A MODEL FOR LOW-LEVEL ANOMALY CIRCULATION AND CLIMATE IN THE TROP

by

RAMASHAN K.

DEPARTMENT OF PHYSICS

Indian Institute of Technology Kanpur

AUGUST 1997

A MODEL FOR LOW-LEVEL ANOMALY CIRCULATION AN CLIMATE IN THE TROPICS

A Thesis Submitted

in Partial Fulfillment of the Requirement

for the Degree of

DOCTOR OF PHILOSOPHY

by

RAMASHAN K.

to the

DEPARTMENT OF PHYSICS

INDIAN INSTITUTE OF TECHNOLOGY - KANPUR

August 1997

CERTIFICATE

It is certified that the thesis work entitled *A Model for Low-level Anomaly Circulation and Climate in the Tropics* by RAMESHAN, K. has been carried out under our supervision and that it has not been submitted elsewhere for a degree.

(Dr. P. Goswami)

Thesis Supervisor
CSIR Centre for Mathematical Modelling
and Computer Simulation
Bangalore 560 037, India

(Dr. P. K. Kalra)

Thesis Supervisor
Department of Electrical Engineering
Indian Institute of Technology
Kanpur 208 016, India

(Programme Co-ordinator) 3/9/97

Head, Department of Physics
Indian Institute of Technology
Kanpur 208 016, India

August 1997

Abstarct

As considerable portion of the energy required to drive the global atmosphere comes from tropical region in the form of precipitational heating, the tropical dynamics play a major role in setting the pattern of world-climate. This heating and associated dynamics in the tropics exhibit a wide range of both temporal and spatial variabilities. It is imperative to understand these variabilities as it leads to a better predictive skill. Over the past few decades much progress has been made with models of different complexities to delineate the main physical processes that give rise to them. Despite these efforts, the general skill in simulating the detailed structure of the tropical variabilities is still limited. One possible reason for this may be the difficulty in modeling of convectively induced internal dynamics which dominates the tropical atmosphere.

Several studies have demonstrated the significant roles played by the moist feedbacks and internal dynamics in the genesis and structure of the tropical variabilities. In particular, it was shown that the introduction of convective time lag (CTL) brings about selective destabilization of the tropical normal modes at observed intraseasonal frequencies. However, these studies involving CTL have been done in an analytical setting. The assumption in these studies that tropical variabilities are largely controlled by convectively forced internal dynamics needs to be examined in a more realistic non-linear setting, for a wider range o observed structures. This thesis examines this question from a number of angle and for a number of time scales ranging from monthly to subseasonal to inter annual. The primary objective here is to formulate and develop a model of th

tropical anomaly circulation incorporating convectively forced internal dynamics. For this purpose, the concept and formulation of CTL has been modified to model the non-linear convective forcing and related circulation anomalies in the lower troposphere of tropical atmosphere.

A brief outline of the overall content and the organization of the thesis is given below

CHAPTER I: Introduction

The tropical atmosphere exhibits a number of variabilities at widely different spatial and temporal scales. Thanks to the large-scale and persistent field experiments of the last few decades, there now exist a number of data sets on the structure of these variabilities. Using these data sets like COADS, it is now possible to examine the spatio-temporal structure of the tropical anomaly circulation for a number of years. These observations impose powerful constraints for modeling and provide the only tool for an objective evaluation of various model simulations. This introductory chapter describes the salient features of tropical variabilities at various scales and discusses their implications for modeling studies.

CHAPTER II: The Driving Mechanisms of Tropical Variabilities

Considerable efforts have been devoted in the past few decades to understand and simulate the tropical variabilities. In particular, a number of studies have explored different feedback mechanisms between convection and large-scale dynamics that can generate the observed structure of tropical variabilities. These modeling efforts can be broadly divided into the three categories: process models, intermediate models and general circulation models (GCM). While the process models help to identify specific physical processes responsible for certain observed variability, they cannot address the question of detailed spatio-temporal structure of the flow. Another limitation of the simple process models is that, being often linear, they cannot accommodate the non-linear and threshold processes. The GCMs, on the other hand, do not suffer from such limitations. However,

the general skill of the GCM in simulating the detailed structure of the tropical variabilities is still limited. The intermediate model stands somewhere in between the process models and the GCMs in their complexity and completeness. In particular, models that address the question of only anomaly circulation for a prescribed (space-time dependent) mean state can be termed intermediate models. Thus the model developed and used in this study is an intermediate model of tropical anomaly circulation. This chapter discusses the general mechanisms of convective forcings in the tropics and their effect on the tropical circulation.

CHAPTER III: The Model Formulation

This chapter describes the physical basis and the formulation of the model-equations. In particular, this chapter describes the concept and the formulation of the CTL for parameterizing the effect of *organized* convection on tropical circulation. A major portion of this chapter is devoted to the derivation of the model-equations. A discussion on the implemented numerical scheme and initial and boundary conditions is also included.

CHAPTER IV: The Monthly Anomaly Fields: Observed vs Simulated Structures

Next, the model's ability to simulate the observed structure of tropical variabilities is examined. For this we examine a quantity

$$\Delta\sigma_\xi(x,y,m) = \frac{|\sigma_{\xi_o}(x,y,m) - \sigma_{\xi_s}(x,y,m)|}{\sigma_{\xi_o}(x,y,m)} \qquad (0.1)$$

where $\sigma_{\xi_o}(x,y,m)$ is the standard deviation of the observed data for the month m (m=1,12 for January to December). The observed data set consisted of the anomaly fields for 12 months for 8 years (1979-1987). The corresponding simulated quantity, $\sigma_{\xi_s}(x,y,m)$ represents the standard deviation from eight one-year model simulations with initial conditions from respective years. Here, ξ denotes either zonal or meridional component of the wind. It was found that both CTL and the structure of moist feedback (EWF), arising from the structure of under-

lying SST, have profound effect on the structure of the variabilities. In particular, it was found that a convective timelag of about 0.5 hour generates fields which can account for a large part of the observed structure of variabilities.

CHAPTER V: The Annual Cycle of the Composit Anomaly Circulation

We next examine the model simulations for the structure related to annual cycle. The sixteen-simulation composite model fields were analyzed to examine the annual cycle for different locations and dynamical conditions. In particular, the results were analyzed for two values of CTL which could generate the structure of the monthly anomaly fields in agreement with the observed structures. It is shown that the model annual cycle exhibits a large part of the spatial (zonal) and temporal characteristics of the observed fields. These findings have important implications for long- and medium-range forecasting in the tropics.

CHAPTER VI: The Spectrum of Oscillations: The Total Spectrum

A prominent feature of the tropical circulation is the existence of a number of oscillations at different temporal and spatial scales. In the intraseasonal scale the most prominent one is the 30-50 day eastward propagating oscillation, while in the interannual scale the most well documented oscillation is the ENSO related variabilities. Hence, one of the requirements of a good tropical-tropospheric model is its ability to generate these variabilities. We have, therefore, examined the existence and structure of oscillations at both intraseasonal and interannual time scales in our model. In particular, a detailed power spectrum analysis of the model simulations for various dynamical conditions as well as for different values of CTL. The model results considered for analysis of ISO were generated by compositing a number of one-year model simulations for different initial conditions, while the existence of longer period oscillations were analyzed using a number of 38-year model simulations. We first investigated the total spectra for both annual and interannual simulations using red noise spectra for identifying significant

peaks. It was found that both the mean conditions (in terms of distribution of SST and mean wind) and CTL affect the genesis of variabilities at different periods. A significant finding was that convective forcing can excite oscillations with interannual period even without ocean-atmosphere coupling. A detailed analysis of each of the significant oscillations is then presented in subsequent chapters.

CHAPTER VII: The Spectrum of Oscillations: The 30-50 Day Oscillation

Perhaps the most prominent and the most well studied intraseasonal oscillation in the tropics is the 30-50 day oscillation. Following its identification in the early seventies, a large number of studies have examined various aspects of this oscillation in detail. Hence, the properties of 30-50 day oscillation provide an excellent testing ground for our model. This chapter, therefore, examines the existence and various properties of this oscillation in detail using a composite one-year model simulation. It is shown that the model can simulate most of the established characteristics of the 30-50 day oscillation. Moreover, a few new features had been revealed in our analysis, which may be verified in a detailed observational study.

CHAPTER VIII: The Spectrum of Oscillations: The Quasi-Biweekly Waves

Another prominent, but less studied oscillation of the tropical circulation is the 10-20 day or quasi-biweekly (QBW) oscillation. Observationally, this oscillation is most prominent over the summer monsoon region; it has not been generally reported over other regions of the globe. The QBW has significant influence on the monsoon circulation and precipitation. So the existence and structure of QBW in our composite model simulation has been examined. Once again it was found that the power spectra of simulated QBW are in close agreement with that of observed. Certain new characteristics to be verified observationaly are also

mentioned.

CHAPTER IX: The Spectrum of Oscillations:i Interannual Varaibilities

After establishing the ability of the model to simulate the structure of the observed intraseasonal oscillations, we address the issue of longer period oscillations. One of the prominent low-frequency oscillations in the tropics is the quasi-biennial oscillation (QBO). Due to the recent observational analyses of the structure of the QBO, it is now possible to address these questions with our model. In particular, we could show that the model simulates a QBO with spatial and temporal characteristics in close agreement with observations.

An important climate variability in the tropics is the El Niño-Southern (ENSO) scale variabilities. Although the most widely held view on the genesis of the ENSO variabilities is ocean-atmosphere interaction, it is possible that the atmospheric dynamics alone can generate interannual oscillations, although their structures are modified by ocean-atmosphere coupling. It was indeed found that the CTL induced convective forcing can generate ENSO scale and longer timescale variabilities. This chapter also discusses the structure of the interannual variabilities with reference to the observed structure for different mean and dynamical conditions. In addition, we address and investigate the important question of inter-relationships among oscillations at annual, biennial and interannual time scales.

CHAPTER X: Convective Couplng and Tropical Variabilities

It has long been held that the most prominent interannual variability in the tropics, *viz.* ENSO, is an ocean-atmosphere coupled variability. However, our findings with the effect of SST-induced distribution of moist feedback on the characteristics of ISO and monthly fields imply that ocean dynamics has considerable impact even on shorter time scale variabilities like ISO. This is also supported by recent observational studies. To investigate the effect of CTL in a coupled environment,

we have formulated ocean-atmosphere coupling involving CTL in terms of convective coupling. The main principle of convective coupling is that ocean-atmosphere coupling, and in particular SST, can affect the atmospheric heating only by modulating atmospheric convection (or column precipitation)-the atmosphere in the large scale is insensitive to the underlying SST as a direct heat source. Since many of the observed tropical variabilities exhibit a predominantly Kelvin wave character, the implications of convective coupling are investigated for the dynamics of Kelvin waves in an analytical setting. It was found that, depending on the mean conditions, convective coupling with a convective timelag, can selectively excite waves over a wide spectrum, from intraseasonal to annual to interannual with observed characteristics. This sets the stage for incorporating CTL in a more realistic coupled model.

CHAPTER XI: Conclusioing Remarks

The last chapter presents the conclusions and scope for future works. The main conclusion that emerges is that a significant part of the tropical variabilities can be understood as forced by convection induced dynamics. The success of this formulation in the present work indicates that it may be useful in parameterizing convection in more complex models.

The present work shows that SST can significantly affect the tropical variabilities even at monthly and other intraseasonal scales. This has been seen in Chapter V to IX, where SST effects the circulation implicitely through its effect on the strength of the EWF, and also in Chapter XI, where SST is included in a coupled and dynamical framework. These findings have important consequences for medium range weather forecasting in the tropics.

It is worth noting that the first-baroclinic mode model developed by us can support a rich spectrum of physics. This chapter also discuss the certain possible improvements in the formulation of moist feedbacks which can improve the quality of simulation of the anomaly fields.

ACKNOWLEDGMENTS

I thank my advisors Dr. P. Goswami and Prof. P.K. Kalra for their guidance, constant encouragement and support. I am grateful to Dr. R.N. Singh and Prof. K.S. Yajnik for allowing me to use the excellent computing facilities at CSIR Centre for Mathematical Modelling and Computer Simulation (C-MAACS) for the numerical modelling part of this work.

Prof. B.N. Goswami (Center for Atmospheric and Oceanic Sciences, IISc., Bangalore) has generously provided the required observational data. I sincerely acknowledge this.

I also thank all scientists and staff in C-MMACS for their co-operation. A special word of thanks to Mr. Thangavalu and Mr. Anil Kumar, C-MMACS scientists, for their computing-help.

My friend Mr. Prasad has been of constant support and help in putting together this thesis. Much needed support and encouragement also came from my fellow graduate students, particularly Gautam, Alok, Koshy, Jimmy, Bala, Salim, Siby, Mansoor and Manoj, at IIT-Kanpur. I am really grateful to these friends who were always ready to help me.

Thanks are also due to Anand, Malay, Prasant, Rajendran and Sajini for their comapany. I thank Malay and Monsoor for patiently reading my thesis and for the valuable suggestions.

I am indebted to my family for their constant support, encouragement and love, without which this could not have been possible.

RAMESHAN K.

Contents

List of Figures

Chapter 1

Introduction

As humanity faces problems like anthropogenic climate change and depletion of the Earth's protective ozone layer, the need for a careful and integrated long term planning of various industrial and developmental activities in order to preserve a delicately balanced bio-geo-ecosphere is becoming more acute. Such long-term policy forecast requires as accurate and reliable as possible a description of the dynamics of the climate system- the role of mathematical models of climate in such decision and policy making thus ranges from helpful to enabling to critical. Accurate forecast of the weather and rainfall patterns, on the other hand, can make significant contribution to a country's economy and the quality of life of its people through better and advance planning of agricultural strategy. This is particularly true for countries like India with an agro-based economy. The advent of high performance computing now allows numerical integration of complex three-dimensional models of the atmospheric general circulation. However, in spite of the tremendous progress made in numerical techniques and computing abilities, accurate simulation and forecasting of the complex atmospheric processes at user specified range and scales still remains a distant goal. This is particularly true in the tropics, where a complex interplay of a number of physical processes makes prediction a challenging task. The tropics, however, play a major role also in the

global context. As considerable portion of the energy required to drive the global atmosphere comes from the tropical region in the form of precipitational heating, the tropical dynamics play a major role in setting the pattern of world-climate. This heating and associated dynamics in the tropics exhibit a wide range of both temporal and spatial variabilities. It is imperative to understand these variabilities for developing better predictive skill. Over the past few decades much progress has been made with models of different complexities to delineate the main physical processes that give rise to them. Despite these efforts, the general skill in simulating the detailed structure of the tropical variabilities is still limited. One possible reason for this difficulty is the dominance of convectively induced internal dynamics in the tropical atmosphere. Several studies have demonstrated the significant role played by the moist feedbacks and internal dynamics in the genesis and structure of the tropical variabilities. These studies have brought out the important role moist processes can play in exciting the observed spectrum of tropical variabilities (Neelin *et al.* , 1987; Lau and Shen, 1988; Goswami and Goswami 1992). With appropriate parameterization of the convective heating process it was found that several observed intraseasonal oscillations in the tropics can be understood as intrinsic modes of the tropical atmosphere. In particular, Goswami and Rao (1993) and Goswami and Mathew (1994) proposed and explored the concept of a convective time lag (CTL) in the genesis and structure of tropical intraseasonal oscillations. A significant finding was that introduction of CTL brings about selective destabilization of the tropical normal modes at observed intraseasonal frequencies.

However, these studies involving CTL have been done in an analytical setting. The implicit assumption in these studies, *viz.* tropical variabilities are largely controlled by convectively forced internal dynamics, needs to be investigated in a more realistic non-linear setting, for a wider range of observed structures. In particular, whether or not the formulation of CTL can be incorporated into a

more detailed model of the tropical atmosphere, with relevant non-linearities needs to be examined. Such a model then can provide the basis for an improved prediction model for the tropics. This question has been examined from a number of angles and for a number of time scales ranging from monthly to subseasonal to interannual. The primary objective here is to formulate and develop a tropical anomaly circulation model incorporating convectively forced internal dynamics. In the present version of the model, we shall focus on a model of intermediate complexity. Thus a relatively simpler dynamical situation with more emphasis on the formulation of convective processes is considered. In particular, the model uses the concept and formulation of CTL to model (non-linear) convective forcing in the lower tropospheric anomaly circulation in the tropics.

A significant contribution to the advancement of understanding and the modeling of the tropical atmosphere came from the large number of observational programmes in the last few decades. Along with these observational programmes, the modeling of atmospheric general circulation made enough advance to be able to supplement the data generated by the observational programmes through comprehensive and objective analysis. Thanks to these large-scale and persistent field experiments combined with model analysis, there now exists a number of data sets on the structure of the atmospheric circulation. Using data sets like the Comprehensive Ocean Atmospheric Data Sets (COADS), it is now possible to examine the spatio-temporal structure of the tropical anomaly circulation for a number of years. Analyses of these data sets enabled the scientists to unravel structures hitherto unknown in the tropical atmosphere. A typical example is the identification of 3-6 day westward propagating wave with a zonal wavelength of about 6000 km. by Liebmann and Hendon (1990) from an analysis of the 7-year reanalysed data from European Center for Medium Range Weather Forecasting (ECMWF). Another example, involving long-term oscillations, is the discovery of quasi-biennial oscillation (QBO) and its interconnections with El Niño-Southern

Oscillation (ENSO). As we shall see, the detailed spatio-temporal structures now exist for most of the variabilities in the tropics. These observations and analyses put powerful constraints on modeling and provide the only tool for an objective evaluation of various model simulations.

Fairly in pace with the observational studies, enormous efforts have been devoted in the past few decades to understand and simulate the tropical variabilities. In particular, a number of studies have explored different feedback mechanisms between convection and large-scale dynamics that can generate the observed structure of tropical variabilities. These modeling efforts can be broadly divided into the three categories of process models, intermediate models and general circulation models. While the process models help to identify specific physical processes responsible for certain observed variability, they cannot address the question of detailed spatio-temporal structure of the flow. Another limitation of the simple process models, which are often linear, is that they cannot accommodate the non-linear processes. The General Circulation Models (GCM), on the other hand do not suffer from such limitations. However, the general skill of the GCM in simulating the detailed structure of the tropical variabilities is still limited. The intermediate models are somewhere in between the process models and the GCM in their complexity and completeness. In particular, models that address the question of only anomaly circulation for a prescribed (space-time dependent) mean state can be termed intermediate models. Thus the model developed and used in this study is an intermediate model of tropical anomaly circulation. The organization of this thesis is given below.

After providing a brief discussion of the various forcings important for the variabilities of the tropical atmosphere, we turn towards developing a model for the anomaly circulation in the tropics incorporating convection induced internal dynamics governed by CTL. The third chapter describes the physical basis of our model and the formulation of the model equations. In particular, this chapter

describes the concept and the formulation of the CTL for parameterizing the effect of *organized* convection on tropical circulation. A discussion on the numerical scheme implemented and initial and boundary conditions is also included.

The crucial step of model calibration and validation was carried out by comparing model simulation of the monthly anomaly fields with the corresponding observed structure. In particular, we consider composite-simulations for a number of values of CTL to determine the range of values that would provide the best simulation of the observed anomaly fields. In addition, this chapter also investigates the effect of different dynamical conditions, like the spatio-temporal structure of evaporation-wind feedback (EWF), on the quality of model simulations. As will be shown, both CTL and the structure of EWF, arising from the structure of underlying SST, have profound effect on the structure of the variabilities.

Next, the model simulations are examined for the annual cycle. For this purpose sixteen one-year model simulations were generated with initial conditions from observed anomaly fields for 1979 to 1987. The simulated fields were then analyzed for the nature of variation through the year. A significant finding was that SST-induced spatio-temporal distribution of moist feedback has profound impact on the structure of the fields. In particular, spatio-temporal variation of the strength of EWF, determined by distribution of SST field, is necessary to simulate the correct distribution of the convective heating. These findings have important implications for long- and medium-range forecasting in the tropics.

A prominent feature of the tropical circulation is the existence of a number of oscillations at different temporal and spatial scales. In the intraseasonal scale the most prominent one is the 30-50 day eastward propagating wave, while in the interannual scale the most well documented oscillation is the ENSO related variabilities. Hence, one of the requirements of a good model of the tropical tropospheric circulation is its ability to generate these variabilities. While it was

shown in earlier studies that moist feedbacks and CTL can give rise to selective excitation of the tropical waves at observed intraseasonal frequencies (Goswami and Rao, 1993; Goswami and Mathew 1994), these studies have been on an analytical setting. In particular, these studies could not investigate the effect of non-linear convective heating. The existence and structure of oscillations at both intraseasonal and interannual timescales in the model simulation are examined. We first investigate the total spectra for both annual and interannual simulations using red noise spectra for identifying significant peaks in the power spectra. It was found that both mean conditions (in terms of distribution of SST and mean wind) as well as CTL affect the genesis of variabilities with intraseasonal period. A significant finding was that convective forcing can excite oscillations with interannual period even without ocean-atmosphere coupling. A detailed analysis of each of the significant oscillations is then presented in subsequent chapters.

The available information on the structure of various tropical oscillations can be exploited to critically evaluate model simulations against the observed structure of these oscillations. Perhaps one of the most prominent and well studied intraseasonal signal in the tropics is the 30-50 day oscillation. Following its identification in the early seventies, a large number of studies have examined various aspects of this oscillation in detail. The properties of 30-50 day oscillation thus provide an excellent testing ground for our model. The existence and various properties of this oscillation are examined using a composite one-year model simulation. It is shown that the model can simulate most of the established characteristics of the 30-50 day oscillation. In addition, model simulations with special dynamical conditions like only-winter and only-summer mean winds have helped to identify the relative roles of the annual cycle of the mean wind and SST.

Another prominent, but less studied oscillation of the tropical circulation is the 10-20 day or quasi-biweekly (QBW) oscillation. Observationally, this oscillation

is most prominent over the summer monsoon region. The QBW has significant influence on the monsoon circulation and precipitation. Therefore the existence and structure of QBW in our composite model simulation are examined.

Apart from the intrascasonal oscillations, the tropical climate is also characterized by a number of long term oscillations. Among these QBO with a period between 19-36 months and ENSO with a period between 3-6 years are most important. The next chapter, therefore, examines the existence and characteristics of these low frequency oscillations in our model simulation. The power spectrum analysis of simulated time series at selected locations shows considerable power at low frequencies close to that observed. It is also shown that the existence of interannual variabilities requires the interannual variabilities in the SST fields.

Many of observational analyses brought out the interconnection between oscillations at different time scales (Murakami *et al.* ; 1986; Philander, 1984) In order to successfully simulate the climate, a model not only has to simulate the individual oscillations, but also their interconnections. This aspect of the model simulations was also investigated. It is shown that the simulated and the observed phase relationships among annual cycle, QBO and ENSO are in good agreement.

It has long been held that the most prominent interannual variability in the tropics, *viz.* ENSO, is an ocean-atmosphere coupled variability. However, Our findings with the effect of SST-induced distribution of moist feedback on the characteristics of ISO and monthly fields imply that ocean dynamics has considerable impact even on shorter time scale variabilities like ISO. This is also supported by observational studies. To investigate the effect of CTL in a coupled environment, we have formulated ocean-atmosphere coupling involving CTL in terms of convective coupling. The main principle of convective coupling is that ocean-atmosphere coupling, and in particular SST, can affect the atmospheric heating only by modulating atmospheric convection (or column precipitation); the atmosphere on the large scale is insensitive to underlying SST as a direct heat source.

Since many of the observed tropical variabilities exhibit a predominantly Kelvin wave character, the implications of convective coupling are investigated for the dynamics of Kelvin waves in an analytical setting. It was found that, depending on the mean conditions, convective coupling with a CTL, can selectively excite waves over a wide spectrum, from intraseasonal to annual to interannual with observed characteristics. This sets the stage for incorporating CTL in a more realistic coupled model.

The last chapter presents the conclusions and scope for future work. The main conclusion is that a significant part of the tropical variabilities can be understood as forced by convetion induced dynamics. We have characterized this convective dynamics through CTL, which represents a timescale for interaction between *organized* convection and large-scale dynamics. The success of this formulation in the present work indicates that it may be useful in parameterizing convective processes in more complex GCMs. A significant finding from the present work is that SST can significantly affect the tropical variabilities even at monthly and other intraseasonal scales. These findings have important consequences for medium range weather forecasting in the tropics. It is worth noting that the first-baroclinic mode model developed by us can support a rich spectrum of physics. While there are several directions in which further improvement is possible and necessary, the ability of the model to simulate a wide range of observed phenomena, with time scale ranging from a few days to several years, indicates its versatility.

Chapter 2

The Driving Mechanisms of Tropical Variabilities

Large-scale convection and circulation anomalies in the tropical atmosphere have been observed to operate with certain characteristic time scales and spatial patterns. In particular, a large part of the tropical variability is determined by the so called intraseasonal oscillations (ISO). Prominent examples of these ISO are the 30-50 day eastward propagating oscillation or the Madden and Julian oscillation (Madden and Julian, 1971,1972), the 10-20 day westward propagating mode (Krishnamurthi *et al.,* 1973; Murakami and Frydrych 1974; Chang and Chen, 1993) and 3-6 day westward propagating wave (Liebmann and Hendon, 1992). A primary question that needs to be answered concerns the mechanism(s) that govern the excitation and dynamics of these variabilities at the observed spatial and temporal scales. The significant role played by these variabilities in the regional as well as global weather systems explains the persistent effort at simulating them through models of varying degrees of complexity. In spite of these efforts, the detailed regional and global manifestations of ISO are still evasive to modeling studies. However, considerable advances in understanding the mechanism of genesis of several of the variabilities have taken place in the recent years through investigation of roles the of moist processes and the interaction of convection

and the large-scale dynamics associated with it. In the longer term scales, much attention has been focussed on the variabilities related to El Niño-Southern Oscillation (ENSO) and, on the role of ocean-atmosphere coupling. Here, an outline of the various mechanisms that may be operative in the genesis of variabilities in the tropical atmosphere is provided.

Tropical Wave Dynamics and Intraseasonal Oscillations

Following Mastsuno (1966), a large number of the theoretical investigations have examined the ISO as manifestation of the internal dynamics of the tropical atmosphere. The idea that the intraseasonal oscillations could be intrinsic unstable modes of that part of the tropical atmosphere situated over the warm ocean pool, and not a globally propagating mode, is also strongly suggested by observational studies.

The most distinctive aspect of the 30-50 day oscillation (namely its slow eastward movement, and equatorial emplacement of its maxima) prompted earlier investigators to search for an analytical explanation of the phenomenon in terms of Kelvin wave dynamics. Parker (1973) interpreted the oscillation as the Kelvin wave mode studied by Matsuno (1966), although the vertical scale of low- frequency Kelvin wave is very small in the absence of heating. Chang (1977) suggested that the vertical-scale can be explained by the effect of strong viscosity.

A fundamental problem in invoking the Kelvin wave dyhamics to explain MJO, the apparent disparity in the phase speed, was addressed by Swinbank *et al.* (1986). They have come up with some evidences that this may be understood in terms of moist Kelvin wave dynamics, if effect of latent heat release on stability is taken into account properly . A simple model-calculation leads to the conclusion that precipitation associated with the Kelvin wave reduces static stability and so decreases the phase speed. They further confirmed these conclusions by GCM experiments in which latent heat-release was increased, first by increasing SST and second by doubling the value of latent heat constant. In both the cases the

period of wave was increased.

Another serious drawback with many studies that introduced tropical wave dynamics to explain ISO is the lack of scale selection at observed (intraseasonal) frequencies. Only wave with highest growth rate will be observable, since by interpretation of linear theory this is the one that draws maximum energy. However, in most studies involving Kelvin wave such a selective excitation (or scale selection) was not achieved. The highest growth rates still occurred at the highest frequency. This resulted in a search for mechanisms that would provide a high-frequency cut-off in agreement with the observed spectra.

CISK and wave-CISK

The concept of conditional instability of the second kind (CISK) was first discussed by Charney and Eliassen and Murakami, and is a simple representation of interaction between small scale convection and large scale dynamics (and hence second kind) in presence of moist processes (and hence conditional). Since its formulation almost 30 years ago, CISK has been employed extensively as an explanation for various tropical phenomena that involve convection. The central point is that CISK cannot work in an atmosphere that is not conditionally unstable.

Recently the commonly held assumption that the mean tropical atmosphere is conditionally unstable has come into question. Betts (1982) noted the correspondence between the observed atmospheric profile and the a virtual moist-adiabatic lapse rate. The virtual moist adiabatic takes into account the effect on buoyancy of the condensed vapor, whereas a moist adiabatic assumes condensate immediately rains out. Xu and Emanuel (1989) analyzed numerous tropical profiles and found that the atmosphere did indeed approximate to a virtual moist adiabatic. Convective towers probably carry their condensate to at least some level so that appropriate adiabatic is a reversible virtual adiabatic rather than an irreversible moist adiabatic.

If atmosphere is neutrally stable, intensification of disturbance will rely critically on the surface fluxes and convection will perform the role of communicating the perturbations in the boundary layer moist entropy to the rest of the atmospheric column. The large scale dynamics would then respond to the rearrangement of the atmospheric mass that surface fluxes and convection supplied. In contrast to the CISK scenario, in this case there is no alternation in the free atmospheric temperature (and hence the pressure distribution) unless the boundary layer moist entropy changes. In recognition of this range of interactions, and to avoid further confusion from use of the term CISK, Neelin and Yu (1993) have suggested the term *convective interaction with dynamics* (CID) to cover all the possibilities.

The CISK has failed to achieve what it was created for. Because the theory predicted highest growth rate at the smallest scale. In other words, it predicted that the only structure that should be seen in the tropical atmosphere are the cumulus clouds, and not, say the tropical cyclones. A modification of the old CISK idea by including the wave dynamics was proposed by Lindzen (1973), and came to be known as wave-CISK. The wave-CISK has been often questioned, since it invokes physically unreasonable negative heating in a linear setting. This happens in the linear theory due to the proportionality of heating to the wave divergence irrespective of their sign.

In several papers, K.M Lau and his co-workers have used a convergent dependent heating scheme to argue that the intraseasonal oscillation is wave-CISK mode that propagate east due to moisture convergence (Lau and Peng 1987; Sui and Lau 1989; Lau *et al.*, 1989). Lau and Lau (1986) have analyzed the 12-year output of a GCM experiment with the objective of describing the spatial and temporal behavior of this tropical variability. The GCM used for this integration is a 9-level, 15- wave number spectral model with realistic distribution of continents and orography. The model physics consists of radiative transfer process, ground

hydrology, moist convective adjustment and ice-albedo feedback. In the course of integration, SST and solar heating were constrained to evolve through successive annual cycles which are identical to each other. Even though some of the characteristics of the simulated oscillation (*ie.* spatial structure, phase relationship between the upper and lower level variables, propagation characteristics and seasonal dependence) are in agreement with the observations, the period of wave number 1 component of model disturbances is shorter than the corresponding observed value.

Hendon (1988), using a two-level model and a CISK-type cumulus heating scheme, identified its structure as that of a nonlinear coupled Rossby-Kelvin mode. The mechanism of propagation is essentially one where the large-scale equatorially trapped CISK disturbance forced by the convection neutralizes the stability that generates it preferentially to the west of its center, thus giving rise to slow eastward propagation.

Evaporation-Wind Feedback

Another mechanism that has been proposed to significantly affect the convective forcing in the tropics is evaporation-wind feedback (EWF). The evaporation anomaly are generally small, but in the delicate balance tropical atmosphere modest gradient in the evaporation can have significant effects on the evolution of the convective activity. The first theories taking into account the effect of surface evaporation were proposed by Emanuel (1987) and Neelin *et al.* (1987) in the context of 30-50 day oscillation. In particular, they had considered the dynamics of Kelvin wave in an equatorial β-plane for a moist neutral atmosphere. Considering a case in which the mean background winds are (implicitly) easterlies, they showed that inclusion of EWF destabilizes the Kelvin wave. However, a major problem was that the growth rate was found to be monotonically increasing with frequency, implying selection at the smallest scale. If the wind speed dependence of evaporation is changed by replacing its instantaneous value by the climato-

logical value, the amplitude of the power in the eastward propagating waves is substantially reduced.

Prescribed vs Dynamical Heating

Lau and Peng (1987) conducted two numerical experiments. The focus was the validation of two widely used heating parameterizations against the key features of the phenomenon. In one of the experiments, the heating was assumed to be localized and pulsating with a period of 40 days. No feedback with the internal dynamics was permitted. Apparently, the horizontal scale of the main circulation was determined both by the scale of the heating and the dissipation. The major disagreement between the response of the model and reality is that both eastward and westward expansion of the wind perturbation are seen in the former, whereas only eastward propagation is seen in the latter.

In their numerical experiment to determine the relative roles of localized heating and wave-CISK, Lau and Peng (1987) removed the unphysical negative heating by prescribing a positive-only heating. Although in their simulation the eastward propagation was captured, the phase speed was about a factor two faster than what is observed. The amplitude was seen to be strongly modulated by the variation in SST. The CISK-induced responses were more strong over the warm ocean. But the geographical preference of the convection was not seen. Strong similarity of the horizontal structure of wind anomalies in the deep tropics to that of the Kelvin wave had prompted them to propose so called *mobile wave-CISK* mechanism by which Kelvin waves were selectively destabilized. Kelvin wave consists of solely divergent winds. Therefore, associated low-level convergence is stronger than that of Rossby waves. Hence, heating source moves eastward along with the Kelvin wave convergence which in turn again excites Kelvin wave further east.

The effect of vertical structure of heating on the phase speed was investigated by Sui and Lau (1989). The convection was parameterized by using a simple

one-dimensional cloud model which took into account the available moisture supply in the lower troposphere and the mean thermodynamic state for the entire troposphere. Consequently, the spatial distribution of convective heating could be determined internally as a function of SST. The major disturbances were seen to propagate eastward with phase speeds of 18 ms^{-1} and 9 ms^{-1} when the maximum heating was near 500 mb and between 700-500 mb respectively. The corresponding time periods were 26 and 52 days. In all the experiments a uniform SST distribution was assumed. However, for the case when heating was related only to boundary layer processes, the value of phase speed (13 ms^{-1}) was in between the phase speeds of two wave- CISK modes discussed earlier. But the wind response in this case was dominated by wave number 2. It was also stated that the boundary layer processes enhance the convection to the east of the deep convection thus reinforcing the eastward propagation.

The oscillations simulated in another study (Lau *et al.* 1987) with the help of a spectral-GCM resemble observations to some extent. This model has same resolution as the model analyzed by Lau and Lau (1986), but the boundary conditions were more idealized. The prescribed SST-distribution was zonally symmetric and function of only latitude, convection was modeled by moist convective adjustment parameterization scheme. The annual mean solar input was prescribed at the top of the boundary and clouds were prescribed as a function of latitude only. There was a sharp contrast between the simulated dynamical and precipitational fields; larger portion of the total variance in the former resided in the wave number 1 and 2, whereas in the latter it resided in the higher modes. Moreover, the small scale precipitation did not propagate steadily at the same phase speed, like those presented in the models where Kuo type scheme was used to calculate heating. Instead, in the course of their eastward journey, they redeveloped in the regions favored by large-scale convection. The simulated circulation patterns at both 200 and 850 mb had strong zonal components. There was a much stronger meridional

component at 850 mb, which presumably produced the frictional stress near the surface.

Teleinduction and Genesis of Super Cloud Clusters

According to Winston the super cloud clusters and their eastward movement originate from what they called as the *supercloud clusters teleinduction mechanism* of initiating new cloud clusters by the existing cloud clusters at some distance (800-1200 km) to its east. Locations close to the cloud clusters, because of the compensating downward motion associated with the existing cloud clusters, are not favored for the emergence of the new cloud cluster. The reason the eastern side is more favored than the western side for new cloud cluster to emerge is due to the fact that the basic flow in the boundary layer, being easterlies, is strengthened by the circulation induced by the existing cloud cluster. Once new cloud is formed it compete with existing cloud clusters for moisture. Since moisture mainly comes from the east in tropical easterly flow, new cloud has the first chance to harness it. He argues that the initiation of the cloud is not caused by the Wave-CISK, but by the circulation features induced by the existing cloud clusters 800-1200 km to the west of it. The wave-CISK is an instability responsible for the growth of the cloud clusters, and cloud cluster teleinduction is the mechanism that brings the dynamical and thermodynamical fields at a particular location towards the critical point beyond which the wave instability starts.

Extra-tropical Influence

The assumption that each new intraseasonal episode of convective activity is initiated by the remnants of the previous oscillation approaching from the west has been the underlying assumption in many theoretical studies. There are also studies which report the potentiality of midlatitude baroclinic eddies in triggering the convective activity. Blade and Hartmann (1993) examine these possible mechanisms responsible for the selection of the preferred period of MJO. For this purpose, a global two-layer nonlinear model with a positive-only CISK type cu-

mulus heating scheme is used. By making the SST in the tropics as a function of longitude, they investigate the relative importance of these two mechanisms in determining the time scale of the oscillation. When the cold SST is sufficiently stable, the CISK-wave propagates efficiently through the stable region in the form of damped moist Kelvin wave, and reemerges in the unstable region where its amplitude grows again. When SST in the stable sector is set close to the instability threshold, the moist Kelvin waves (MKW) slow down and decay before reentering the unstable region. However, the CISK perturbation periodically regenerates over the warm water in response to the local buildup of instability. This shows that MKW in this case is a forced response, and has no impact on the genesis of the next convection. This implies a new mechanism for setting the time scale of the oscillation, alternative to that of simple zonal propagation around the globe. A *recharge-charge* theory is proposed whereby, the time scale of the disturbances is set by the growth and duration times of the convective episode together with the recharging time of the static stability in the convective region. Also shown is how midlatitude baroclinic eddies provide the quasi-stochastic force necessary to excite each new intraseasonal episode by organizing a region of subtropical convection, which then grow and expand towards equator due to the effect of latent heating.

Ocean-Land-Atmosphere Interaction

The question, as to whether atmospheric variabilities at intraseasonal and shorter time scales are entirely forced by internal atmospheric instability or whether coupling between ocean and atmosphere play a role is still not fully answered. Most of the linear theories assume the availability of steady source of energy for the maintenance of the basic state. The source of energy for the sustained cumulus heating (on the subseasonal time scale) is usually not addressed. Convection for such long period requires a steady supply of moisture from the ocean. It is found that in this time scale the latent heat flux from the ocean to

atmosphere is of considerable amount. The study by Krishnamurthi *et al.* (1988) indicate that oscillation of both the wind and the SST contribute to a strong coupling of atmosphere and the ocean at this time scale. The amplitude of SST variation at this time scale are of the order of 0.5° to 1.0°C and most pronounced SST oscillation in the SST occurs over the equatorial western pacific ocean and the Bay of Bengal. It is conceivable that one degree enhancement of SST over these climatological warm oceans can affect the convection and their propagation.

Oscillations of intraseasonal time scale have been observed in the tropical oceans. For example Mysak and Mertz (1984) reported a 40-60 day oscillation of long shore current and sea surface temperature in the western Indian Ocean. It is worth noting that 40-50 day signals have been found in many oceanographic parameters, e.g., surface current over the Indian Ocean (McPhaden, 1982); sea level in the coastal regions of South America (Enfield and Lukas, 1984) and sea surface temperature in the Somali current (Mysak and Mertz, 1984). The dynamical model study by Webster and Chou (1980) hints at the possibility that this intraseasonal variability could be an outcome of interaction of the ocean or the ground hydrological cycle with atmosphere.

At annual, interannual and longer time scales the importance of ocean-atmosphere interaction has been recognized for a long time. A conceptual model for the ENSO based on sustained ocean-atmosphere interaction was proposed by Bjerkness (1969). A significant finding was that a coupled equatorial ocean-atmosphere system can sustain unstable oscillations, although the linear equatorial ocean and the atmosphere may by themselves be stable. In the conventional explanation, ENSO can be understood as a manifestation of equatorial Kelvin wave dynamics and associated delayed oscillator mechanism. In this scenario (Cane and Zebaik, 1985; Schopf and Suarez, 1988; Battisti and Hirst, 1989; Philander, 1992), oceanic wave dynamics and the reflection of the wave from boundary determine the structure and growth rate of coupled instability. Hence, it was argued that ENSO type

oscillations should be absent over the tropical Atlantic and Indian oceans. Nevertheless, several observational studies suggest that ENSO related variabilities are present also outside the tropical Pacific. A global relation of the surface pressure anomalies to the ENSO cycles was demonstrated by Krishnamurthi *et al.* (1986). Barnett (1985) presented the evidence of eastward propagation of surface wind and pressure anomalies from equatorial Indian Ocean to Central Pacific. Yasunari (1987) suggested that ENSO should be considered as a global phenomena in a land-ocean-atmosphere coupled environment.

The relationship between these features observed in the ocean and their counterparts in the atmosphere remains to be ascertained. Thus, coupled atmospheric model may necessary for a complete understanding of this complex global phenomena. The question of role of ocean-atmosphere coupling in the genesis of sub-seasonal scale variabilities will be taken up in more detail in the present study.

From an analysis of the various mechanisms presented above, and their relative success in explaining the genesis of tropical variabilities, the most universal one appears to be convection induced internal dynamics through interaction between convection and large scale dynamics. However, the scope and the representation of interaction between convection and large scale dynamics is rather broad, encompassing mechanisms like CISK and EWF. Indeed, as described below, the current, most successful representation of interaction between convection and large scale dynamics is a combination of CISK, EWF and convergence feedback in presence of an explicit moisture equation.

Interaction between Convection and large-scale Dynamics

Observations indicate that deep convection often occurs over the regions of large scale moisture convergence. It is, therefore, reasonable to assume that evaporation only regulates the amount of moisture available for the precipitation. Seager and Zebiak's study (1994) is related to the interaction between convection and

dynamics in a new linear primitive equation model wherein a new method of integration had been employed. An idealized sea surface temperature distribution, representing the climatological warm pool area with a maximum at 100°E and a cold region with maximum at 140W°, is used when simulations were performed for two different types of heating schemes. The simulated behaviors were changed radically when heating was evaluated by Betts-Miller convection scheme. Contrary to what is common in wave CISK-studies, but in agreement with the observations, eastward propagating disturbances do not remain coherent around the globe. They are seen only over the warm-pool regions and die out over the cold region. The phase speed of convection in this case is less than one third of that in the wave-CISK case. If the evaporation wind feedback were removed, then a moisture convergent mode is seen with a single disturbance that would encircle the globe in about 60 days. If the effect of moisture convergence is suppressed, then almost all deep convection and propagation is suppressed and the weak modes present have only half the amplitude of those present in the experiment with full moisture equation. The model characteristics were not altered much when the dominance of moisture convergence over the evaporation wind feedback was reduced by assuming a higher value of the surface exchange coefficient. This is not true when one of the feedbacks is absent. No eastward propagation is apparent in the presence of only moisture convergence. The conclusion is that for different values of the surface evaporation time scale, either the EWF or low-level convergence of moisture can create eastward propagating deep convective mode. The periodicity is longer when full moisture equation is used.

A successful application of the formulation of interaction between moist feedback induced convection and large scale dynamics to explain the genesis and structure of ISO was made by Goswami and Goswami (1992). In particular, it was shown that the combined effect of EWF, convergence feedback and dissipation can selectively destabilize the mixed Rossby-gravity wave at 3-6 day time

scale. The spectral characteristics of this selectively destabilized wave matched very well with the observed 3-7 day westward propagating wave (Liebmann and Henden, 1991). However, the formulation of Goswami and Goswami, (1992) could not account for the scale selection at two other major ISO observed in the tropics viz. the 30-50 day oscillation and the 10-20 day oscillation.

Moisture Dynamics and Convective Time Lag

As mentioned earlier, other major drawback of most of the studies involving CID to explain ISO is their inability to produce selective excitation of the tropical wave with observed spectral characteristics. Besides, often only a particular ISO is addressed. If one has to build up a consistent model of anomaly circulation in the tropics, a mechanism that can generate under appropriate dynamical conditions all the major oscillations in the tropics is needed. A reason for this failure might be due to the diagnostic status assigned to moisture variable. In particular, most of these studies consider a balance equation for the moisture variable so that the precipitational heating is determined by a balance between surface evaporation, column convergence and column precipitation. Such a formulation is not likely to be valid in a general situation, where the storage of moisture will determine the scales at which the heating will be most effective. In other words, while the moist feedbacks can bring about the essential destabilization, the dynamics of moisture variable determines the selective destabilization. The role of an explicit moisture dynamics in the excitation of tropical waves was formulated and examined by Emanuel (1988) and Goswami and Rao (1994). Goswami and Rao, by introducing the concept of a convective time lag in an explicit moisture equation, showed that convection induced internal dynamics can selectively destabilize Kelvin wave with observed spectral characteristics. Subsequently, Goswami and Mathew (1994) investigated the dynamics of equatorial waves in presence of an explicit moisture equation with a convetive time lag. Goswami and Mathew (1994) showed that the 3-4 day westward propagating wave (Liebmann and Mathew, 1991) and the 10-20

day westward propagating wave observed over the summer monsoon region could be understood as selectively destabilized tropical normal modes. However, the total anomaly circulation in the tropical lower troposphere contains a much wide range of variabilities than the these ISO. The question arises therefore, whether the analytical model of Goswami and Rao (1994) and Goswami and Mathew (1994) can be generalized to provide an acceptable representation of the low-level variabilities in the tropics. In the chapters that follow this question is examined in detail.

Chapter 3

The Model Formulation

In the background of the large number of analytical studies and simple process models, it can be expected that convective internal dynamics determines a large part of the anomaly circulation in the tropics. This convective internal dynamics, of course, would depend on the embedding mean state. Since the mean state embodies the effects of various large-scale forcings as well as boundary conditions, proper inclusion of the mean condition and convective internal dynamics should enable us to simulate large part of tropical circulation. This is the working hypothesis for developing our model of anomaly circulation in the tropics.

The spatial similarity of apparently disconnected modes like ISO and ENSO of tropical atmosphere (Lau and Chan, 1988; Wieckmann, 1983; Wang and Murakami, 1988) is rather intriguing. So is the phase-locked nature of the variabilities at the low frequency end of the spectrum. It has been proposed (Lau and Chan, 1988) that ISO might trigger the low frequency mode like ENSO. There might exist a common dynamical link which could selectively cascade energy from one mode to other. In view of this, it is essential to identify the connection between various components of these variabilities. This is possible only if all these variabilities are brought under a common dynamical framework. There have been a few theoretical and modeling (Lau and Shen, 1988; Hirst and Lau, 1990) attempts

made in this direction. An alternative view of interaction of convection and dynamics in the tropics is proposed to develop a unified dynamical framework for the oscillations at different time scales.

A characteristic of the geophysical fluid is their large horizontal dimension compared to vertical extent. So they behave like shallow fluids. The shallowness can be quantified by aspect ratio, $\delta = D/L$. D and L are typical vertical and horizontal scales of the atmosphere respectively. For a synoptic situation in the tropics with horizontal scale of 1000 km. and vertical scale comparable to the height of tropopause, the aspect ratio is the order of 10^{-2}. This has profound effect on the vertical dynamics of the geophysical fluids and has led to a class of models known as shallow water model.

3.1 The Shallow Water Approximation

Perhaps Laplace was the first to apply shallow-water equations on a rotating sphere to study oscillations of the atmosphere. Since then this model had been used with appropriate modification to study the dynamical processes of relevance to both ocean and atmosphere. Gill (1980) was able to capture the wind and pressure distribution patterns similar to those observed in the tropics when the model was forced by a prescribed heating.

3.2 The Basic Equations

The horizontal components of momentum equation can be written as,

$$\frac{\partial \tilde{u}}{\partial t} + \tilde{f}_x + \tilde{u}\frac{\partial \tilde{u}}{\partial x} + \tilde{v}\frac{\partial \tilde{u}}{\partial y} + \tilde{w}\frac{\partial \tilde{u}}{\partial z} + \frac{1}{\tilde{\rho}}\frac{\partial \tilde{p}}{\partial x} + \tilde{F}_x = 0 \qquad (3.1)$$

$$\frac{\partial \tilde{v}}{\partial t} + \tilde{f}_y + \tilde{u}\frac{\partial \tilde{v}}{\partial x} + \tilde{v}\frac{\partial \tilde{v}}{\partial y} + \tilde{w}\frac{\partial \tilde{v}}{\partial z} + \frac{1}{\tilde{\rho}}\frac{\partial \tilde{p}}{\partial y} + \tilde{F}_y = 0 \ . \qquad (3.2)$$

where $\tilde{u}$, $\tilde{v}$, and $\tilde{w}$ denote x, y and z components of velocity respectively, whereas

$\tilde{p}$, the pressure and $\tilde{\rho}$ the density of air. The x and y components of momentum dissipation are given by $\tilde{F}_x$ and $\tilde{F}_y$ respectively. The terms $\tilde{f}_x$ and $\tilde{f}_y$ are the components of Coriolis force. The vertical momentum equation reduces to a simple hydrostatic balance under shallow water approximation.

The nonlinearity in the advective term seems to play a secondary role (Gill and Phillips, 1986) in many of the dynamical scenarios in the tropics. Zebaik (1990) evaluated the terms in the vorticity budget for selected monthly surface wind anomaly fields over the tropical Pacific Ocean. He arrived at the conclusion that nonlinear advection terms are of second order importance. So the equations are linearized using conventional method wherein the total fields are partitioned into a mean term and a perturbation term. Exploiting the smallness of the perturbation terms, the equations 3.1 and 3.2 are simplified as

$$\frac{\partial u}{\partial t} - \beta y v + U\frac{\partial u}{\partial x} + V\frac{\partial u}{\partial y} + \frac{1}{\overline{\rho}}\frac{\partial p}{\partial x} + F_x = 0 \tag{3.3}$$

$$\frac{\partial v}{\partial t} + \beta y u + U\frac{\partial v}{\partial x} + V\frac{\partial v}{\partial y} + \frac{1}{\overline{\rho}}\frac{\partial \rho}{\partial y} + F_y = 0 \tag{3.4}$$

The mean zonal wind (U), meridional wind (V) and vertical velocity (W) are characterized by $U = U(x, y, t)$, $V = V(x, y, t)$ and $W = 0$. In the case of ρ, the *Boussinsesq approximation* is evoked wherein it is treated as a constant in horizontal momentum equations and as a function of z in the vertical momentum equation. As the terms involving meridional and zonal gradients of mean wind are in general small, they are neglected. The zonal and meridional components of anomaly wind are denoted by u and v. The F_x and F_y stand for x and y components of horizontal friction. The Coriolis parameters in an equatorial β-plane can be approximated as $-\beta y v$ and $\beta y u$ respectively.

The energy equation is given by

$$\frac{d\tilde{\theta}}{dt} = \dot{Q} \tag{3.5}$$

Here $\dot{Q}$ is the source term of total energy with Q as the perturbation heating. Linearization of equation 3.5 about a basic state having mean potential temperature ($\bar{\theta}(z)$) gives:

$$\frac{\partial \theta}{\partial t} + U\frac{\partial \theta}{\partial x} + V\frac{\partial \theta}{\partial y} + w\frac{d\bar{\theta}}{dz} + F_\theta = Q, \tag{3.6}$$

The horizontal gradients of mean potential temperature are neglected due to its small value. The cooling term is represented by F_θ. At this stage a spatially and temporally uniform value of $\frac{d\bar{\theta}}{dz}$ is assumed.

3.2.1 Incompressibility and Hydrostatic Balance

Although in general the atmosphere is compressible, it can be shown that for large scale dynamics incompressibility is a reasonable approximation. The continuity equation is, then, linearized to obtain

$$\frac{\partial u}{\partial x} + \frac{\partial v}{\partial y} + \frac{\partial w}{\partial z} = 0 \tag{3.7}$$

The observation that scale of motion in vertical plane is very small compared to that in the horizontal plane helps to simplify the vertical component of equation to a hydrostatic relation which can be written as

$$\frac{\partial \tilde{p}}{\partial z} + \tilde{\rho} g = 0, \tag{3.8}$$

where g is the acceleration due to gravity.

A simple linear relationship between perturbation potential temperature and pressure used in earlier studies is adopted here. The details of the derivation and assumptions which lead to this simplification are given below.

The equation of state can be written as

$$\frac{\overline{p}+p}{\overline{p}} = \frac{(\overline{\rho}+\rho)(\overline{T}+T)}{\overline{\rho}\overline{T}}. \tag{3.9}$$

After some cancellation and neglecting the product ρT, equation 3.9 gives

$$\frac{\rho}{\overline{\rho}} + \frac{T}{\overline{T}} = 0 \quad , \tag{3.10}$$

when we assume, for simplicity, that the fractional changes in temperature are much greater than those in pressure.

The Poisson's equation may be linearized to obtain

$$\frac{\theta}{\overline{\theta}} = \frac{T}{\overline{T}} - \frac{R}{C_p}\frac{p}{\overline{p}} \quad . \tag{3.11}$$

The last term in the right hand side of this equation is dropped, based on the above assumption. Now, hydrostatic relation (3.8) may be written as

$$\frac{1}{(\overline{\rho}+\rho)}\frac{\partial(\overline{p}+p)}{\partial z} + g = 0 \tag{3.12}$$

But the relation $(\overline{\rho}+\rho)^{-1} \approx \frac{1}{\overline{\rho}}[1-\frac{\rho}{\overline{\rho}}]$ and $\frac{\partial \overline{p}}{\partial z} = g\overline{\rho}$ give

$$\frac{1}{\overline{\rho}}\frac{\partial p}{\partial z} + g\frac{\rho}{\overline{\rho}} - \frac{\rho}{\overline{\rho}^2}\frac{\partial p}{\partial z} = 0 \tag{3.13}$$

The equations 3.11 is used to modify equation 3.13.

$$\frac{1}{\overline{\rho}}\frac{\partial p}{\partial z} - g\frac{\theta}{\overline{\theta}} = 0 \tag{3.14}$$

We may write the equation 3.14 as,

$$\frac{\partial}{\partial z}\left(\frac{p}{\overline{\rho}}\right) + \frac{p}{\overline{\rho}}\frac{\partial}{\partial z}(ln\,\overline{\rho}) - g\frac{\theta}{\overline{\theta}} = 0 \tag{3.15}$$

Further approximation is possible only if oscillations having vertical wavelengths less than half of the scale height of density are considered. Under this condition the magnitude of the second term is negligible. Now we may rewrite equation 3.15 as

$$\frac{\partial}{\partial z}\left(\frac{p}{\overline{\rho}}\right) - g\frac{\theta}{\overline{\theta}} = 0 \tag{3.16}$$

3.2.2 The Vertical Structure

In the present formalism the tropical atmosphere is represented by the shallow water equations describing the horizontal structure of the first baroclinic mode on an equatorial β-plane. Though a number of modes may be required to tackle general problems, a remarkable degree of success had been achieved in understanding certain aspects of tropical atmosphere behavior by using even single mode (Krishnamurthi *et al.*, 1976; Anderson, 1976 and Bannon 1979). Hantel and Baader (1978) indicated that, when suitably averaged in horizontal and time the heating rate increases from zero at the surface to a maximum at about 500 mb, and then fall off above that. The wind in lower troposphere is oppositely directed to that in the upper troposphere. The horizontal velocity is zero in mid-level, whereas the vertical velocity is maximum there. This characteristics of first baroclinic mode can be mathematically represented as the following vertical structures of the model fields:

$$u = u_a(x, y, t)\,cos(z/H) \tag{3.17}$$

$$v = v_a(x, y, t)\,cos(z/H) \tag{3.18}$$

$$w = w_a(x,y,t)\,sin(z/H) \tag{3.19}$$

$$(\theta, Q) = (\theta_a, Q_a)\,sin(z/H)\frac{\overline{\theta}}{\overline{\theta}_o} \tag{3.20}$$

$$p = p_a\,cos(z/H)\frac{\overline{\rho}}{\overline{\rho}_o} \tag{3.21}$$

We have neglected higher-order modes, as the first baroclinic mode provides a reasonable approximation for tropics. This vertical structure has been used in several studies (Davey, 1985; Lau and Shen, 1988; Davey and Gill, 1987; Goswami and Goswami, 1991). The $\overline{\theta}_o$ and $\overline{\rho}_o$ are characteristic values of $\overline{\theta}$ and $\overline{\rho}$. This structure is bounded by rigid horizontal plane at $z = \pi H$ and $z = 0$. Substituting 3.19 and 3.21 in 3.16

$$\frac{p_a}{\overline{\rho}_o} = -gH\frac{\theta_a}{\overline{\theta}_o} \tag{3.22}$$

The perturbation vertical velocity (w) expressed as

$$w_a = -H\left\{\frac{\partial u_a}{\partial x} + \frac{\partial v_a}{\partial y}\right\} \tag{3.23}$$

is obtained by removing vertical structure from the continuity equation by using 3.17, 3.18 and 3.19.

3.2.3 Moisture Dynamics

Although the importance of moist dynamics in the tropical variabilities has been emphasized in many works, most of them do not consider explicit moisture dynamics. In these studies, unlike in the present case, convective heating is determined by a balance between column convergence and surface evaporation.

The equations 3.3, 3.4 and 3.6 describing the evolution of perturbations of zonal and meridional wind components at the lower layer and the mid level potential temperature perturbation θ_a respectively are supplemented by a fourth equation describing the evolution of depth integrated moisture:

$$\frac{\partial q}{\partial t} + \Gamma \left\{ \frac{\partial u_a}{\partial x} + \frac{\partial v_a}{\partial y} \right\} = E - P \tag{3.24}$$

Here E is the gain due to evaporation from the surface and P is the loss due to precipitation in the column and

$$\Gamma = -H \int_0^{H_o} \frac{dq^*}{dz} f(z) dz. \tag{3.25}$$

In the above expression, H_o represents a height relevant for moisture dynamics. The unit of q^* is kgm^{-3}. The f(z) is a non-dimensional structure function representing the vertical structure of the dynamical fields. Since our model is formulated for the first baroclinic structure, we consider H_o = H. For simplicity, $\frac{dq^*}{dz}$ is assumed to be independent of height and its value is estimated by assuming $q^*(H) = 0$, and a climatological value for $q^*(z = 0)$. In the tropics moisture concentrations tends to fall off with height over a vertical distance small compared with that of the first baroclinic mode. It should be noted that the explicit time-dependence of the moisture variable in our study allows us to avoid assuming a permanently convective region assumed in many studies (*e.g* Lau and Shen, 1988; Goswami and Goswami 1991). In our formalism a non-convective (convective) region can evolve to a convective (non-convective) region by the dynamics of moisture variable.

3.2.4 The Convective Time Lag and Precipitation

The models of tropical dynamics are sensitive to how convection is handled. Most frequently used theories for interpreting intraseasonal oscillations are based on Wave-CISK (Lau and Peng, 1987; Miyahara, 1987; Hendon, 1988; Chang and Lim, 1988; Wang, 1988; Kirtman and Vernekar, 1993; and Blade and Hartmann, 1993) and evaporation wind feedback mechanisms (Neelin, 1987; Emanuel, 1987).

In majority of these works precipitation was estimated from a steady state moisture budget equation. The linear versions of these theories suffer from scale selection problem. Moreover, Wave-CISK mechanism often produces eastward propagating waves with higher phase speed compared to the observed one. The EWF implicitly depends upon the presence of mean easterlies. In fact, wind is observed to be weak easterly or even westerly in locations (*ie.* Indian and western Pacific oceans) where intraseasonal signal is strong. The studies by Numagati and Hayashi (1991) and Numagati (1993) found out that the convective adjustment scheme produces more realistic simulation of convective complexes and its propagation characteristics. Though the parameterization of convective heating used in the present study can be classified as convective adjustment scheme, conceptually it is different. In the present formulation, precipitation brings the moisture variable q to its equilibrium value $\overline{q}$ over a time scale τ; thus, it can be expressed as

$$P = \frac{q - \overline{q}}{\tau}. \tag{3.26}$$

In other words, the moisture variable does not relax back to its equilibrium value $\overline{q}$ immediately but does so over a moisture relaxation time scale τ. Several studies have emphasized the role and importance of a convective time-lag in tropical circulation (Betts, 1986; Betts and Miller, 1986; Emanuel, 1993; Goswami and Rao, 1994; Goswami and Mathew, 1994; Neelin *et al.*, 1994). The concept and the effect of a moisture relaxation time scale were also discussed in GR. The basic philosophy is that for organized large-scale precipitation in the tropics, the process cannot be considered instantaneous; it has a characteristic relaxation time scale which can be typically a few hours. Seager *et al.*, (1995) have also used a time-lag of a few hours, although in a different context.

It should be noted that the CTL embodies our hypothesis and it is not possible

to assign a precise value to it at present. However, we shall assume that the CTL time scale of a few hours. It is obvious from the above equation that as model moisture evolve in time, regions of negative precipitation may appear. In the numerical version of this model, this limitation has been overcome by setting the value of precipitation to zero wherever it is less than zero.

3.2.5 The Evaporation Wind Feedback

Using well known bulk aerodynamic formula, the perturbation evaporation E may be expressed as

$$E = \rho_s C_d W(q_s - q_o), \tag{3.27}$$

where ρ_s is air density in the boundary layer, C_d the moisture flux coefficient, W the surface wind speed, and q_s the saturation specific humidity at sea surface. The q_o represents specific humidity at the surface, which is determined by sea surface temperature SST (in units of K) via following empirical relation:

$$q_o = 10^{-3}[18 + 0.67(SST - 300)]. \tag{3.28}$$

This empirical relation has been used by Wang and Li (1993) and is derived from monthly mean Comprehensive Ocean-Atmosphere Data Set (COADS) for the tropics where SST is higher than 295 K. This expression for evaporation can be further simplified. For this purpose the Clausius-Clapeyron equation is integrated from a reference temperature T_r to SST, which yielded

$$q_s(SST) = q_s(T_r)\left\{1 + \frac{L_v}{R_v T_r^2}(SST - T_r)\right\} \tag{3.29}$$

where R_v is gas constant for water vapor. Inserting 3.28 and 3.29 into 3.27 we get,

$$E = \rho_a C_d K_q W (SST - T_*), \tag{3.30}$$

where coefficient $K_q = 6.95 \times 10^{-4} K^{-1}$ and $T_* = 293.2$ K. This equation implies that the evaporation rate increases with SST. Because the empirical relation was used, strictly speaking, equation 3.30 can be applied only to the tropical regions where SST exceeds 22°C. The evaporation rate is assumed to be independent of SST and is given by $1.8 C_E W K_q$, when SST is below 293.2 K.

A closed set of model equations constructed by using equations 3.3, 3.4 3.6, 3.22, 3.23, 3.25, 3.24 and 3.26 is given below.

$$\frac{\partial u_a}{\partial t} - \beta y v_a + U\frac{\partial u_a}{\partial x} + V\frac{\partial u_a}{\partial y} - \frac{gH}{\overline{\theta}}\frac{\partial \theta_a}{\partial x} + Ru_a = 0 \tag{3.31}$$

$$\frac{\partial v_a}{\partial t} + \beta y u_a + U\frac{\partial v_a}{\partial x} + V\frac{\partial v_a}{\partial y} - \frac{gH}{\overline{\theta}}\frac{\partial \theta_a}{\partial y} + Rv_a = 0 \tag{3.32}$$

$$\frac{\partial \theta}{\partial t} + U\frac{\partial \theta}{\partial x} + V\frac{\partial \theta}{\partial y} - H\frac{d\overline{\theta}}{dz}\left\{\frac{\partial u_a}{\partial x} + \frac{\partial v_a}{\partial y}\right\} + R\theta_a = Q_a \tag{3.33}$$

$$\frac{\partial q}{\partial t} + \Gamma\left\{\frac{\partial u_a}{\partial x} + \frac{\partial v_a}{\partial y}\right\} = E - P \tag{3.34}$$

The F_u, F_v and F_θ are expressed as Ru_a, Rv_a and $R\theta$ respectively

The atmospheric heating proportional to precipitation is in the form

$$Q_a = \eta P; \tag{3.35}$$

where, $\eta = \dfrac{L_v}{C_p H \rho_a}$.

The L_v and C_p denote latent heat of vaporization of water and specific heat of air respectively. While density of the air is represented by ρ_a, the value of the tropopause height is given π times H .

3.3 The Basic State

In this study, the incorporation of effects of advection by mean wind and the effect of mean SST through evaporation would enable us to investigate the model's

response to temporal and spatial inhomogeneity present in the mean state of the tropical atmosphere. The climatological monthly fields for meridional and zonal components of the wind and SST were derived from monthly mean COADS from the year 1979 to 1987. The anomalies for individual year had been calculated by deducting (9-year) climatological mean from the total field of the each year. These anomalies form the initial fields for the control runs. The mean SST fields also decide the temporal and spatial variation EWF.

3.4 Numerical Scheme

Owing to the presence of non-linearities in our equations it is not easy to obtain analytical solutions in general. Besides, we would like to investigate the detailed spatial and temporal evolution of the fields in a general setting. Hence, the model equations have to be numerically integrated with a suitable scheme. This has been done by using explicit finite difference methods in both space and time. Symbolically this can be written as,

$$\Psi_k^{n+1} = \Psi_k^{n-1} + 2\Delta t \Phi(\Psi_{k-1}^n, \Psi_k^n, \Psi_{k+1}^n, F), \tag{3.36}$$

where Ψ represents any one of the dependent variables , Δt the time step and Φ the generalized forcing term. The time level and spatial grid point are identified by the subscript n and superscript k respectively. The numerical integration is initiated by using the forward difference scheme. This is inevitable, as Leap- Frog scheme can be utilized only if values of dependent variable are supplied at all time levels. The spurious mode inherent in this time-integration scheme is eliminated by using Asselin (1 2-1 in time) filter (Shapiro, 1970) at every 48th time step. The model leapfrogs with time step of 500 sec. To avoid two-grid interval noise, the variables are staggered on the Arakawa-C grid. The same resolution is used in longitude and latitude: ie., 2°. While boundary conditions prescribed in the zonal

direction are periodic, the fields are forced exponentially to zero in meridional directions through spongy layers implemented over 5 points near the boundaries. The integration domain in the meridional direction is 90^{o} on either side of the equator. In our formalism, the moisture variable can assume any positive or negative values allowed by the equation 3.24. But there are physical bounds on the magnitude of the moisture anomaly. Since a positive q would imply a rise above (near) saturated reference state, allowing very large value would make it unphysical supersaturation. On the other hand, permitting too large a negative value would make the total moisture content very small or even negative, which is unphysical. We, therefore, impose this bound through the condition

$$q = \begin{cases} q_{-} & \text{if } q < q_{-} \\ q_{+} & \text{if } q > q_{+} \end{cases} \tag{3.37}$$

Although the lower and the upper bounds can in principle be different, we have taken them to be symmetrical about zero. Besides, it was found that a symmetrical bound with $q_{+} = q_{-} = 5kg\,m^{-2}$ produces the daily rates of precipitation which were in best agreement with observation.

Chapter 4

The Monthly Anomaly Fields: Observed vs Simulated Structure

The anomaly fields in the tropics show a high degree of spatio-temporal variabilities. They also exhibit characteristic organization at various spatio-temporal scales. While there has been a large number of attempts to simulate specific variabilities like 30-50 day oscillations, it is a prerequisite of a model of atmospheric circulation to be able to simulate the structure of the anomaly fields. The dynamics of the anomaly field (as against the structure of a specific oscillation) are subjected to a number of forcings determined by geophysical conditions and mean state. Moreover, tropics are never dynamically isolated from the extra-tropics, especially at large spatio-temporal scales. However, the major forcing for the anomaly circulation in the tropics is still likely to be the convective forcing. The convective forcing itself is not independent of the mean conditions; for example, the convective activity seems to closely linked to the underlying SST fields. It is reasonable to expect that a proper representation of convective forcing along with the effect of mean state should explain a fair portion of tropical variabilities. To examine this hypothesis and to validate our model, a comparison of the spatio-temporal structures of the simulated vs the observed fields is made. The convective forcing in our model is determined by precipitational heating which

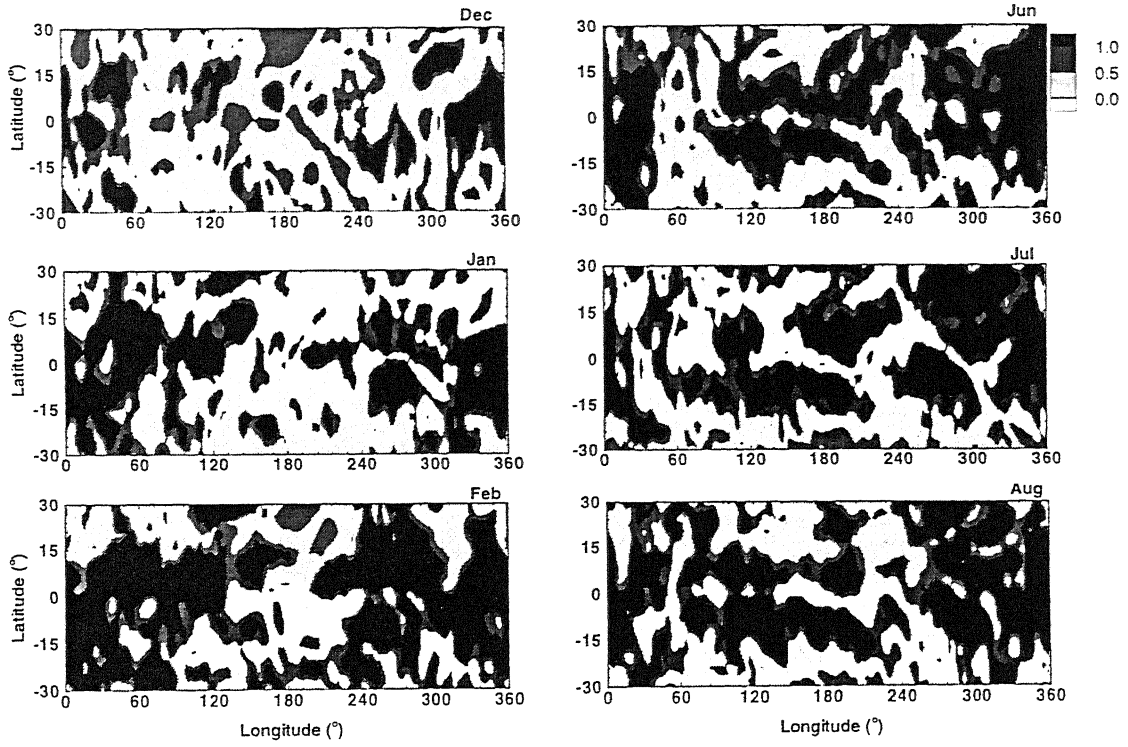

Figure 4.1: Longitude-latitude structure of the $\Delta\sigma_u$ field with uniform EWF for $\tau = 0.5$ hr.

depends on large-scale convergence, EWF and CTL. However, many of the parameters (in particular CTL) cannot be determined precisely. In addition, we need to identify and assess relative roles of various moist processes and CTL in the quality of our model simulation. However, the anomaly fields are also influenced by the mean circulation and underlying SST distribution. Finally, there is the question of the sensitivity of model to initial conditions. Thus there are at least three major issues that need to be addressed:

1. Role of CTL

2. The effect of SST-induced distribution of EWF

3. Sensitivity to initial conditions

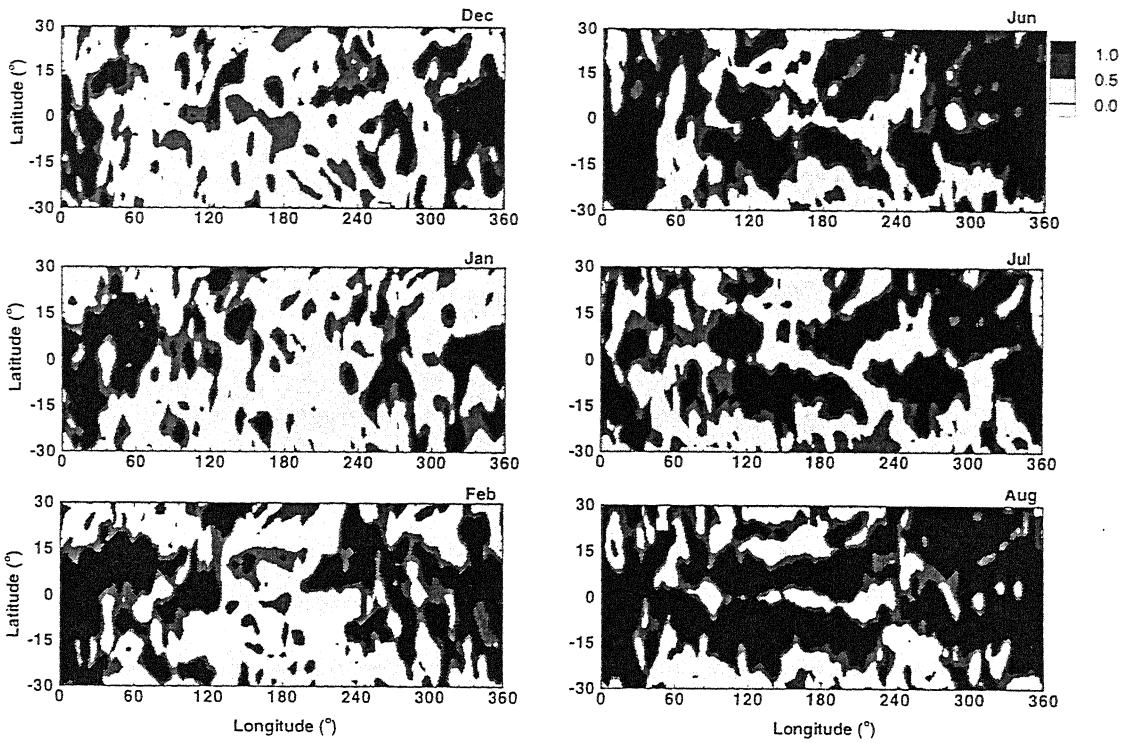

Figure 4.2: Same as the Fig 4.1, but for $\tau = 1.5$ hr.

The first of these issues, *viz.* the role of CTL, is also related to the model calibration. While in earlier analytical studies a CTL of about six to twelve hours was used, these studies were aimed at investigating mechanisms of specific low-frequency variabilities like 30-50 day oscillation and 3-5 day oscillation. As mentioned earlier, the basic idea had been that specific ISO arises from convective forcing organized at specific scales. However, while considering the dynamics of the anomaly fields the possibility remains that even smaller period organizations also contribute to the genesis and the dynamics of the variabilities. Indeed, since the larger scale organizations are dependent on the organization at smaller scales, it is possible that the smallest organizational time scale determines the subsequent hierarchy of organization. In this scenario, the relevant convective timelag should be comparable to the cumulus time scale. Since we still do not have a way of

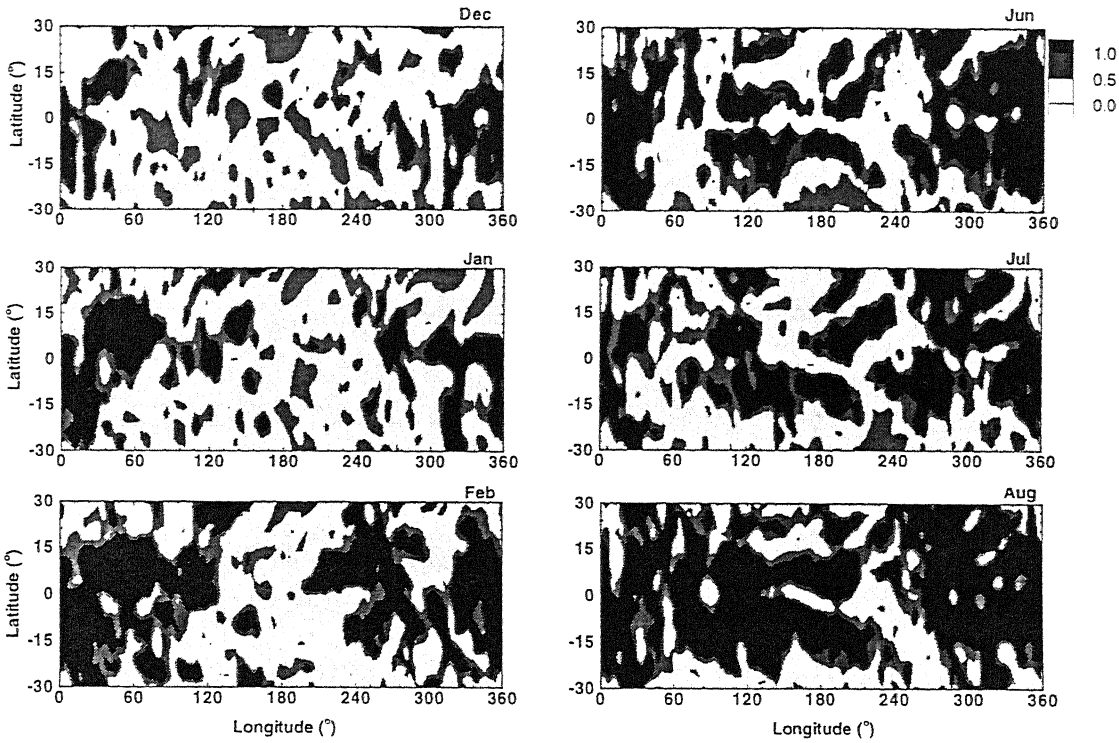

Figure 4.3: Same as the Fig 4.1, but for $\tau = 3.0$ hr.

precisely determining the value of CTL, a number of values for CTL, from the cumulus scale to the meso-scale, is considered. A comparison of quality of the simulations for the various values of CTL then provides a way of choosing an appropriate value of CTL. The second issue, ie. the role of mean conditions, is significant in view of the fact that many of our model processes like EWF depend (implicitly as well as explicitly) on the mean conditions. For example, the quantity Δq appearing in for EWF depends on the underlying SST through the dependence of surface humidity on SST. This dependence can introduce complex spatio-temporal variations in the strength of EWF. As we shall see, this affects the structure of the variabilities to a large extend. In addition, the presence of a space-time dependent advective mean wind has considerable effect on the evolution and structure of the variabilities.

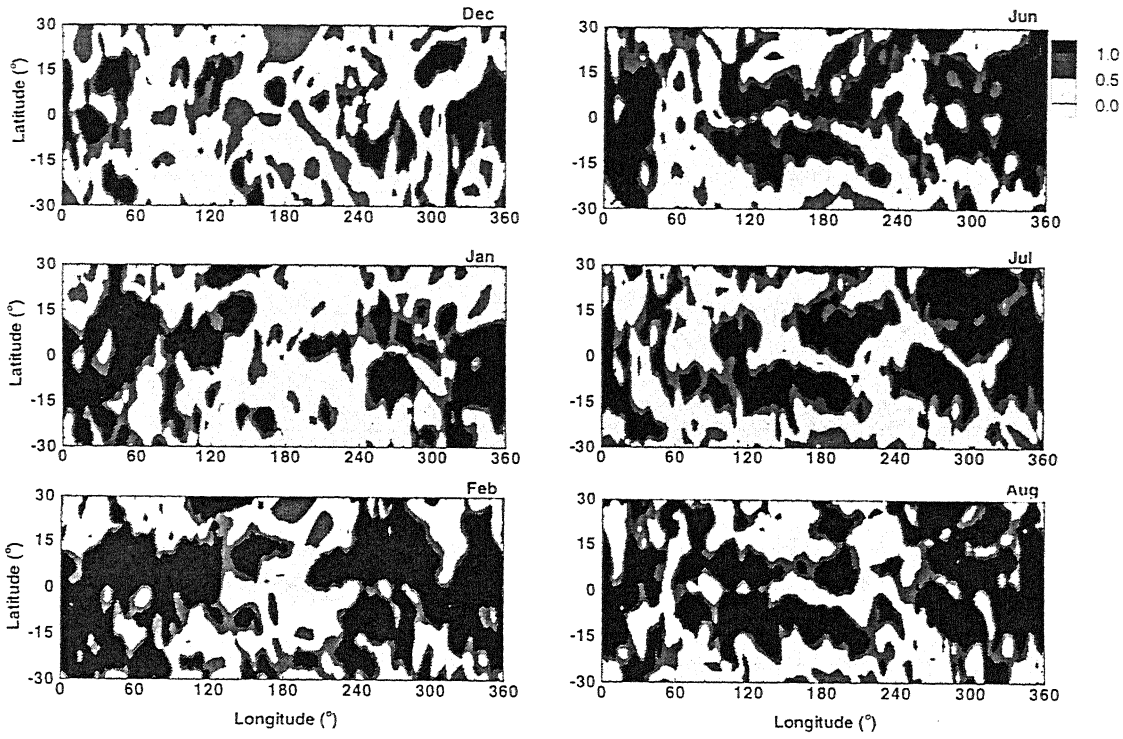

Figure 4.4: Same as the Fig 4.1, but for $\tau = 6.0$ hr.

4.1 Design of the Experiments

To compare the model simulated variability with the observed structure in a statistical sense, we have considered the structure of the observed standard deviation of the variables u and v for the period 1979-1987. The observed fields are generated by subtracting the 9-year monthly-mean for the above period for each month and each year. The observed data set is taken from COADS available on a $2^o \times 2^o$ grid. The simulated precipitation is compared with the observed positive-anomaly precipitation. The monthly mean SST fields were also obtained from the COADS for the same periods. As discussed in Chapter 3, we consider a domain of simulation that is global in the zonal direction and from 30°S to 30°N in the meridional direction, embedded in a numerical domain of meridional extent

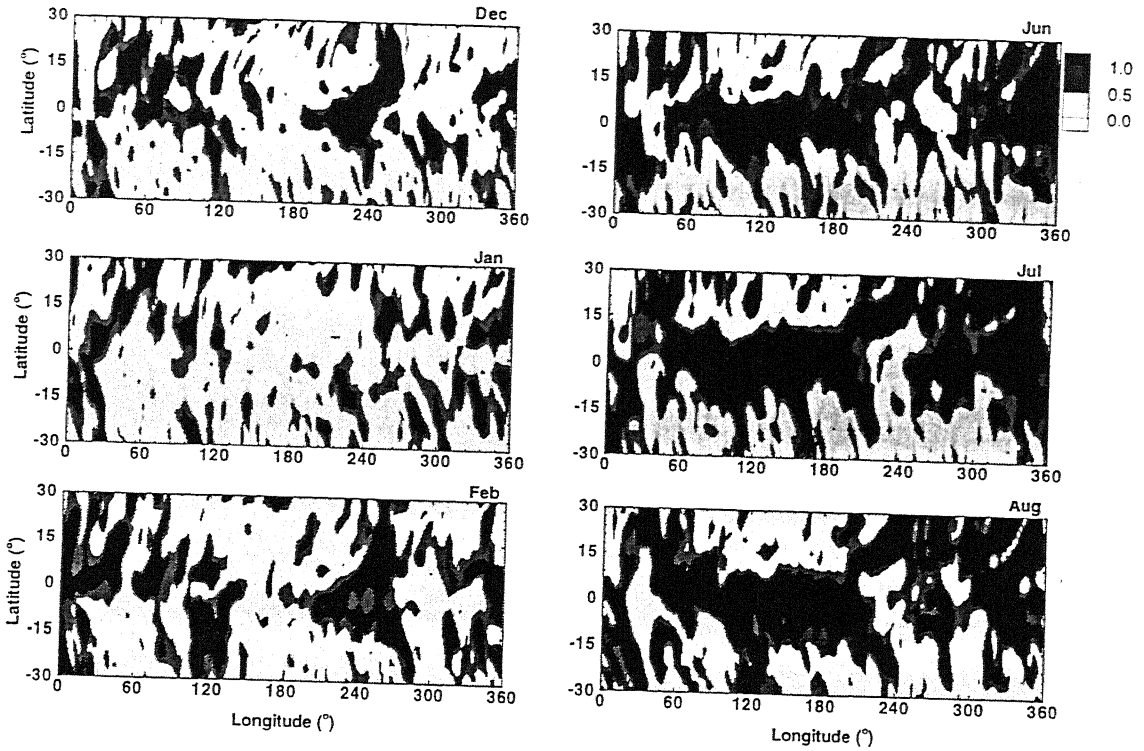

Figure 4.5: Same as the Fig 4.1, but for $\Delta\sigma_v$

180° and symmetric about the equator. All the simulations were also carried out on a $2^\circ \times 2^\circ$ grid, with a time step of 500 sec. The experiments can be categorized into the following two sets:

1. SetI: Uniform strength of EWF, mean wind prescribed from monthly-mean wind for the period 1979-1987 for each month.

2. SetII: Non-uniform strength of EWF determined by the distribution of monthly-mean SST; mean wind prescribed from monthly-mean wind for the period 1979-1987 for each month.

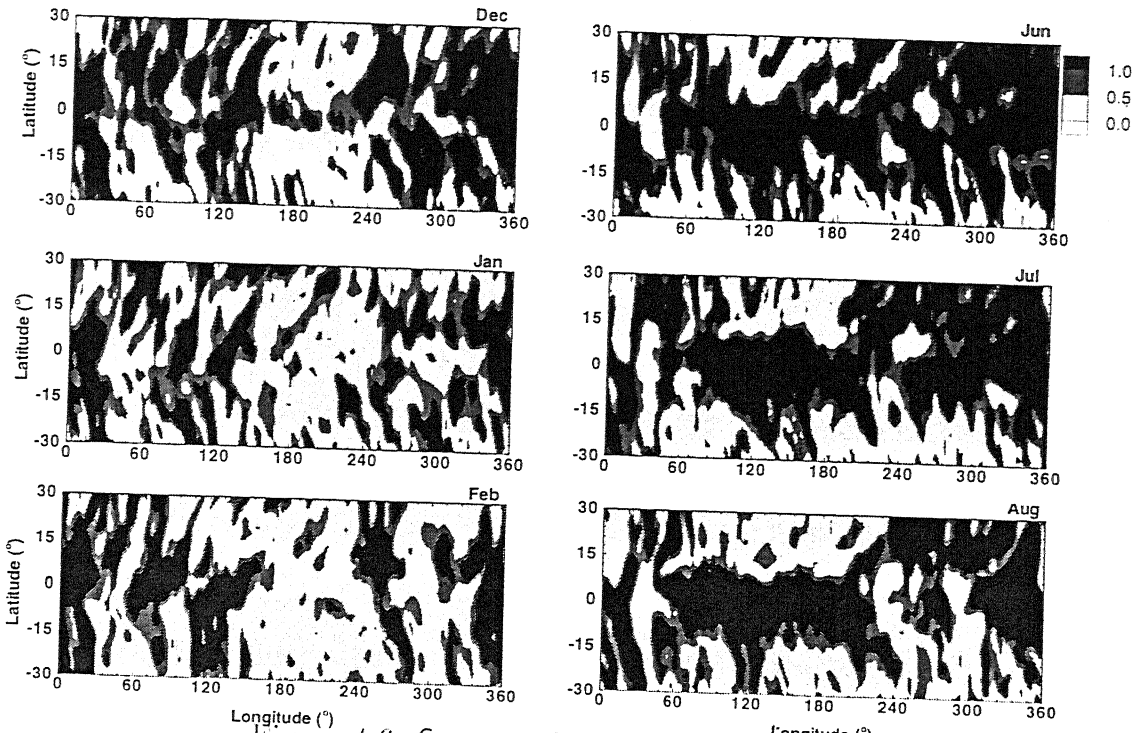

Figure 4.6: Same as the Fig 4.5, but for $\tau = 1.5$ hr.

4.2 Method of Analysis

To create the monthly anomaly fields, the longitude-latitude structures of the simulated fields were written every five days and then averaged over a month. The simulated structure of standard deviation is obtained by compositing model simulations for each month from 16 one-year model integrations. Out of these 16 model simulations, eight were with initial conditions taken from the observed anomaly fields for the month of January and the other eight with initial conditions derived from the observed anomaly fields for the month of June for the respective year. In all the cases, both the observed and the composite simulated fields were normalized to their respective maximum, so that any error due to difference in the magnitudes is filtered out. This allows us to discuss exclusively the quality of

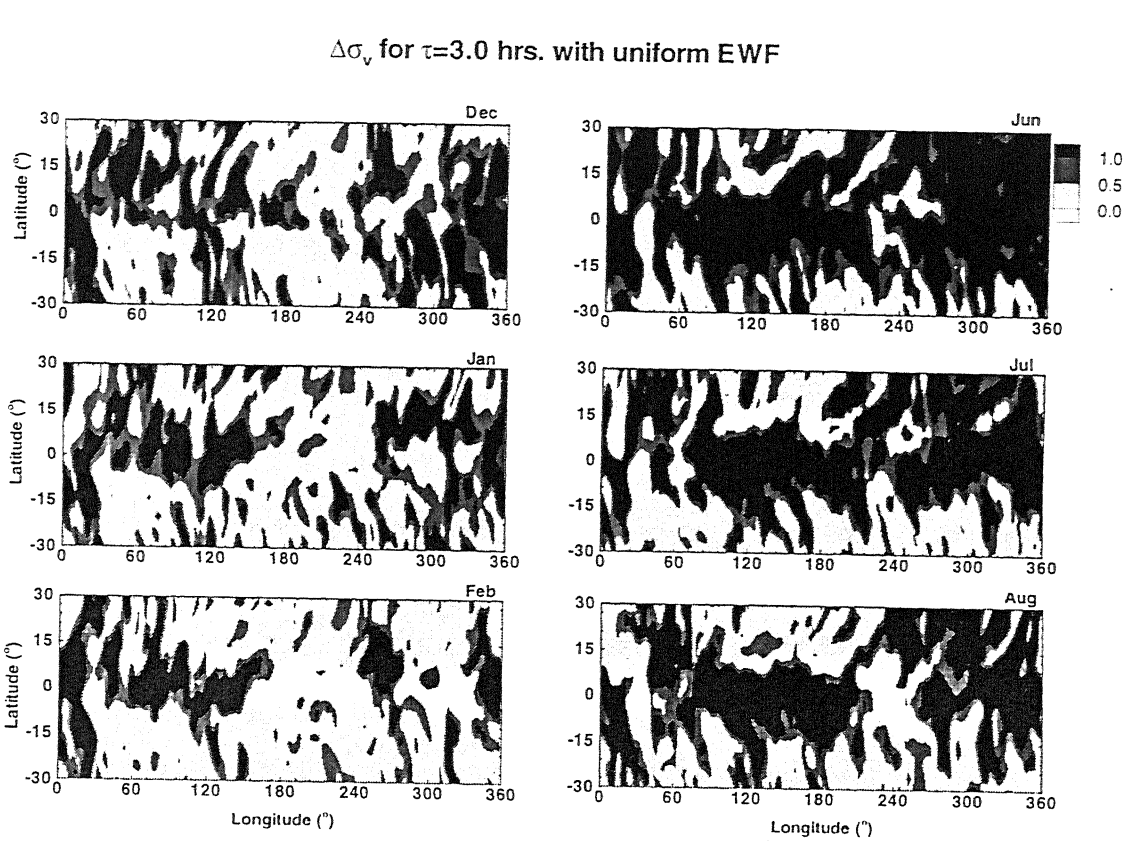

Figure 4.7: Same as the Fig 4.5, but for $\tau = 3.0$ hr.

the simulation in terms of spatio-temporal distribution of the variabilities. Since the magnitudes of the simulated fields depend on the strengths of various model parameters, many of which cannot be determined precisely, we do not address the issue of magnitudes of the simulated fields. However, for reasonable values of the model parameters the distributions of the simulated fields are close to the observed.

To assess the quality of simulation we define and use the normalized magnitude of the difference between the observed and simulated standard deviations, given by

$$\Delta\sigma_\xi(x,y,m) = \frac{|\sigma_{\xi_o}(x,y,m) - \sigma_{\xi_s}(x,y,m)|}{\sigma_{\xi_o}(x,y,m)} \tag{4.1}$$

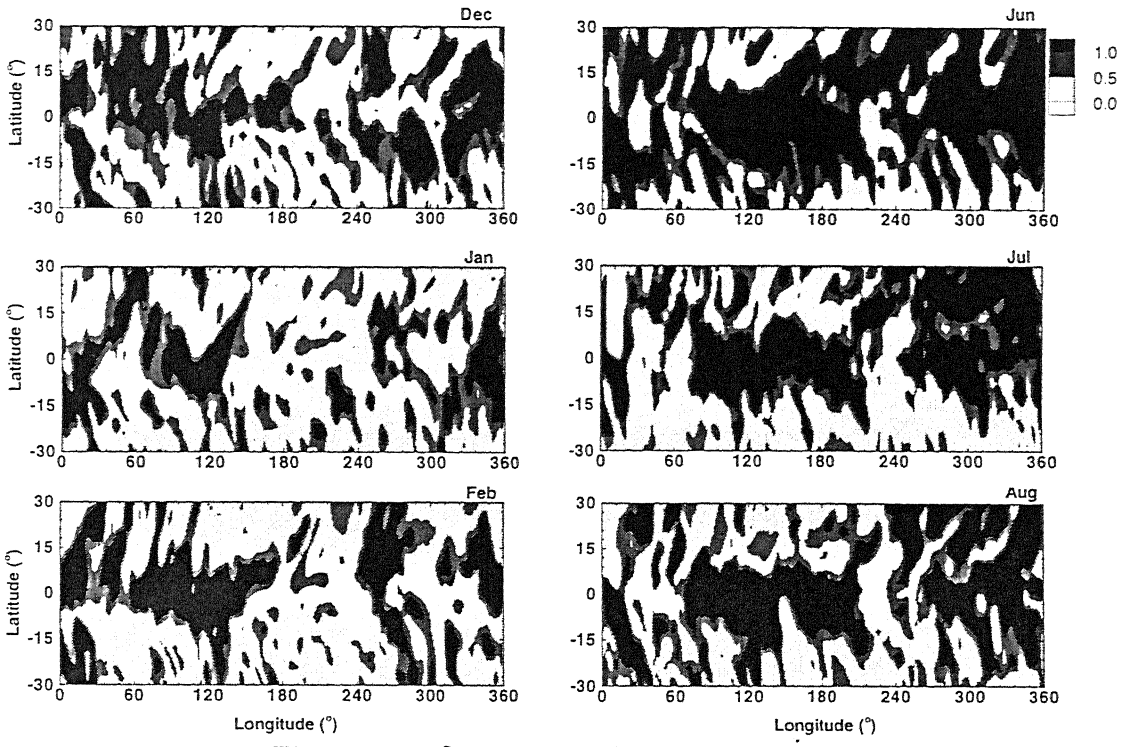

Figure 4.8: Same as the Fig 4.5, but for $\tau = 6.0$ hr.

where, $\sigma_{\xi_o}(x, y, m)$ represents the standard deviation of the observed monthly anomaly field ξ (for the period 1979-1987) at the point (x, y) for the month m. The corresponding simulated quantity is represented by $\sigma_{\xi_s}(x, y, m)$. It should be noted that since the difference between the observed and the simulated standard deviations is divided by the *local* value of the observed standard deviation, the range of $\Delta\sigma$ lies between zero and infinity. While $\Delta\sigma_\xi(x, y, z)$ provides a quantitative and objective measure of the ability of the model to simulate the tropical variabilities, an important question concerns the ability of the model to respond to different initial condition. This aspect is analyzed by comparing model simulations for different initial conditions.

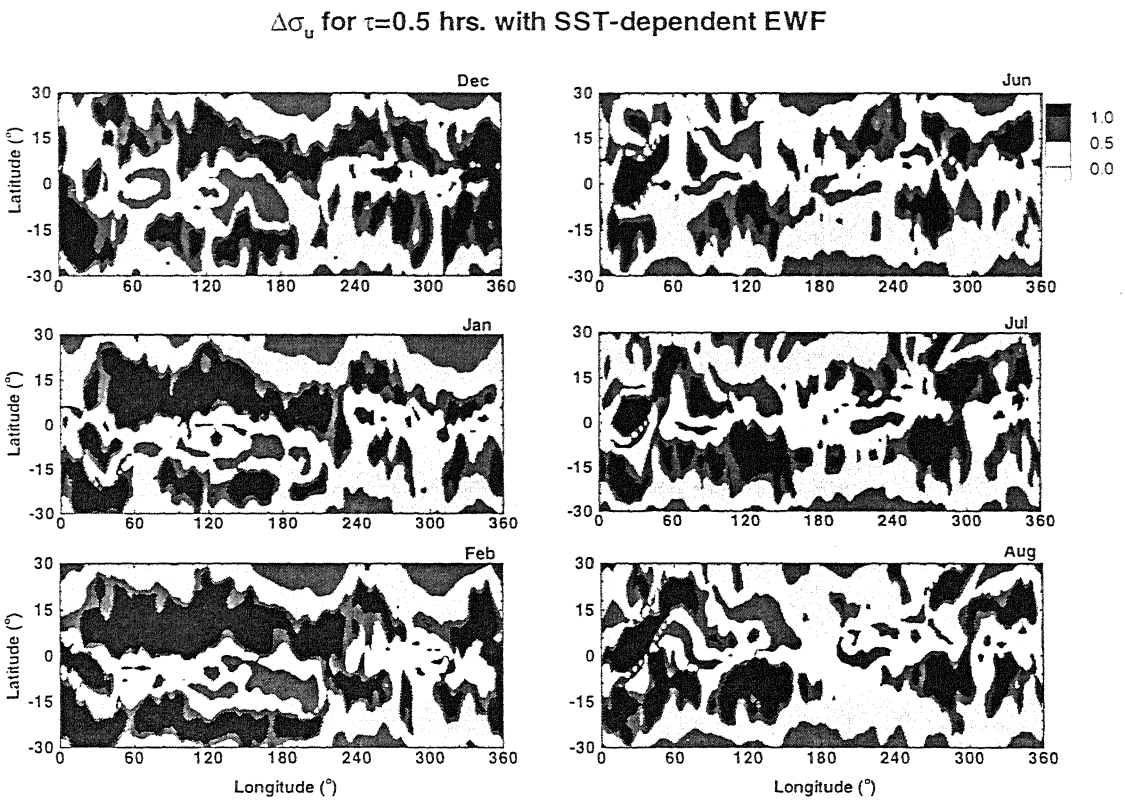

Figure 4.9: Longitude-latitude structure of the $\Delta\sigma_u$ field with SST-dependent EWF for $\tau = 0.5$ hr.

4.3 Results

For each of the sets of experiments I and II, a composite-simulation is constructed from 16 simulations corresponding to winter and summer initial conditions for the eight year period extending from 1979-1987. In the following we shall present the longitude-latitude structure for the six months, three winter months of December, January, February and three summer months of June, July and August. For each of the fields u and v the results are presented for the four values of CTL: 0.5, 1.5, 3.0 and 6.0 hours.

Simulation with uniform EWF: Figures from 4.1 to 4.4 show the longitude-latitude structure of the difference between standard deviations ($\Delta\ \sigma_u$) of the normalized observed and composite simulated u-fields for the period 1979-1987.

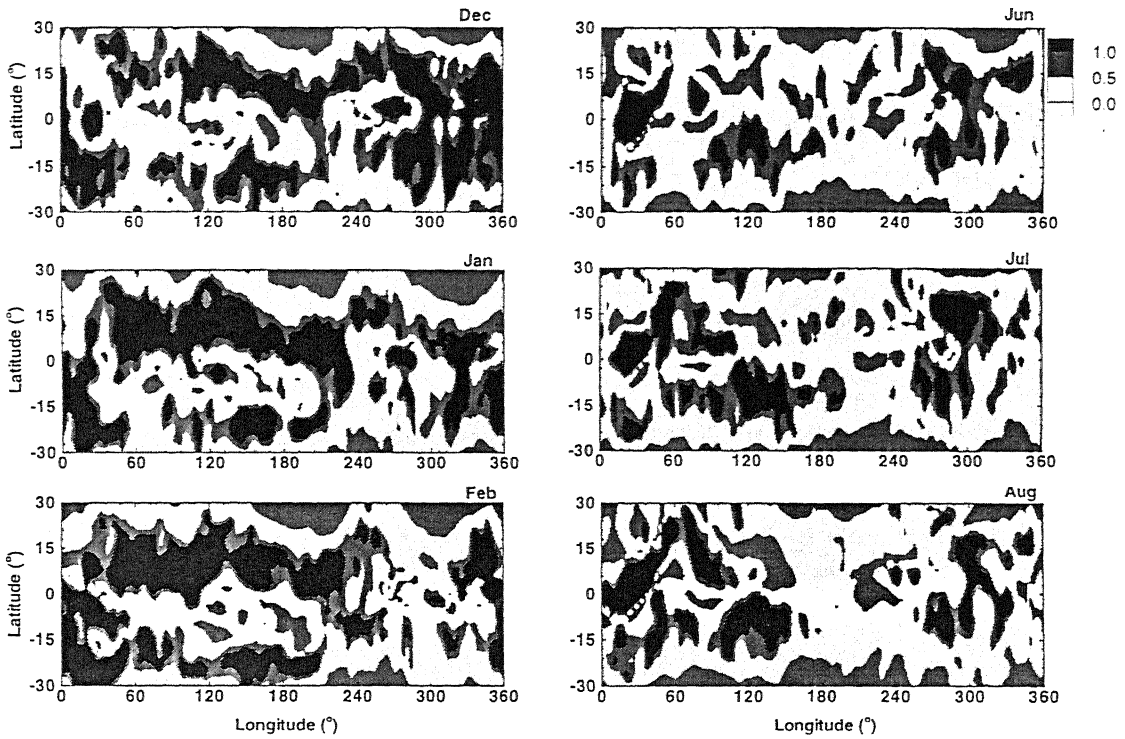

Figure 4.10: Same as the Fig 4.9, but for $\tau = 1.5$ hr.

A constant value of EWF corresponding to a spatially and temporally averaged mean condition is used. As indicated in the figures, the results are shown for four values of CTL, from 0.5 hours to 6 hours. The corresponding results for the meridional wind are shown in figures 4.5-4.8. In all these figures, the darkest shade represents difference between the observed and the simulated variabilities equal to or greater than 100% of the local observed variability. A careful examination of the figures from 4.1 to 4.8 reveals that over most of the tropics, and especially in the summer months, the error is greater than 100%. It is intriguing that the simulations in the winter months are better than those in the summer months. A similar observation holds also for the v. This perhaps indicates that our parameterization of convective forcing is not adequate for strongly convective summer months. In particular, it appears necessary to take into account the structure of

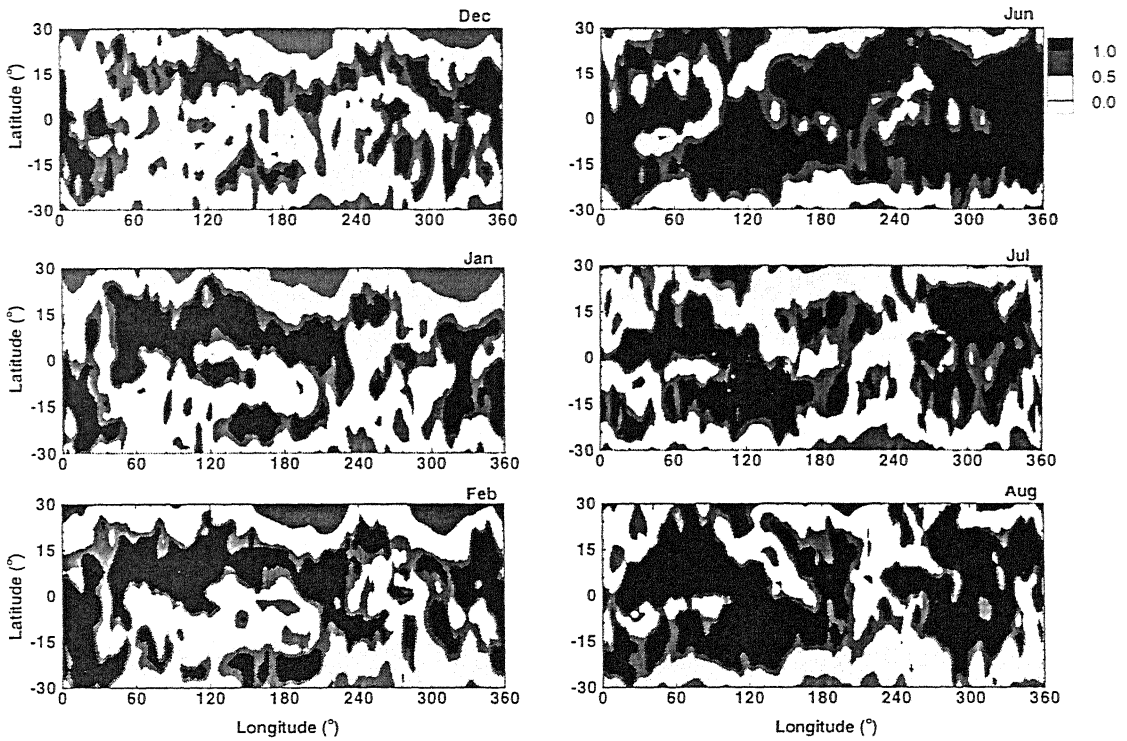

Figure 4.11: Same as the Fig 4.9, but for $\tau = 3.0$ hr.

the underlying SST field and its effect on the strength and distribution of moist processes.

Simulation with SST-dependent EWF: As discussed in context of our model formulation, SST can implicitly affect moist processes in our system at least in two ways: through its effect on the amount and distribution of the mean column integrated moisture and through its effect on the magnitude and distribution of Δq, which controls the strength of EWF. Although it is difficult to evaluate the relative importance of these two effects a prior, we shall focus on the second effect because a large number of studies have shown the significant role of EWF in the genesis and dynamics of tropical oscillations.

The longitude-latitude structure of the $\Delta\ \sigma_u$ field for winter and summer months for four values of CTL are shown in figures 4.9 to 4.12. As can be

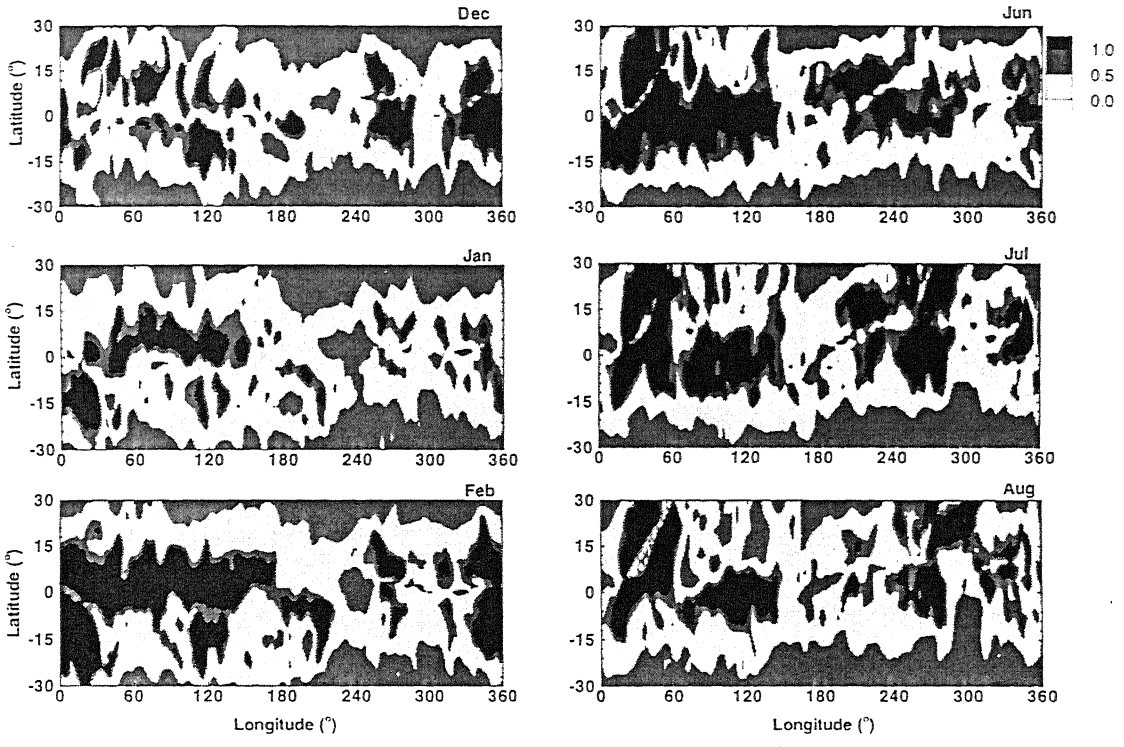

Figure 4.13: Same as the Fig 4.9, but for $\Delta\sigma_v$

between the observed and the simulated dynamical fields should arise from an actual year to year variability in the simulated fields. This ability to respond to different initial conditions is essential for the model of tropical climate. This issue is ,hence, addressed by comparing simulations for two different years with corresponding initial conditions. For this purpose, two simulations corresponding to 1979 (normal year) and 1982 (an El Niño year) had been chosen. The initial condition for each one-year simulation is given as monthly anomaly fields for the month of January of the respective years. So far we have focussed only on the dynamical fields. The very important issue of the simulation of the precipitation field has not been addressed. In this section we address these two issues together. However, in view of the fact that it is only an SST-dependent EWF and a value of $\tau = 0.5$ hr. gives rise to the best simulation of the dynamical fields, only these

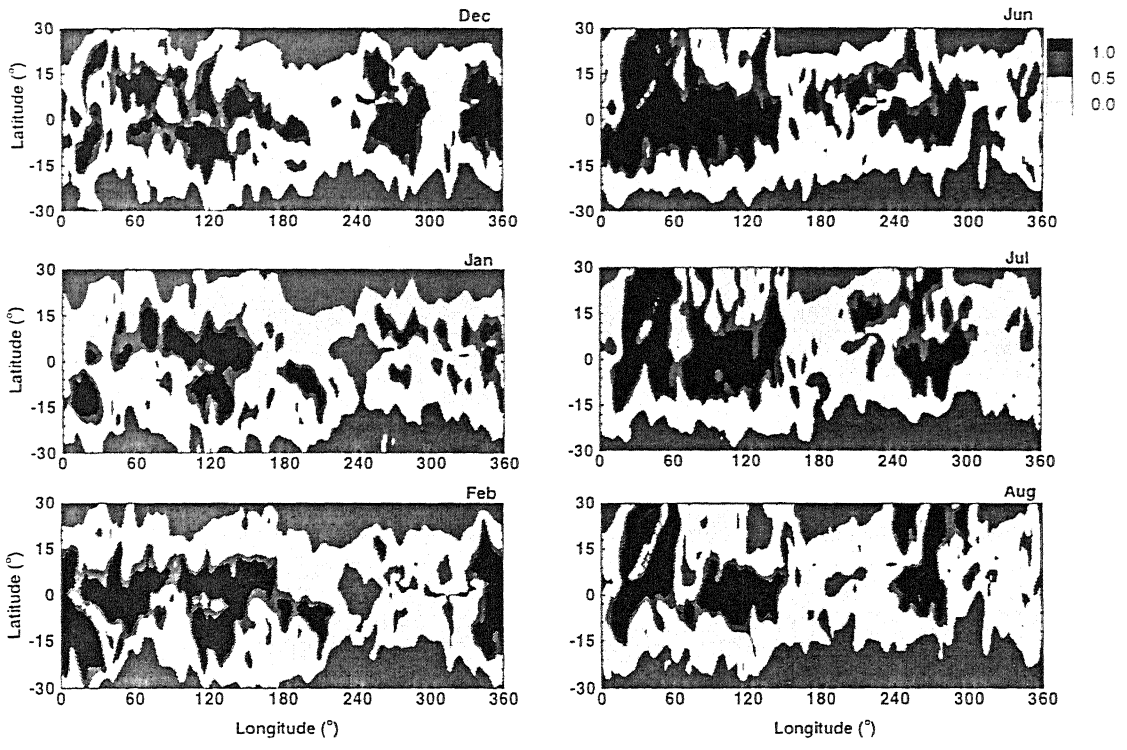

Figure 4.14: Same as the Fig 4.13, but for $\tau = 1.5$ hr.

simulations are analysed. Figures 4.17 and 4.18 compare the simulated structure of monthly precipitation fields for 1979 with corresponding observed structures for the same year. The results for the year 1982 are presented in figures 4.19 and 4.20. In each of these cases only positive part of the observed anomaly is considered, as the simulated precipitation is only positive. In each of the figures the left panels are for simulated precipitation while corresponding observed monthly anomaly precipitation (positive part) is shown in the right panels. Once again, only the distribution of the fields are emphasized. Hence the figures are prepared according to their respective maximum and minimum and no comparison of magnitudes should be made.

A distinct aspect of the simulated precipitation fields, as can be seen from the figures 4.17 to 4.20, is their clear shift from the southern to northern latitudes

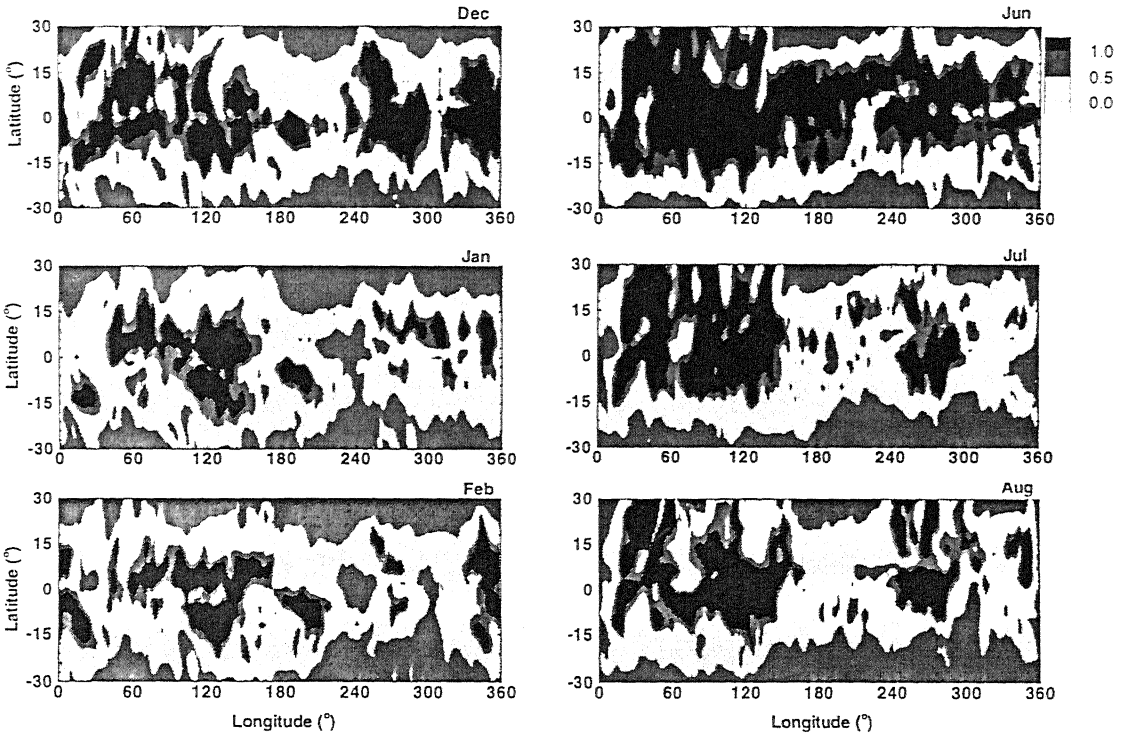

Figure 4.15: Same as the Fig 4.13, but for $\tau = 3.0$ hr.

as the season progresses from winter to summer. This tendency is also clearly present in the observed fields, although the north-south shift is not as total in the observed fields as in the simulated ones. The absence of precipitative heating in the Southern Hemisphere in summer (Northern Hemisphere in winter) in the simulated fields also affects the wind fields (not shown here). A comparison of the precipitation fields for the winter months for 1979 (figure 4.17) and 1982 (figure 4.19) shows a fair amount of variability among the two observed fields (right panels). The simulated fields (left panels) tend to follow the observed ones, but with lesser degree of spatio-temporal variability. Similarly observations also hold for the summer precipitation fields (figures 4.18 and 4.20). However, a distinctive feature of the observed precipitation fields for 1982 summer (an El Niño year) is a southern hemisphere preference which the simulated fields follow only weakly.

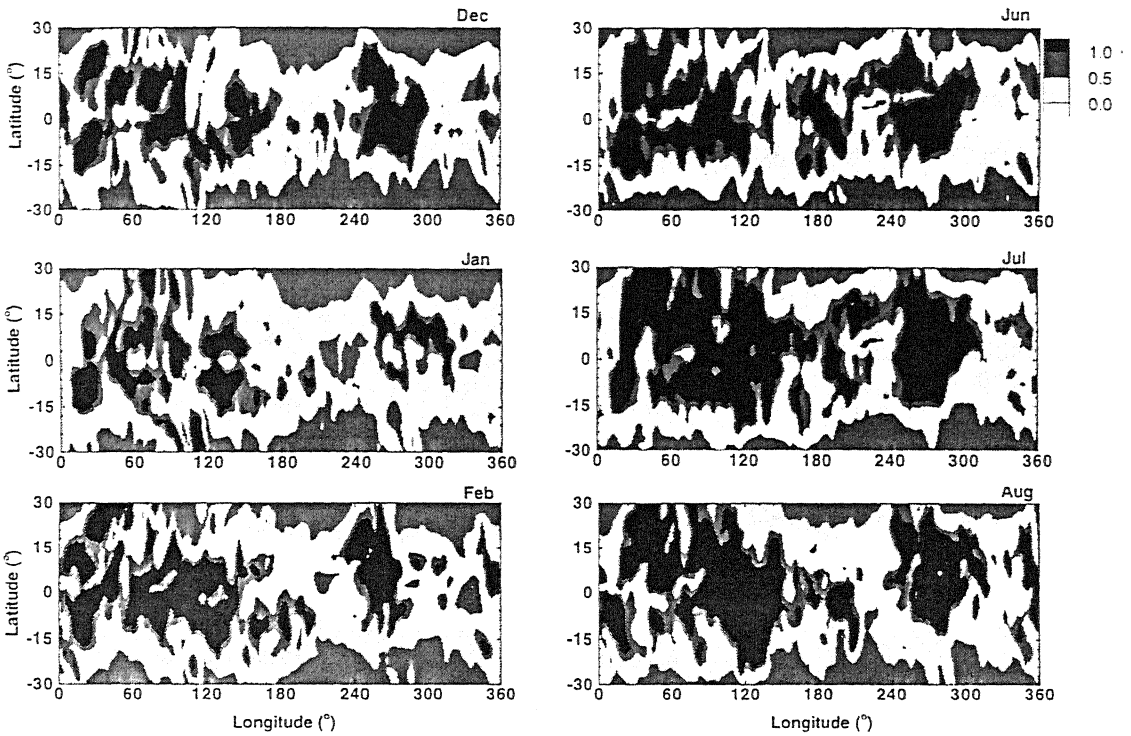

Figure 4.16: Same as the Fig 4.13, but for $\tau = 6.0$ hr.

This hints at the need for a more detailed and sophisticated implementation of the spatio-temporal distribution of convective forcing.

4.4 Conclusions

The main conclusion that emerges from the above experiments is that convection -induced internal (anomaly) dynamics can explain a large part of the tropical variabilities. This is particularly true when SST-induced spatio-temporal variations of the strength of EWF is included. As we have emphasized above, the difference between the observed and the simulated (composite) variabilities in this case is less than 50% of the local observed variability over most of the tropical belt, and especially over the equatorial belt of 15°S to 15°N. The larger error in the higher

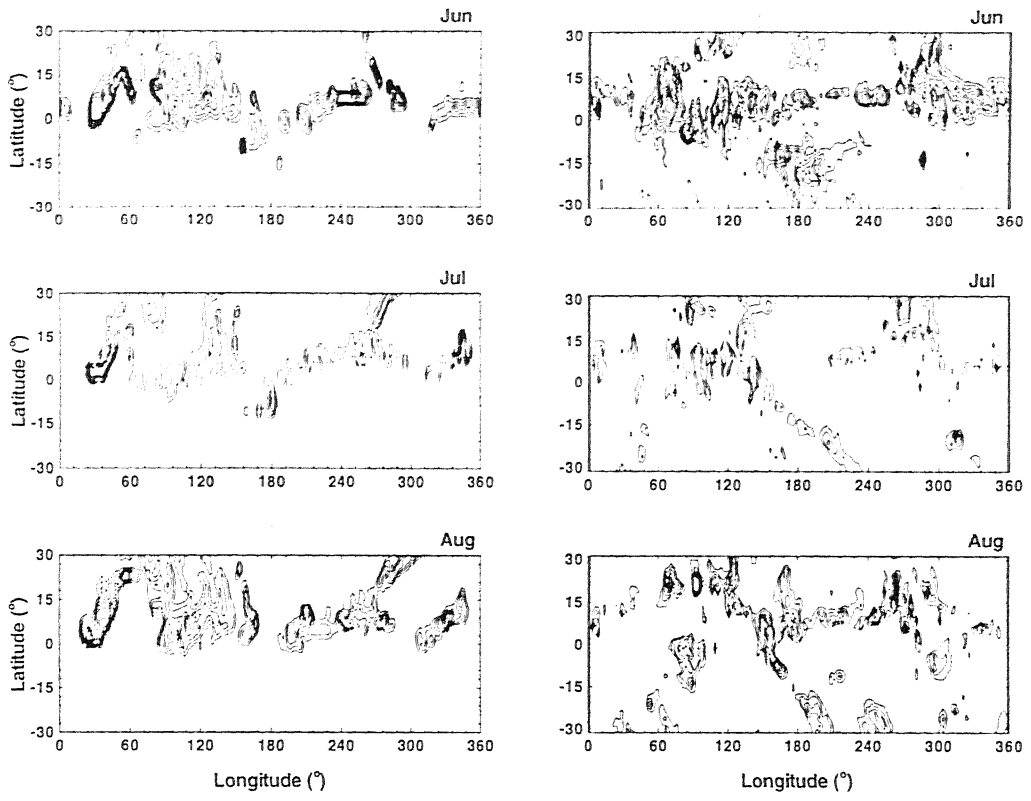

Figure 4.17: Comparison of simulated precipitation (left panels) with anomaly precipitation (right panels) for the summer months of 1979. Only the spatial distributions for each of the months are considered, as the maximum and the minimum values and contour interval are different for different cases.

latitudes is not altogether surprising since our model with its β-plane approximation is not expected to be valid at higher latitudes. There are regions even in the equatorial belt where the model fails (with error more than 100%) in a systematic way. In particular, these regions are essentially continental. Obviously, our model with its all-ocean lower boundary, fails to capture the variabilities controlled by land processes. The fact that this happens systematically raises hope for improving performance by including ground hydrology.

Another interesting fact arises from these experiments is that for both the representations of strength of EWF (Expt Set I and Set II), the simulations show less errors for the summer hemispheres than for the winter hemispheres. This points to the fact that convection plays a greater role in the structure of tropical variabilities in the summer than in the winter. Since our model emphasizes

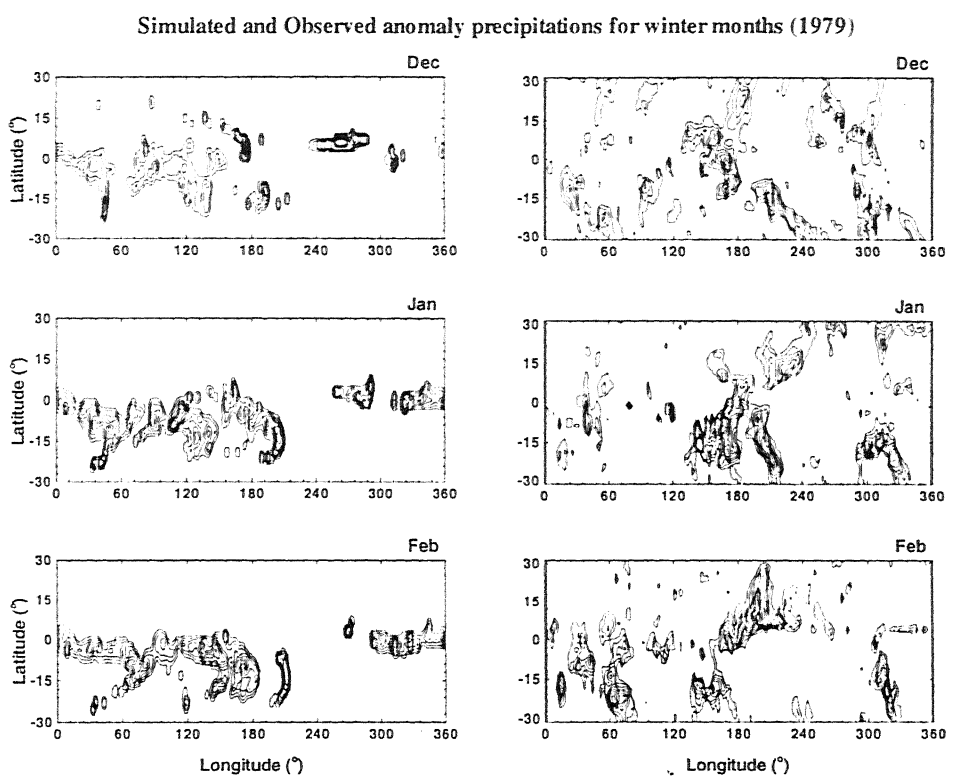

Figure 4.18: Same as figure 4.17, but for winter months

convection-induced dynamics of the tropical variabilities, it fails to account for the *winter-time forcing* which would account for (a large part of the) remaining variability. One way of improving our model would be, therefore, to identify and parameterize this component of the forcing. From a comparison of the results from Set I and Set II, it is clear that the spatio-temporal variations in the strength of EWF induced by mean conditions should be taken into account . In the present case, we have represented this dependence of EWF on mean conditions through its implicit dependence on SST according to equation 3.29. Considering the profound effect of the distribution of EWF on the quality of simulation, it is very important to properly formulate the representation of EWF in terms of the mean conditions. Also, it will be interesting to carry out the above experiments with mean conditions derived from a GCM in place of monthly mean data as used in the present case.

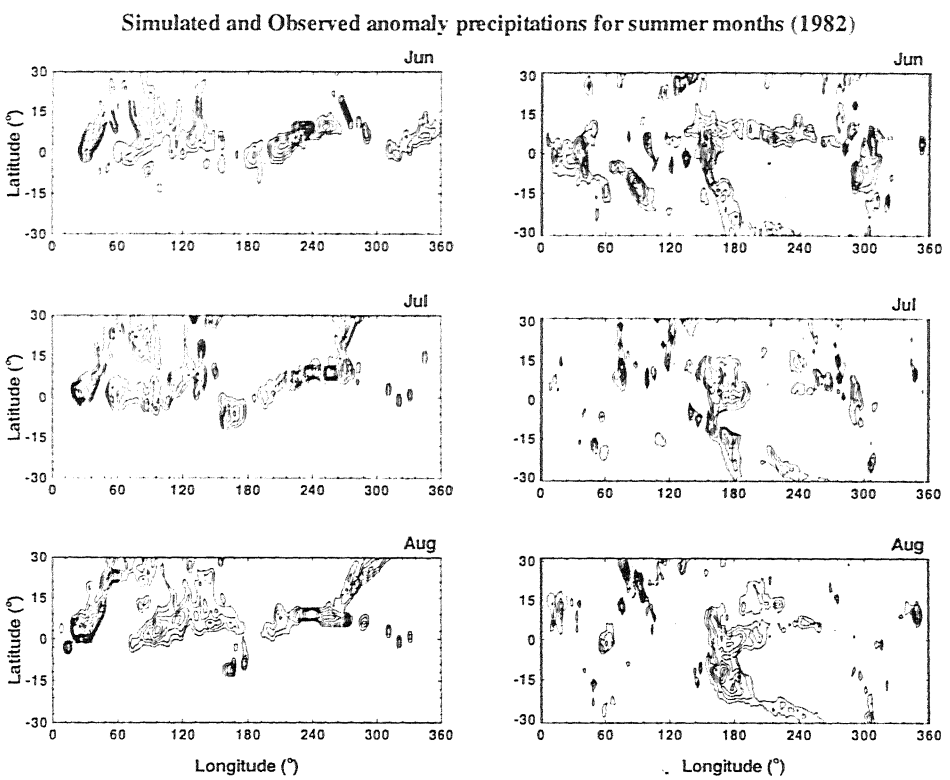

Figure 4.19: Same as figure 4.17, but for 1982

One purpose of the present study has been to investigate the effect of the value of the CTL in the quality of the model simulations. As has been emphasized earlier, the CTL embodies the underlying hypothesis of our dynamical model, and a precise value of CTL cannot be assigned. Although earlier analytical studies of GR and GM had used a CTL of a few hours, these studies were aimed at the mechanisms of particular intraseasonal oscillations. Following this argument outlined above, we have considered four values of CTL, from half an hour, corresponding to cumulus organization scale to six hours, corresponding to meso-scale convective systems. Indeed, as can be seen from the results of Set I and Set II, a much smaller value of CTL less than 6 hours is needed for capturing the detailed structure of monthly anomaly fields. It would appear that a more appropriate value of CTL lies around an hour, or so.

An important conclusion that arises from the present study is that SST can

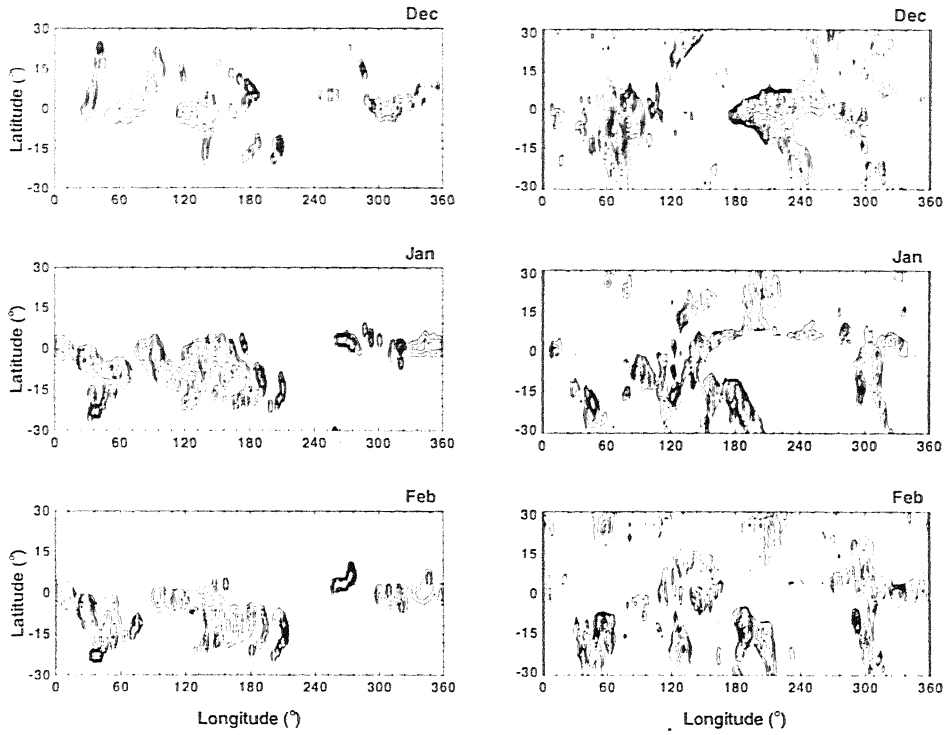

Figure 4.20: Same as figure 4.17, but for winter months 1982

play a significant role in the structure of tropical variabilities even at monthly and shorter time scales. This is evident from the fact that a correct distribution of the convective heating over the equator is simulated only when the SST-induced spatio-temporal distribution of EWF is taken into account. Although SST may not affect the tropical dynamics at monthly or shorter time scales as a direct heat source, it can affect the atmospheric convective heating. However, for this it is necessary that the parameterization of convection is sensitive to SST distribution.

Another success of the present model is its ability to capture the year-to-year variabilities in the observed anomaly fields, in particular precipitation. Thus, for example the observed anomaly precipitation field for 1979 August shows a much stronger field in the northern hemisphere than the corresponding field in 1982. These differences in the observed fields are present in the simulated fields to a large extent. However, the simulated fields do not possess as much variability

as in the observed fields both temporally as well as spatially. In view of the crucial role played by the spatio-temporal structure of moist processes further improvement in the formulation of moist processes is likely to be necessary to bridge the gap between observation and simulation.

The present study shows the convection induced internal dynamics, governed by a CTL, is quite successful in accounting for a large part of the tropical variabilities in terms of their monthly structure. However, the tropical atmosphere also exhibits a number of characteristic variabilities at intraseasonal and longer time scales. Since these oscillations are an important feature of tropical circulation, a good model of tropical variabilities should be able to support these oscillations. We investigate this aspect in the next chapter.

Chapter 5

The Annual Cycle of the Composite Anomaly Circulation

The anomaly circulation in the tropics exhibits a pronounced annual cycle with distinct zonal characteristics. The annual cycles of convection in the tropical Indian Ocean and Pacific Ocean follow their own characteristic seasonal march. The mean annual cycles present in the wind and SST can significantly affect the anomaly circulation. In our model with moist feedbacks, and its implicit dependence on mean SST, the annual cycle in SST can also affect the anomaly fields.

A characteristic feature of the mean annual cycle in the tropics is the association of the convective maximum with the Intertropical Convergence Zone (ITCZ). This convective maximum is often seen to move from north to south and back following the annual cycle of solar heating. However, this annual march also exhibits pronounced regionality, especially over the tropical Indian Ocean and the Pacific, due to the effects of land-ocean distribution and local ocean-atmosphere interaction. Thus, over the tropical Indian Ocean-Australia area, the convective maximum moves not only meridionally but also zonally (Lau and Chan, 1983). Since the dynamics of the anomaly circulation in our model are significantly affected by the mean wind and SST, we expect the anomaly circulation also to

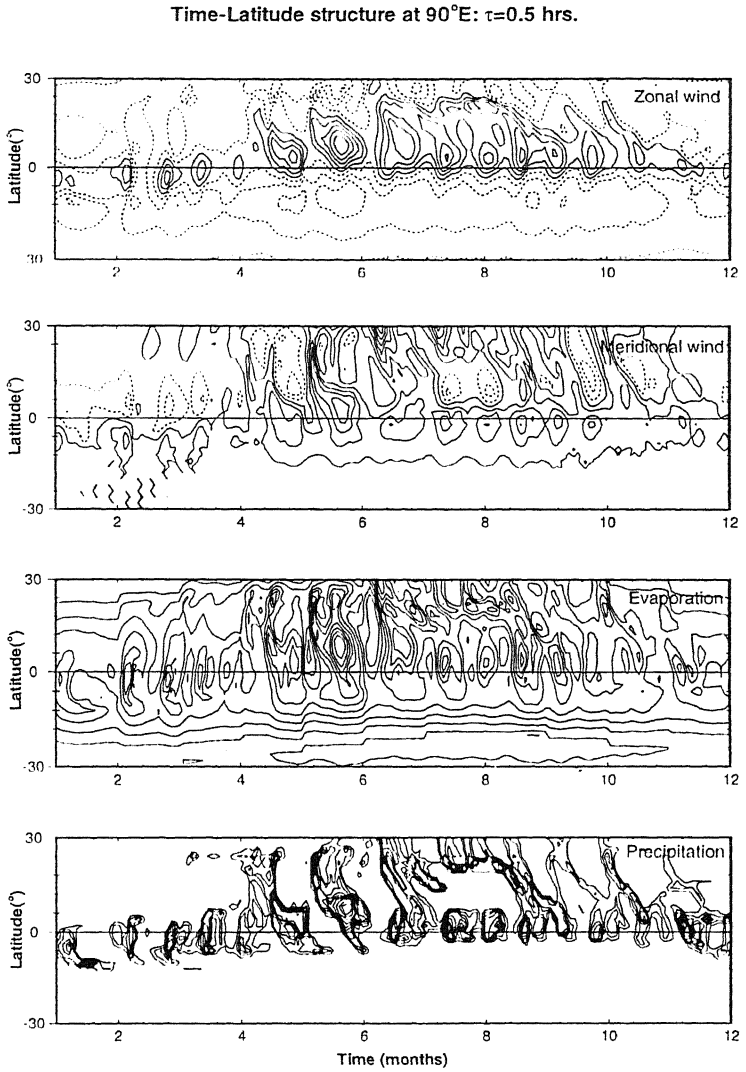

Figure 5.1: Time-latitude structure of the unfiltered model fields. The negative contours are dashed

exhibit a characteristic annual cycle. Since there is no external forcing in our model related to annual cycle, the model annual cycle should closely match the mean annual cycle. Therefore, the model annual cycle is first compared with the mean annual cycle. The question of an annual cycle intrinsic to the convection induced anomaly circulation will be taken up subsequently.

Analysis of eight-year (1974-1982) monthly mean Outgoing Longwave Radiation (OLR), obtained from monthly means of daily averages on a 2.5×2.5 grid, by Meehl (1987) reveals the several interesting features about the spatial struc-

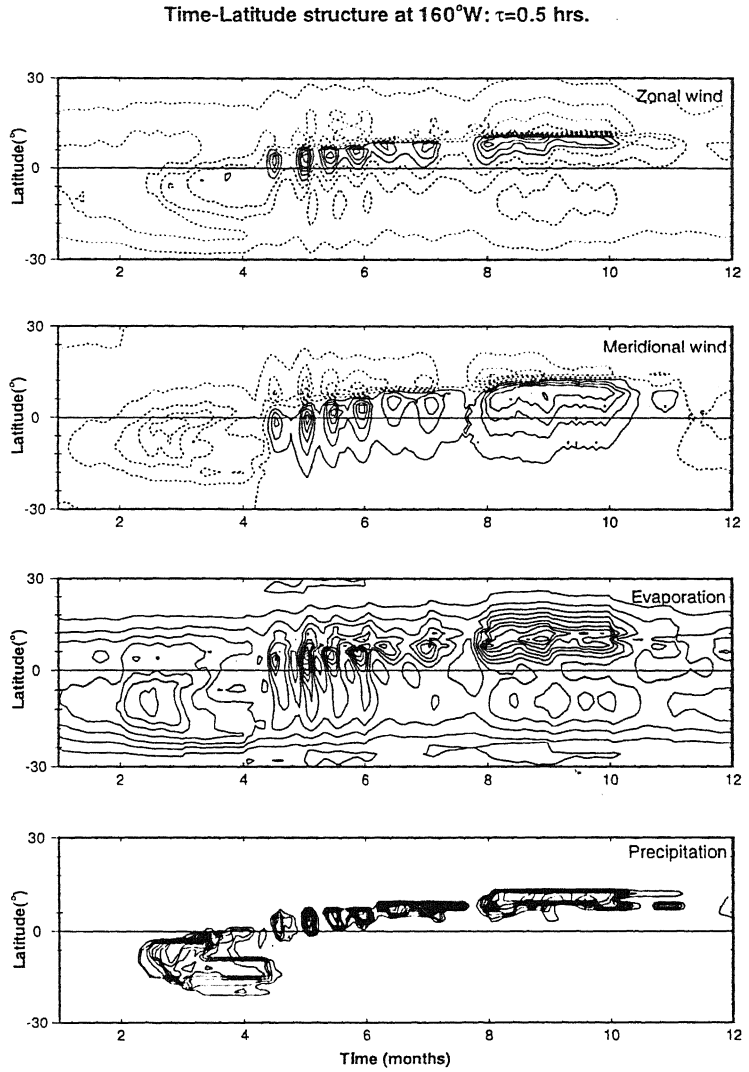

Figure 5.2: Same as the figure 5.1, but for 160°W

tures of the annual distributions of variables like OLR, clouds and precipitation. Although in our model there is no explicit computation of OLR, the changes in OLR are often used to study implied relative fluctuations in the deep convection and associated rainfall in the tropics (Liebmann and Hartmann, 1982; Lau and Chan, 1983; Weickmann *et al.*, 1985). Hence, the observed structures of both OLR and precipitation are compared with our simulated precipitation fields.

To examine the model simulations for the annual structure of the variabilities the composite one-year model simulations generated with initial conditions from observed anomaly fields for 1979 to 1987 are used. Once again, the simulated

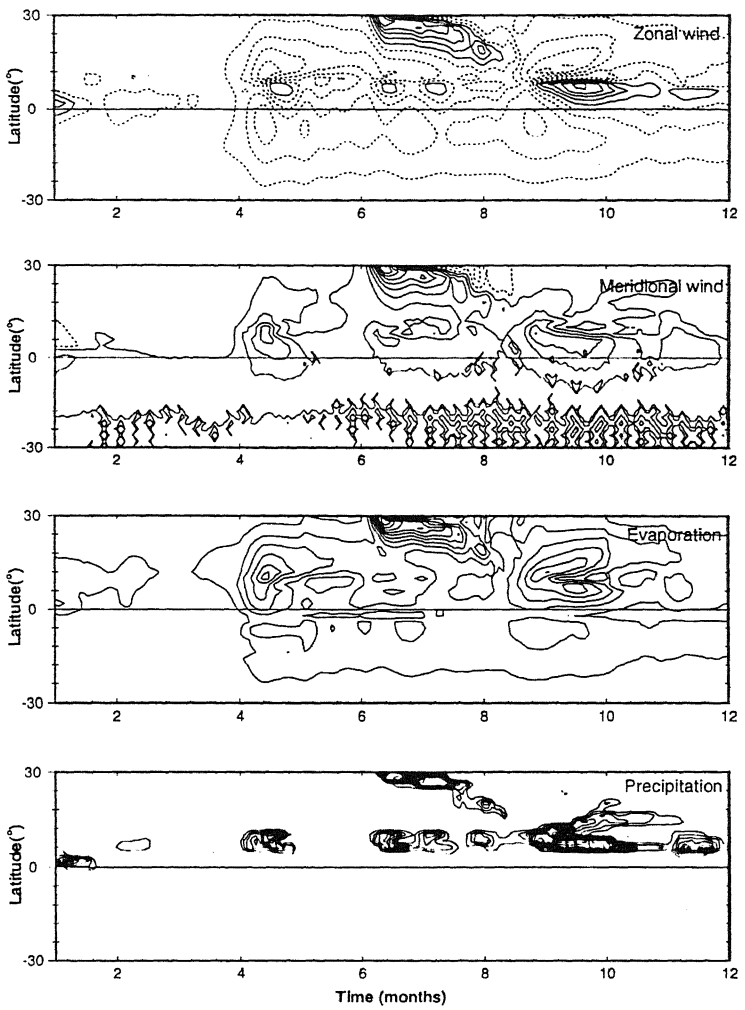

Figure 5.3: Same as the figure 5.1, but for 80°W

annual cycles for different mean and dynamical conditions are analyzed to identify and assess the relative roles of various processes in the genesis and structure of the anomaly annual cycle. The issues of the structure of the annual cycle specific to certain well-known oscillations will be taken up in the later chapters.

As we have seen earlier, only a value of CTL between 0.5-1.5 hours can generate the observed structure of the variabilities with reasonable success. To determine the role of the value of CTL on the structure of the simulated annual cycle, we have examined the four composite one-year simulations, one for each value of the CTL. It is found that only τ =0.5 or 1.5 hours gives rise to the observed

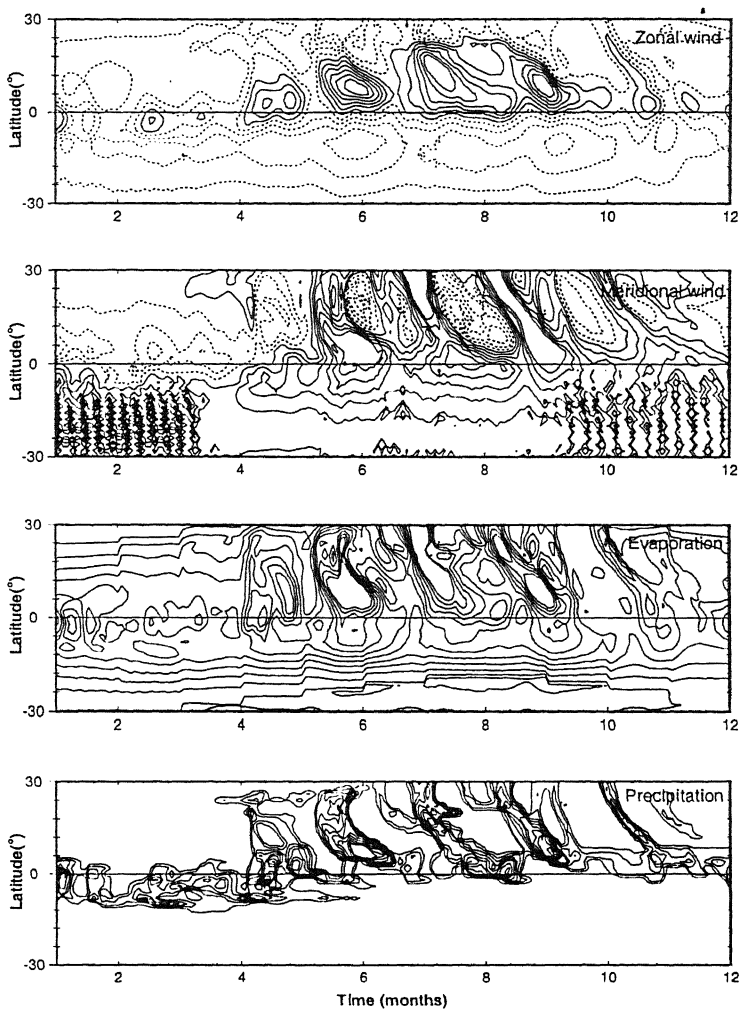

Figure 5.4: Same as the figure 5.1, but for $\tau = 1.5$ hr.

characteristic. Therefore, the results presented here are only for these two values of CTL. In addition, as we have found, a uniform strength of EWF, implying a uniform SST, does not simulate the structure of the variabilities. In particular, SST dependent EWF is necessary to simulate the correct distribution of the convective heating. Hence, only cases of non-uniform strengths of EWF are considered to examine its role in the anomaly annual cycle.

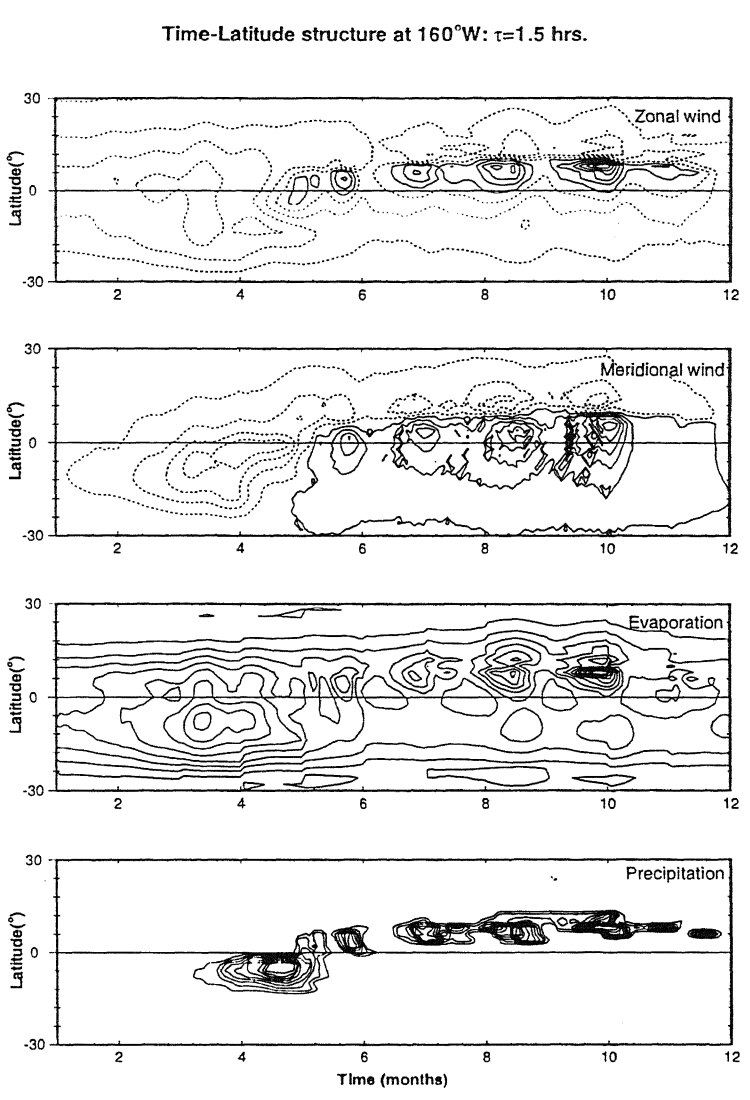

Figure 5.5: Same as the figure 5.4, but for 160°W

5.1 Time-Latitude Structure

The annual cycles in the form of time-latitude diagrams at three zonal locations are shown in figures 5.1 to 5.3 for $\tau = 0.5$ hours. The corresponding results for τ =1.5 hours are shown in figures 5.4 to 5.6. A comparison of the results for the two values of CTL shows that although there are certain differences between the two simulations, the essential characteristics are very similar. However, these differences are more marked over the off-equatorial areas and especially over the northern tropics.

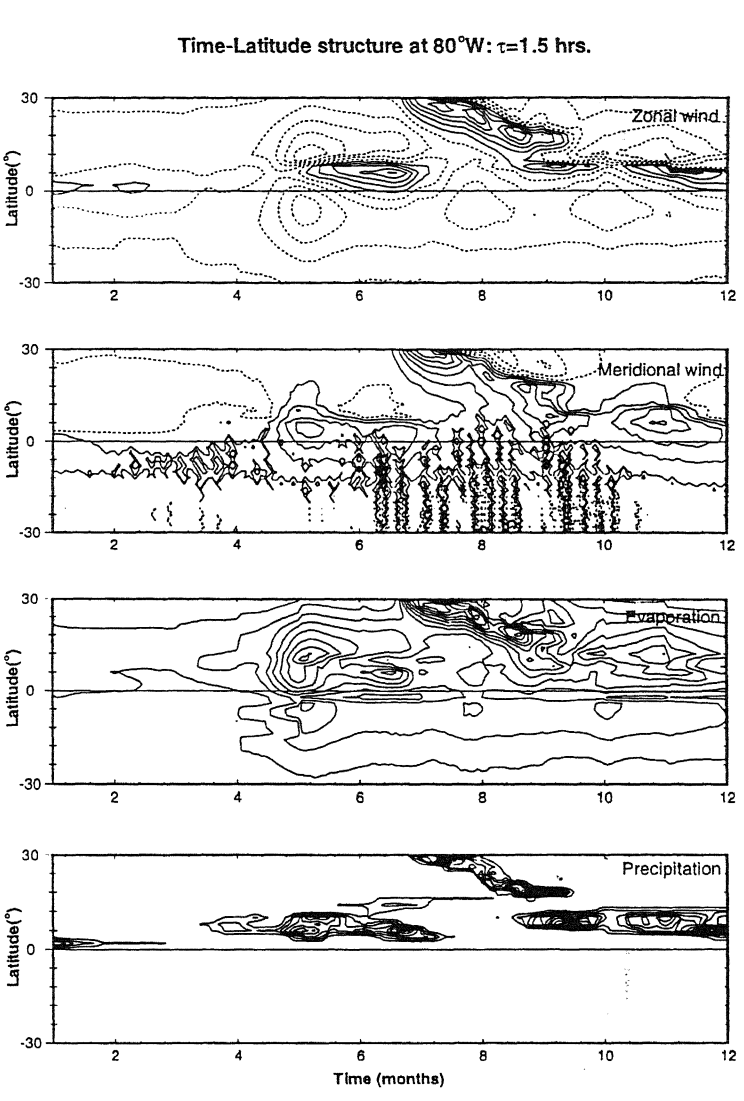

Figure 5.6: Same as the figure 5.4, but for 80°W

A remarkable feature of the time-latitude structure for both the values of CTL is a distinct zonal character of the annual cycle. In particular, the precipitation field over the monsoon region shows a clear shift from the Southern Hemisphere to the Northern Hemisphere and back with the march of the season. Such a cross-equatorial movement is much less pronounced over the Central and the Eastern Pacific. From an analysis of eight-year monthly mean OLR, Meehl (1987) showed that the dominant convective activity in the northern latitudes in the tropics is found during the monsoon. The monthly anomaly (zonal means covering 45 to 155°E and 155°E to 90°W; annual average zonal mean subtracted from

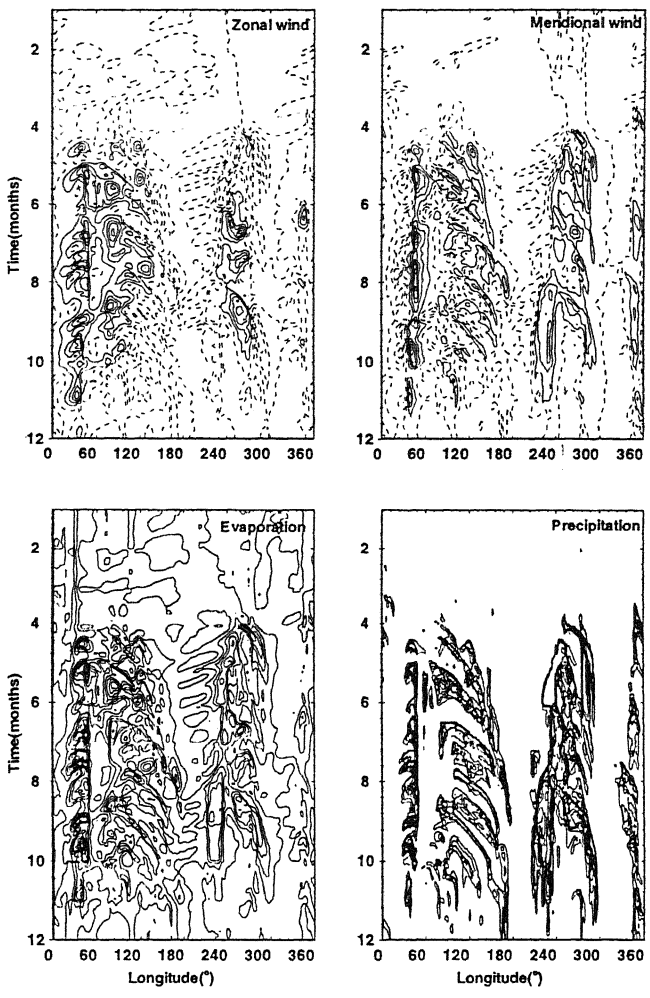

Figure 5.7: Time-longitude structure of the unfiltered model fields. The negative contours are dashed

the zonal mean for each month) fields of OLR and cloud also show a relative convective maximum north of the equator in July-August and south of the equator in January-April. Thus the monthly anomaly fields also tend to follow a cycle similar to the annual course of the sun. Such a trend is clear in the simulated annual cycles of the zonally averaged fields over the monsoon sector centered at 90°E (Figures 5.1 and 5.4) and also over the Pacific Ocean centered at 160°W (Figures 5.2 and 5.5).

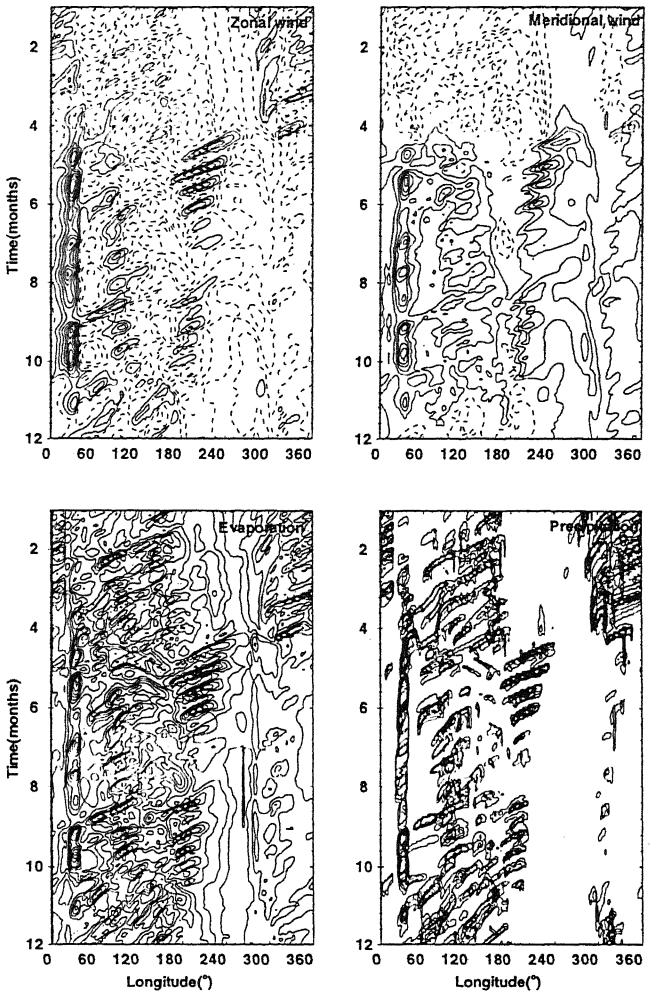

Figure 5.8: Same as the figure 5.7, but over the equator

5.2 Time-Longitude Structure

The similarities in the simulations with the two values of CTL can be seen also in the time-longitude diagrams for the unfiltered anomaly fields for one year period. The time-longitude diagrams for the model fields for $\tau = 0.5$ hours for three latitudinal locations, equator, 10°N and 10°S, are shown in figures 5.7 to 5.9, respectively. The corresponding results for $\tau = 1.5$ hours are shown in figures 5.10 to 5.12 respectively.

For both the values of CTL, there is a strong annual cycle over 10°N between

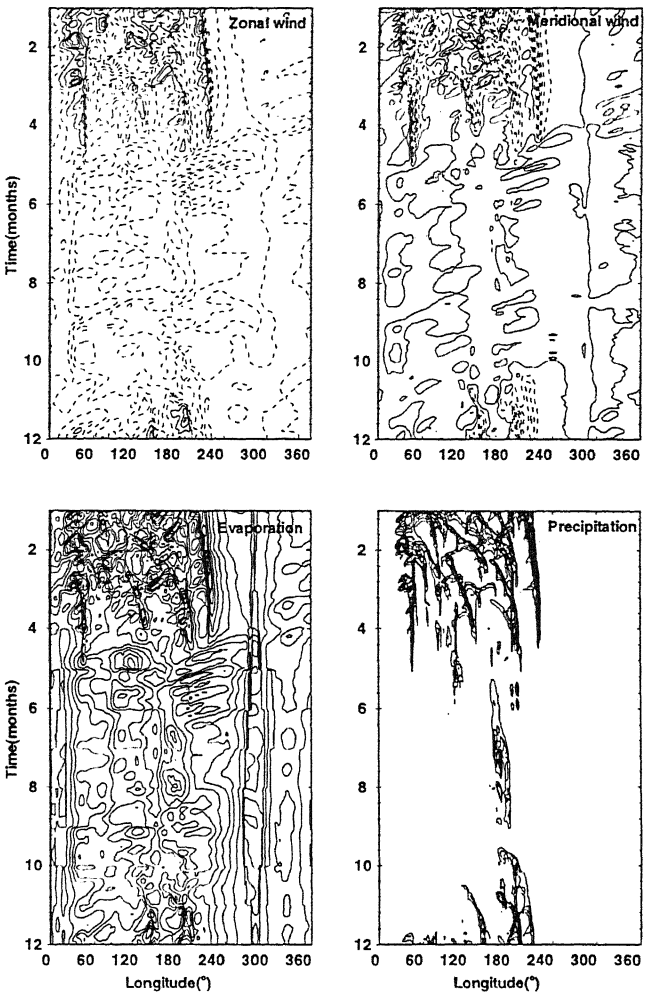

Figure 5.9: Same the as figure 5.7, but for 10°S

40-120° and 240-300° (in all x-t plots the longitudes continuously increase from left to right), marked by strong westerlies and southerlies in the summer months. However, over other longitudinal positions the annual cycle is rather weak. In particular, there is no reversal of wind. We also note that the annual cycle of zonal and meridional winds do not quite coincide, although they overlap, in terms of their longitudinal characteristics. The annual cycle of both u and v at 10°S for τ =0.5 hours (figure 5.9 are confine to the zonal location between 60-240°, a characteristic also shared by precipitation. However, evaporation is present throughout the year, although with temporal variation in strength. The precipi-

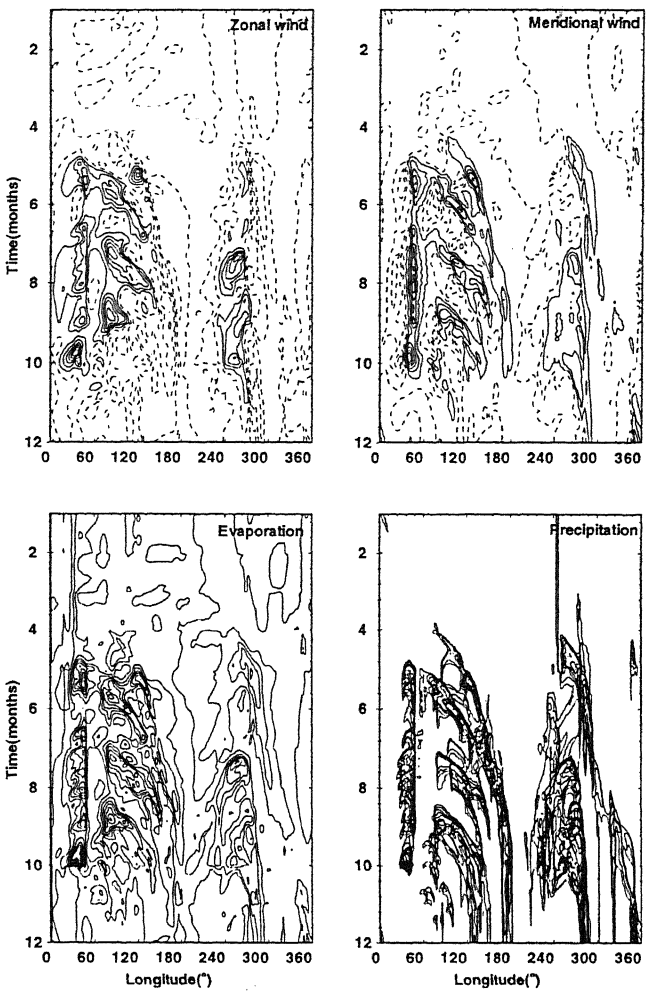

Figure 5.10: Same the as figure 5.7, but for $\tau = 1.5$ hr.

tation seems to occur only when the strength of evaporation reaches a threshold value. The former is always accompanied by strong southerlies (northerlies) in northern (southern) hemespheric summer (figures 5.7, 5.9, 5.10 and 5.12). This clearly brings out the role of cross-equatorial wind in the anomaly annual cycles. In the 10°N the precipitation is seen only with westerlies, but in the 10°S it is present in easterlies also. This behavior is common to both values of τ used.

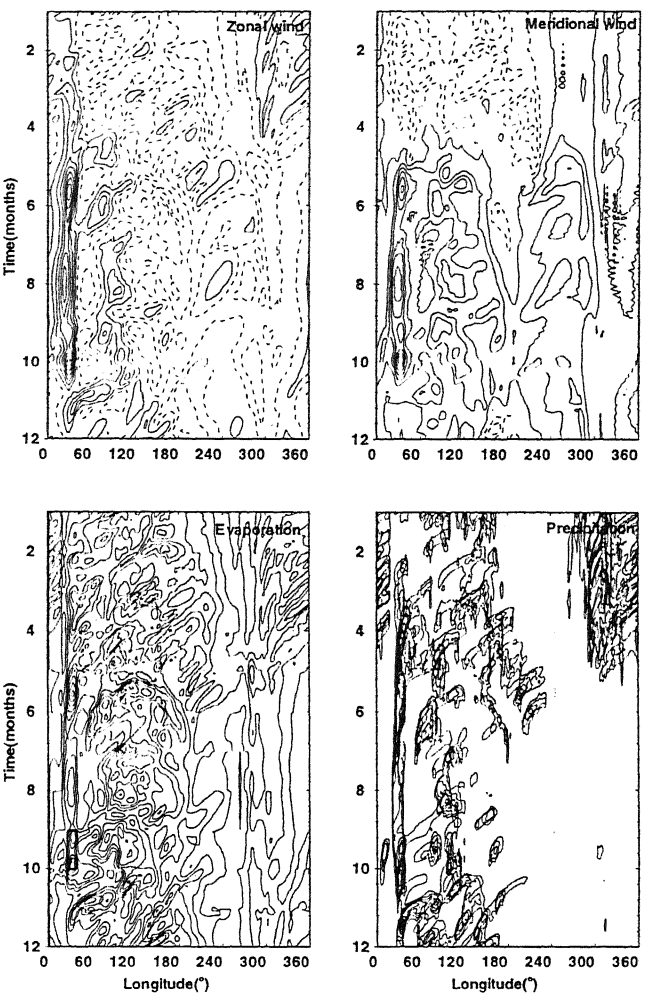

Figure 5.11: Same the as the figure 5.10, but over the equator

5.3 The Role of the Mean Annual Cycle

An important question at this point is how much of the annual cycle of the anomaly circulation is induced by the annual cycle of the mean fields. For example, the monsoonal region is characterized by the well-known seasonal reversal of wind, which may induce an annual cycle also in the anomaly circulation. Similarly, the annual march of the SST, through its influence on EWF, can significantly affect the anomaly annual cycle. On the other hand, it is possible that the convection induced internal dynamics generate an annual cycle that is intrinsic to

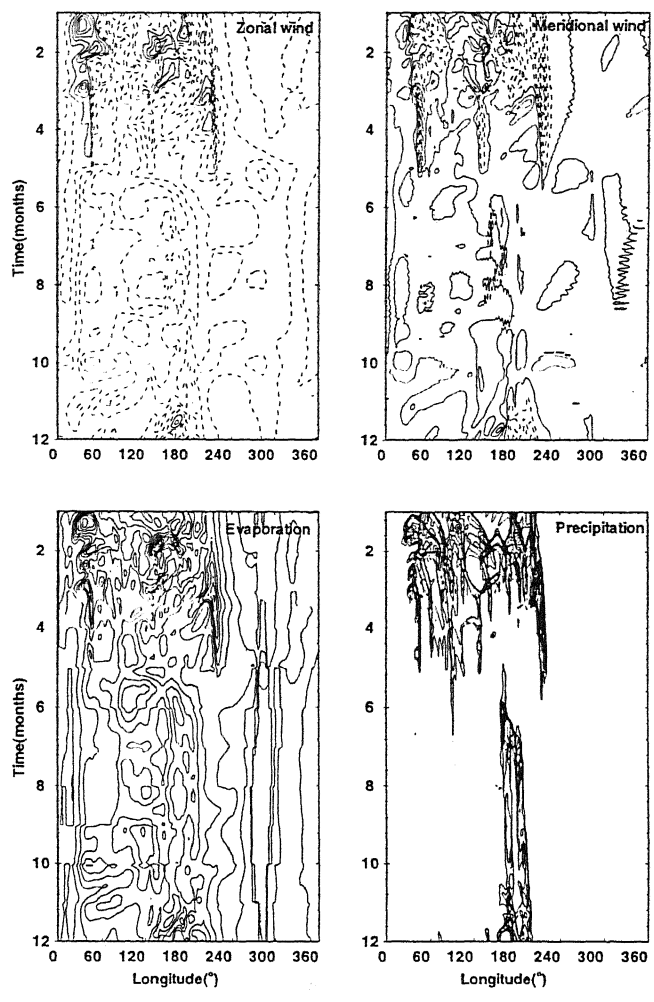

Figure 5.12: Same the as figure 5.10, but for 10°S

the tropical dynamics. To examine these questions we analyze the annual cycles in the one-year model simulations with the annual cycles of mean wind and SST suppressed. We shall consider the time-latitude structure of the model fields at three longitudes (ie. 90°E, 80°W and 160°W) to examine the effects of the mean annual cycle on the anomaly circulation.

5.3.1 Role of the Annual Cycle of the Mean Wind

To study the role of the annual cycle of the mean wind on the anomaly annual cycle, we have analyzed the annual cycles from the two one-year simulations

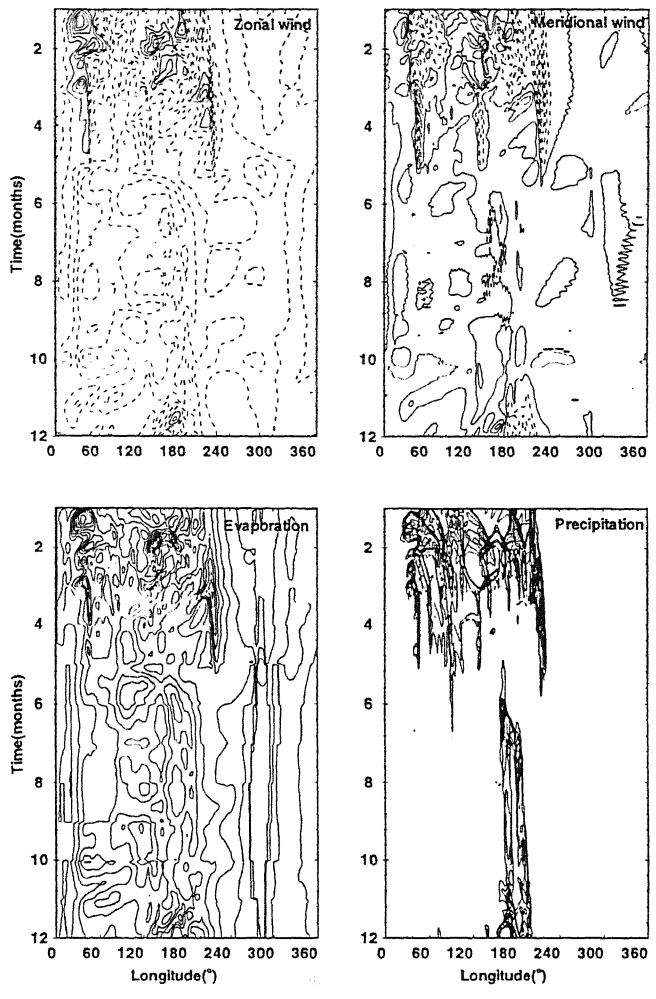

Figure 5.12: Same the as figure 5.10, but for 10°S

the tropical dynamics. To examine these questions we analyze the annual cycles in the one-year model simulations with the annual cycles of mean wind and SST suppressed. We shall consider the time-latitude structure of the model fields at three longitudes (ie. 90°E, 80°W and 160°W) to examine the effects of the mean annual cycle on the anomaly circulation.

5.3.1 Role of the Annual Cycle of the Mean Wind

To study the role of the annual cycle of the mean wind on the anomaly annual cycle, we have analyzed the annual cycles from the two one-year simulations

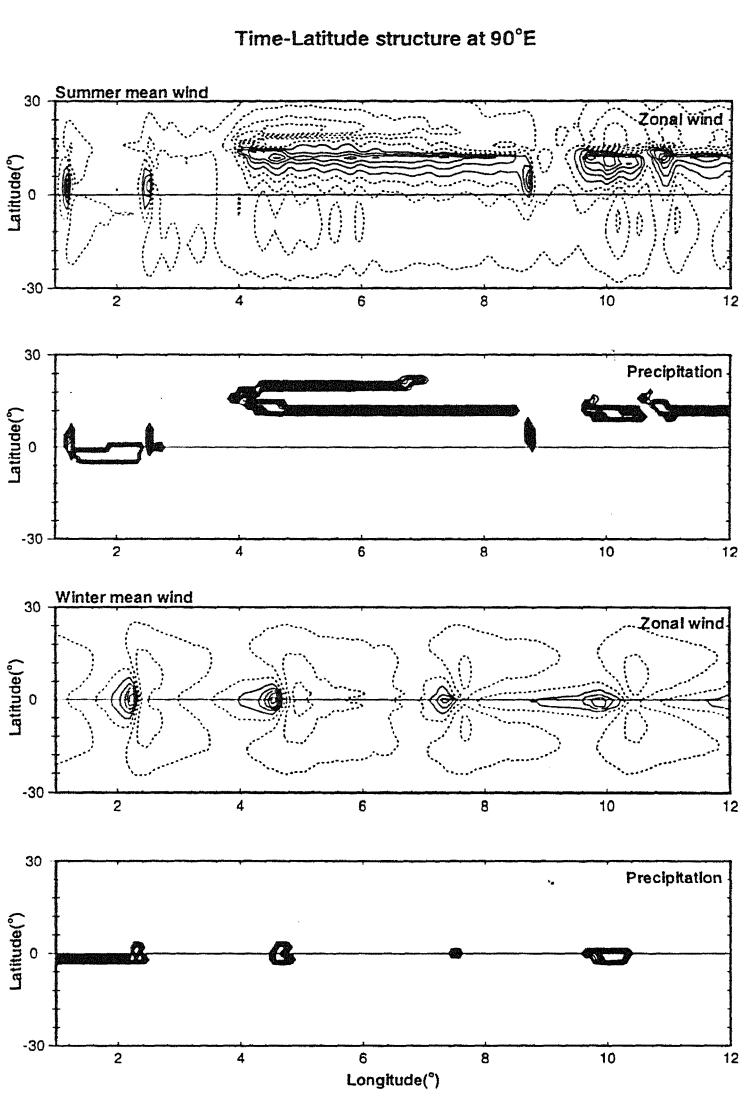

Figure 5.13: Time-latitude structures for summer mean wind (first two panels from the top) and winter mean wind (third and fourth panels). Negative contours are dashed.

with winter and summer mean winds. Thus in the first experiment (of summer mean winds) the mean winds were prescribed by averaging the 9 years of (1979-87) monthly mean winds in the summer months from June to August, while in the second experiment (winter mean winds) the mean winds were obtained by averaging the 9 years of climatological monthly mean winds in the winter months from December to February. In both of these experiments the annual cycle of SST was kept intact. In particular, the northward march of high SST with season could still affect the model dynamics through its effect on the strength of EWF.

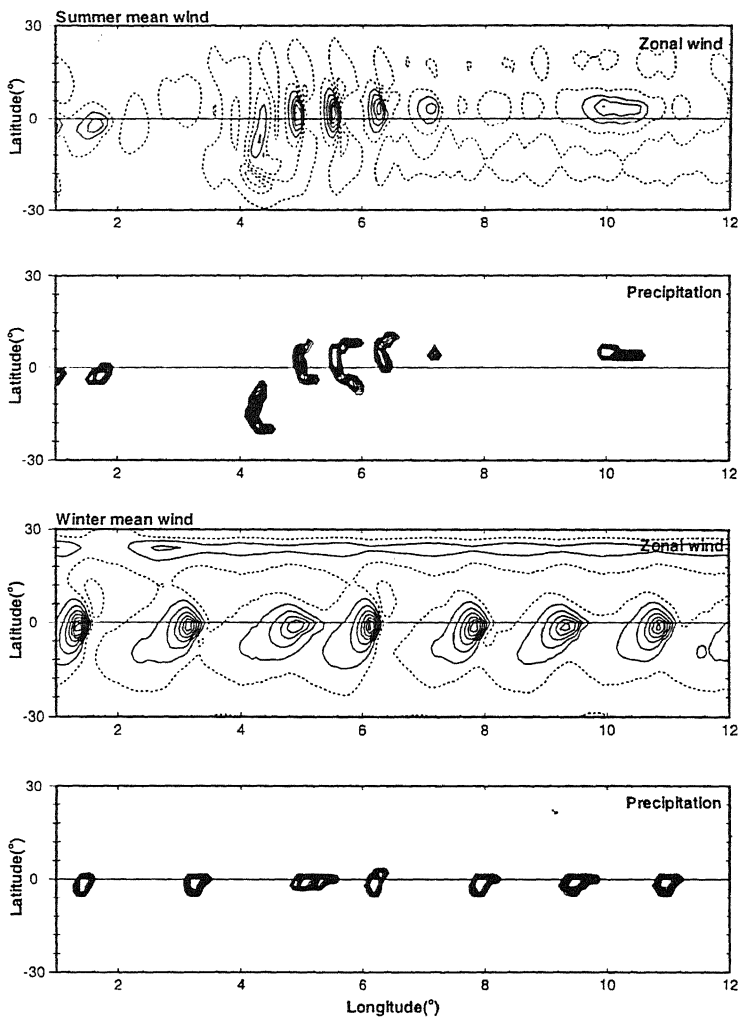

Figure 5.14: Same as the figure 5.13, but for 160°W

Figures from 5.13 to 5.15 show the time-latitude structure of the model zonal wind and precipitation for the cases of only-summer-mean-wind and the only-winter-mean-wind for three zonal locations respectively. It can be seen that the pronounced annual cycle over the monsoon sector disappears in the absence of the annual cycle of the mean wind. This is especially true in case of the winter mean winds, which shows an equator centered structure throughout the year. However, in case of the only-mean-summer-wind, there is a weak annual cycle, although the pronounced north-south shift seen over the monsoon sector with the mean annual cycle is no longer present. We note that in presence of the summer mean

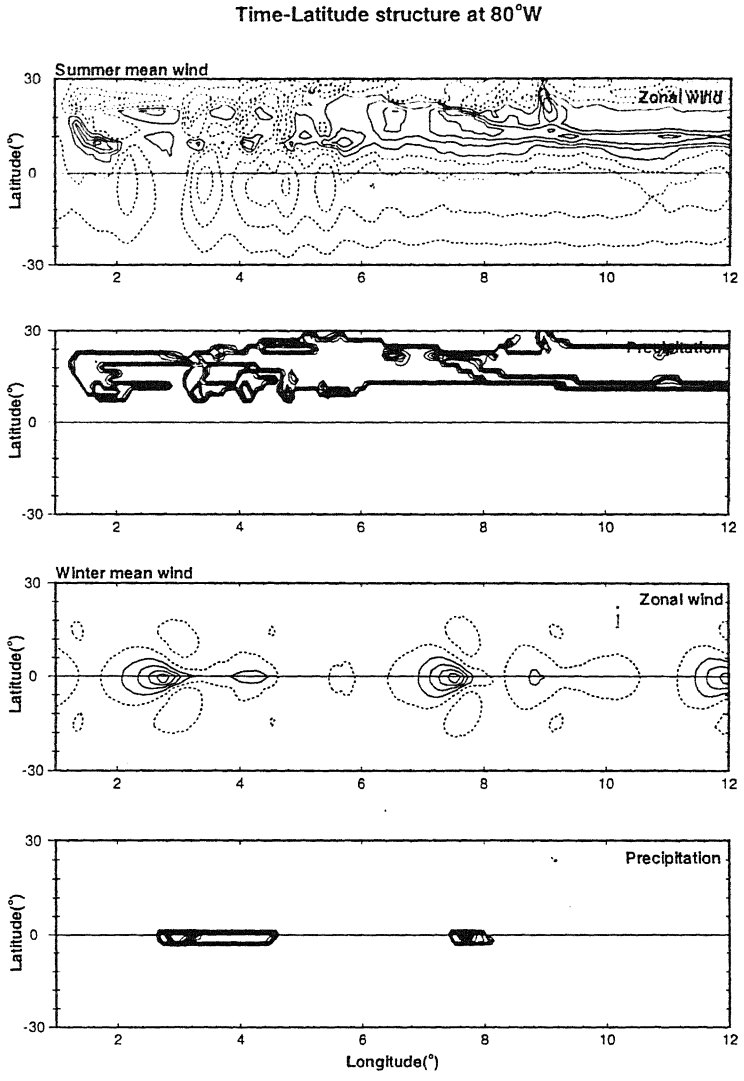

Figure 5.15: Same as the figure 5.13, but for 80°W

winds the model dynamics respond to the location of higher SST in the northern latitudes in the summer months, while no such seasonal change appears in case of the only-winter-mean-wind. Another distinction between the model fields with summer mean winds and with the winter mean winds is that the fields with summer mean winds tend to exhibit a higher degree of spatio-temporal variability, with shorter periods and larger north-south asymmetry. Indeed, in the case of the only-winter-mean-wind, the fields are quite periodic, with a periodicity of about two months. This issue of the difference in the periodicities will be taken up when the characteristics of the intraseasonal oscillations in these cases are

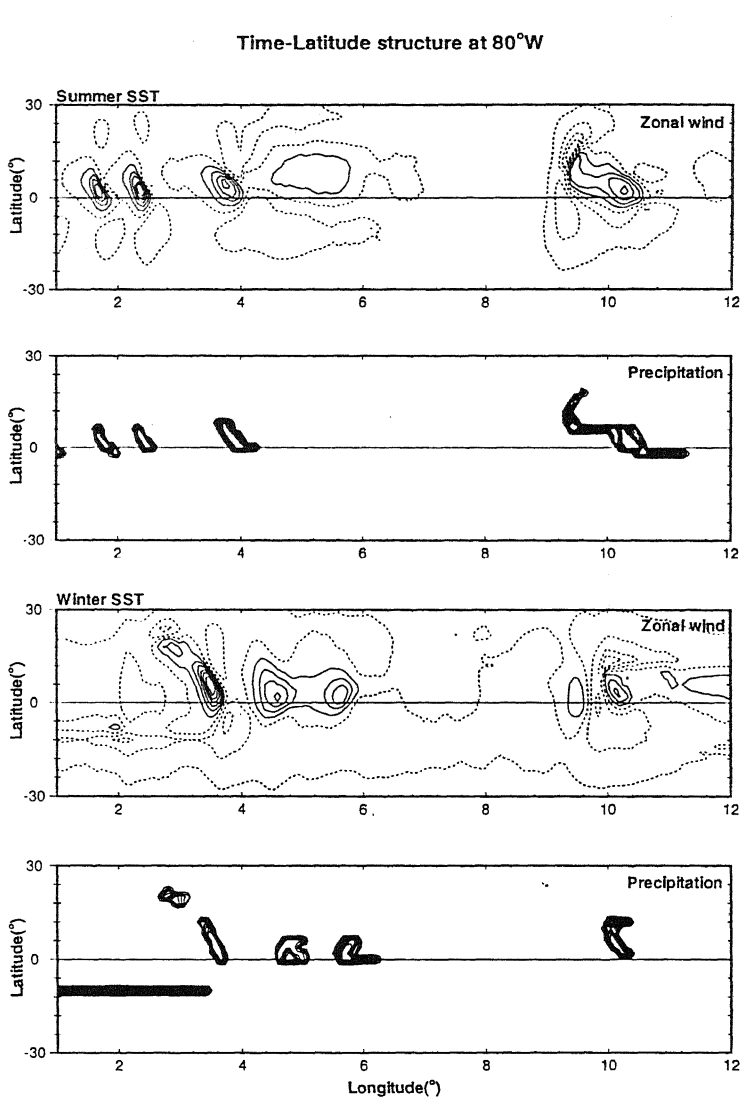

Figure 5.16: Time-latitude structures for summer SST (first two panels from the top) and winter SST (third and fourth panels). Negative contours are dashed.

discussed. Another difference between the u-field from the two simulations over 90°E is the appearance of the westerly anomalies at 16°N during the summer months persisting into the winter. In fact, there are westerlies centered at the equator all throughout the year in the case of the winter mean winds. However, in the case of summer mean winds these equator-centered westerly anomalies appear only during the first three months. A comparison of the u-field with only-summer-mean-wind with the corresponding structure with the annual cycle of both mean wind and SST show that the main difference between two cases is

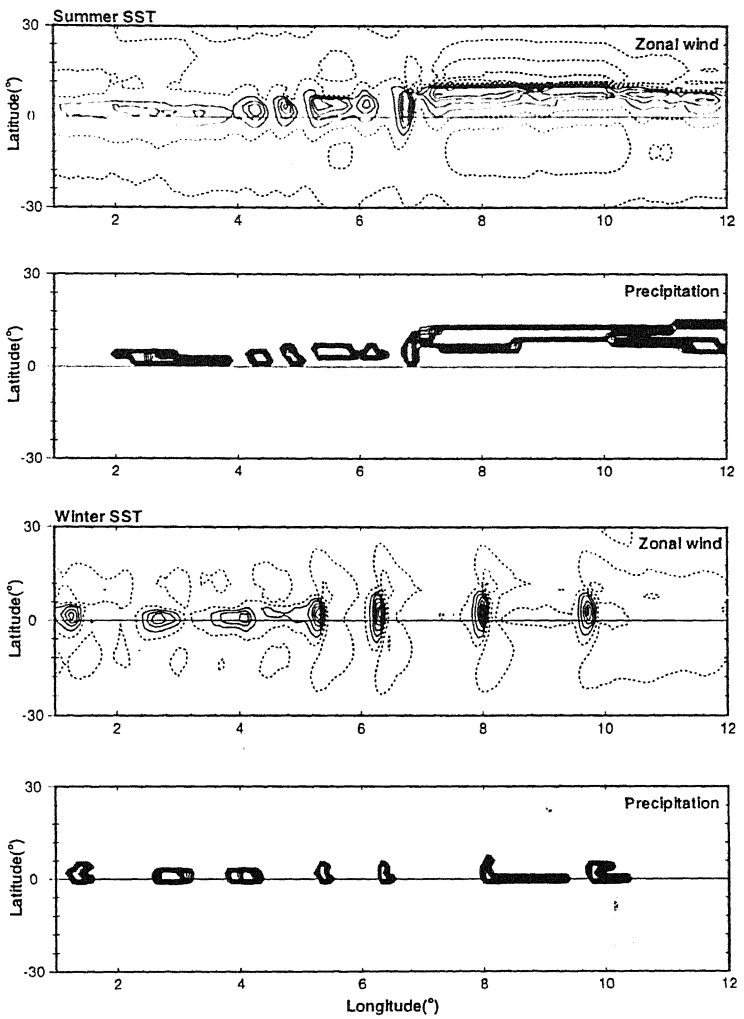

Figure 5.17: Same as the figure 5.16, but for 160°W

the absence of the equatorward shift in the post monsoon months in the absence of the annual cycle of the mean wind. Thus the north-south migration of the westerlies with season may appear to be primarily due to the annual cycle of the mean wind. However, this conclusion is not true, as we shall see when we examine the structure in the absence of the annual cycle of the mean SST. Both the zonal wind and precipitation are localized too far north in the summer months in the absence of the mean wind.

In contrast to the monsoon region, the annual cycle of the mean wind does not seem to influence the latitudinal distribution of either the zonal wind or

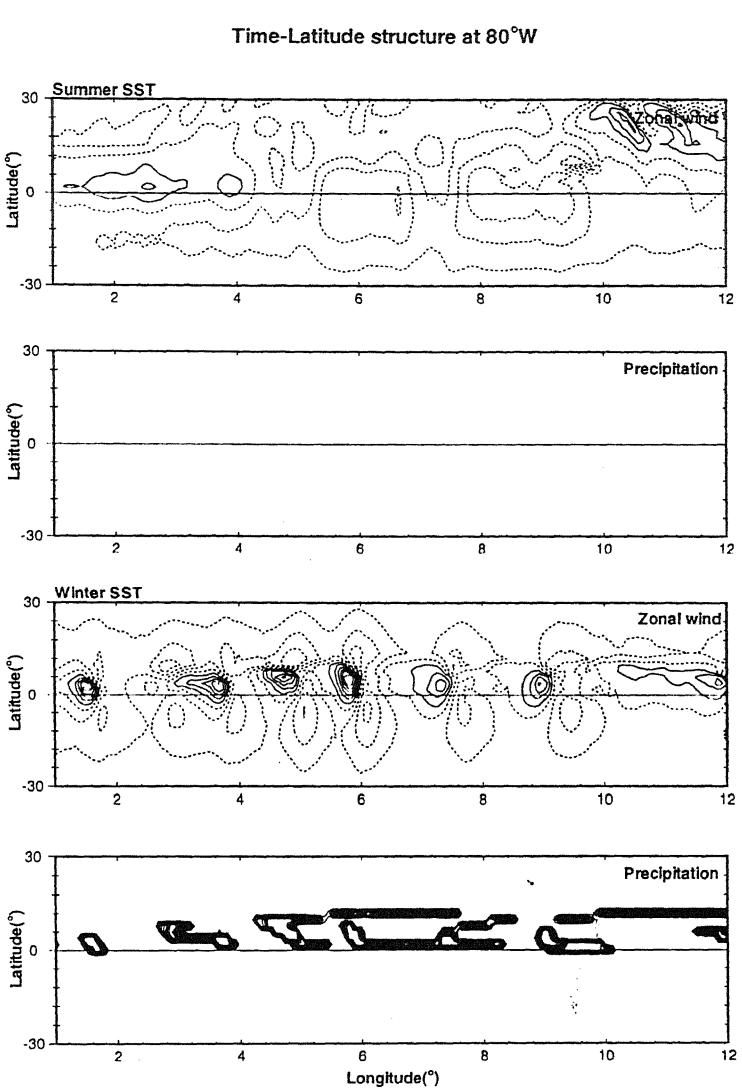

Figure 5.18: Same as the figure 5.16, but for 80°W

precipitation over the Eastern or Central Pacific. However, it seems to have much greater influence on the temporal distribution.

5.3.2 Role of the Annual Cycle of SST

The relevance and significance of SST-dependent EWF in the context of simulating the structure of anomaly fields have been noted earlier. Now we examine the role of the mean SST annual cycle in the annual cycle of the anomaly fields. The time-latitude diagram of the model zonal wind and precipitation are shown in figures 5.16 (90°E), 5.17 (160°W) and 5.18 (80°W) for summer and winter SST

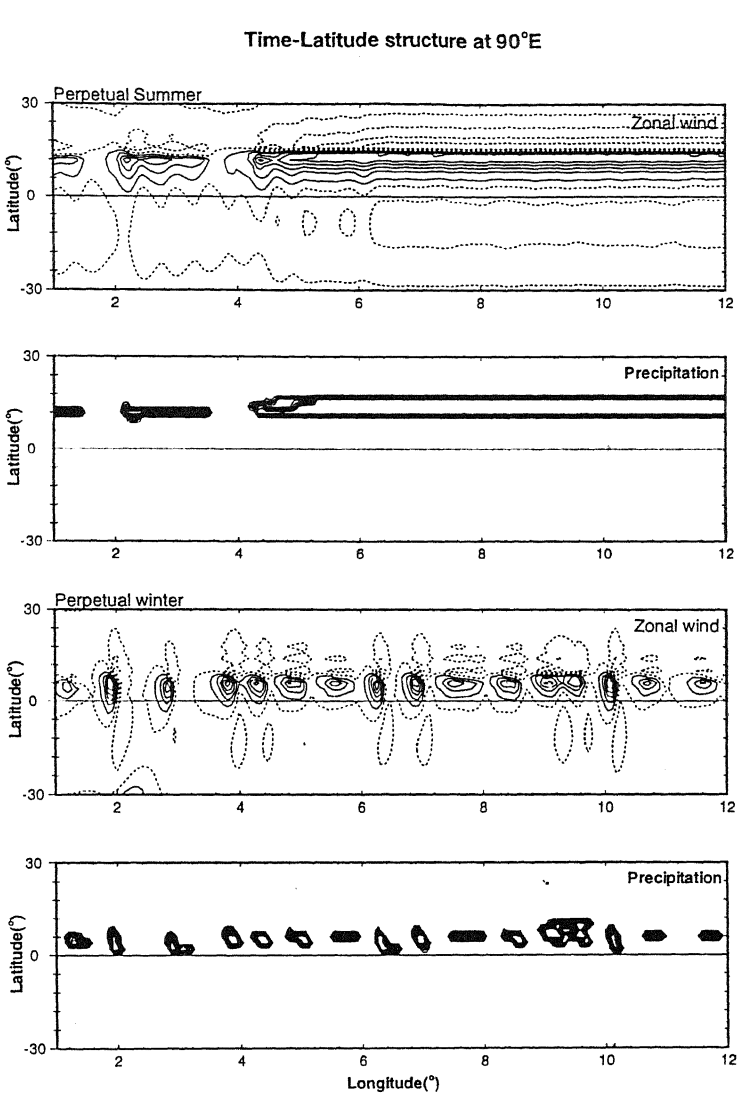

Figure 5.19: Time-latitude structures for perpetual summer (first two panels from the top) and perpetual winter simulations (third and fourth panels). Negative contours are dashed.

simulations as indicated in the panels. A comparison of the annual cycles with summer and winter mean winds (5.14) at 90°E with the corresponding results for summer and winter SST simulations (5.16) shows that the northward shift seen over the monsoonal region in the summer months is essentially due to the annual cycle of SST. However, the fields do not return to southern latitudes when the annual cycle of mean wind is absent. The winter simulations are, however, generally much more periodic and equator centered. Figure 5.18 shows that zonal wind and precipitation are predominantly centered in the Northern Hemisphere,

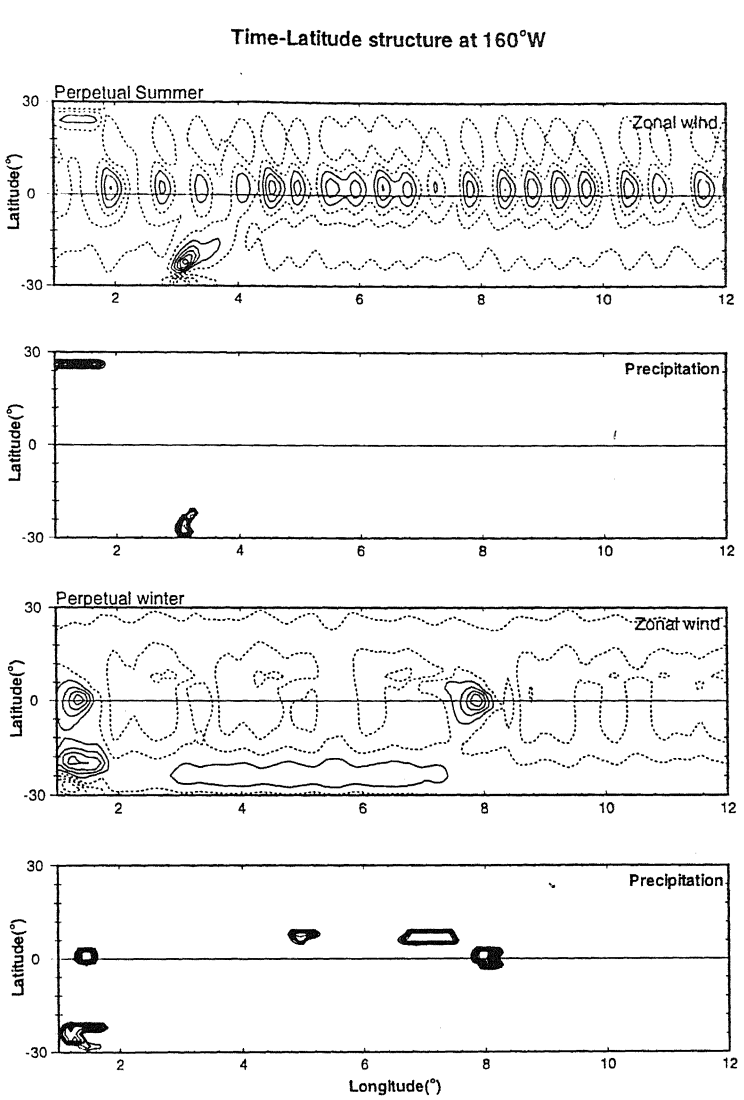

Figure 5.20: Same as the figure 5.18, but for 160°W

although the SST maximum would be in the Southern Hemisphere. In contrast, over 90°E and 160°W the fields for winter SST simulations are more or less equator centered. These features point to the conclusion that the annual cycle of the total anomaly fields in the tropics is a complex combination of effects due to the annual cycles of the mean wind and SST.

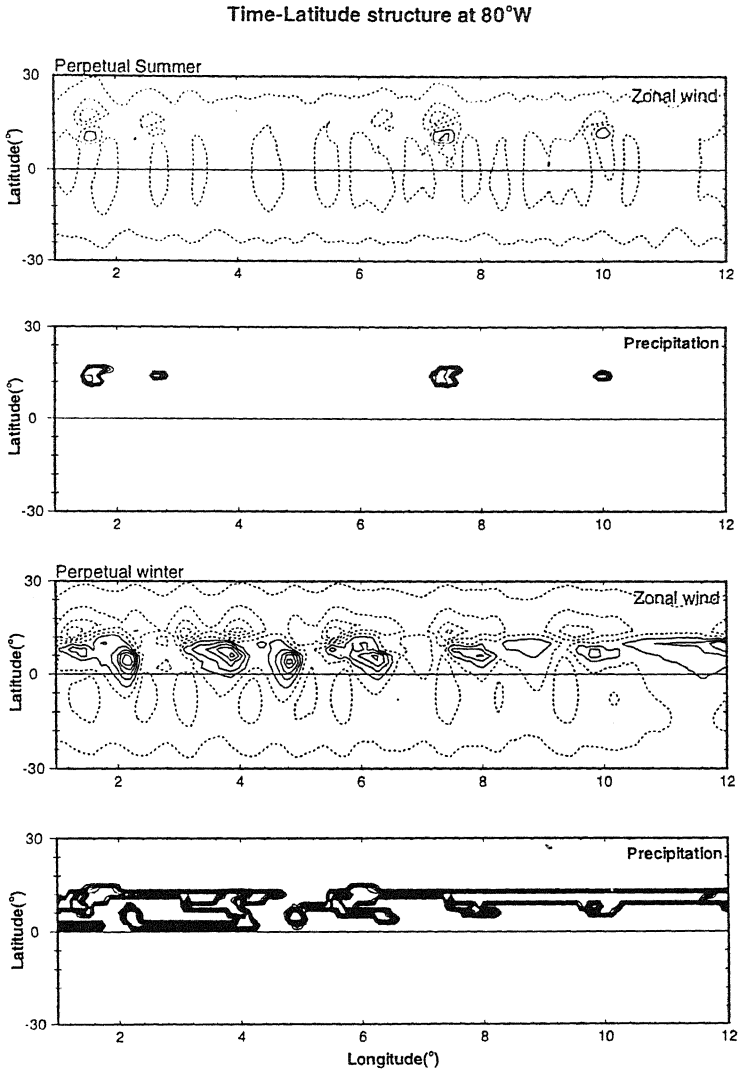

Figure 5.21: Same as the figure 5.18, but for 80°W

5.3.3 Perpetual Summer and Perpetual Winter Simulations

The time-latitude structures of the model simulation when annual cycle of both mean wind and mean SST are suppressed are given in figures 5.19 to 5.21, for the three longitudes. Each of the figures shows zonal wind and precipitation for the perpetual summer (summer mean wind and summer SST) and perpetual winter (winter mean wind and winter mean SST).

As expected, in the absence of both the mean annual cycles, the anomaly cir-

culation shows no significant change with season. However, the simulated time-latitude structures of the model fields are quite different over three longitudes, emphasizing the role of the spatial structure of the mean fields in the anomaly circulation. In particular, both the monsoon and the Eastern Pacific regions are characterized by equatorial westerlies for perpetual summer simulation, while the Eastern Pacific region is characterized by anomaly easterlies for perpetual summer. Another interesting feature is a reversal of the zonal wind from westerly for perpetual summer to easterly for perpetual winter at 160°W, with a similar but reversed effect at 80°W. In contrast, there is no appreciable change at 90°E where the zonal wind is predominantly westerly for both perpetual summer and perpetual winter. A scrutiny of the zonal wind for perpetual winter over 160°W (5.20) and for perpetual summer over 80°W (5.21) shows the signature of a seasonal scale variability in the form of a reversal of the (dominant easterly) wind to westerly winds. The significant fact is that these westerly bursts coincide with episodes of precipitation over these locations. Since for perpetual summer and perpetual winter there is no external contribution to the temporal variability of the anomaly fields, this seasonal cycle is essentially intrinsic to the convectively forced tropical circulation.

5.4 Conclusions

The annual cycle of the anomaly circulation in the tropics appears to be essentially determined by the annual cycles of the mean wind and SST. Indeed, as we have seen with our perpetual summer and perpetual winter simulations, there is no significant change in the circulation pattern with the march of the season in the absence of the mean annual cycles. This is not surprising, since our model does not contain any other seasonally varying forcing. This implies that variabilities associated with the 30-50 day oscillations or QBW do not have any overall contribution to the seasonal variations. This point is examined further in

connection with the structure of intraseasonal oscillation.

An important point brought out by our simulation is the important role played by the annual cycle of the mean SST. The GCM simulations indicated that relatively small SST anomalies over the equator can give rise to large diabatic heating through the release of latent heating (Rowntree, 1979; Julian and Chervin 1978; Kesavamurthy, 1982). The atmospheric response to this diabatic heating can also induce an annual cycle in the anomaly circulation. While the mean wind and SST may influence each other to produce the observed mean anomaly cycle, the annual cycle of the anomaly circulation is determined by a combined effect of the two mean annual cycles. Neither of the mean annual cycle alone can give rise to a characteristic annual cycle. However, the mean SST and the mean wind in the summer and the winter affect the anomaly circulations differently. An interesting point is the higher degree of variabilities in presence of the summer mean fields. This has an important implications for the predictability in the tropics.

It can be seen from figures 5.19-5.21 that there is , however, a weak annual cycle intrinsic to the convection induced internal dynamics. This is particularly prominent over the Pacific regions, with a rather prominent seasonal-scale (200 days) variabilities.

Chapter 6

The Spectrum of Oscillations I: The Broad Spectrum

The existence of a broad spectrum of oscillations spanning the intraseasonal to interannual time scale makes modeling of the tropical atmosphere a challenging task. These oscillations are an integral part of the tropical dynamics, and they have important implications for the climate and predictability in the tropics. The simulation of these variabilities, therefore, has been a major testing ground for both GCM and for models of intermediate complexity. Nevertheless, most of the efforts in simulating the tropical intraseasonal oscillations have focussed primarily on 30-50 day oscillations. As we have seen, there are at least two other significant oscillations at intraseasonal time scale in the tropical atmosphere. In addition, the tropical atmosphere exhibits several longer period oscillations, prominent ones being the quasi-biennial oscillation (QBO) and the El Niño-Southern Oscillation (ENSO) type interannual oscillations.

The detailed evolution and structure of these oscillations with widely separated time scales are, no doubt, influenced by external and internal forcings of relevant time scales. For example, it is quite likely and is suggested by several studies that the evolution and the structure of the interannual variabilities are significantly affected by the ocean-atmosphere coupling. Indeed in the currently held scenario,

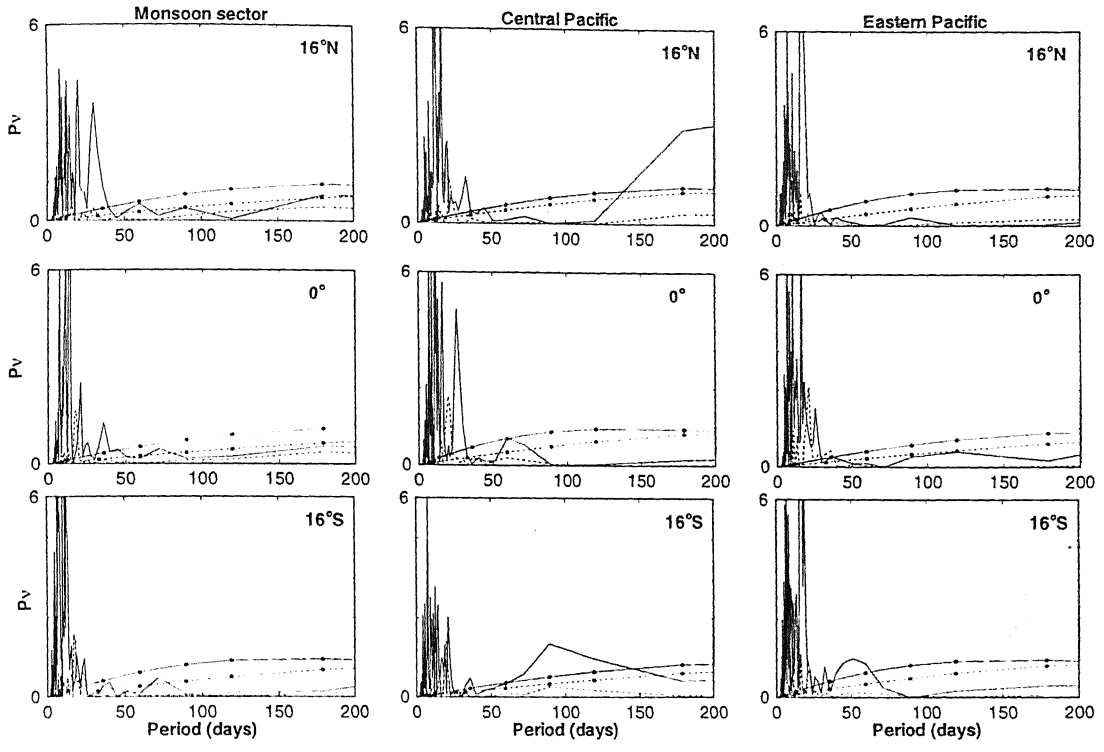

Figure 6.1: Power spectra of unfiltered time series of the model u field from composite annual simulation for uniform EWF plotted with $\nu P(\nu)$ as the ordinate and period as abscissa. The solid line for τ =0.5 hr. and dashed line represent τ =1.5 hr. The corresponding red noise spectra are marked with symbols.

the ENSO variability is an ocean-atmosphere coupled instability. However, the question of *genesis* of these variabilities can be addressed separately. In particular, it is possible that the different oscillations are excited by the same basic mechanism, while their detailed evolution and structure are modulated by the forcings operative at spatio-temporal scale of particular oscillations.

We investigate these questions with our model of convective tropical atmosphere. Previous analytical studies have already shown that convection-induced internal dynamics in presence of a CTL of a few hours can selectively excite intraseasonal oscillations at 30-50 day (Goswami and Rao 1994, hereafter GR), 10-20 day and 3-5 day scales (Goswami and Mathew 1994, hereafter GM). However, for our model simulation of the monthly anomaly fields, it was found that

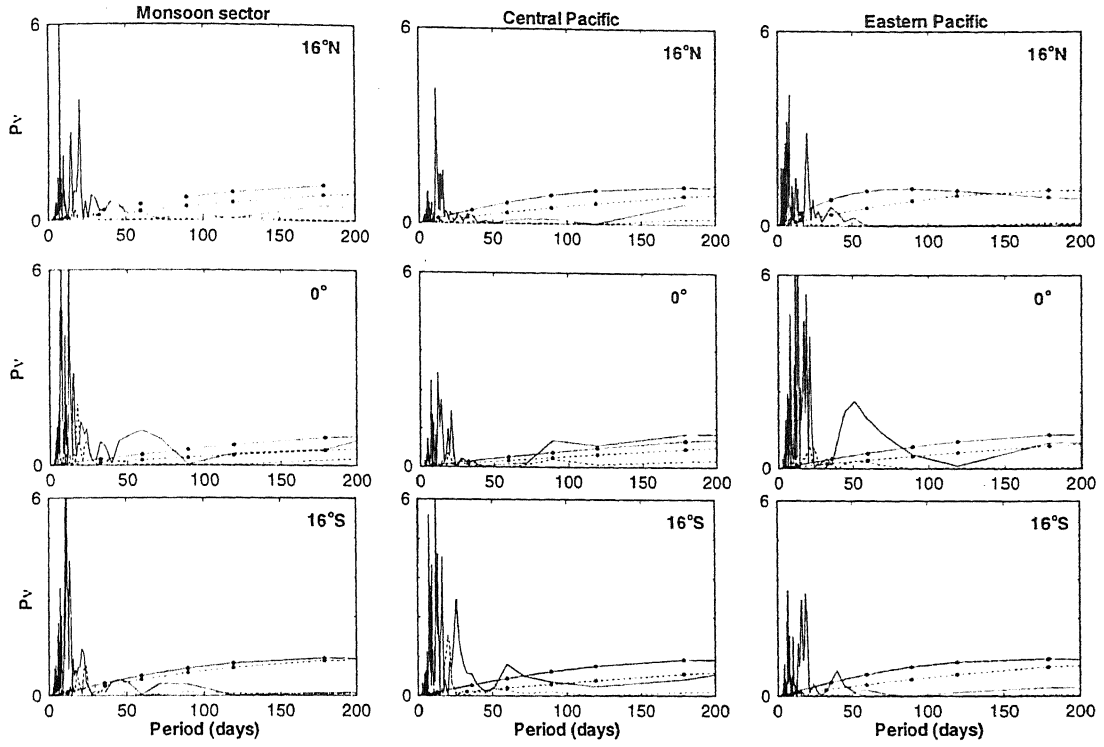

Figure 6.2: Same as figure 6.1, but for meridional wind

the most appropriate value of CTL is between 0.5 and 1.5 hours. This is not surprising, since the monthly anomaly fields contain contributions not only from the low frequency waves but also from the convection organized at smaller scales. Indeed, it was found that while the most appropriate value of CTL for selective excitation of Kelvin wave at 30-50 day time scale is about twelve hours (GR), the corresponding value for the higher frequency ISO is about six hours (GM). Besides, the spectrum and the nature of oscillations in presence of the non-linear heating processes and the observed space-time dependent mean states may be quite different. An important question is whether convection induced internal dynamics could support any longer period oscillation without ocean-atmosphere coupling (but may be with SST-induced variations in distribution of convective feedbacks). In particular, if our model is to provide an effective simulation of the tropical anomaly climate, a single value of CTL (chosen from a range) should be

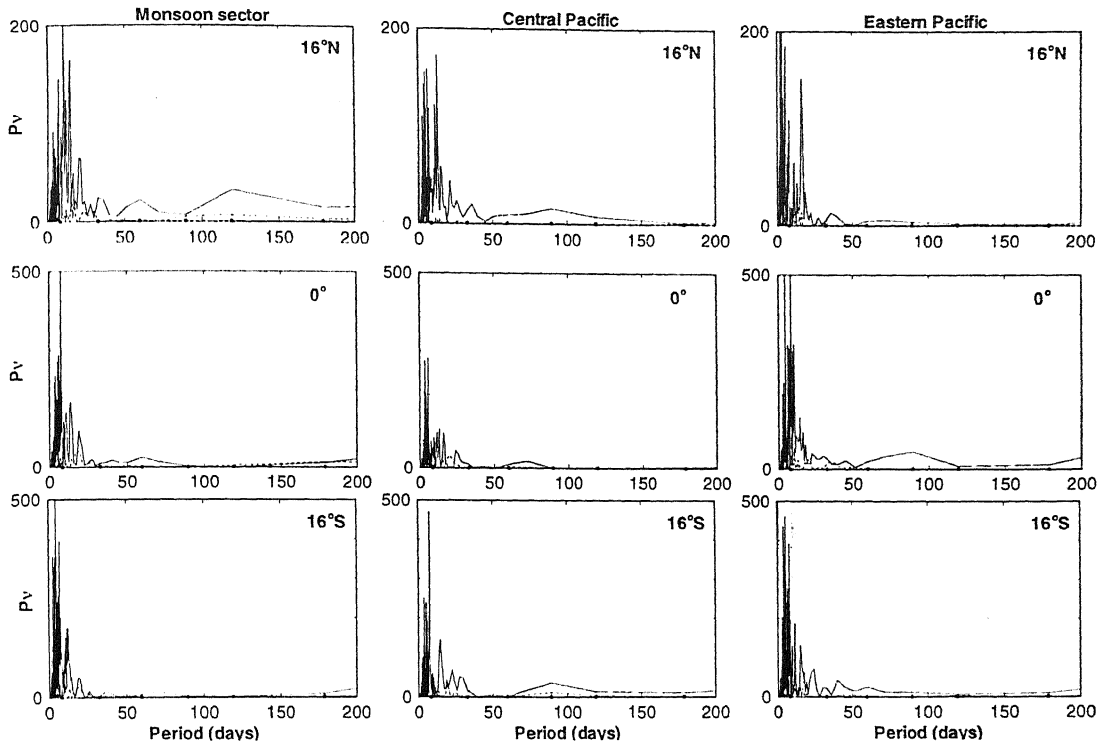

Figure 6.3: Same as figure 6.1, but for precipitation

capable of simulating the entire range of observed oscillations under appropriate dynamical conditions. Therefore the question of the existence of oscillations at various time scales and the relative roles of various processes in their genesis and structure is investigated.

6.1 Design of the Experiments

Given that the observed circulation in the tropics exhibits a wide spectrum of oscillations, an important question to be answered concerns the minimal and relevant physics that can support these oscillations. In particular, it is important to identify and ensure mechanisms that can support certain well-known phenomena like the 30-50 day eastward propagating oscillation. While the detailed structure of each major oscillations in the model will be addressed and described subse-

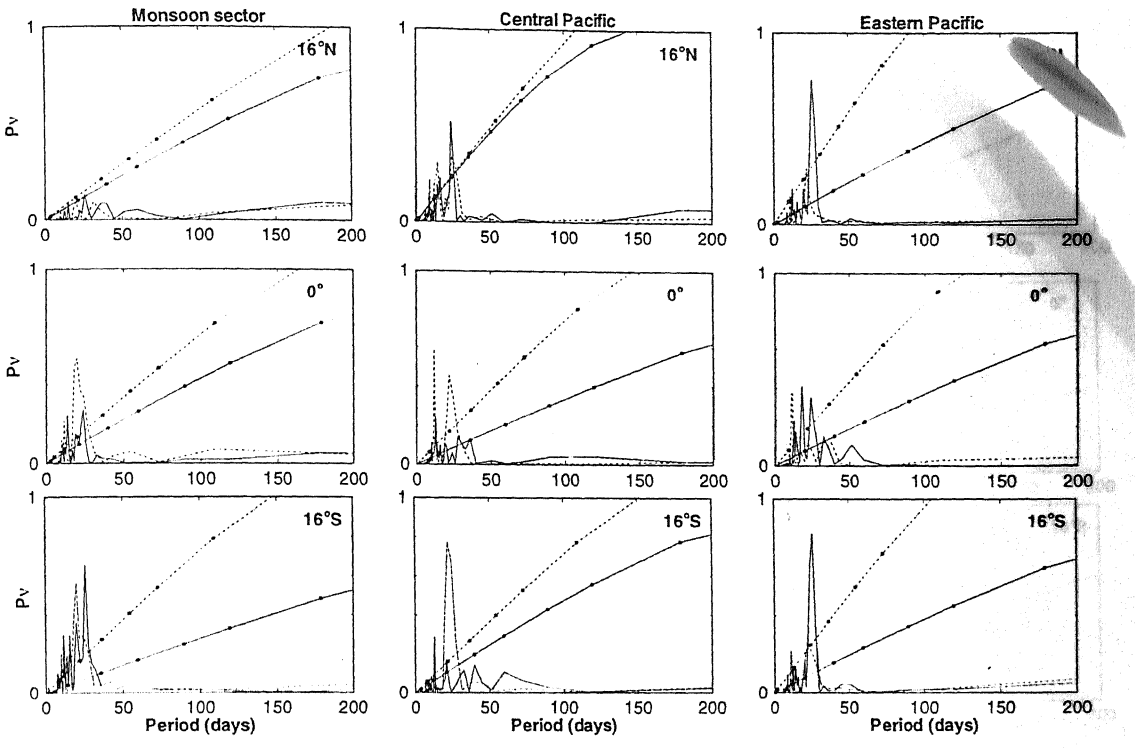

Figure 6.4: Power spectra of unfiltered time series of the model u field from composite annual simulation for uniform EWF plotted with $\nu P(\nu)$ as the ordinate and period as abscissa. The solid line for τ =3.0 hr. and dashed line represent τ =6.0 hr. The corresponding red noise spectra are marked with symbols.

quently, our primary goal here is to examine the existence of these oscillations and to identify the primary mechanism of their genesis. Most of the earlier studies have simulated, as we have mentioned earlier, only a particular oscillation or at the most a part of the spectrum at a given time. But for a model to be successful in simulating the tropical climate it must be capable of simulating all the relevant observed periodicities. This requirement is getting stronger in view of the interconnection among the oscillation with widely separated time scales. Hence, a large number of experiments to identify the effects of various dynamical and mean conditions on the genesis and structure of tropical oscillations is carried out. The analyses were done using model simulations from both one-year integrations and much longer 38-year simulations. A brief description of these

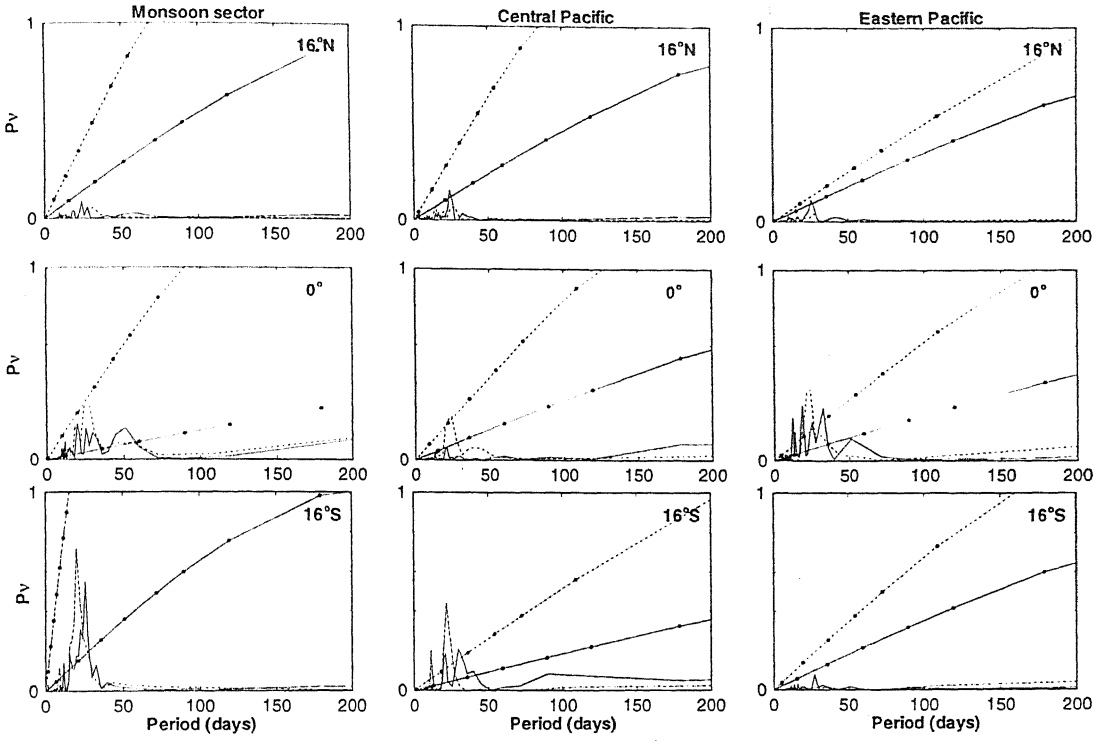

Figure 6.5: Same as figure 6.4, but for meridional wind

two sets of experiments is given below.

6.1.1 Composite Annual Simulation

To examine the existence and the characteristics of the intraseasonal oscillations, we have carried out a number of (sixteen) one-year simulations with different initial conditions. The initial conditions are obtained by subtracting the climatological mean monthly fields from the monthly mean fields for a particular year. For the one year simulations we have used the 9-year (1979-1987) data set from Comprehensive Ocean Atmosphere Data Sets (COADS). The monthly mean SST fields were also taken from the same data set. The sixteen initial conditions for the sixteen one-year simulations were obtained from eight winter (January) and eight summer (corresponding June) monthly anomaly fields obtained from the observed data. The results of the sixteen simulations were then composited with

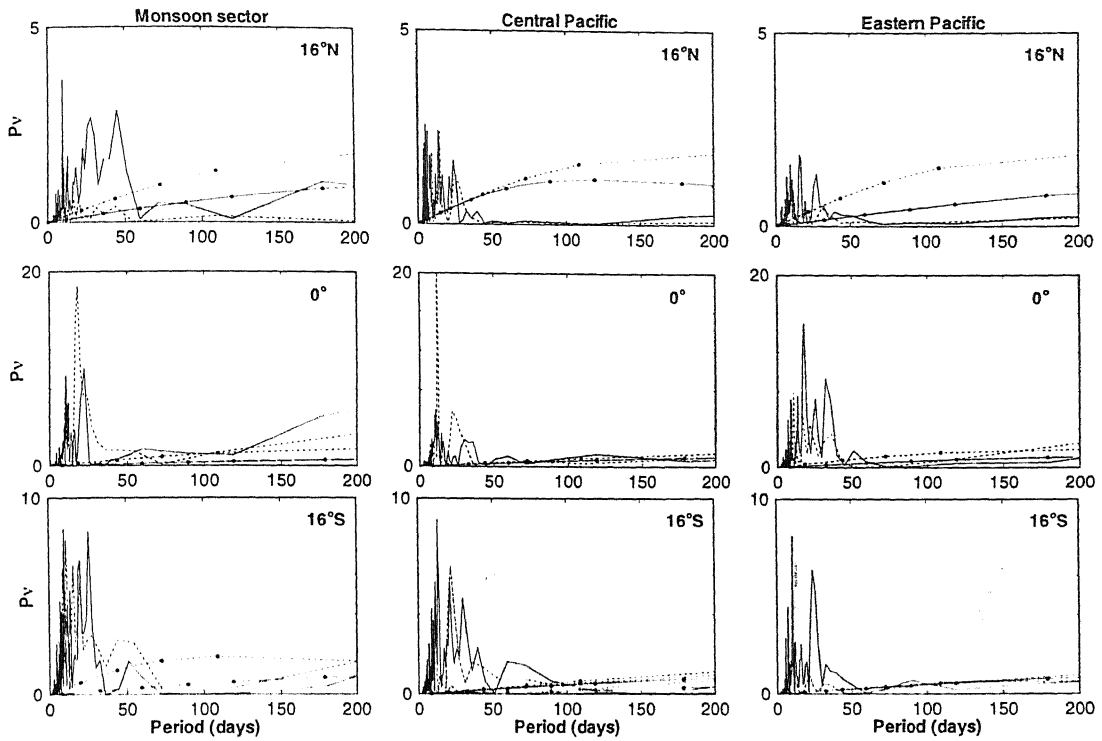

Figure 6.6: Same as figure 6.4, but for precipitation

equal weights to arrive at a composite one-year simulation. This procedure is repeated for each of the four values of CTL considered in our study.

6.1.2 Long-term Simulations

To generate a model simulation suitable for investigating the broad spectrum of tropical oscillations, we have integrated the model for thirty eight years with a given observed initial condition. The observed initial fields are obtained by subtracting the 38-year mean for January from the monthly mean January field for a particular year (1950). The mean fields of zonal and meridional wind components are given as the 38-year mean monthly winds obtained by taking the mean of observed monthly mean surface fields for zonal and meridional wind components from the 38-year (1950-1987) COADS. The mean SST field is also taken from the same data set.

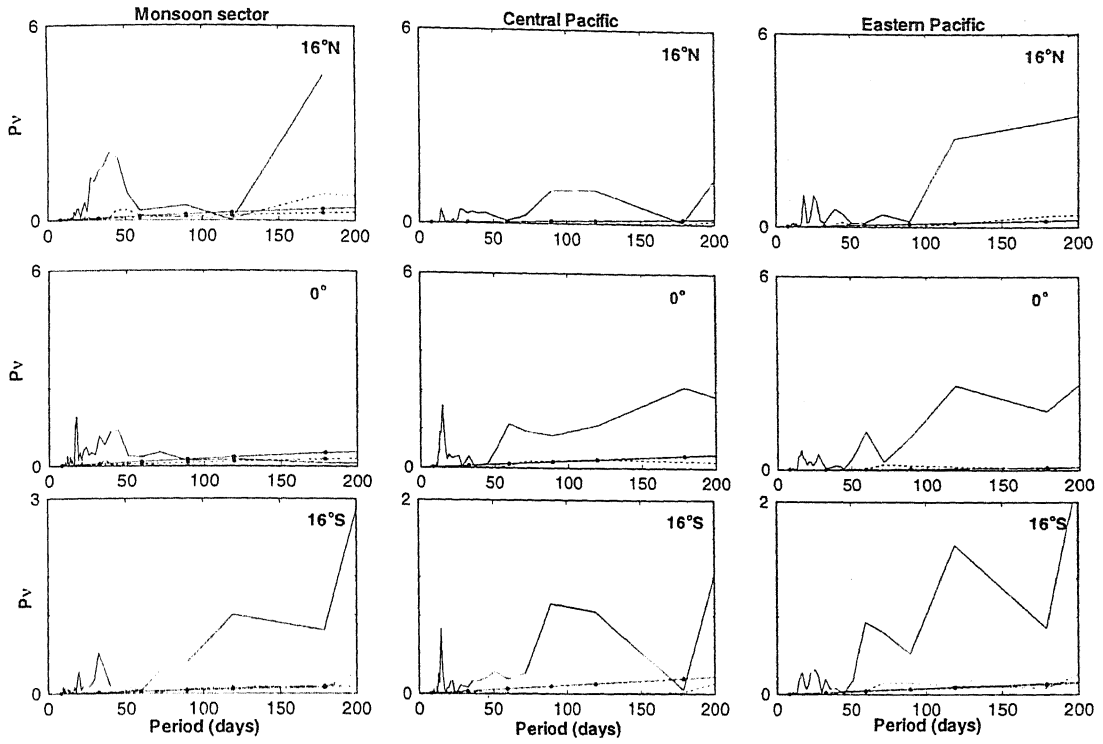

Figure 6.7: Power spectra of unfiltered time series of the model u field from composite annual simulation for SST dependent EWF plotted with $\nu P(\nu)$ as the ordinate and period as abscissa. The solid line for τ =0.5 hr. and dashed line represent τ =1.5 hr. The corresponding red noise spectra are marked with symbols.

We have used two different data sets for obtaining the mean states and initial conditions for the annual and long-term simulations with the purpose of obtaining a more objective evaluation of the model simulations.

Both the annual (composite) and the long-term simulations were repeated to examine the existence and structure of the oscillations under different mean and dynamical situations. The detailed design of the simulations with emphasis on the different aspects is discussed below.

a) Role of Convective Timelag

As we have argued earlier, the values of CTL used in earlier analytical studies may have to be changed in presence of non-linear processes and complex mean fields. Indeed, we have already seen in chapter 4 that it was with a smaller value

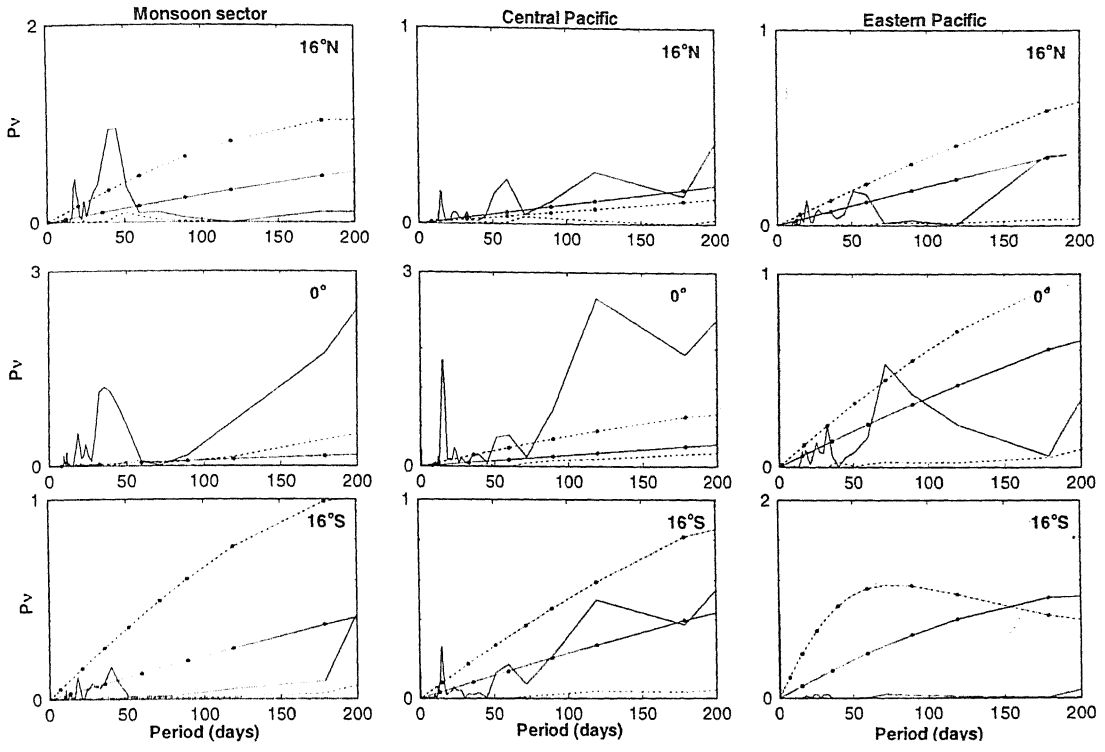

Figure 6.8: Same as figure 6.7, but for meridional wind

of CTL; from 0.5 hour to 1.5 hour, that the detailed structure of the anomaly fields are better simulated. However, the adopted value of CTL must also be able to support the observed spectrum of tropical variabilities. Therefore, four values of CTL, from 0.5 hour to 6.0 hours, are considered. For the annual composite simulation, this gives 16×4=64 one-year simulations, as the model is integrated for sixteen different initial conditions for each value of CTL. For the long-term simulation, this results in four 38-year model integrations.

b) Uniform Strength of Evaporation-Wind Feedback

A spatially and temporally uniform strength of EWF represents a mean condition in which the underlying SST field is also spatially and temporally uniform. In the case of one-year integration, this would mean the absence of the annual cycle and the spatial variation of SST field. In the case of long-term simulation this would imply spatially uniform SST field devoid of any seasonal as well as in-

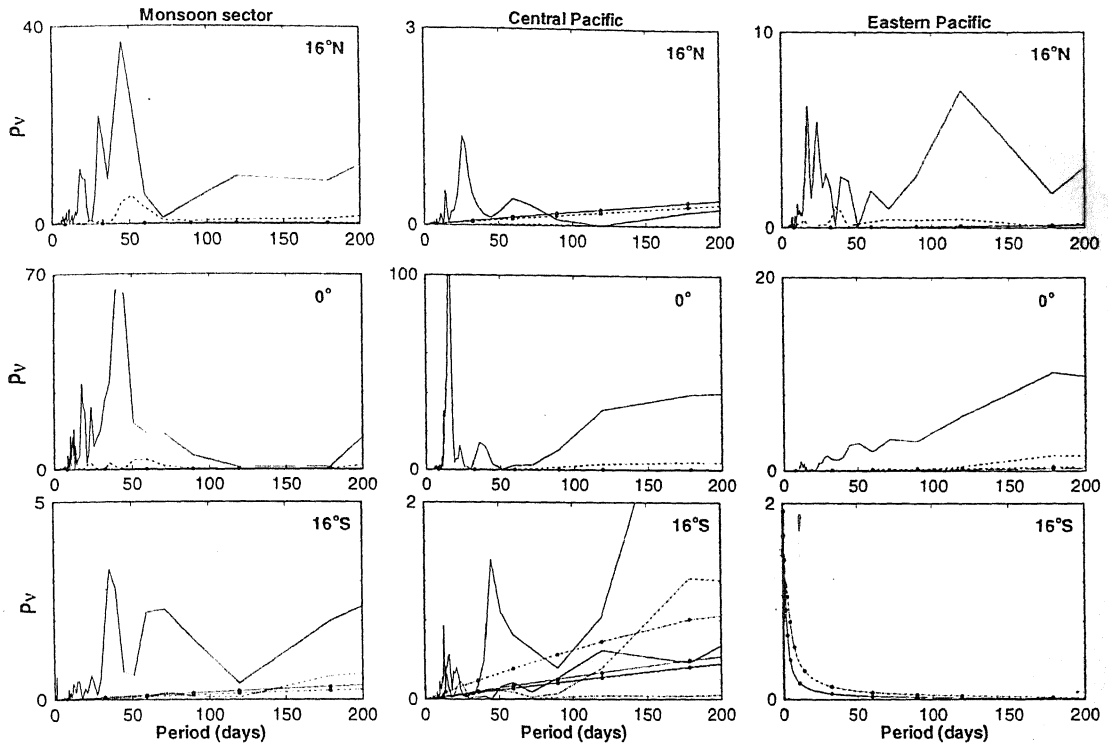

Figure 6.9: Same as figure 6.7, but for precipitation

terannual variabilities. As we have already seen, a uniform strength of EWF can not simulate the spatial structure of the monthly anomaly fields well, signifying the importance of the structure of the SST field in the simulation of the tropical variabilities. We shall examine this issue in the context of intraseasonal and interannual oscillations. Thus sixteen-integration-composite one-year simulations were generated for each of the four values of the CTL with a uniform strength of EWF.

c) Role of SST-induced Spatio-Temporal Variations of EWF

One of the moist processes that has been shown to play a significant role in the dynamics of tropical variabilities is EWF. This is also true in the present study, in the context of the structure of the anomaly fields. We have seen that the inclusion of dependence of EWF on underlying SST, through dependence of Δq on SST, has profound effect on the structure of simulated variabilities. The corresponding

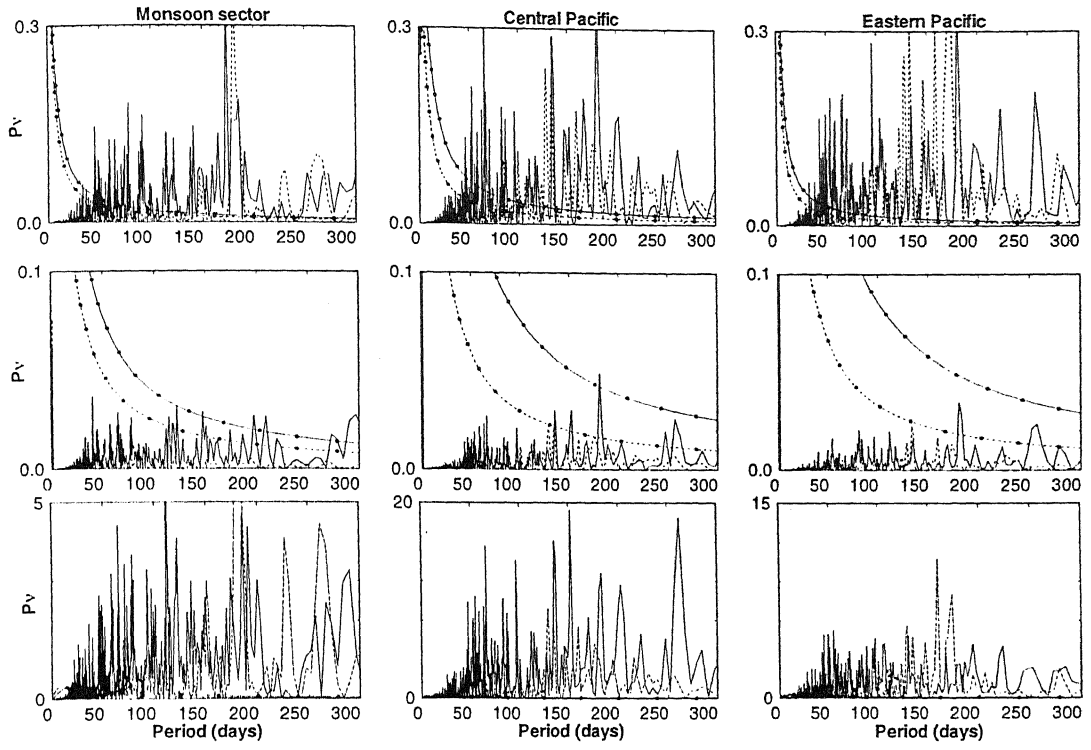

Figure 6.10: Power spectra of unfiltered time series of the model u field from long term simulation for total SST dependent EWF plotted with $\nu P(\nu)$ as the ordinate and period as abscissa. The top row is for zonal wind, middle for meridional wind and the last row for precipitation. The solid lines for τ =0.5 hr. and dashed lines represents τ =1.5 hr. The corresponding red noise spectra are marked with symbols.

effects on the genesis and structure of ISO are investigated here. Both the annual and the interannual integrations were therefore repeated to investigate the role of SST-induced spatio-temporal structure of strength of EWF on the genesis of the oscillations.

d) Role of the Annual Cycle of the Mean Wind

The mean circulation in the tropics is characterized by a pronounced seasonal reversal of winds over the monsoon region. It is known that this annual cycle of the mean wind significantly affects the anomaly circulation in the tropics. To examine the effects of the seasonal variation of the mean wind on the intraseasonal oscillations, we have carried out two one-year simulations with winter (Decem-

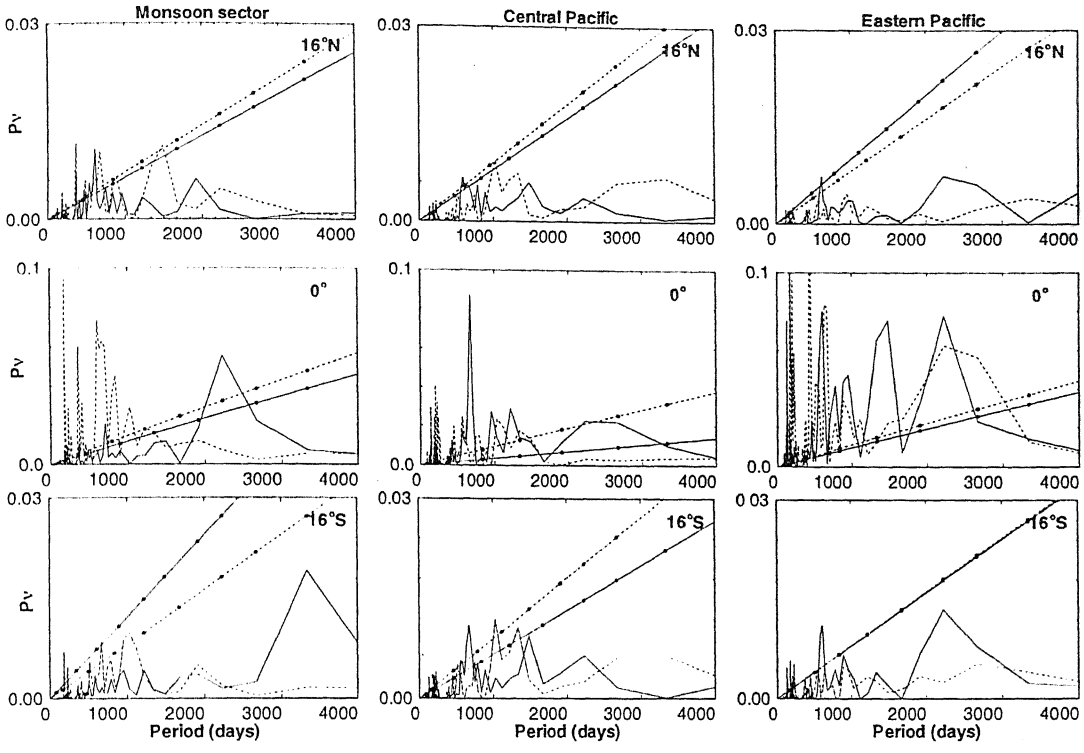

Figure 6.11: Power spectra of unfiltered time series of the model u field from long term simulation for SST dependent EWF plotted with $\nu P(\nu)$ as the ordinate and period as abscissa. The solid line for τ =0.5 hr. and dashed line represent τ =1.5 hr. The corresponding red noise spectra are marked with symbols.

ber, January and February mean) and summer (June, July and August mean) background winds with a given initial condition.

e) Role of Interannual Variability of SST

In the current scenario, many of the low frequency (longer than a year) variabilities of the tropical atmosphere are viewed as resulting from ocean-atmosphere interaction. While there can be little doubt that the ocean-atmosphere interaction plays a crucial role in the *structure and evolution* of these low-frequency variabilities, it is worthwhile to investigate whether the question of *genesis* of some of these oscillations can be addressed in the context of (convection induced) atmospheric dynamics alone. To address this question, we have generated long term simulations without the effect of the interannual variabilities of SST.

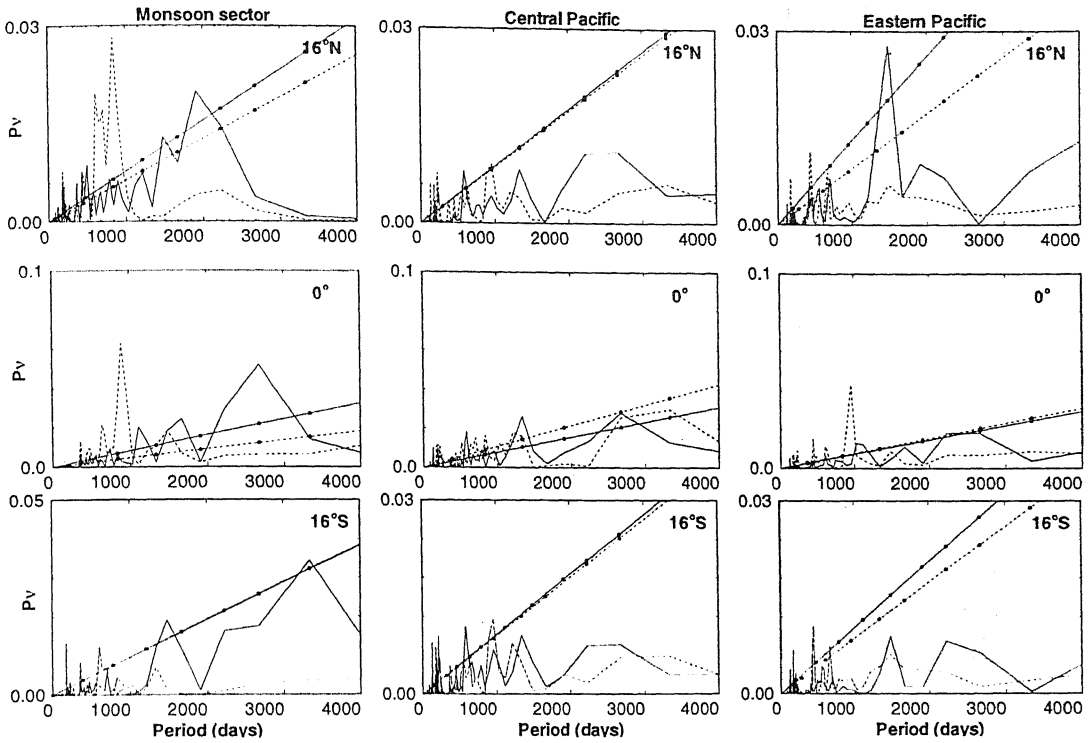

Figure 6.12: Same as figure 6.11, but for meridional wind

6.2 Method of Analysis

To verify the presence of both intraseasonal and longer term oscillations, the time series from the various numerical experiments are subjected to a power spectrum analysis. The significance of peaks are tested against the corresponding red noise spectra. Both the 38-year and one-year simulations are subjected to this analysis. While the long term simulations are primarily used to investigate longer period oscillations, we also look for certain intraseasonal oscillations. These results from the long-term simulation on intraseasonal oscillations are then compared with the results for the same oscillation from the composite one-year simulations. This provides a cross-validation of the two simulations with different mean fields, initial conditions and periods of integration. For all the simulations, the time series were constructed by creating zonal area averages over three re-

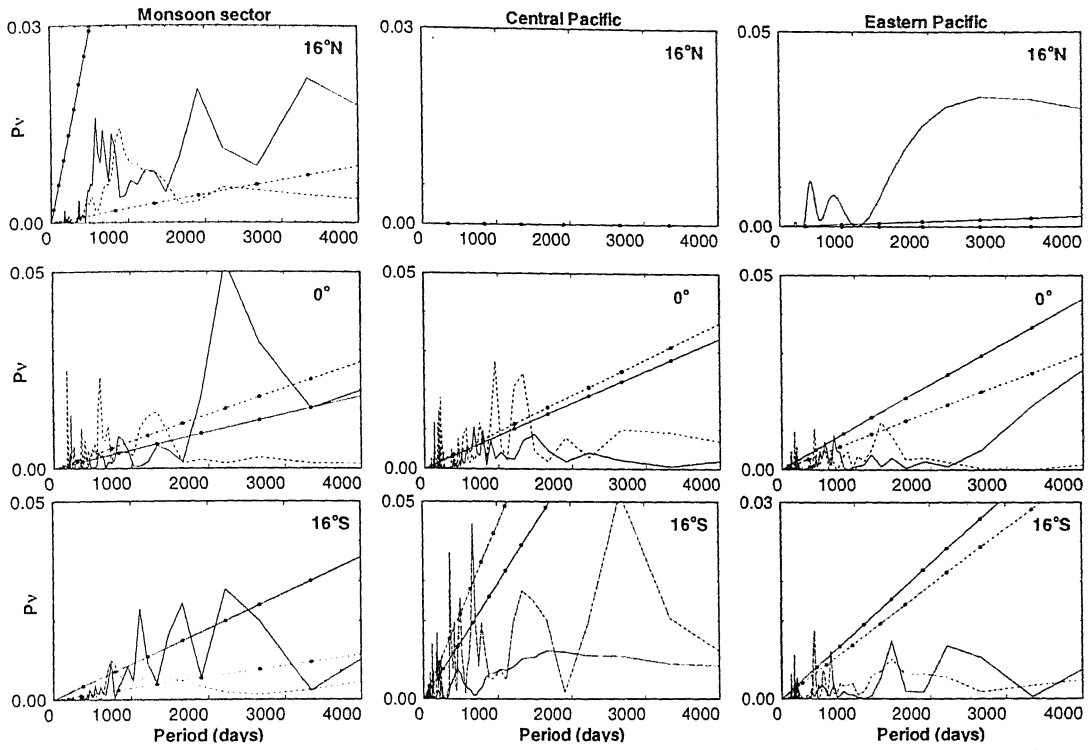

Figure 6.13: Same as figure 6.11, but for precipitation

gions: monsoon sector (60-120°E), Central Pacific (170°E-130°W) and Eastern Pacific (110-50°W). These zonal averaged time series were then recorded at three latitudinal locations: centered around 16°N, the equator and 16°S.

6.3 Results

6.3.1 Intraseasonal Oscillations

In view of the significant role played by the ISO in tropical dynamics, the ability to simulate some of the characteristics of these oscillations can be considered as a prerequisite for any model for tropical dynamics. We, therefore, first analyze our model simulations in terms of existence of the intraseasonal oscillations. A more detailed analysis of their zonal and meridional structures will be presented subsequently. Figures from 6.1 to 6.3 show the power spectra from the composite

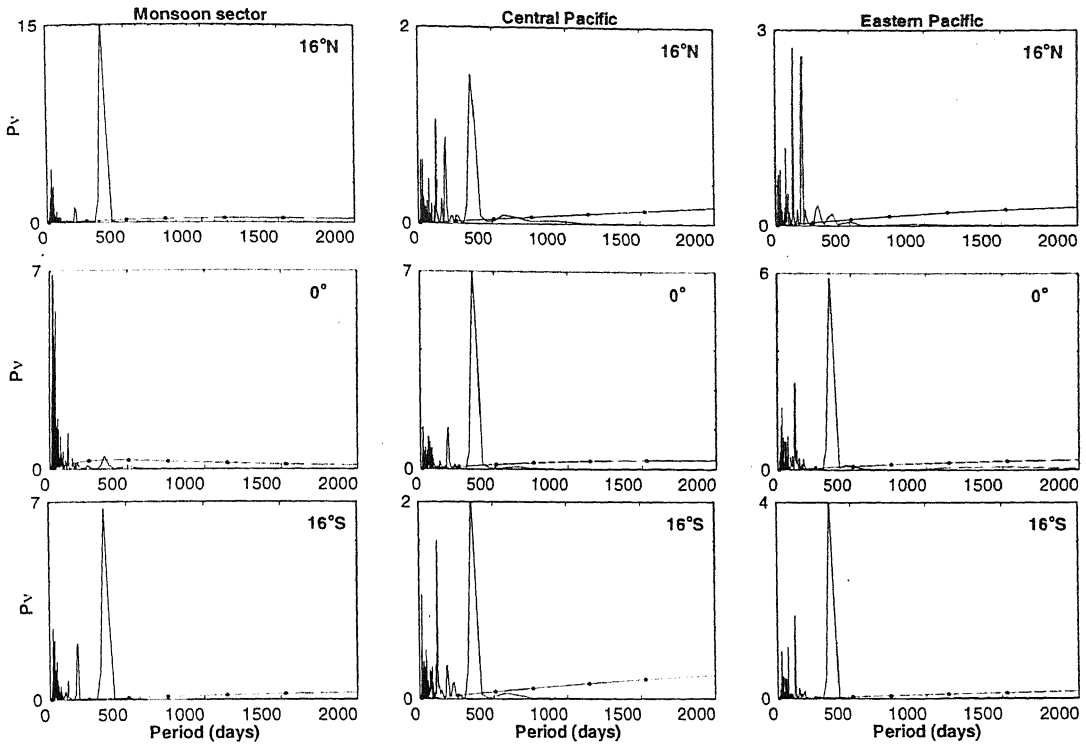

Figure 6.14: Power spectra of unfiltered time series of the model u field from long term simulation for climatological SST dependent EWF plotted with $\nu P(\nu)$ as the ordinate and period as abscissa. The solid line for τ =0.5 hr. and dashed line represent τ =1.5 hr. The corresponding red noise spectra are marked with symbols.

one-year model simulation with a spatially and temporally uniform strength of EWF at different locations as indicated in the panels. The solid and the dashed curves in each panel represent the power spectra for the two values of CTL, 0.5 and 1.5 hours respectively. The red noise spectrum corresponding to each value of CTL is represented by the corresponding curve with solid circles. The corresponding figures for τ =3.0 and 6.0 hours are shown in figures 6.4 to 6.6. As can be seen from these figures, neither value of CTL can give rise to significant power at relevant intraseasonal periods. Especially, the power above the red noise level is not seen at 30-50 day scale- the most prominent intraseasonal periodicity in the tropics. As we have seen in chapter 4, a uniform distribution of strength of EWF fails to simulate the observed structure for any values of CTL. Along with

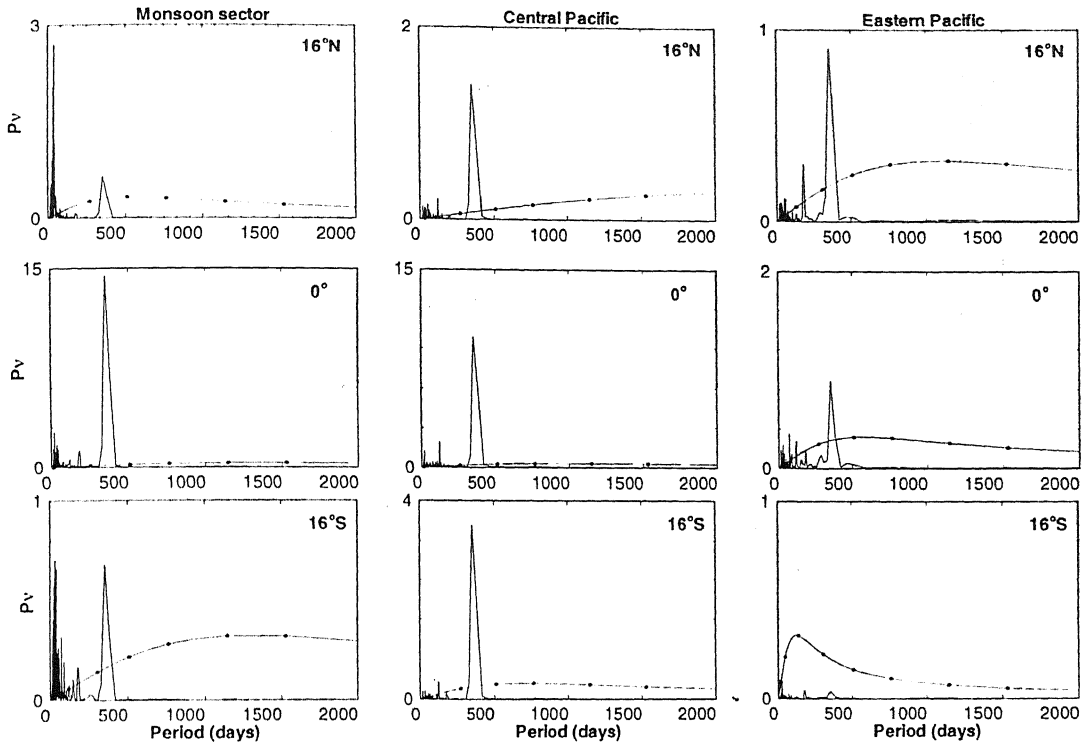

Figure 6.15: Same as figure 6.14, but for meridional wind

our present finding of the power spectrum, it now appears that a proper simulation of the tropical variabilities must involve a spatial and temporal distribution of the strength of EWF.

The power spectra with a (SST induced) space-time dependent strength of EWF are shown in figures from 6.7 to 6.9. Once again, the solid line and the solid line with solid circles represent, respectively, the power spectrum for $\tau = 0.5$ hour and the corresponding red noise spectrum. The corresponding spectra for $\tau = 1.5$ hour are represented by the dashed line and the dashed line with filled circles. As can be seen from these figures, the power spectrum shows significant power in a number of frequencies, corresponding to 3-7 days, 10-20 days and 30-60 days. However, the power is not always above red noise level in all locations, except for the 30-50 day wave, which exhibits a strong signal everywhere. The quasi-biweekly (or 10-20 day) oscillation also shows considerable power in several

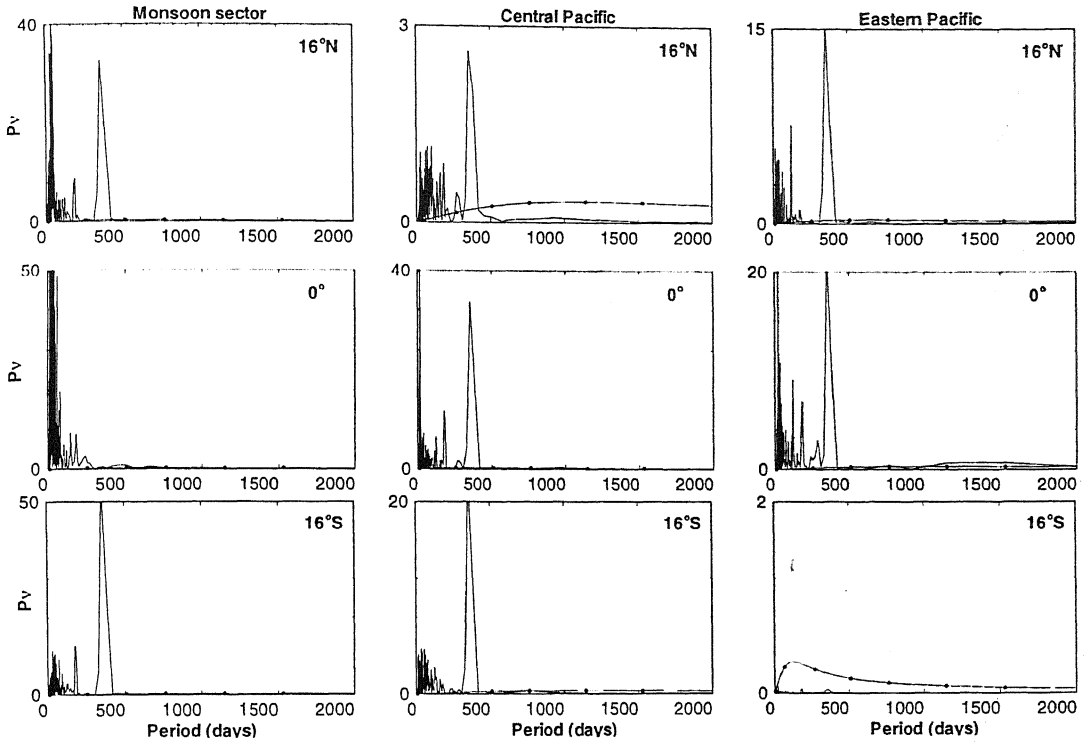

Figure 6.16: Same as figure 6.14, but for precipitation

locations. However, there appears to be only marginal power, although it is above the red noise level in many locations, at 3-7 day range. However, considering that our time series are obtained by averaging over rather large zonal extents, a process which might have weakened the signal, we shall consider the detailed structure of the oscillations at all these observed periods.

6.3.2 Interannual Oscillations

The tropical atmosphere is also characterized by a number of long period oscillations. Prominent among these are the quasi-biennial oscillations with a period between 18-36 months and the ENSO-type interannual oscillations with a period between 3-6 years. There is also evidence for decadal and interdecadal oscillations. We have, therefore, examined our 38-year model simulations for existence of oscillations at various observed frequencies. To validate our long-term simulation

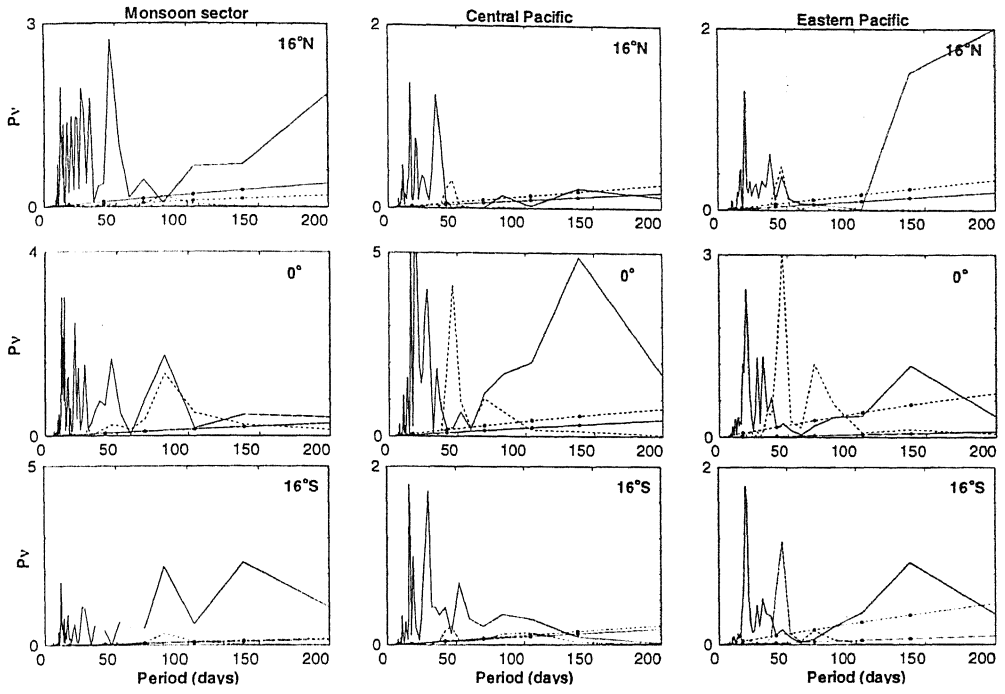

Figure 6.17: Power spectra of unfiltered time series of the model u field from one year simulation with winter and summer wind plotted with $\nu P(\nu)$ as the ordinate and period as abscissa. The solid line for summer wind+annual cycle in SST and dashed line for winter wind+ annual cycle in SST. The corresponding red noise spectra are marked with symbols.

and to check consistency with our one-year simulations, we have first examined the time series (written every two days) from our long-term simulation for the existence of intraseasonal oscillations. The results of this analysis are presented in figure 6.10, for two values of $\tau = 0.5$ hour (solid line) and 1.5 hour (dashed line). These results represent the power spectra of unfiltered time series model zonal wind (top panels), meridional wind (middle panels) and precipitation (bottom panels) at the equator. As indicated in the figures, the results are shown for the three zonal locations. Only the part of the power spectrum with a period less than annual time scale has been emphasized to examine the existence of prominent peaks at intraseasonal period above red noise level (lines with solid symbols).

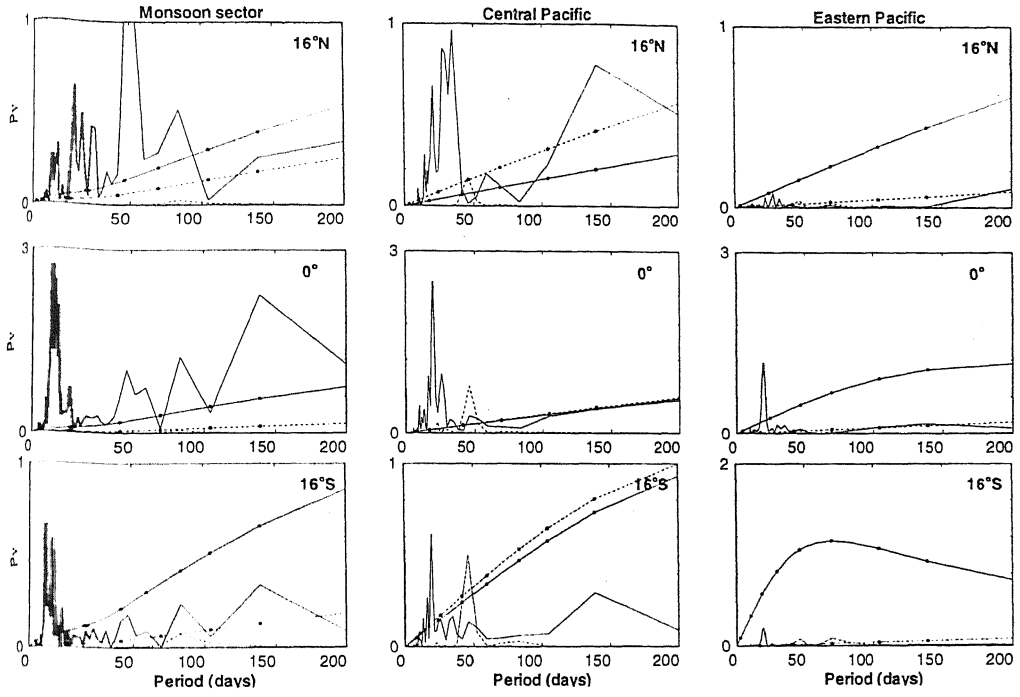

Figure 6.18: Same as figure 6.17, but for meridional wind

A prominent feature of the power spectra is the existence of a broad-band peak at intraseasonal frequency for the zonal wind and precipitation. However, the power in the meridional wind is generally below the red noise level at intraseasonal time scales. This is consistent with the results from the composite one-year simulation which show weak power for the meridional wind over most locations. The broad bands for the zonal wind and precipitation are, of course, indicative of substantial interannual variations of the characteristics of 30-50 day oscillations, a point we note for future investigation. However, the important conclusion for the present is that the two simulations with their different initial condition and mean fields generate simulations with a high degree of consistency. However, the long-term simulation also exhibits a strong annual cycle with very large power. To delineate the longer term oscillations with relatively weaker power, corresponding to quasi-biennial, interannual (3-7 years) and longer term (7-8 years) we have taken

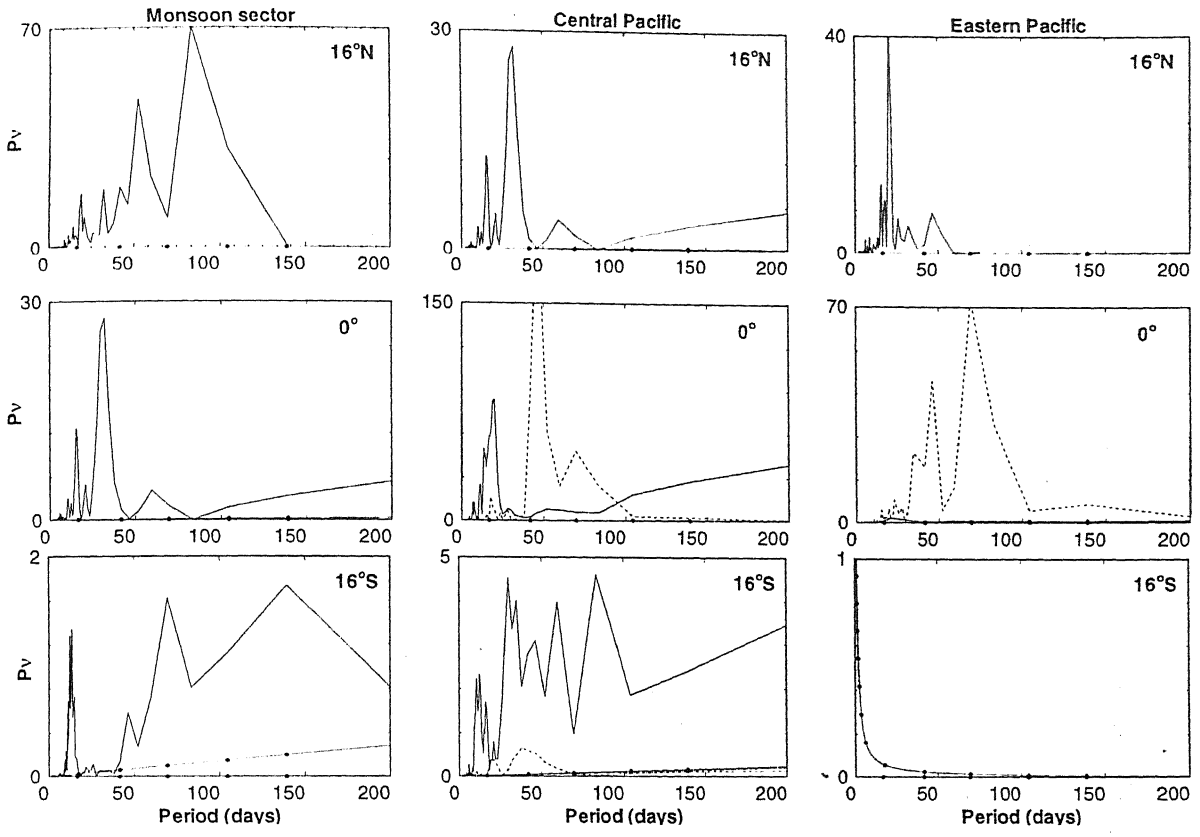

Figure 6.19: Same as figure 6.17, but for precipitation

a 10-month running average of our model time series. The results are shown in figures from 6.11 to 6.13. Most of these peaks are prominent only for one value of CTL, *viz* 0.5 hour. This is consistent with our finding that the value of $\tau = 0.5$ hour also generates the best simulation of the monthly structures of the tropical variabilities.

6.3.3 Role of the Mean Annual Cycle

There are two ways in which the mean annual cycle influences the dynamics in our model. While the annual cycle of the climatological mean winds is incorporated through the advection, the annual cycle of SST enters through its effect on the strength of EWF. In the following section we shall describe the relative roles of

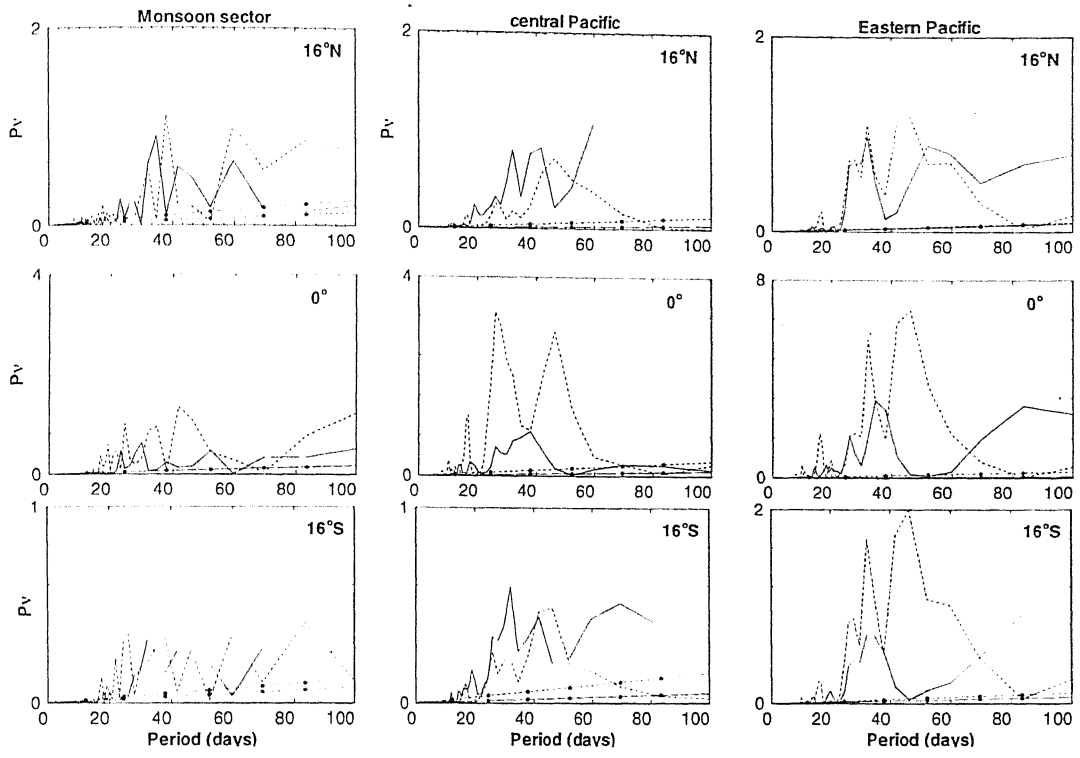

Figure 6.20: Power spectra of unfiltered time series of the model u field from one year simulation with winter and summer SST plotted with $\nu P(\nu)$ as the ordinate and period as abscissa. The solid line for summer SST+annual cycle in the wind and dashed line for winter SST+ annual cycle in the wind. The corresponding red noise spectra are marked with symbols.

the annual cycles of the mean wind and SST.

6.3.4 Role of Annual Cycle of Mean Wind

The results of the experiment to determine the role of the annual cycle of the mean wind are shown in figure 6.17 to 6.19. The nine panels in figure 6.17 show the power spectra for the zonal wind for one-year simulations with only winter (December, January, February) and summer (June, July, August) averaged mean winds at different locations as indicated in the panels. The solid line represents the power spectra for the summer mean wind run and the solid line with symbol represents the corresponding red noise spectrum. The power spectra and the

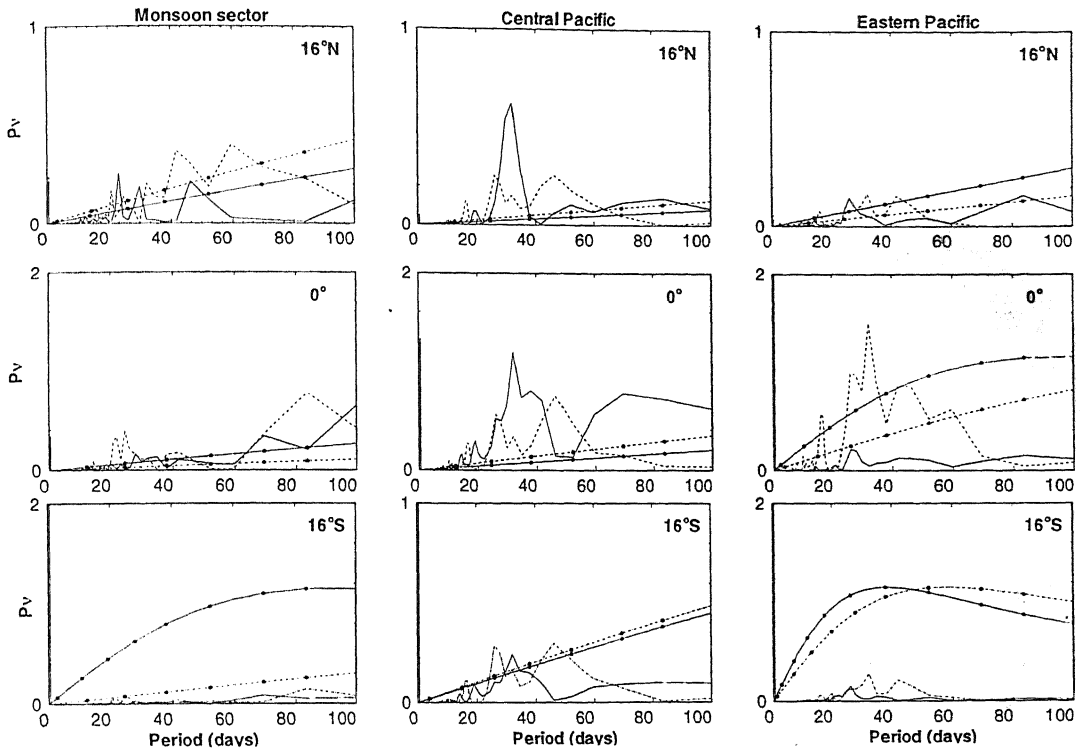

Figure 6.21: Same as figure 6.20, but for meridional wind

corresponding red noise for the winter mean wind simulation are represented by the dashed line and the dashed line with symbol, respectively.

As can be seen from figure 6.17, there are prominent peaks at intraseasonal frequencies for both the summer and the winter simulations. However, in almost all cases the peaks in the power spectra are located around distinct frequencies for the winter and the summer simulations. Figure 6.17 shows a remarkable and persistent winter-summer asymmetry in the genesis of the intraseasonal oscillations. In particular, while the peak at the power spectra occurs almost always around 50 days for the winter simulation, it is located at around 30 days for the summer simulation. The differential response to the winter and the summer mean winds, therefore, appears to be a primary mechanism for the broad band nature of the 30-50 day oscillations. A more detailed analysis of the effect of the annual cycle of the mean wind on the other characteristics of the 30-50 day oscillations will be

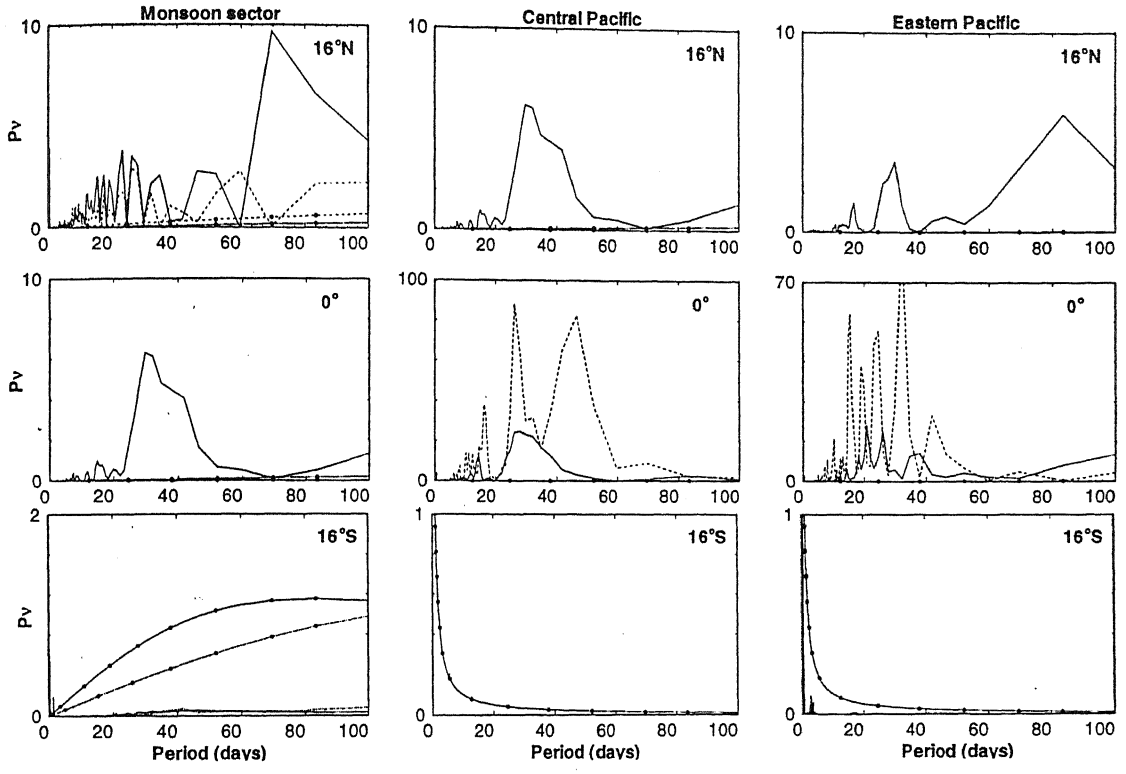

Figure 6.22: Same as figure 6.20, but for precipitation

discussed in connection with the structure of 30-50 day oscillations. The effect of the annual cycle of the mean wind, however, is much more prominent on the oscillations of the meridional wind component, shown in figure 6.18. In particular, there is very little power above red noise at 30-50 days at most locations. This is especially true for the winter mean wind (dashed line), and over the eastern Pacific region. The effect of the annual cycle on the tropical oscillations can be seen from figure 6.19, which shows the power spectra of precipitation with summer mean wind (solid line) and winter mean wind (dashed line). The corresponding red noise spectra are represented by the lines with symbols. As can be seen from this figure, the 30-50 day signal in precipitation is excited by only the summer (winter) mean wind in the monsoon sector (eastern Pacific). This feature can be verified by analyzing data over the two sectors specifically for the winter and the summer months. Indeed, it is already known that the 30-50 day signal over the

monsoon region is prominent only in the summer season.

6.3.5 Role of the Annual Cycle of SST

Although it is often argued that the oceanic processes do not have significant influence over the oscillations at intraseasonal time scales, such a scenario is not supported by observations. For example, Krishnamurti *et al.* (1988) found significant modulation of the air-sea fluxes at 30-50 day time scales. Significant oscillations at 30-50 day time scales of the oceanic variables, in particular SST, have been reported by a number of authors. Since in our formalism SST plays a significant role through its modulation of the strength of EWF, it is necessary to examine the effect of the spatio-temporal distribution of SST on the structure of the intraseasonal oscillations. The results of the experiment to determine the role of the annual cycle of the SST are shown in figures 6.20 to 6.22. The nine panels in figure 6.20 show the power spectra for the zonal wind for one-year simulations with only winter (December, January and February) and summer (June, July and August) averaged SST at different locations as indicated in the panels. The solid line represents the power spectra for the summer SST-run and the solid line with symbol represents the corresponding red noise spectrum. The power spectra and the corresponding red noise for the winter SST simulations are represented by the dashed line and the dashed line with symbol respectively. The winter-summer asymmetry in terms of the positions of the peak, apparent in winter-wind and summer-wind runs, is not present in this case. There is clear dominance of power for the winter-SST run over summer-SST in most of the locations. However, both u and v (figures 6.20 and 6.21) spectra continue to exhibit much weaker power over the off equatorial positions.

Role of Interannual Variability of SST

At the interannual time scale, the most important effect in our simulation is likely to be the interannual variability of SST. The analyses of our model re-

sults from long-period simulation show that the ability of the model to generate interannual oscillations at observed interannual periodicities. However, these interannual oscillations are likely to be the response of the atmospheric dynamics to the interannual variations in the moist feedback induced by the interannual variability in the SST, which in turn may be due to ocean-atmosphere interaction.

Perpetual Winter and Perpetual Summer Simulations

As we have seen above, the annual cycle of mean wind and SST effect in the genesis of ISO in somewhat similar but still has its own characteristics. To investigate the effect of absence of both the annual cycles (mean wind and SST), we have generated two one-year simulations with only winter mean wind and winter SST (perpetual winter) and with only summer mean wind and summer SST (perpetual summer). The power spectra at different locations exhibited (not shown here) peaks at intraseasonal time scale at several locations. However, the periodicity of the perpetual summer was found to be generally around 20 days, while that for perpetual summer was about sixty days in many cases. This is consistent with our findings with the summer and winter mean winds that summer (winter) mean conditions favor short(long) period oscillations.

6.4 Conclusions

A noteworthy feature of the simulations discussed here is the persistent appearance of an oscillation at 30-50 day time scale for diverse dynamical conditions. It appears that the genesis of 30-50 day oscillation is not crucially dependent on the details of the mean field. However, the observed 30-50 day oscillation is characterized by several other properties, in particular, its well known eastward phase propagation. While the excitation of a 30-50 day and other intraseasonal oscillations may not crucially depend on the structure of the mean fields, the detailed properties of the oscillations may. We will discuss this in more detail in subsequent chapters.

Another effect of the annual cycle of the mean wind is that while there are significant peaks at higher frequencies for summer mean wind, there is very little power above 30-50 day time scale for the winter mean wind. Thus, the existence of ISO at 3-7 day and 10-20 day time scales may crucially depend on the annual cycle of the mean wind.

The model is capable of supporting interannual oscillations at observed interannual variabilities also. This is essentially in response to the interannual variation in the SST-induced convective forcing; the interannual variabilities disappear when the interannual variability in SST is removed (figures 6.14 to 6.16). While the question of excitation of interannual variability in SST has to be addressed, which is likely to be determined by ocean-atmosphere coupling, the success of the model in simulating these interannual oscillations without any explicit ocean-atmosphere coupling implies that our atmospheric model can respond to the SST induced forcing so as to give rise to the observed variabilities.

Chapter 7

The Spectrum of Oscillations: The 30-50 Day Waves

One of the most well investigated intraseasonal oscillations (ISO1) in terms of observation is the 30-50 day oscillations. The 30-50 day oscillation was first detected by Madden and Julian (1971, 1972) in the spectral and cross-spectral analyses of time series of tropical station data and is now also referred to as the Madden and Julian Oscillations (MJO). Subsequently, a large number of observational studies reported the presence of a spectrum of oscillations with periods ranging from 10 to 90 days. Until recently most of the studies on ISO1 were based on data sets which were sparce and insufficient for a systematic analysis of phenomena on intraseasonal time scales. However, these studies had helped to bring out the broad characteristics of the ISO1. As revealed by these observations, the 30-50 day oscillations take the form of an eastward moving circulation cell in the equatorial zonal plane and are most prominent in the zonal velocity and surface pressure, with the amplitudes maximum near the equator. The frequency responses are rather broad, with convective signals having comparable power in the time periods ranging from 30-95 days and the zonal wave numbers lying between 1 and 3. Comparatively, the dynamical fields possess much narrower peaks concentrated in zonal wave number 1 and time periods of 50-60 days. We shall

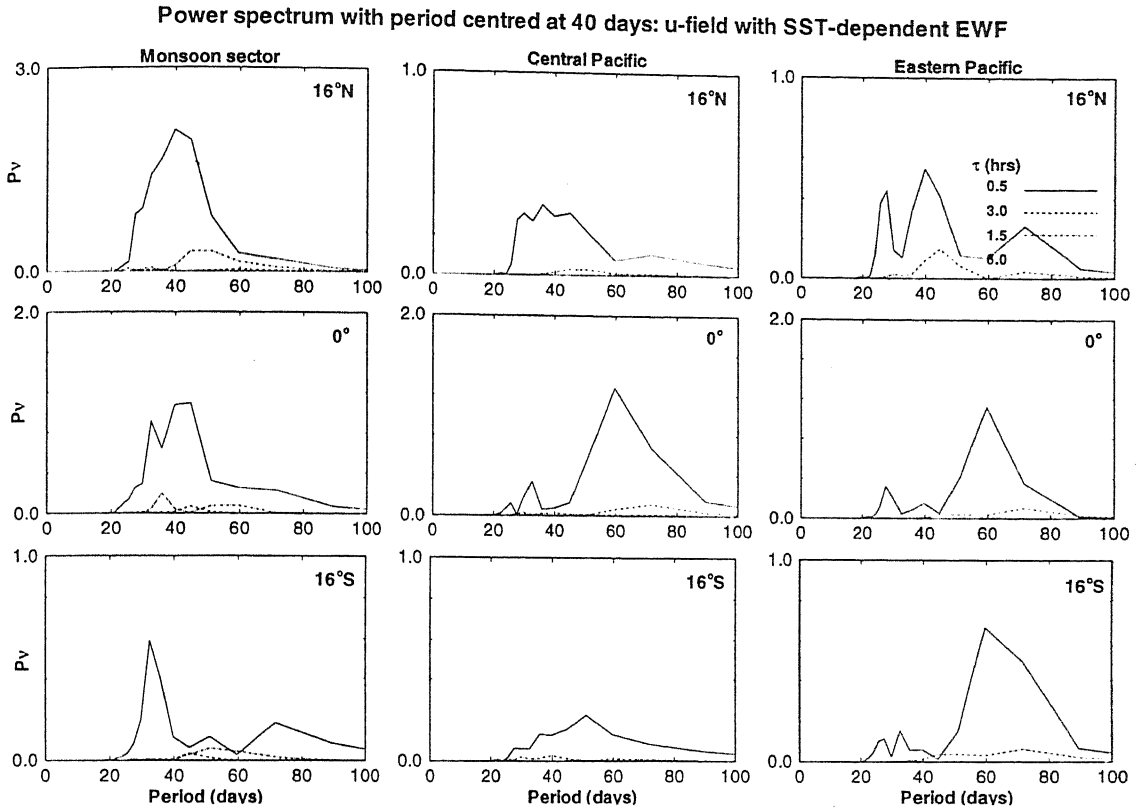

Figure 7.1: Power spectra of zonal wind filtered at 30-50 days plotted for four values of CTL with $\nu P(\nu)$ as the ordinate and period as abscissa, where P is the power and ν is the frequency. For each value of CTL the fields have been normalized to their respective maxumum.

refer to these eastward propagating oscillations with time period of several weeks as ISO1 which is, observationally, the most prominent intraseasonal oscillation in the tropics. Its other feature is that the wind perturbation appears to propagate around the globe but strong convection appears to be confined within the Indian Ocean/western Pacific sector. Detailed analysis of several recent data sets has helped to bring out the rich structure and dynamics of ISO1. Using the cross covariance between outgoing long wave radiation (OLR): wind and temperature, Hendon and Salby (1994) constructed a composite life cycle of ISO1. This displays characteristics of both forced and radiating responses. The forced response is basically a coupled Rossby-Kelvin wave (Gill, 1980) that migrates eastward with the convection anomaly at about 5 ms^{-1} across the eastern hemisphere.

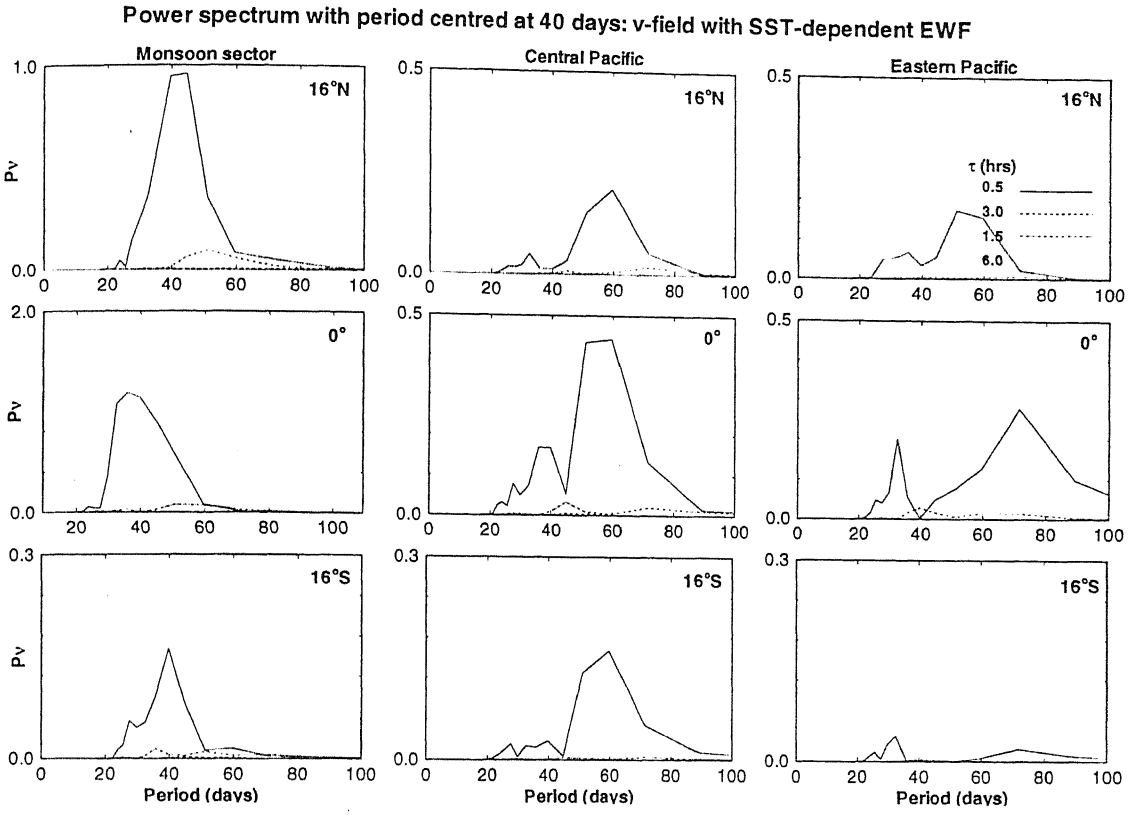

Figure 7.2: Same as Fig. 7.1, but for meridional wind.

The radiating response appears as a Kelvin wave, which propagates eastward at about 10 ms^{-1} into the western hemisphere away from the convective anomaly. Energetics deduced from the covariances between convection, temperature, and vertical motion indicate a close relationship between the relative phase of these quantities and amplification of ISO1. During the growth-stage of anomalous convection, the heating, temperature and vertical velocity are positively correlated. This is consistent with the relationship needed for growth via production and conversion of eddy available potential energy (EAPE). Nevertheless, the heating perturbation is nearly in quadrature with the temperature anomaly, which implies little production of EAPE after its maturity.

As a modulator of precipitation, the ISO have a special appeal to the meteorologists belonging to monsoon regions where agriculture is the main source of income. Also, the fact that midlatitude circulations are teleconnected to ISO1 is

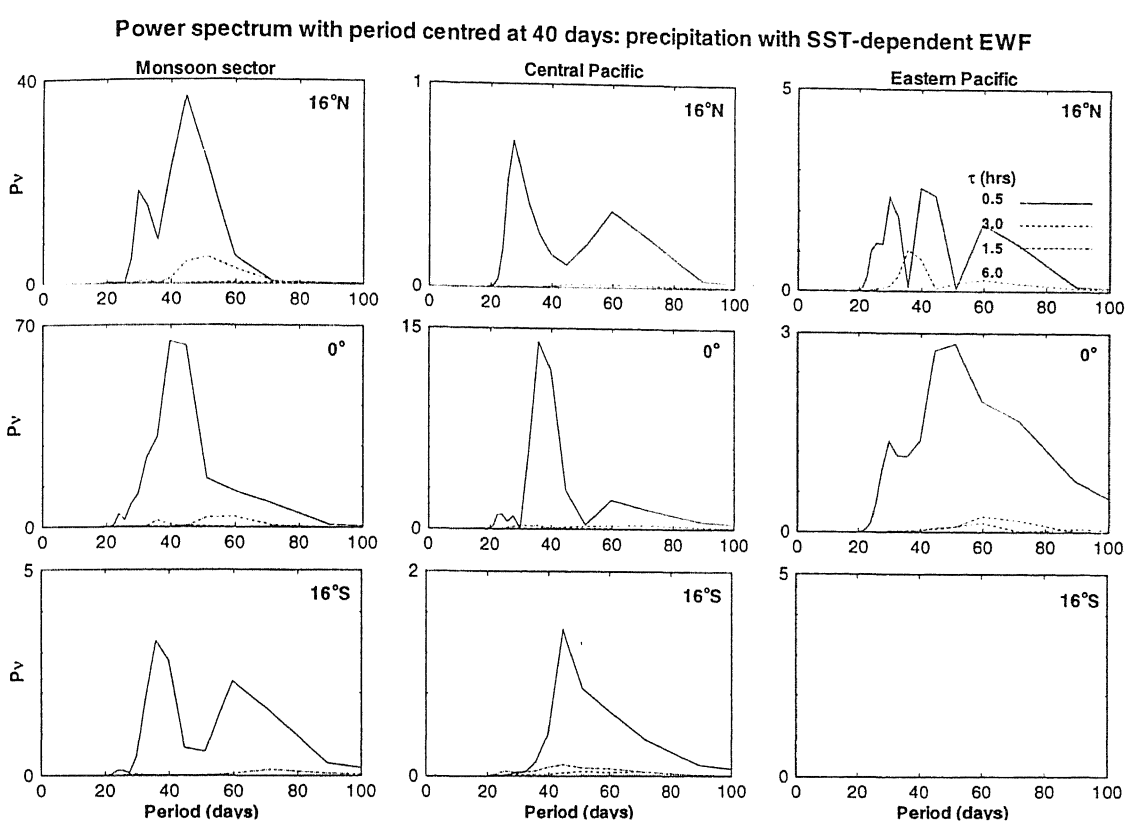

Figure 7.3: Same as Fig. 7.1, but for precipitation.

corroborated by many observations. There are some evidences that the formation of incipient vortex related to tropical cyclone may be related to ISO1 (Nakazawa, 1986). Considering its potentiality in influencing global weather systems, it is not surprising that special attention has been devoted to modeling and simulating these tropical variabilities. However, even after many years of efforts, the regional and global manifestations of ISO1 are still evasive to modeling studies. Considerable insight has been gained on the mechanism of selective excitation at preferred time scales of the oscillation and on the interaction of convection and the large-scale dynamics associated with it. However, a clear picture of organized convection and its relationship to the circulation in general is still lacking. These modeling studies have shed considerable light on the mechanism of genesis and evolution of ISO1.

The most distinctive aspect of the oscillation, namely its slow eastward move-

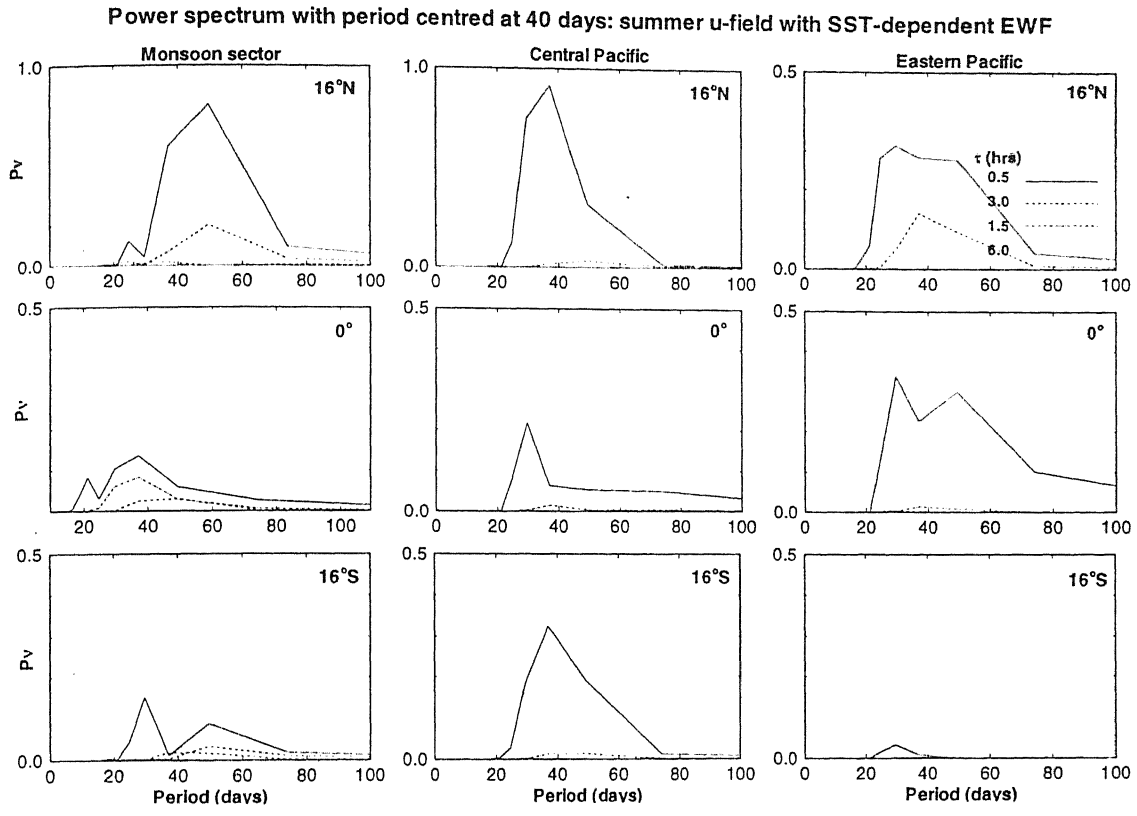

Figure 7.4: Same as Fig. 7.1, but for summer months.

ment and equatorial emplacement of its maxima, prompted earlier investigators to search for an explanation and analytical formulation of the phenomenon in terms of Kelvin wave dynamics. Parker (1973) interpreted the oscillation as a Kelvin wave in an equatorial β-plane mode studied by Matsuno (1966), although the vertical scale of low-frequency Kelvin wave is very small in the absence of heating. Murakami *et al.* (1984) studied the three dimensional structure and phase propagation of the 40-50 day oscillation and concluded that its major energy source is the conversion of potential energy to kinetic energy. Hayashi and Sumi (1986) have studied 30-40 day oscillation in a GCM for ocean covered earth. They have used a flat lower boundary with a specified zonally symmetric temperature. The precipitation and zonal wind anomaly have a large eastward propagating wave number 1 component. This study suggests that the zonal inhomogeneities in the climatological tropical convection and orography are not essential to the exis-

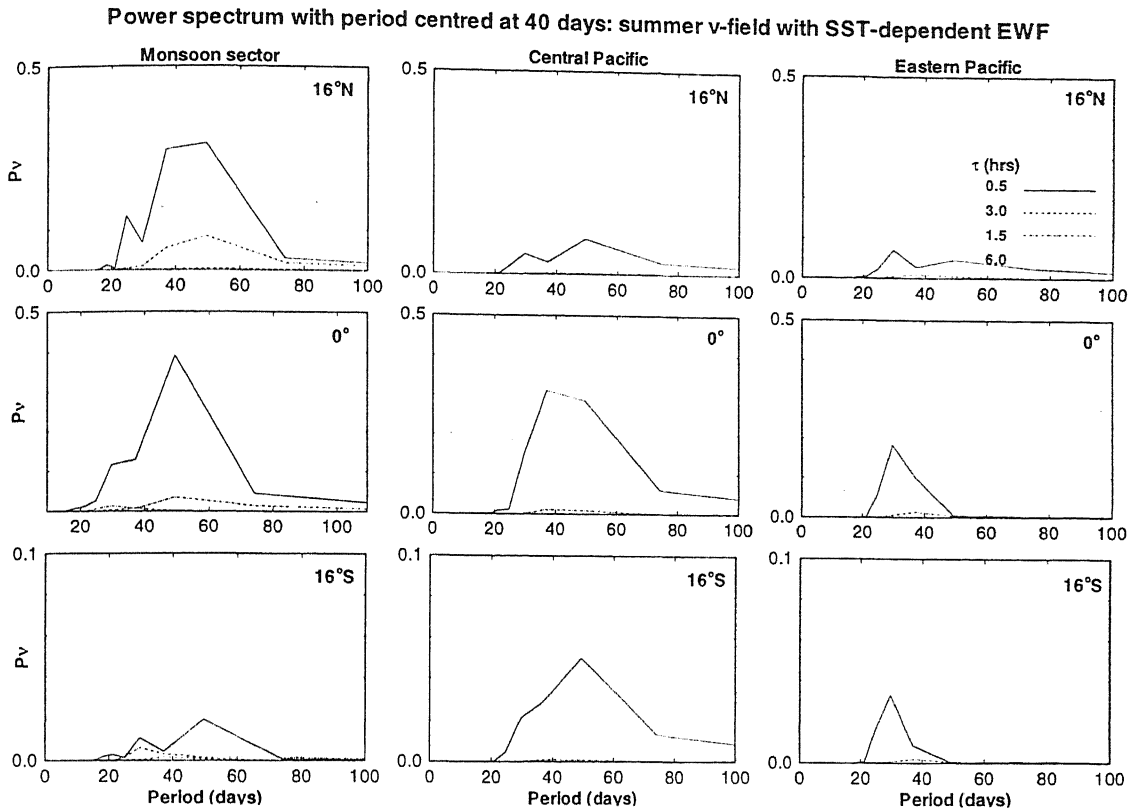

Figure 7.5: Same as Fig. 7.1, but for meridional wind in summer months.

tence of the ISO1. Using a fully stratified tropical model which includes cumulus friction and Hadley cell basic state circulations, they showed that some eastward propagation of tropical circulation features can occur even when the anomaly heating remain fixed in one position.

A fundamental problem in invoking the Kelvin wave dynamics to explain ISO1, the apparent disparity in the phase speed, was addressed by Swinbank *et al.* (1986). They have come up with some evidence that this may be understood in terms of moist Kelvin wave dynamics, if effect of latent heat release on stability is properly taken into account. A simple model-calculation leads to the conclusion that precipitation associated with the Kelvin wave reduces static stability and so decreases the phase speed. These conclusions were further confirmed by two GCM experiments in which latent heat-release was increased, first by increasing SST and second by doubling the value of latent heat constant. In both cases the wave

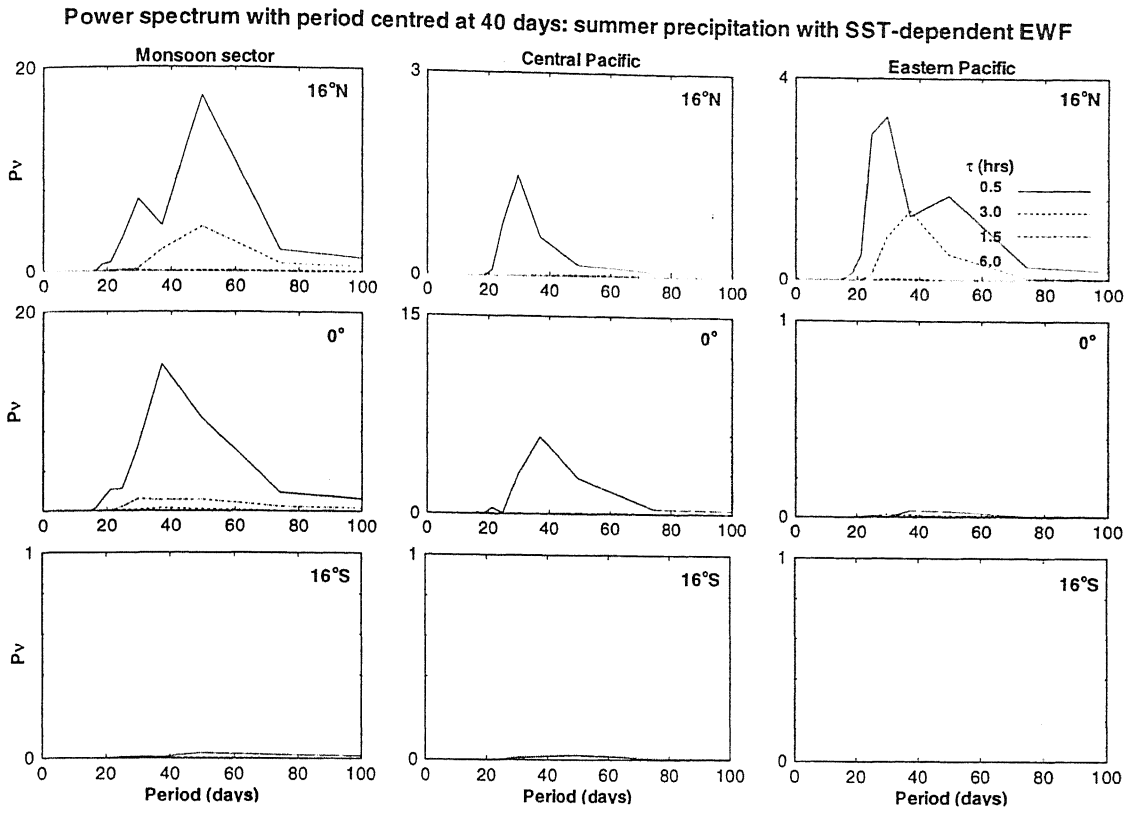

Figure 7.6: Same as Fig. 7.1, but for precipitation in summer months.

period was increased. The role of the moist feedbacks, and in particular EWF on the stability and dynamics of the Kelvin wave was investigated by Neelin *et al.* (1987) and Emanuel (1987). Though this mechanism destabilizes the Kelvin wave, the selection at observed period could not be attained.

One of the most successful mechanisms of genesis of ISO1 was provided by Goswami and Rao (1994) involving Kelvin wave dynamics in presence of an explicit moisture dynamics governed by a convective time lag. In particular, the model could successfully predict excitation of the Kelvin wave at 30-50 day time scale with observed spectral characteristics. Thus, our present model with a convective time lag is well suited for investigation of ISO1. However, as mentioned above, the recent analyses reveal a structure of ISO1 that has strong spatio-temporal dependence. These observed characteristics provide powerful constraints for model simulations as well as for any mechanism proposed for

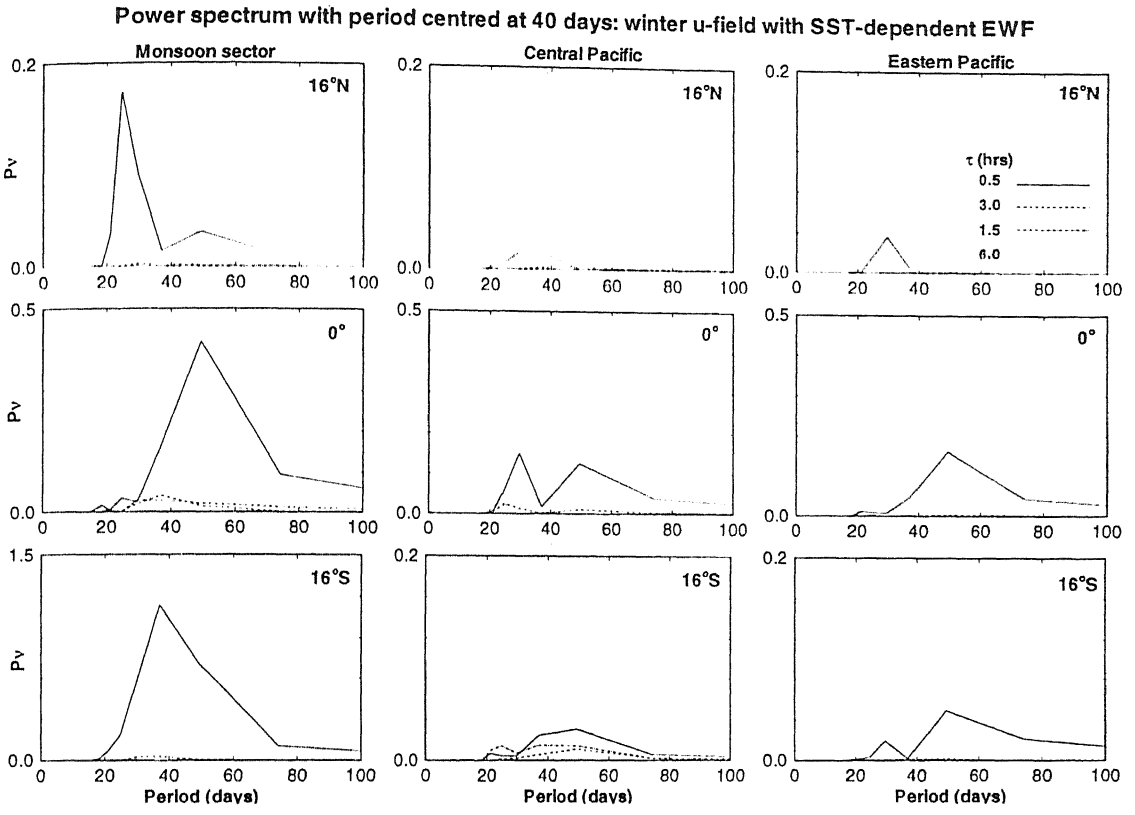

Figure 7.7: Same as Fig. 7.1, but for winter months.

the 30-50 day oscillations. We, therefore, first analyze our model simulations in terms of existence and structure of the 30-50 day oscillation. As we have seen earlier, only an SST-dependent EWF can generate a satisfactory simulation of the tropical monthly anomalies. The significant power in 30-50 day oscillation is present only for SST dependent EWF, although the high frequency part of the spectrum peaks above red noise level even for a uniform strength of EWF. Thus it seems the SST-dependent EWF is more relevant for the dynamics of ISO1 in general. Besides being considered the SST-dependent EWF, a few special cases will also be discussed to isolate and identify the relative role of the mean wind. We first consider the composite one-year model simulations for different dynamical conditions. A certain specific issue will then be addressed using both interannual and one-year simulations from specific experiments.

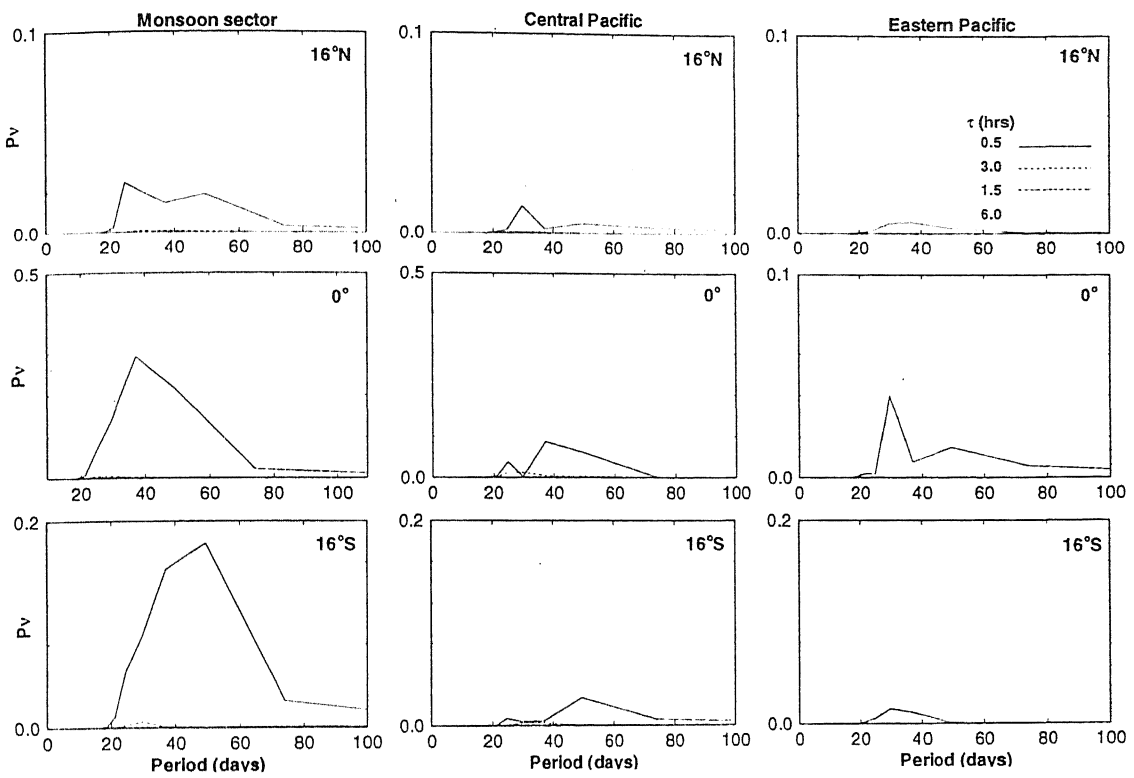

Figure 7.8: Same as Fig. 7.1, but for meridional wind in winter months.

7.1 The Characteristics of the Power Spectrum

As we have seen, our model of the tropical atmosphere supports a prominent signal at 30-50 days at different locations and under different dynamical conditions. Although this global scale phenomenon is present throughout the year, its strength and behavior vary with location as well as with the season. We shall address this issue first in terms of the power spectra of the composite model simulation filtered at 30-50 days at different locations. The unfiltered time series have been generated by averaging the fields over a zonal extent of 60° centered at 90°E (Monsoon sector), 80°W (Central Pacific) and 160°W (Eastern Pacific). We shall consider three latitudinal positions, *viz.* the equator, 16°N and 16°S.

(a) Analysis of the 12-month data

Figures 7.1 to 7.3 show the power spectra of the model u, v and precipitation

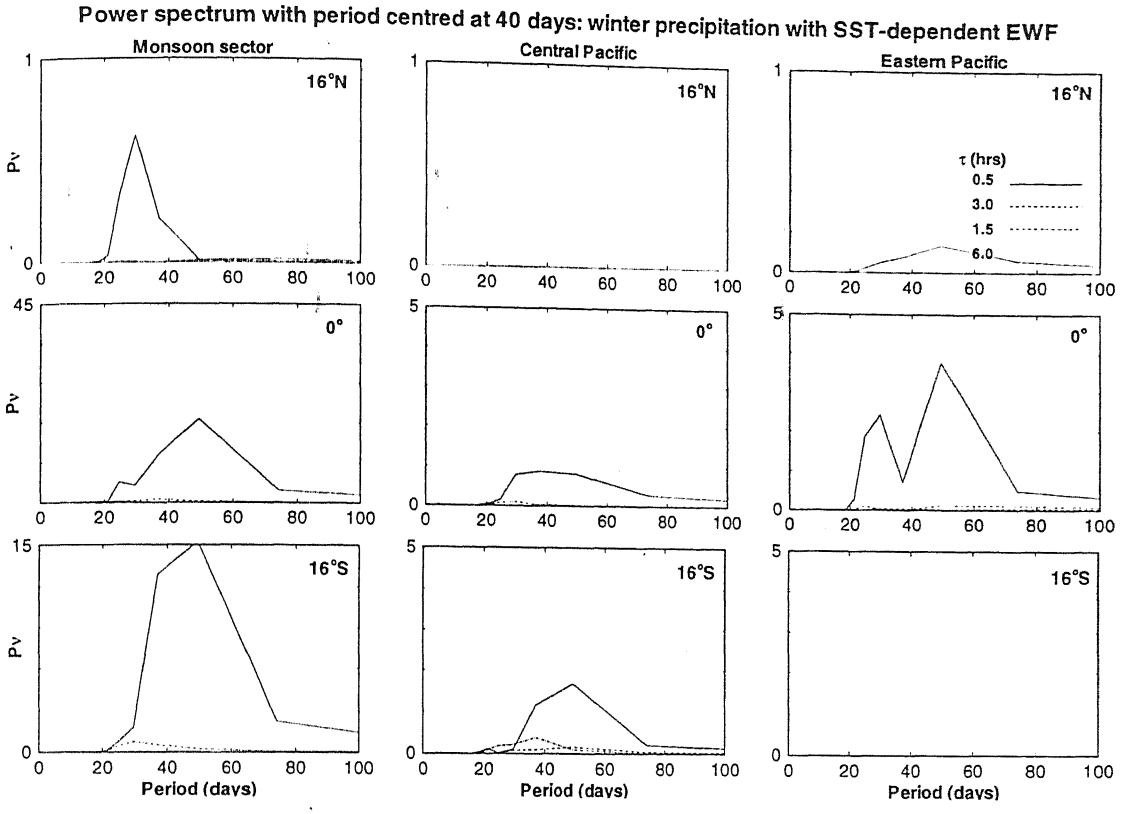

Figure 7.9:. Same as Fig. 7.1, but for precipitation in winter months.

fields from the composite one-year simulation filtered at 30-50 days respectively. The results represent an analysis of an entire year data of at different locations. The four curves in each panel represent the power spectra for four different values of CTL. As can be seen from these figures, the model in general supports ISO with 30-50 day time scale. However, it is evident that only $\tau = 0.5$ hr. gives rise to the most significant signal at 30-50 days time scale. A much quoted feature of this ISO is its presence in the dynamical field throughout the globe. Indeed, as can be seen from figure 7.1 there are almost equally strong signals for all the three zonal sectors, especially over the equator. Another significant characteristic of the power spectra is its larger amplitude over the equator compared to that at higher latitude, implying an equatorially trapped nature. The corresponding results for the model v are shown in the figure 7.2. The conclusions similar to those for the model u also hold for the v. But the power of v is relatively less

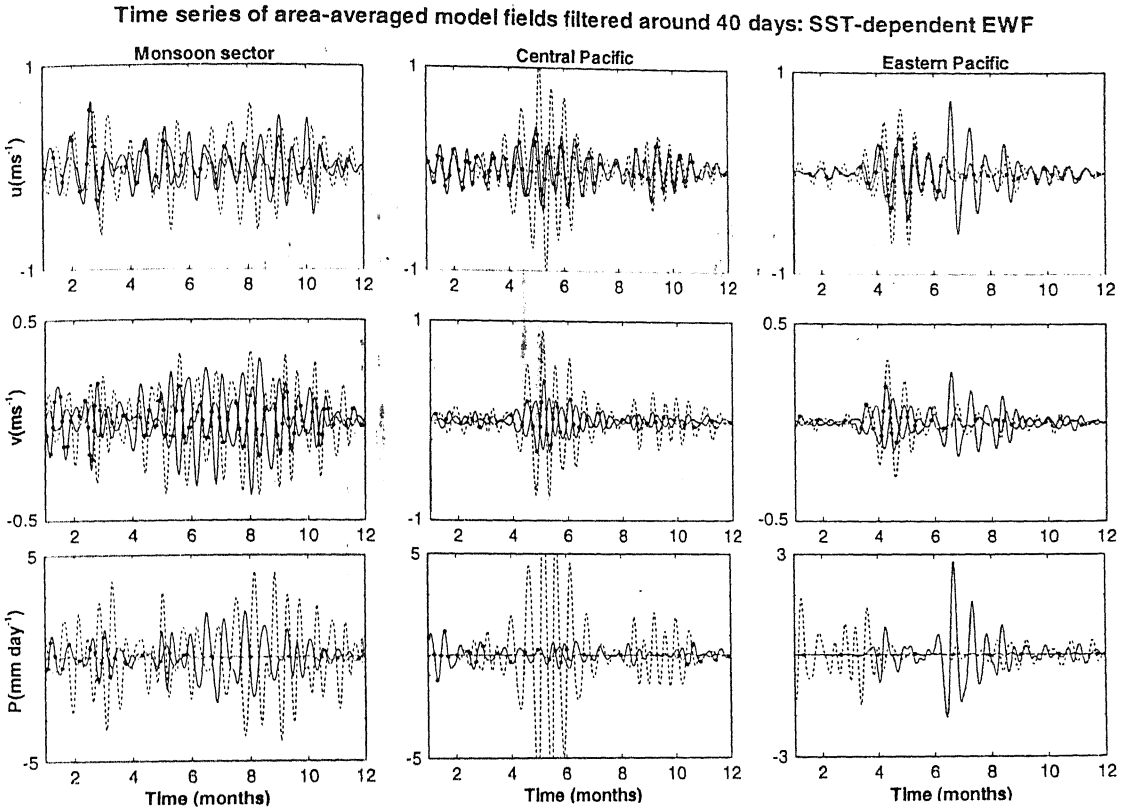

Figure 7.10: The time series of zonal and meridional wind components and precipitation filtered around 40 days. The solid, dashed and solid with symbol lines represent 10^oN, 0^o and 10^oS respectively.

than the corresponding value for the u. In contrast to the u and v, the power spectra for precipitation show pronounced zonal as well as latitudinal variations. In particular, the signal over the monsoon region is much stronger than over the other two regions. Similarly, in the meridional direction the strongest signal appears over the equator.

(b) Analysis of Summer and Winter Fields

The activity of ISO shows pronounced seasonality. This seasonality is understandable, if its major energy source is the large-scale convection associated with the seasonally migrating ITCZ. It was found that the related cloud activity favors the summer hemisphere and the general location of ITCZ (Zangvin, 1975; Wang and Rui 1990; Weickmann *et al.* 1985). To examine this we have separately

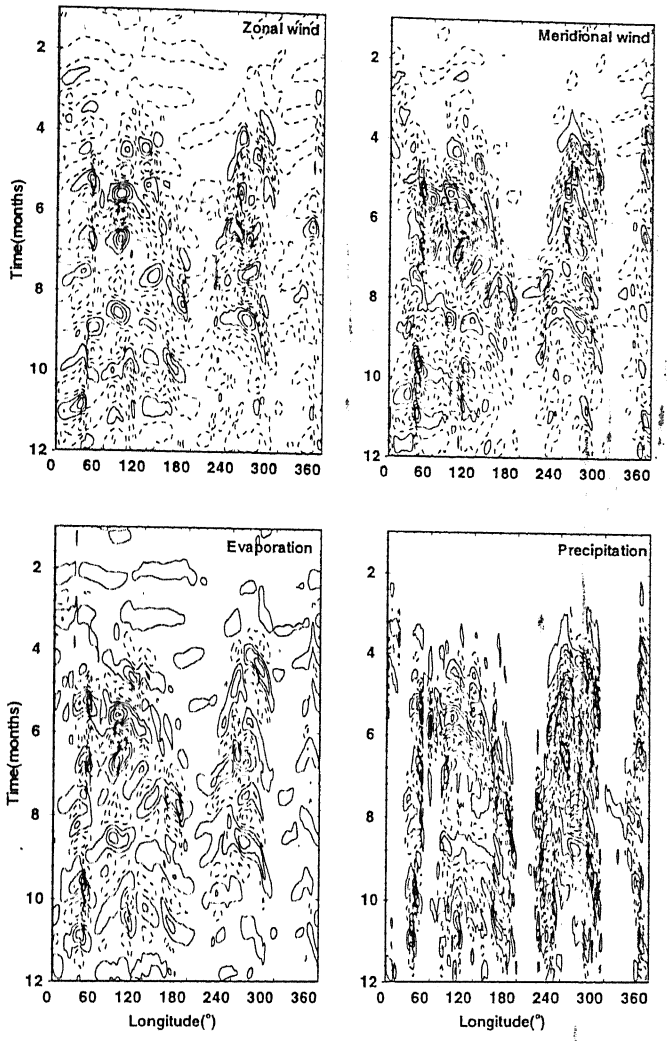

Figure 7.11: The time-longitude structure of model fields from a composite one-year simulation at 10°N for τ =0.5 hr.; filtered at 30-50 day. Negative contours are dashed

studied the power spectra of time series of the filtered model fields for the winter (January to May) and the summer (June to October) months. Figures 7.4 to 7.6 show, respectively, the power spectra of the filtered model u, v and precipitation fields for the summer months at different zonal and latitudinal regions. The corresponding results for the winter months are shown in figures 7.7 to 7.9.

A comparison of the figures 7.4 and 7.1 shows that the equatorial trapping seen for the u for the complete year is not supported by the summer fields, which show comparable and sometimes even more power in the higher latitude than over the

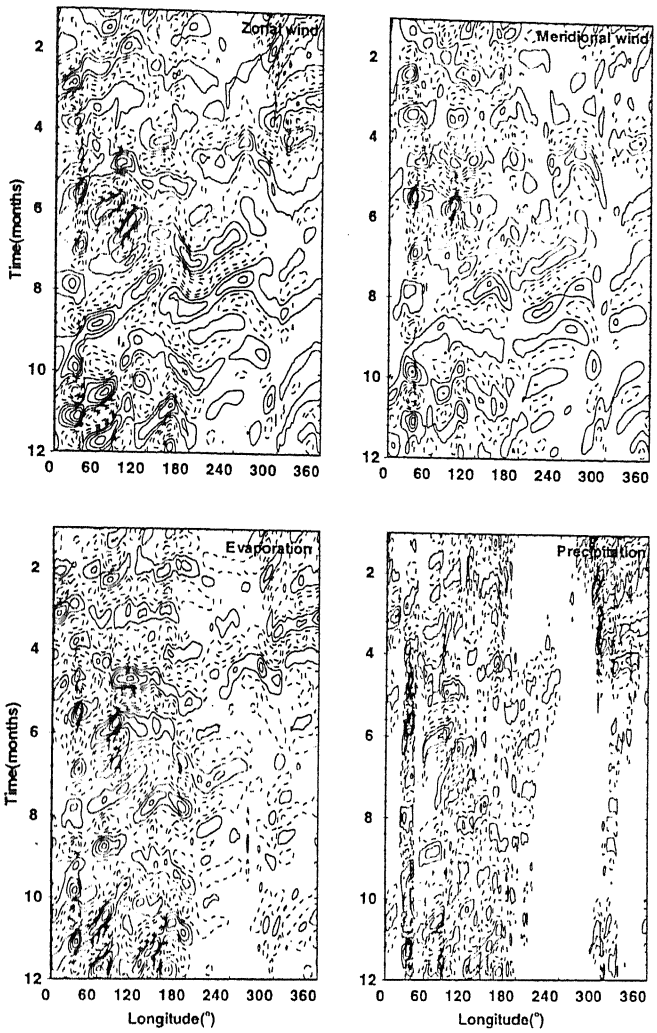

Figure 7.12: Same as Fig 7.11, but over the equator.

equator. This difference is much more pronounced over the monsoon region than over the Pacific sectors. This observation has been made by Nishi (1989) and Handon and Salby (1994) who noticed that the amplitude of the signals do not drop away from the equator as rapidly as the simulated tropical circulation does. These anomalous signals show high degree of symmetry when the convection neighbors the equator. In addition, more the anomalous convection away from the equator, greater its asymmetry at the equator. This fact could be pointed out as one of the reasons why the power at higher latitudes in the monsoon region is more than over the equator in summer.

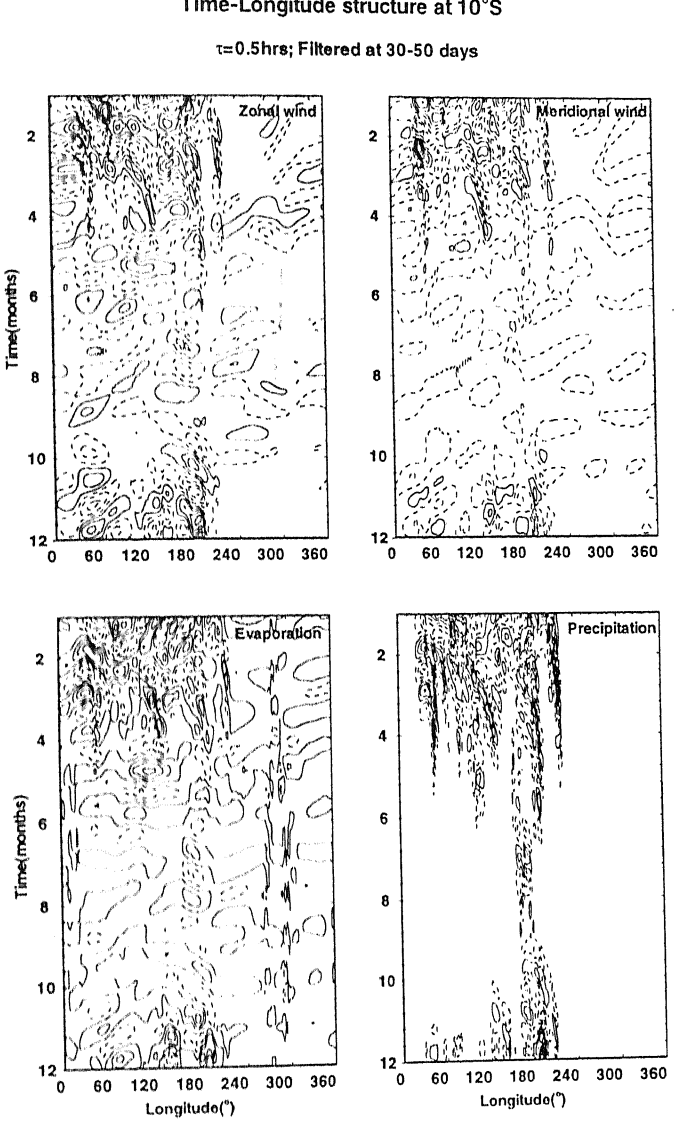

Figure 7.13: Same as Fig 7.11, but over 10^oS

Murakami *et al.* (1986) utilized OLR data over a tropical belt between 45^oN and 45^oS during the eight years of 1975-77 and 1979-83. They found that over the Northern and Southern Hemispheres in the monsoon region, modes in the 20-90 day period band were more pronounced during the summer than winter.

The characteristics of 30-50 day oscillations also show considerable zonal variations. The analysis of OLR data (from 1974 to 1986) carried out by Lau and Chan (1988) revealed the following facts. The peaks in spectra of OLR in 30-50 day range are mostly confined to the tropical area west of dateline ($80^o - 120^o$E). Along the equator the signal is most pronounced in the Indian Ocean region and drop

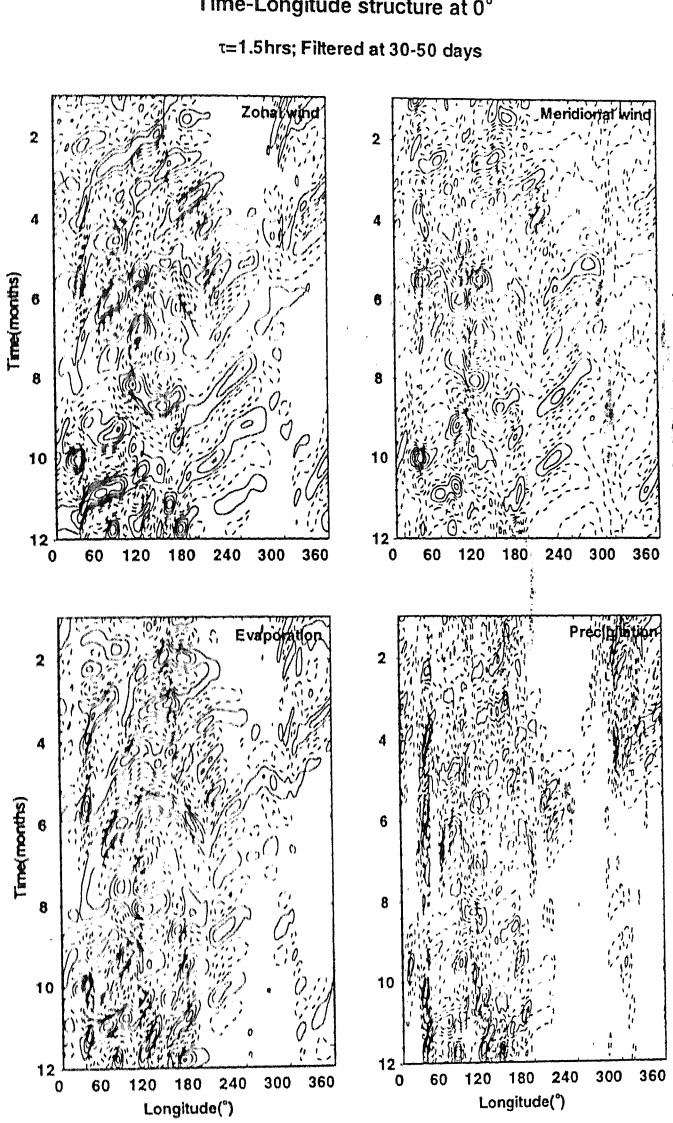

Figure 7.15: Same as Fig 7.14, but over the equator

observed period was found to change from 50 days in boreal winter to about 35 days in boreal summer over the Indian ocean regions (Hartmann *et al.*, 1992). A comparison of figures 7.4 and 7.7 clearly shows that, over the equator and 16°S in the monsoon sector the spectral peaks of zonal wind shift from a higher period in winter to a lower one in summer. In particular, over the equator this shift is from about 50 to 35 days, in accordance with Hartmann *et al.* 's finding. The most remarkable difference in the power spectra of the summer precipitation field from those for the full year is the absence of any significant power in the southern Hemisphere. Like in mean convection, the anomaly convection is dominant in the

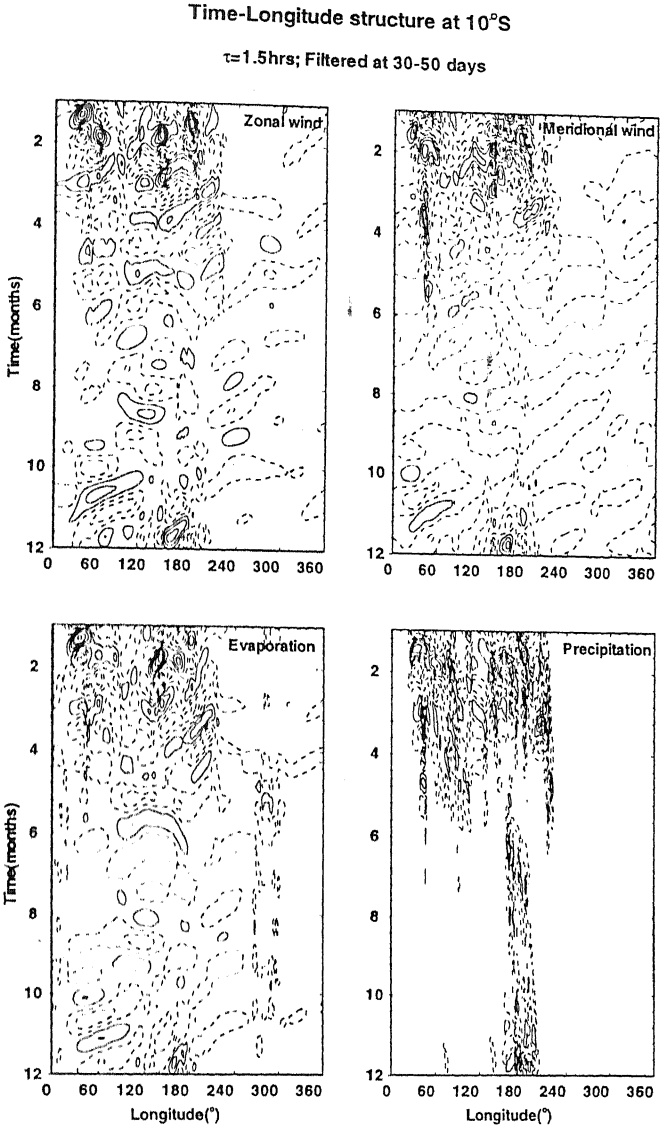

Figure 7.16: Same as Fig 7.14, but over 10°S

summer hemisphere.

(c) Time Series of Model Fields

To investigate the phase relationships between various model fields, we have examined the time series of the filtered model fields at different locations as shown in figure 7.10. In each panel, we consider variables at three latitudes: equator (dash line), 16°N (solid line) and 16°S (solid line with symbol). As before, the model fields have been averaged over three zonal regions as indicated in the panels. The top, middle and the bottom panels represent, respectively, the zonal wind, meridional wind and the precipitation field, as indicated in the figures. It

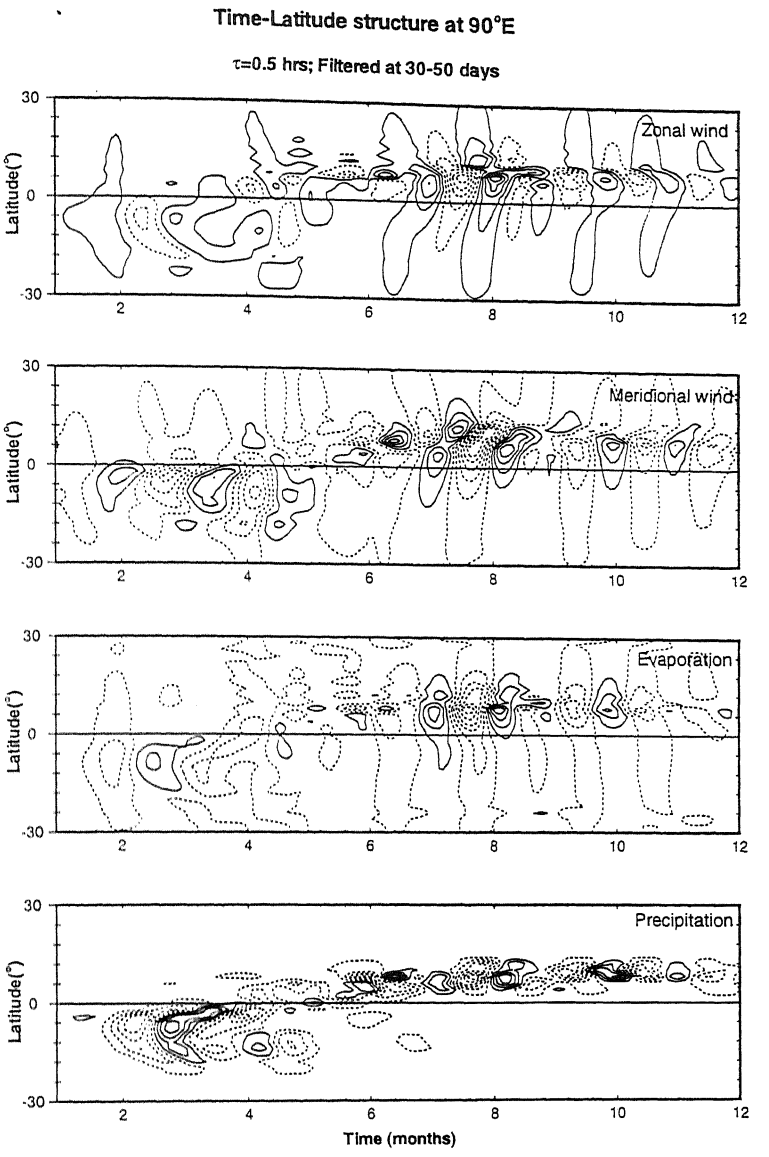

Figure 7.17: The time-latitude structure of model fields from a composite one-year simulation at the 90°E for τ =0.5 hr.; filtered at 30-50 day. Negative contours are dashed

is evident from the figure 7.10 that zonal wind at all the latitude in the Central Pacific and Eastern Pacific are almost in phase. But, no such clear relationship is seen among the zonal wind at three latitudes in the monsoon sector. In meridional components the striking feature is the out of phase nature of wind at 16°N and 16°S. This statement is more valid in the monsoon sector and Central Pacific. This implies a converging/diverging pattern with a periodicity of 30-50 days. The amplitudes of all three variables undergo modulation with period more than 100 days. This amplitude modulation is very clear in the Central Pacific.

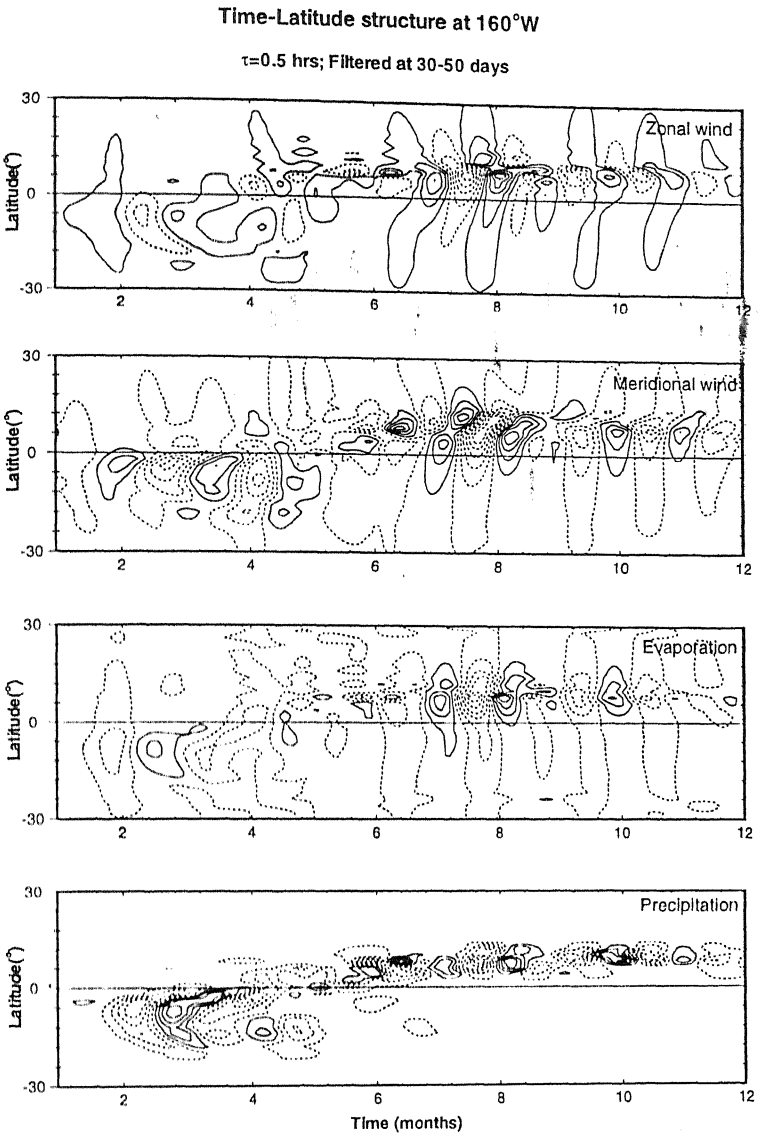

Figure 7.18: Same as the Fig 7.17, but over 160°W

7.2 Time-Longitude Structure

After presenting the power spectra and filtered time series, it would be more revealing to look at the time-longitude structure of the various dependent variable. An analysis using the Hovmöller diagram would make the case stronger, if the simulated tropical disturbances with maximum power in the period mentioned in the last section agree also with observed direction of phase propagation. Figures 7.11 to 7.13 show the time-longitude structures of the filtered model fields for $\tau = 0.5$ hr. at three latitudes: equator, 16°N and 16°S. The figures 7.14 to 7.16

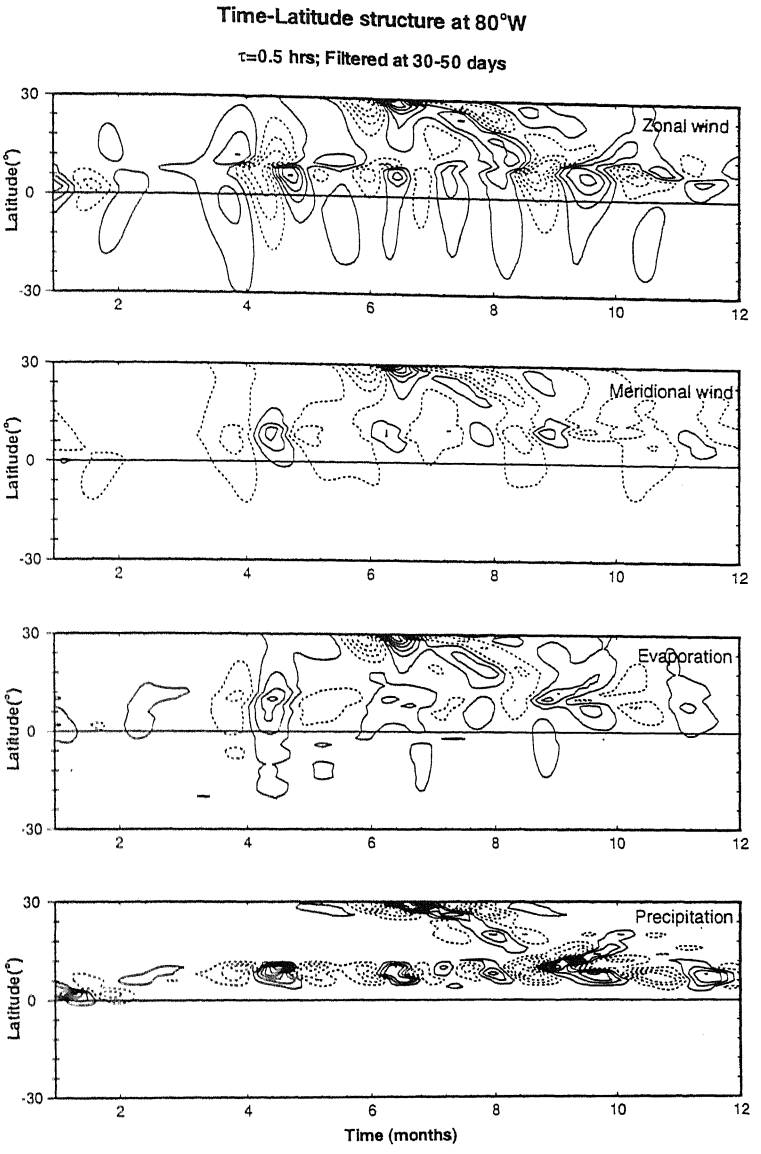

Figure 7.19: Same as the Fig 7.17, but over 80°W

are for $\tau = 1.5$ hr. All the variables are bandpass filtered at 30 to 50 days periods. From a scrutiny of the figures from 7.11 to 7.16 the following observation can be made. The fields at the equator show characteristic oscillation throughout the year, with nearly equal strength. In contrast, the fields at the northern and the southern latitudes show a distinct seasonal variation. In particular, the fields in the southern hemisphere in the (northern hemispheric) summer (winter) months are rather weak. This is consistent with the results shown in the power spectrum analysis. The modeled variabilities propagate both westward and eastward. This agrees well with what Wang and Rui (1990) had reported. They studied OLR

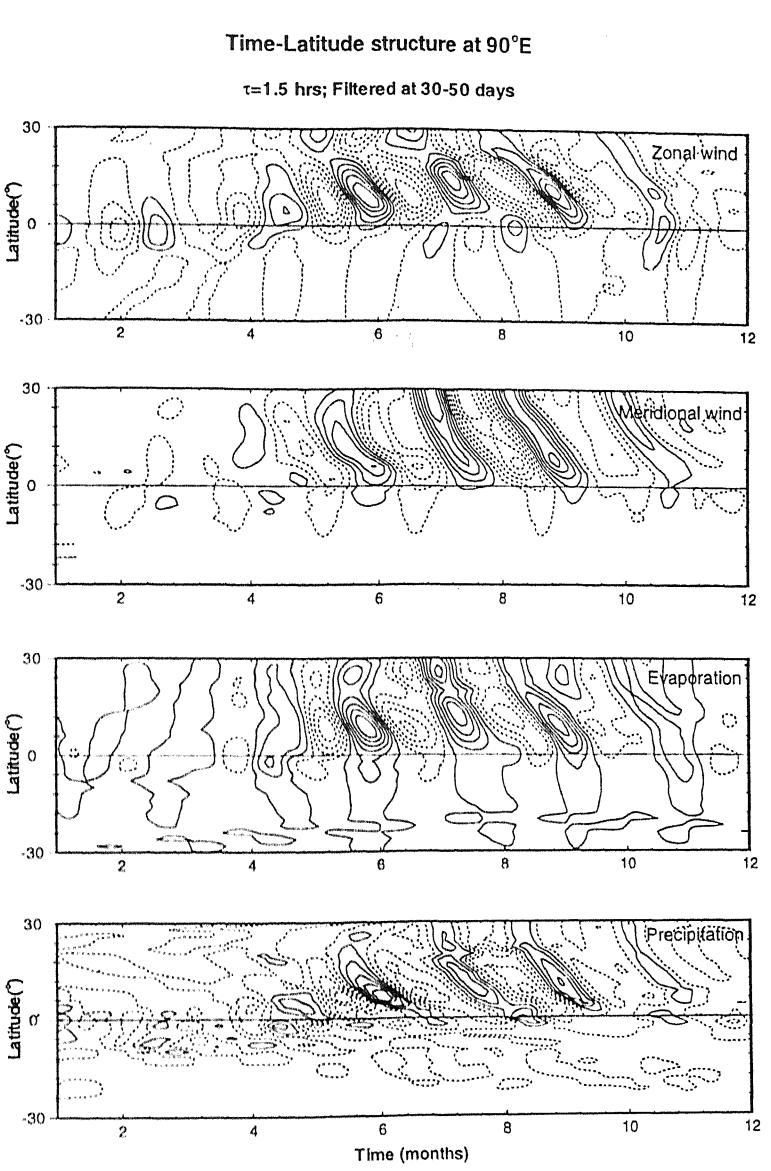

Figure 7.20: Same as the Fig 7.17, but for $\tau = 1.5$

data and summarized various behaviors of large-scale tropical cloud complexes. About 122 tropical intraseasonal convection anomalies were seen during a 10-year period (1975-85). Of those, the majority moved east (77), 27 moved northward with no connection to an eastward moving waves, and 18 moved westward.

Several studies (Lau and Chan 1983, 1986; Weickman *et al.*, 1985) had contributed toward better understanding of 30-50 day wave. Nakazawa (1988) studied the structure of the eastward-moving cloud masses with 3 hourly geostationary OLR data. His main findings were the following. The eastward moving cloud systems were composed of several super cloud clusters (SCC) which moved in the

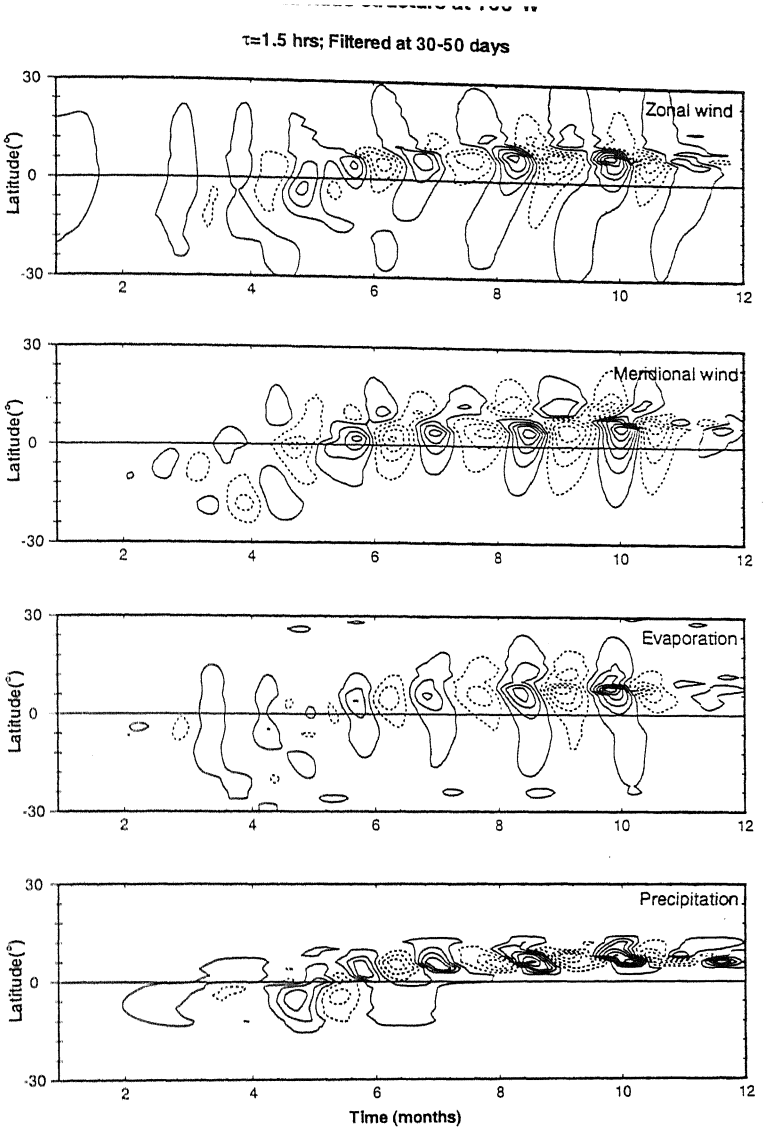

Figure 7.21: Same as the Fig 7.20, but over 160°W

same direction. Each SCC, in turn was, composed of a number of smaller cloud cluster (CC) that propagate westward. The area of each SCC was of the order of $10^3 km$ and that of CC was an order of magnitude less. The life time of CC was only 1-2 days. The genesis of CC took place to the eastern side of matured one. He noted that this behavior was confined to within 15° of the equator. Beyond that the cloud movement on all spatial scales tends to be westward. The OLR anomalies follow upper level divergence and are strongest over the Indian and Pacific Oceans. They are very weak over the cooler water of the Eastern Pacific and Atlantic Oceans and weak over south America and Africa. The OLR

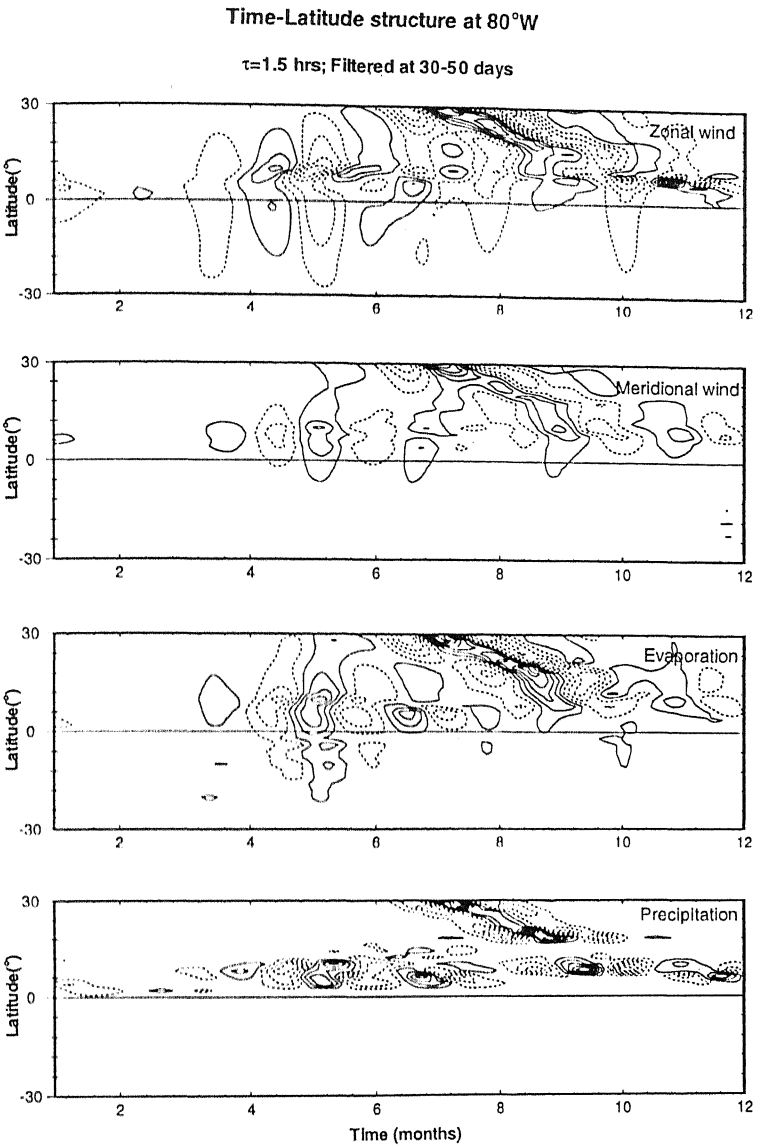

Figure 7.22: Same as the Fig 7.20, but over 80°W

anomaly is found to be strongest in the summer hemisphere. Nakazawa (1995) confirmed the hierarchic structure of the tropical convection by examining its behavior during TOGA-COARE IOP from November 1992 to February 1993. The eastward propagation speed of super cluster was about 6 deg/day. Apart from eastward moving super clusters, also seen over central Pacific along the equator was westward moving super clusters. The phase speed of these cloud-complexes were about 3 degree/day. Another interesting feature revealed by using twice-daily JMA/GANAL global analysis data set was that active convective regions correspond well with lower-level westerlies and convergence (upper level easter-

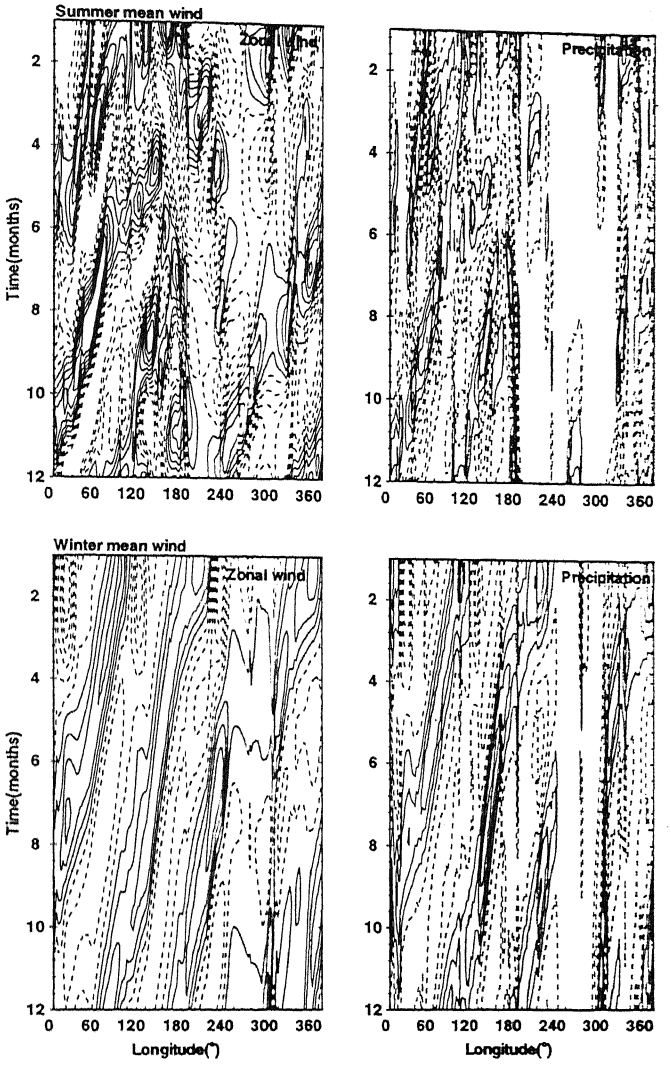

Figure 7.23: Time-longitude plot for winter and summer mean wind simulations but with annual cycle of SST. Only zonal wind and precipitation over the equator are shown. Negative contours are dashed

lies and divergence). The ISO signals were strong in the region between Indian Ocean and the dateline. However, if planetary scale ISO was dominant, the signal was found all over the globe. Using space-time spectral analyses, Guber (1974) and Zangvil (1975) showed the evidence of eastward-propagating cloudy areas in the equatorial region. The latter also demonstrated that this was more prominent over the summer hemisphere. The x-t structures of precipitation shown in the figures 7.11 to 7.13 and the observational structures mentioned above studies match remarkably well. A paper by Weickmann and Khalsa (1990) presents

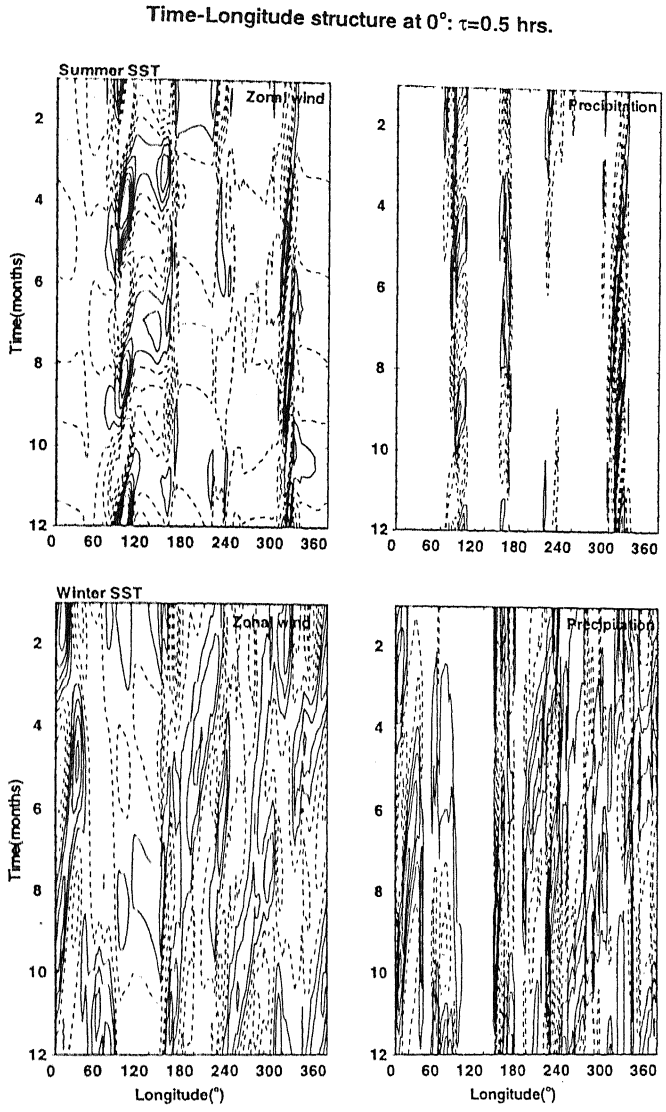

Figure 7.24: Time-longitude plot for perpetual winter and summer SST simulations, but with annual cycle in mean wind. Only zonal wind and precipitation over the equator are shown. Negative contours are dashed.

an analysis of the behavior of the 30-60 day oscillation between September 1981 and April 1982 that uses raw OLR data and dynamical quantities subjected to a 5-day running mean. The time-longitude diagrams of OLR anomaly clearly show three regions of convection; a large area covering Indian Ocean- Western Pacific region and two small regions over Africa and South America. This geographical confinement of convection is also very clear in the model simulated precipitation. What is very clear from Weickmann and Khalsa's (1990) observational analysis and model simulation is that 30-60 day periodicity in the Indian Ocean-Western

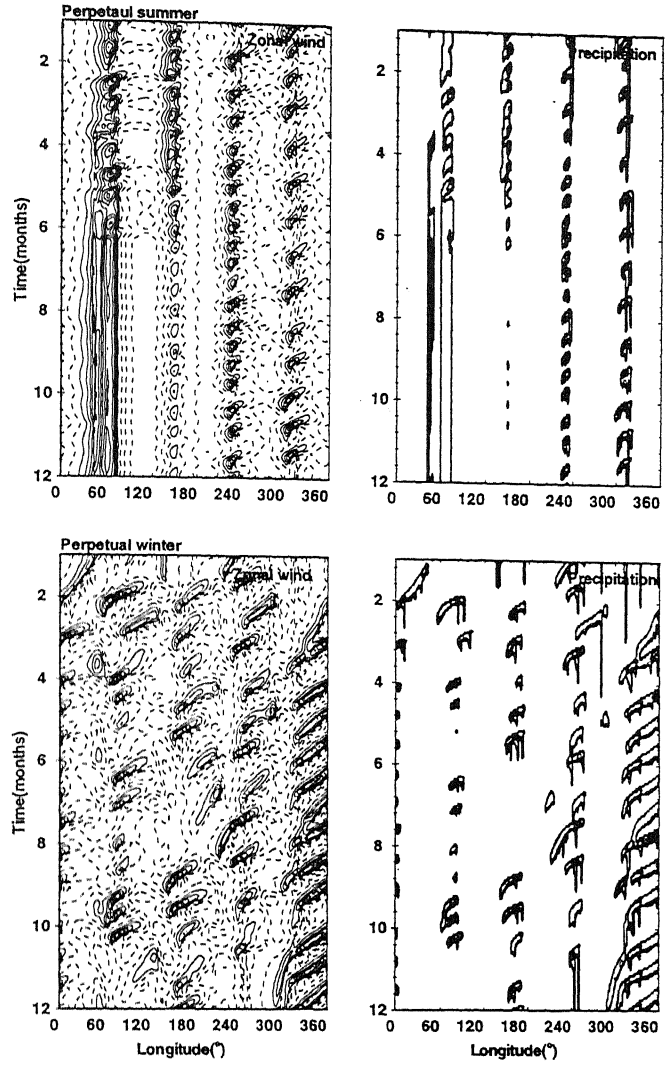

Figure 7.25: Time-longitude plot for perpetual summer and winter simulations. Only zonal wind and precipitation over the equator are shown. Negative contours are dashed

Pacific region is not determined by the time it takes for a propagating convective disturbance to make it around the world. Convection dies out over the Eastern Pacific. The times of intense convection over the Indian Ocean-Western Pacific region are separated by relatively quiescent periods that are approximately 30-60 days apart. We also found that the eastward movement of the pattern is not a smooth propagation with almost constant speed. Instead, shifting of patterns may occur during the evolution. In the Northern hemispheric summer monsoon region between 60° and 160°E a series of time-clustered, partially space over-

lapping disturbances in association with 40-50 day disturbances have also been reported (Murakami *et al.*, 1984).

Besides eastward propagating signal, strong standing oscillations are also evident in Western Pacific, Central Africa and South America where active convection is persistent (Hsu *et al.*, 1990; Knutson and Weickmann 1987). From figures 7.11 to 7.16 we see not only this regionality of the stationary mode but also the propagating signals that radiate from them. Other noteworthy features are a) the concomitancy of precipitation and westerly wind, b) at 10°N and 10°S evaporation is out of phase with zonal wind whereas at the equator they are in phase.

7.3 Time-Latitude Structure

In addition to zonal propagation, the poleward and equatorward movement of the signals were also revealed in many observational analysis. Wand and Rui (1990) further classified the eastward moving complexes into three, based on their propagation characteristics. First, those confined within ±15° of the equator during their life time, which were named as EE mode. The NE and SE modes move eastward along the equator until 100°E, whereupon they traverse in north-east and north-south direction respectively. Third type (EN) were seen over the Indian and /or the Western Pacific, which exhibited complex eastward and northward movements. The EE mode occurred during the 6 months period from December to May. Members of the second group that moved to the southeast near 100°E (SE) were reported only from November through April, indicating relation to the ITCZ and Australian monsoon. Those that moved to north-east (NE) occurred primarily, but not exclusively, in northern summer, again associated with the ITCZ and the East Asian monsoon. The major formation region is west-central equatorial Indian Ocean. There is also, a secondary source just west of equatorial Africa. The maximum intensification rate of the TICA were in the

central Indian Ocean, with secondary areas of intensification near 160°E north of the equator and the one extending from Australia to the date line south of the equator.

To find how well the model can capture this aspect of propagation we also give in figures from 7.17 to 7.22 the time-latitude structures of the filtered model fields at three longitudinal locations: 90°E, 160°W and 80°W. Out of this six figures, first three are for τ =0.5 hr. and the rest for τ =1.5 hr. All the variables are bandpass filtered at 30 to 50 day periods. Figures 7.17 to 7.22 reveal that all the fields are equatorially trapped. The simulations show distinct seasonal cycle at all the three longitudes. The meridional migration is largest in the Monsoon sector and decreases from east to west. In the Eastern Pacific this always remains in the northern hemisphere, showing that the anomaly zonal wind, to a certain extent, follows the mean seasonal cycle.

The maximum of the zonal wind is closer to the equator in winter than in summer, in particular in the Monsoon sector and Eastern Pacific. During January, in the Central Pacific the zonal wind shows northward propagation emanating from 5°S. In summer the zonal wind moves equatorward in the monsoon sector whereas in the Central Pacific and the Eastern Pacific it also shows northward propagation. A very distinct intrusions of waves from the subtropics are visible in the Eastern Pacific. These characteristics are, to a large extent, applicable to all other variables shown in the figures.

7.4 The Role of Mean Fields

An important question of the source of energy for the sustained cumulus heating (at the subseasonal time scale) is usually not addressed. Convection for such long period requires a steady supply of moisture from the ocean. It is found that on this time scale the latent heat flux from the ocean to atmosphere is of considerable amount. The study by Krishnamurthi *et al.* (1988) indicates that oscillation

of both the wind and the SST contribute to a strong coupling of atmosphere and the ocean at this time scale. The amplitudes of SST variation at this time scale are of the order of 0.5°C to 1.0°C and most pronounced SST oscillations occur over the equatorial Western Pacific Ocean and the Bay of Bengal. It is conceivable that a one degree enhancement of SST over these climatological warm oceans can affect the convection and their propagation. Thus the spatio-temporal distribution of the SST fields is likely to play a crucial role in the structure of 30-50 day oscillation. In our model the SST-distribution affects the model dynamics through its implicit effect on the strength of EWF. In addition, the spatio-temporal structure of the mean winds is expected to have considerable influence on the regional characteristics of the ISO1.

To investigate this aspect in detail, we have carried out two simulations, first with only the annual cycle of the mean wind (ie., with no annual cycle of SST) and then with only annual cycle of SST (ie., with no annual cycle of mean wind). In the former case we carry out two simulations, one with winter (January to May) mean SST and the other with summer (June to October) mean SST. Similarly in the case with only the annual cycle of SST we analyze two simulations: one with winter mean wind and the other with summer mean wind. In addition, two more simulations are carried out in the setting of perpetual winter (winter mean wind and winter SST) and a perpetual summer (summer mean wind and summer SST) mean conditions. In all these cases only one value of CTL is used (τ =0.5 hr). As we have seen earlier, there is significant power above the red noise at 30-50 day time scale, for all these special cases. Hence, we shall consider here the simulated fields filtered at 30-50 day scale for further analysis.

The time-longitude diagram for zonal wind and precipitation at the equator for summer and winter mean winds are shown in 7.23. The corresponding figures for summer and winter SST and perpetual summer and perpetual winter are shown in 7.24 and 7.25, respectively. It was found that the power spectrum had significant

peaks around 50 days for winter mean wind and winter SST and around 30 days for summer mean wind and summer SST. The model fields for two fields have been accordingly filtered. The most striking feature in the figure 7.23 is the absence of any clear eastward propagation. Indeed, both for the summer and the winter mean winds, the fields now exhibit westward propagation, irrespective of the zonal locations. The absence of zonal variations is particularly striking in the winter mean wind simulation. Thus the spatial structure of the mean wind alone is not sufficient to bring about the observed variations in the zonal characteristics of the 30-50 day waves.

An interesting conclusion that emerges from an examination of figure 7.24 for summer and winter SST is a more or less stationary behavior of the fields. Thus, from a synthesis of the results from 7.23 and 7.24, we may state that the phase propagation itself is induced by the annual cycle of the SST (and in particular associated temporal structure of EWF) while the direction of phase propagation is determined by the annual cycle of the mean wind.

7.5 Conclusions

A large part of intraseasonal variability in the tropics occurs in the 30-50 day wave. It is also intimately connected with the variabilities of monsoon rainfall. As detailed analyses of observed data sets bring out richer spatio-temporal structure of the 30-50 day oscillation, the emphasis of the model simulations must include not only genesis but also these detailed properties of 30-50 day oscillation. It is noteworthy that our model using convection-induced dynamics with convective time lag succeeds in simulating many of the observed features of the 30-50 day oscillation. This is consistent with and reflective of the fact that our model can simulate a large part of the variability of the monthly anomaly fields. However, there are also certain important aspects of 30-50 day oscillation which our simulations do not capture well. One such feature is the well known northward propagation

of 30-50 day oscillation over the monsoon region. As can be seen from figure 7.17, the model fields filtered at 30-50 days show weak northward propagation over the monsoonal region in the summer months but equatorward propagation in the winter months. This feature is most pronounced in the meridional wind field, while it is nearly absent in the evaporation field. The fields at 90°E are also much more equatorially confined with no significant amplitude beyond 15°N. In contrast, the fields at 80°W show much more off equatorial distribution with pronounced equatorward propagation in the northern hemisphere. Verification of some of these features may need further analysis of observed data with higher spatial resolution. Another very important aspects of 30-50 day oscillation and tropical oscillation, in general, is the interconnection between oscillations at different time scales. Our model with its ability to simulate the broad spectrum of tropical oscillations is suitable for investigating this aspect. Some of these issues will be addressed in the subsequent chapters.

Chapter 8

The Spectrum of Oscillations: The Quasi-Biweekly Waves

The existence of certain prominent periodicities in the summer monsoon rainfall has been known for several decades. In particular, the Indian monsoon region exhibits a 10-20 day (or quasi-biweekly, QBW) oscillation. This oscillation is characteristic of the summer monsoon region and significantly affects the distribution of monsoonal rainfall (active and break conditions), and is not well documented over other parts of the tropics. Although the QBW is not reported in the winter hemisphere, it is possible that more detailed analyses of now available observed data sets for the global tropics may reveal new features. With our model it is possible to investigate the existence and spatio-temporal structure of this oscillation in detail. The agreement of the simulated features with observations then provides a basis for further investigation of the predicted features in the observed data.

The questions regarding the characteristics of the QBW range from one of the genesis of these waves to the variation of the characteristics of these waves in space and time. While there has been a large number of theoretical investigations of the 30-50 day eastward propagating wave, very few studies have addressed the question of dynamical mechanism of 10-20 day wave. A consistent dynamical scenario

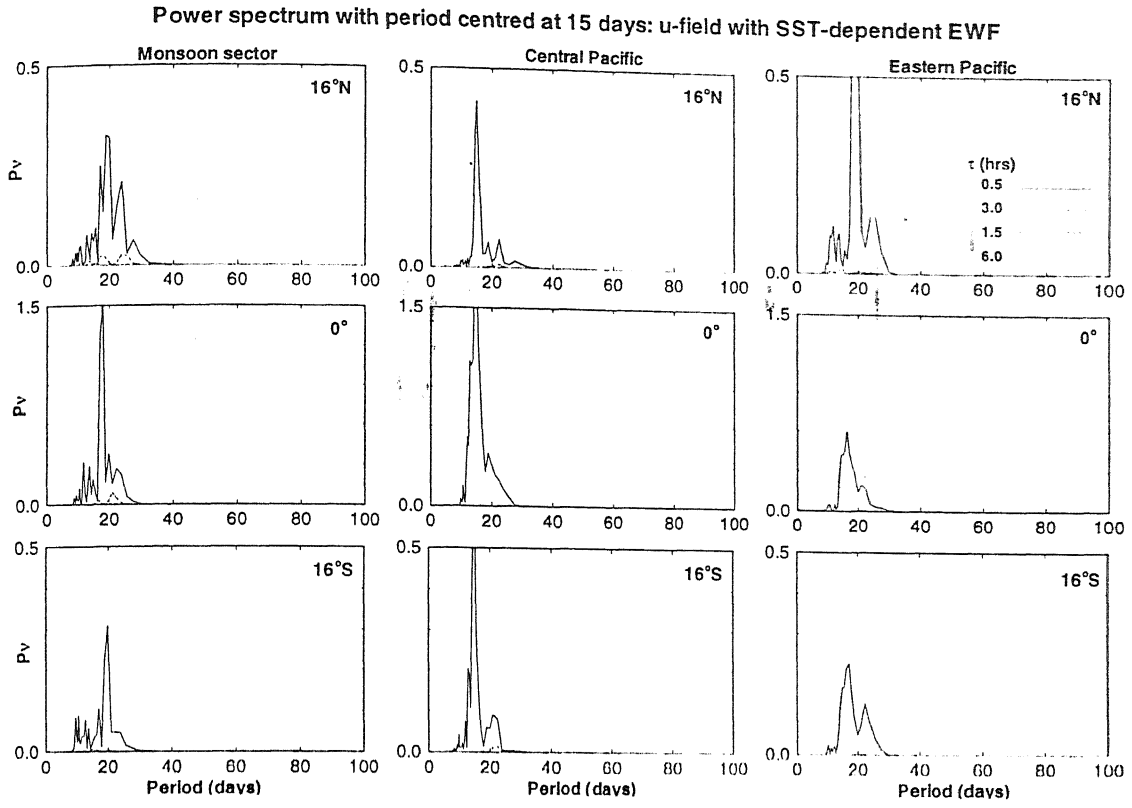

Figure 8.1: Power spectra of zonal wind filtered at 10-20 days plotted for four values of CTL with $\nu P(\nu)$ as the ordinate and period as abscissa, where P is the power and ν the frequency. For each value of CTL, the fields have been normalized to their respective maximum.

for the genesis of 10-20 day wave as well as for another major intraseasonal wave (*viz.* the 3-6 day wave) was advanced by Goswami and Mathew (1994). In particular, it was shown in Goswami and Mathew (1994) that the same mechanism that selectively destabilizes the MRG wave at 3-6 day time scale in presence of mean easterlies excites the 10-20 day wave in presence of mean westerlies. Since the mean westerlies are characteristic of the Indian summer monsoon region, it provides an explanation for the presence of the 10-20 day wave over the northern summer tropics. A significant finding in Goswami and Mathew (1994) was that the 10-20 day wave appeared as a mode distinct from either MRG wave or Kelvin wave. Indeed it was shown that this mode can be expected only in a moist tropical atmosphere in presence of mean westerlies. These analytical results thus

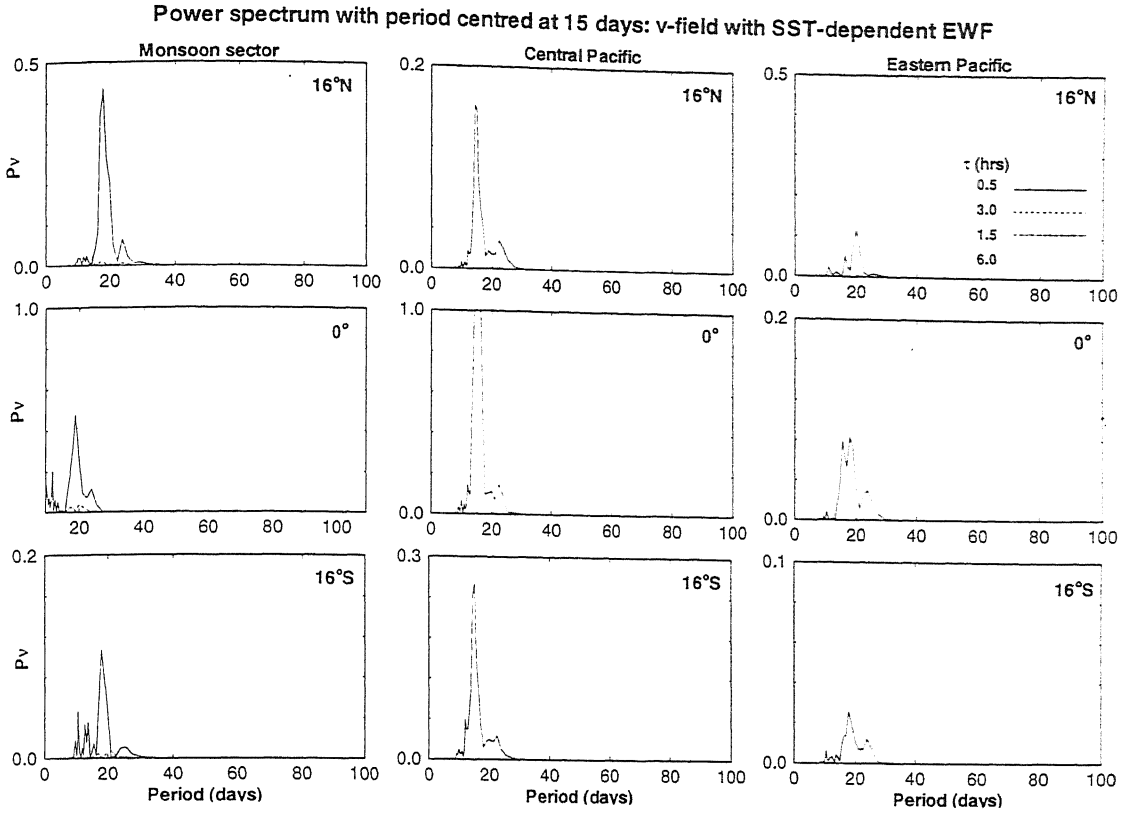

Figure 8.2: Same as the fig 8.1, but for meridional wind

provide a conceptual basis for examining the existence and the characteristics of the 10-20 day wave in our model with CTL and non-linear heating. In particular, we would like to address certain questions regarding the detailed structure of the 10-20 day oscillations which cannot be addressed with simple analytical models. The availability of observational analyses from recent works make such an effort worthwhile. To analyze the general properties of the 10-20 day oscillation in our model simulation, we shall once again consider the composite one-year model simulations for different dynamical conditions. In order to investigate the existence of any significant oscillation in the 10-20 day period, first the time series from the composite one-year model simulation has been analyzed. It was shown that with τ =0.5 hour, there exists a significant peak in the 10-20 day range above the corresponding red noise level. We shall, therefore, investigate the characteristics of the 10-20 day oscillation in our model simulation with the available

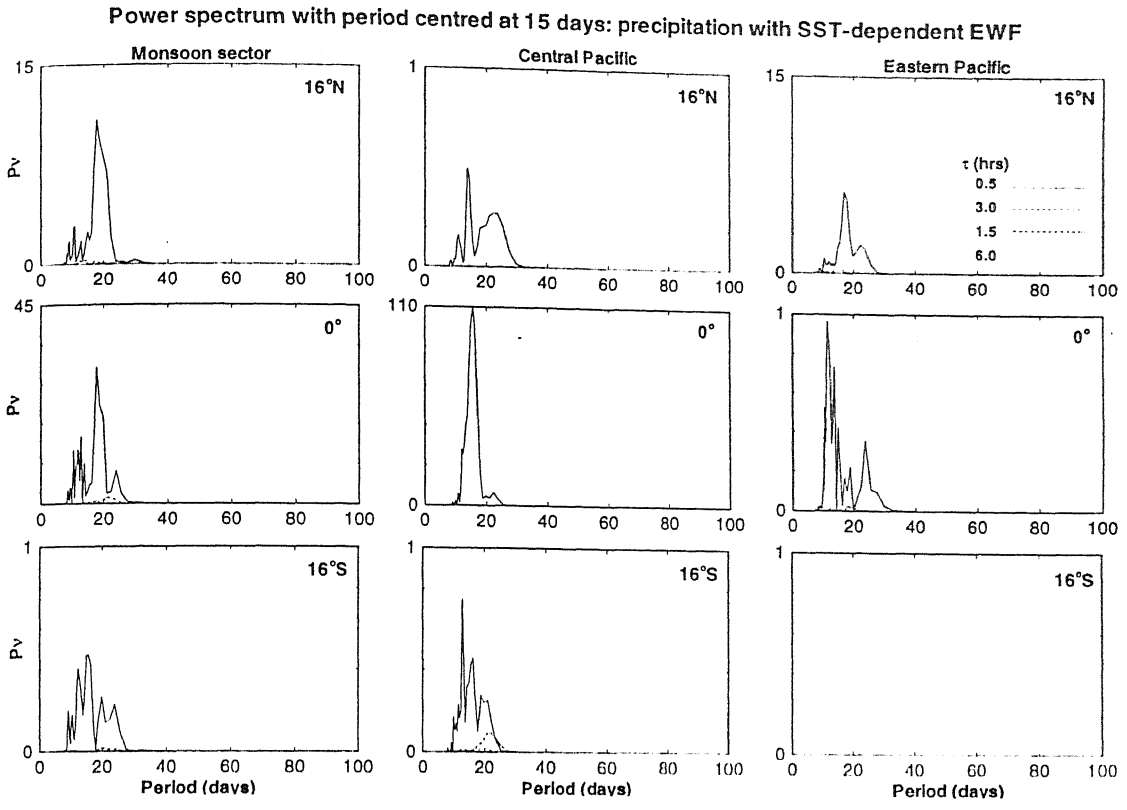

Figure 8.3: Same as the Fig. 8.1, but for precipitation

observations acting as the constraints in the model. We have seen that, in the context of monthly anomaly fields that an SST-dependent evaporation-wind feedback (EWF) gives rise to the best simulation. This point has been also verified in the case of simulation of the annual cycle. Hence, we shall consider only the case of SST-dependent EWF to investigate the structure of QBW in our simulation. But four values of CTL are used to examine the effects of CTL and compare this to its effect on the 30-50 day wave.

8.1 The Characteristics of the Power Spectrum

While most earlier analyses focussed on the 10-20 day oscillation of the summer monsoon rainfall, recent analyses with more comprehensive data sets indicate that the QBW may be more generic for the tropical circulation. Preliminary analyses

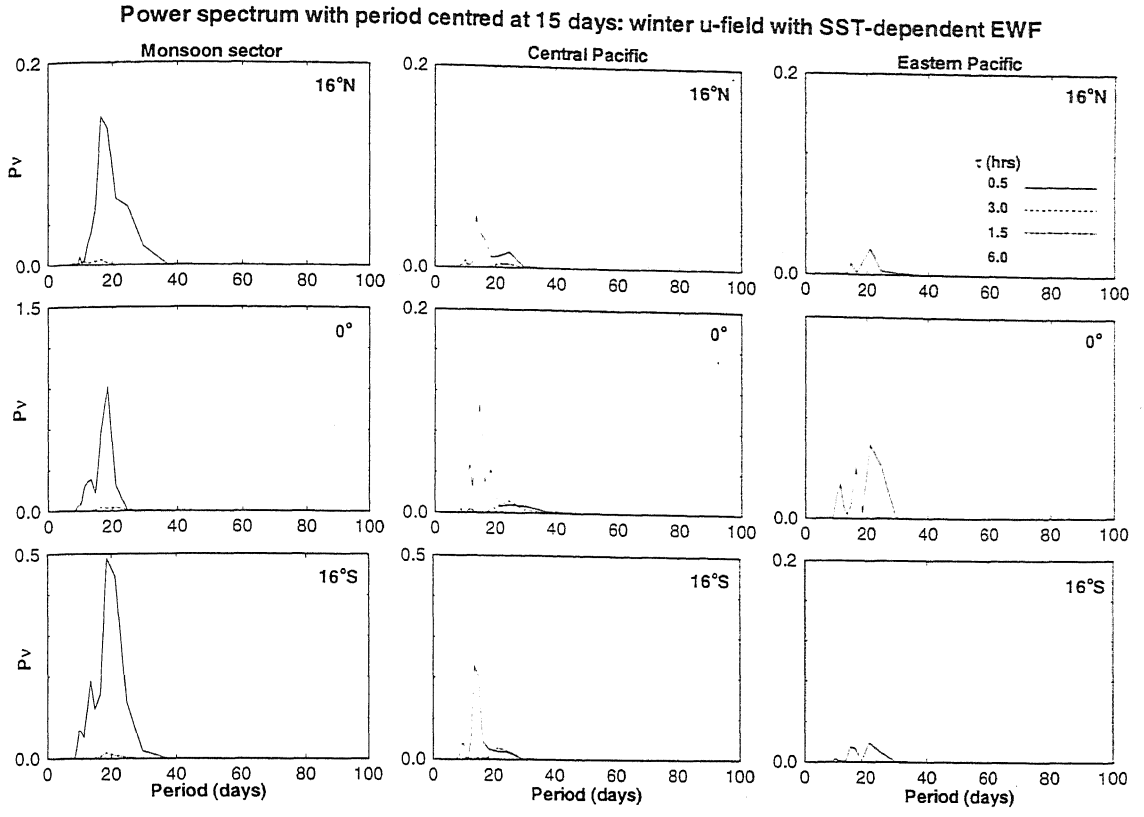

Figure 8.4: Same as the fig 8.1, but for winter months

of our model simulation also indicate significant power at the QBW range above red noise at several locations. Hence the behavior of the 10-20 day wave in our model simulation is examined as a function of location and season. This issue is addressed in terms of the power spectra of the composite model simulation filtered at 10-20 days at different locations. In addition, we have also analyzed the model simulations separately for the winter (January to May) and the summer (June to October) seasons filtered at 10-20 days. As before, the unfiltered time series were generated by averaging the fields over a zonal extent of 60° centered at 90°E (Monsoon sector), 80°W (Central Pacific) and 160°W (Eastern Pacific). We shall consider three latitudinal positions, *viz.* equator, 16°N (NH) and 16°S (SH).

Figures 8.1 to 8.3 show the power spectra of the model u, v and the precipitation fields from the composite one-year simulation filtered at 10-20 days. As seen from these figures, the model in general supports ISO with 10-20 day time scale,

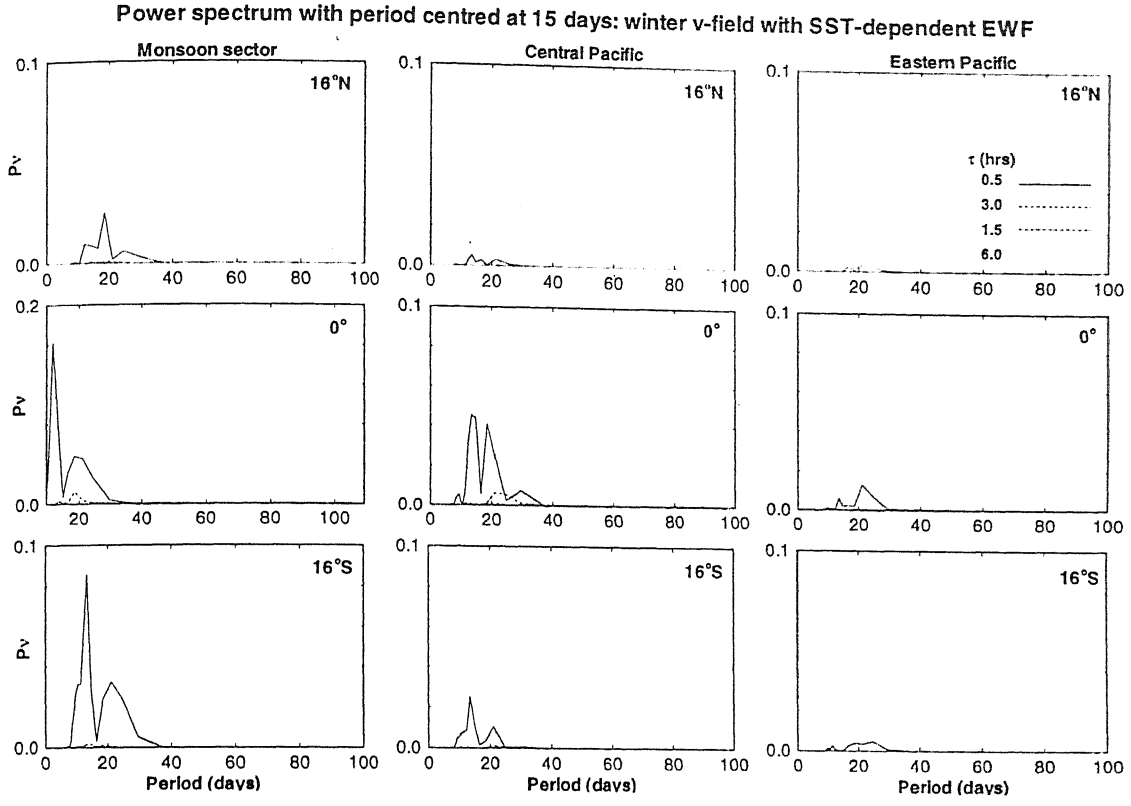

Figure 8.5: Same as the Fig 8.4, but for meridional wind

although the power is relatively weaker than that of the 30-50 day waves in the model simulation. However, since our model fields are normalized to its maximum value for ease of comparing results for different values of CTL, the smallness of power is not necessarily an indicator of weakness of the spectrum in the absolute sense. From figures 8.1-8.6 we see, once again, that it is $\tau = 0.5$ hr. that gives rise to the strongest signal at 10-20 days time scale.

A striking feature in figure 8.1 and, to some extent also in figures 8.2 and 8.3, is the comparable power at 10-20 day period at all the longitudinal positions. This may at first glance appear to be contrary to observational analyses which show the QBW more prominently over the monsoonal region. However, it is possible that the variability in the QBW scales at particular location also depends on the seasons. This question can be examined by analyzing the model fields for winter and summer separately. The figures 8.4 to 8.6 present the results of power

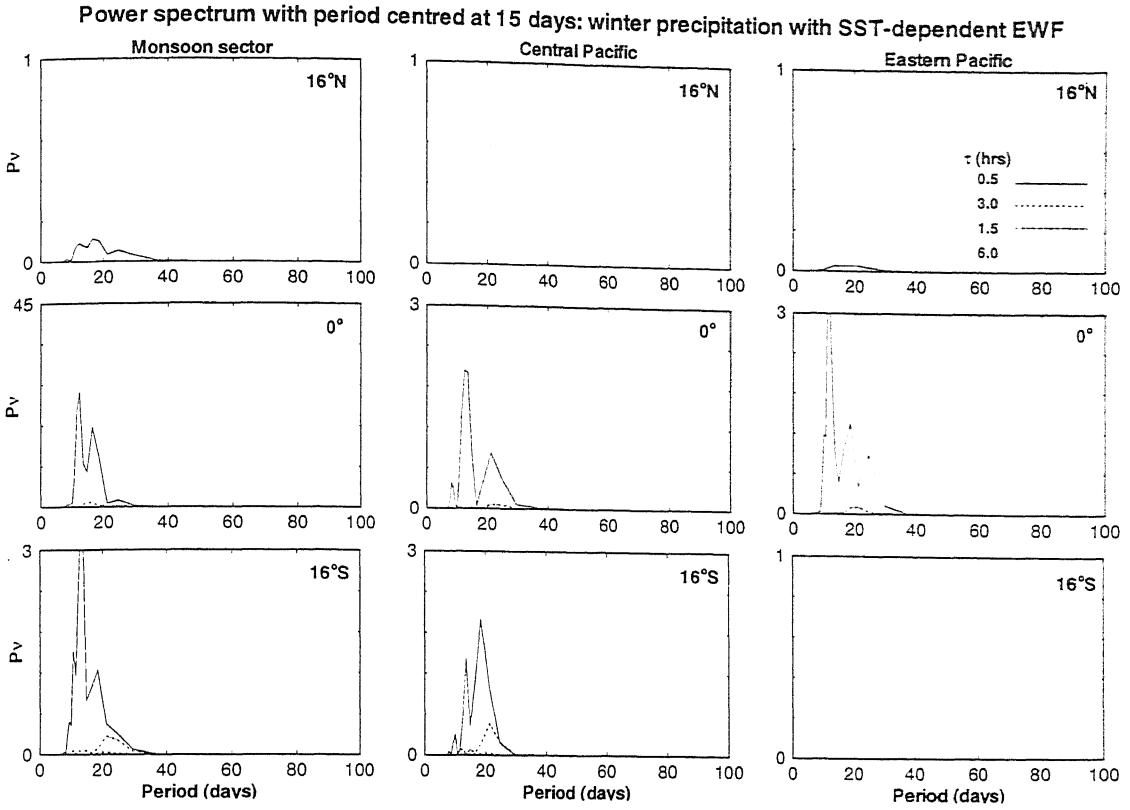

Figure 8.6: Same as the Fig 8.4, but for precipitation

spectrum of variables u, v and precipitation for a 10-20 day for the winter months respectively. The corresponding results for the summer months are shown in figures 8.7 to 8.9. As indicated in the figures, the results are presented for three latitudinal regions, around 16°N (top panels), around the equator (middle panels) and around 16°S (bottom panels), and also for three zonal locations: monsoonal area (left row), Central Pacific (middle row) and the Eastern Pacific (right row). In both the figures, there is ample power around 10-20 days in the monsoonal region, but very small for the other zonal regions. Indeed, the power in general monotonically decreases as we move from the monsoon region towards the eastern Pacific region. In addition, comparison of figures 8.4 to 8.6 with the corresponding figures for the summer months reveals that while in the summer months the power is higher in the Northern Hemisphere, it is higher in the Southern hemisphere in the winter months, as expected. This may imply that the 10-20 day oscillation

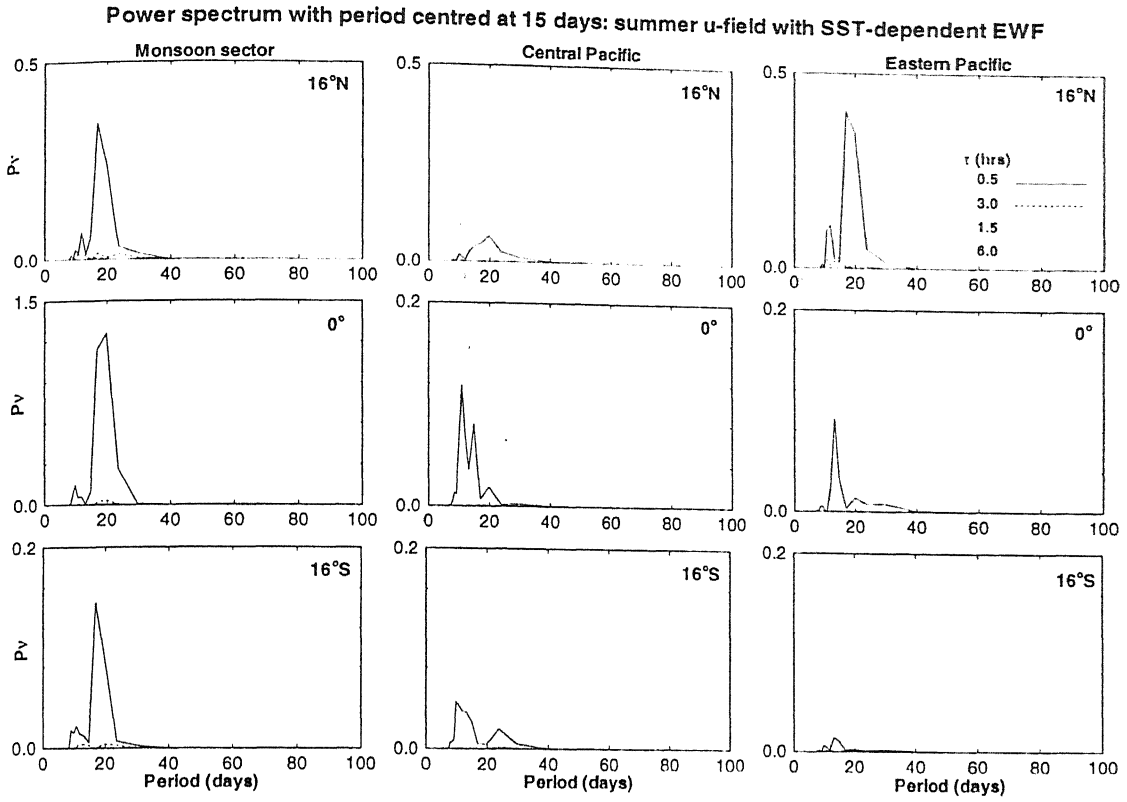

Figure 8.7: Same as the Fig 8.1, but for summer months

appears as a response of the anomaly circulation to the changing mean conditions over the summer monsoon region. In all the figures from 8.1 to 8.6, the results are shown for four values of CTL adopted in this study. It is noteworthy that only one value of CTL, *viz.* 0.5 hour, gives consistently good results.

The figure 8.7 shows the power spectrum of the model u filtered at 10-20 days for summer months. As we see from this figure, the summer u shows strongest signal only over the monsoon region in general. A similar conclusion holds for the summer v, shown in figure 8.8, although the amplitudes over the Southern Hemisphere are somewhat weaker. In contrast to the u and the v fields, the power spectra for the summer precipitation, shown in figure 8.9, show marked variations with latitude. In particular, only two locations, *viz.* the NH monsoon region and the equatorial Central Pacific region, support a significant signal in the summer precipitation field. We have not yet come across any detailed observational analy-

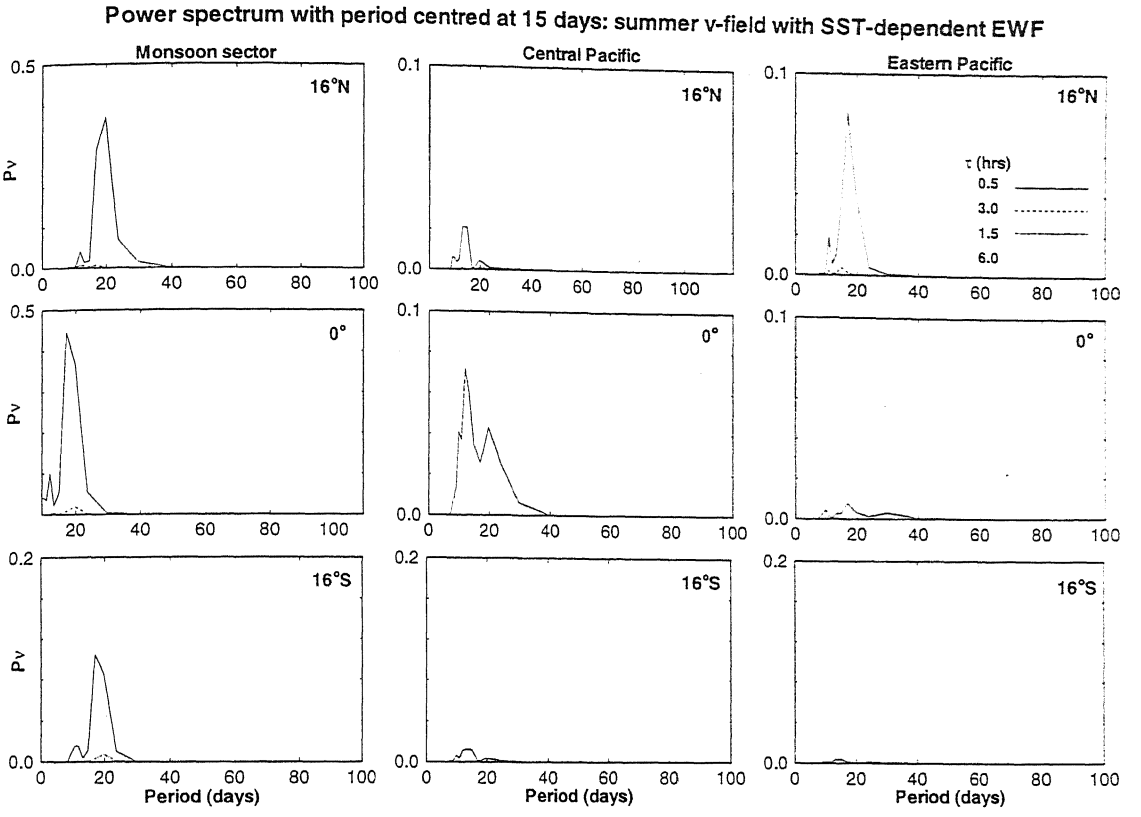

Figure 8.8: Same as the Fig 8.7, but for meridional wind

sis for precipitation with which we could compare our finding. However, with the availability of global high resolution data sets these predictions can be verified.

8.2 Time Series of Model Fields:

To investigate the phase relationships between various model fields, we have examined the time series of the filtered model fields at different locations as shown in figures 8.10 and 8.11. In each panel, we consider variables at three latitudes: 16°N (solid line), equator (dashed line) and 16°S (solid line with symbol). As before, the model fields have been averaged over three zonal regions as indicated in the panels. The top, middle and the bottom panels represent, respectively, the zonal wind, meridional wind and the precipitation field. The filtered time series is shown for both winter and summer separately (figures 8.10 and 8.11).

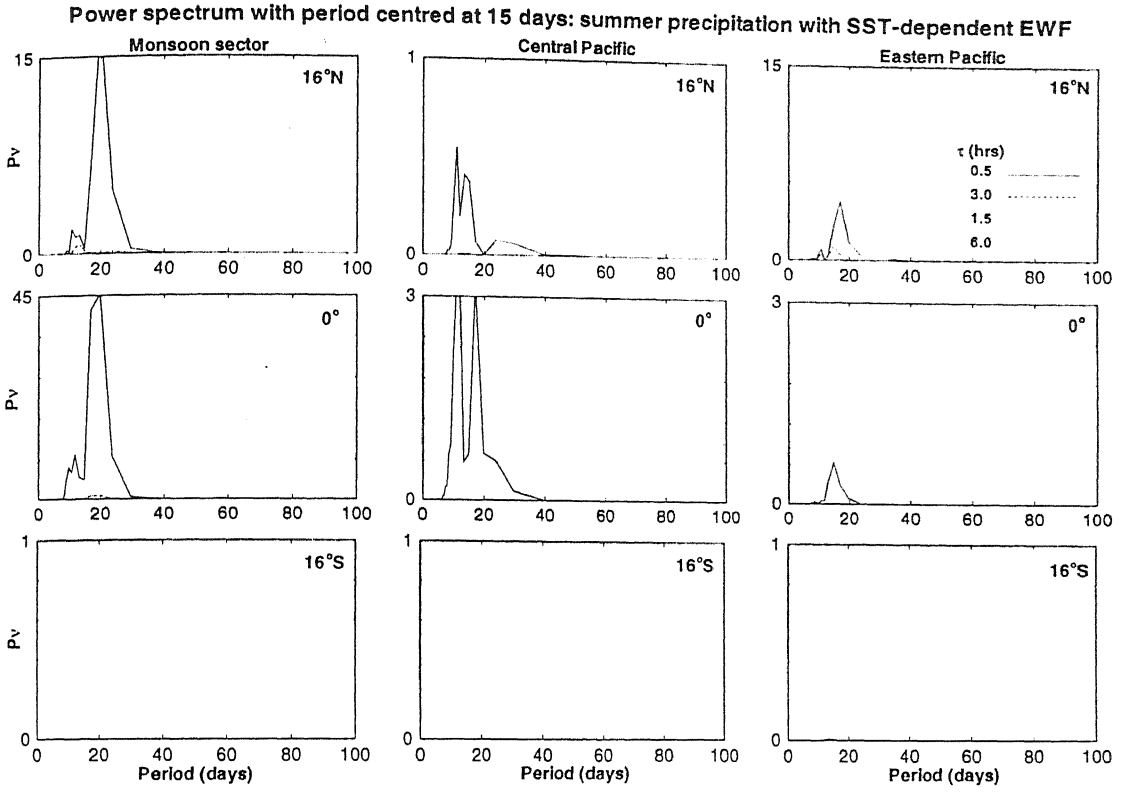

Figure 8.9: Same as the Fig 8.7, but for precipitation

These figures reveal several interesting features. The zonal components of wind at all latitudes considered are in phase in all the three longitudes shown, albeit the amplitudes decrease from east to west. In winter months amplitudes are of comparable magnitude in all three longitudes. This is not true in the case of the summer months (figure 8.11). While in Eastern Pacific zonal wind at 16°N has a large value in the case of Monsoon sector it is the equatorial zonal wind that dominates. There seems be to less change with season in the Central Pacific. In terms of phase relationships among the components of zonal wind at different latitudes, the winter season shows a more consistent picture; all are more or less in phase. The meridional components at 16°N and 16°S are out of phase irrespective of the season. Nevertheless, a dramatic change takes place in precipitation from summer to winter: In summer precipitation is weak in Southern Hemisphere whereas it is so in Northern Hemisphere in winter. This shows the seasonal migration of

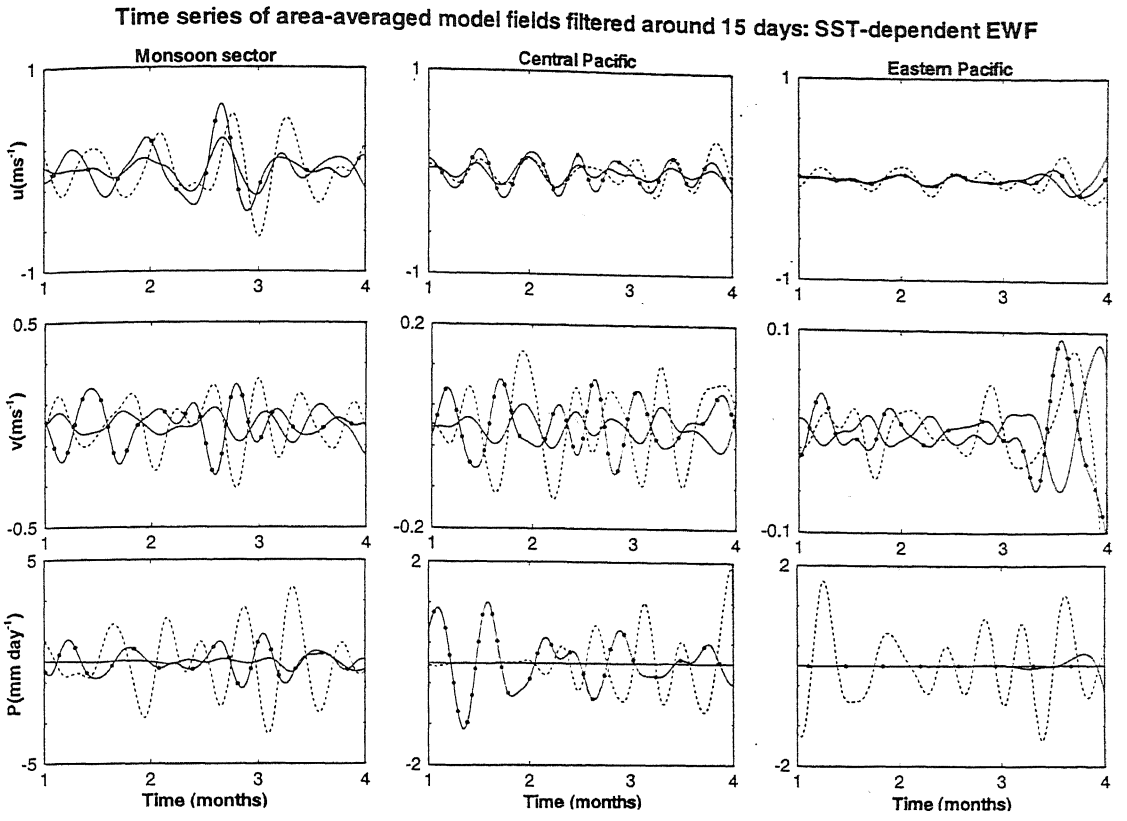

Figure 8.10: The time series of zonal and meridional wind components and precipitation filtered around 15 days for the winter months. The solid, dashed and solid with symbol lines represent fields at 10°N, 0° and 10°S respectively.

convective anomaly with season, similar to the mean precipitation. Precipitation over equator in Monsoon sector and Central Pacific do not change much from winter to summer.

8.3 Time-Longitude Structure

The westward propagation of the 10-20 day monsoon mode first was reported by Krishnamurti and Ardunay (1980). There is now considerable information about the zonal phase propagation characteristics of the QBW. Chen and Chen (1993), for example, report clear westward propagation of 850 mb meridional wind filtered at 10-20 days at 5°N. However, at 20°N, and especially over the Monsoon sector in the summer months, eastward propagation is also seen between 60-120°E. In

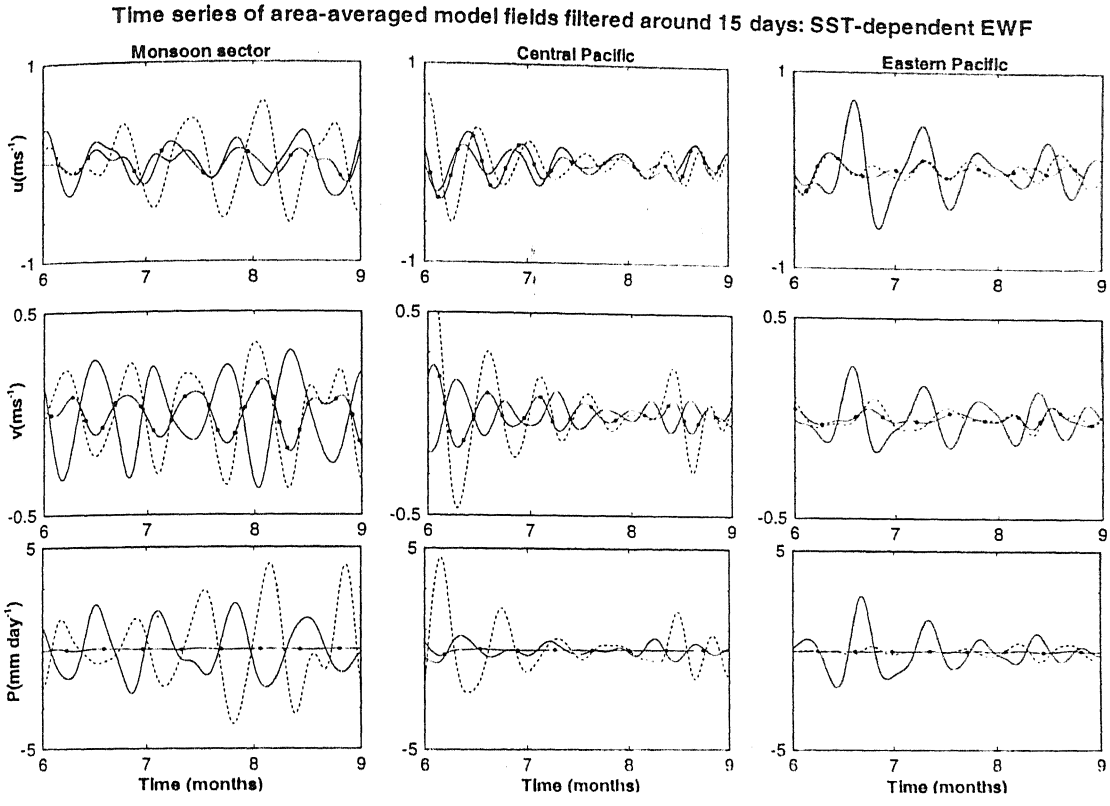

Figure 8.11: Same as the Fig 8.10, but for summer months

fact, this eastward propagation in the analysis of Chen and Chen (1993) is much more pronounced between 80 and 120°E and during May-July. Although the analysis of Chen and Chen (1993) is only for a single summer (of 1979), and may not be typical, it provides a good testing ground for our model simulation of the characteristics of the 10-20 day mode.

The time-longitude structure of the filtered model fields for the entire twelve months of the model simulation are shown in figures 8.12 to 8.14, for three latitudinal locations. These figures indicate a mixture of eastward and westward phase propagation for the 10-20 day oscillation. In particular, the fields show an essentially westward propagation over most longitudes over the equator. This feature is, thus, in close agreement with the finding of Chen and Chen (1993) whose analysis shows clear westward propagation over 5°N, i.e close to the equator. In contrast, the fields at 16°N show, especially during the summer months, and over

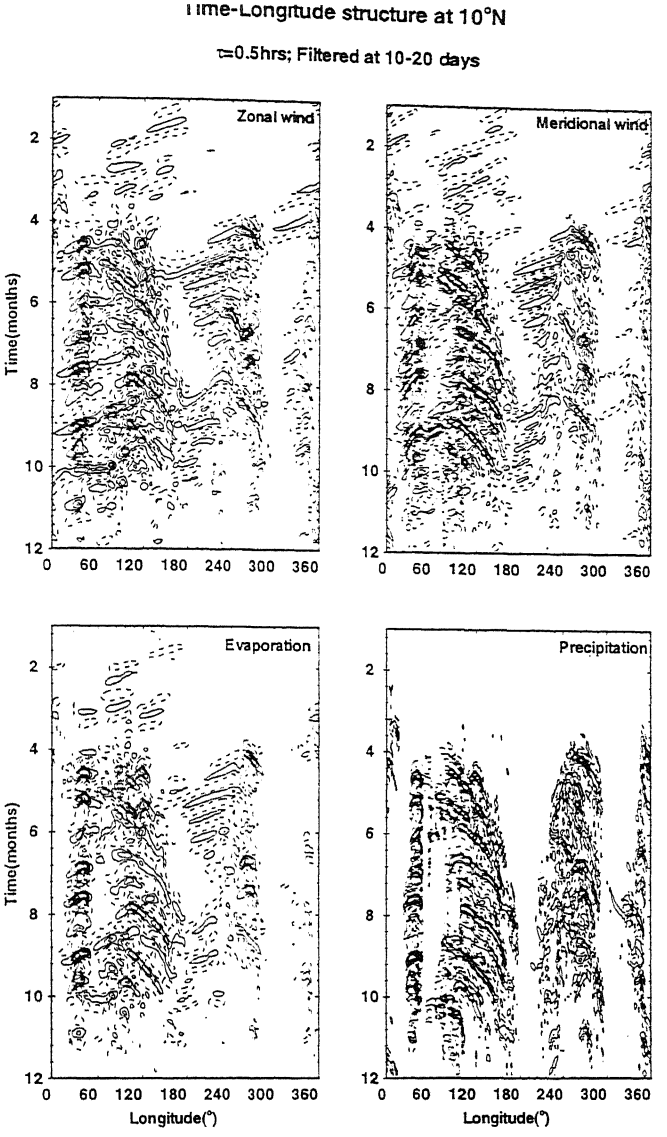

Figure 8.12: Time-longitude structure of the model fields from a composite one-year simulation at 10°N for τ =0.5 hr. Negative contours are dashed.

80-160°E, shows a clear eastward propagation. This eastward propagation begins to reverse to westward propagation around the end of August. Our model simulations are, thus, in excellent agreement with the observed features reported by Chen and Chen (1993). Indeed, the conspicuous stationary belt centered around 40°E at the equator and more prominently at 16°N, can also be seen in the analysis of Chen and Chen (1993). The time-longitude structure at 16°S (figure 8.14) shows that the fields are rather weak over the Southern Hemisphere, especially in the summer months, thus making the 10-20 day mode more characteristic of

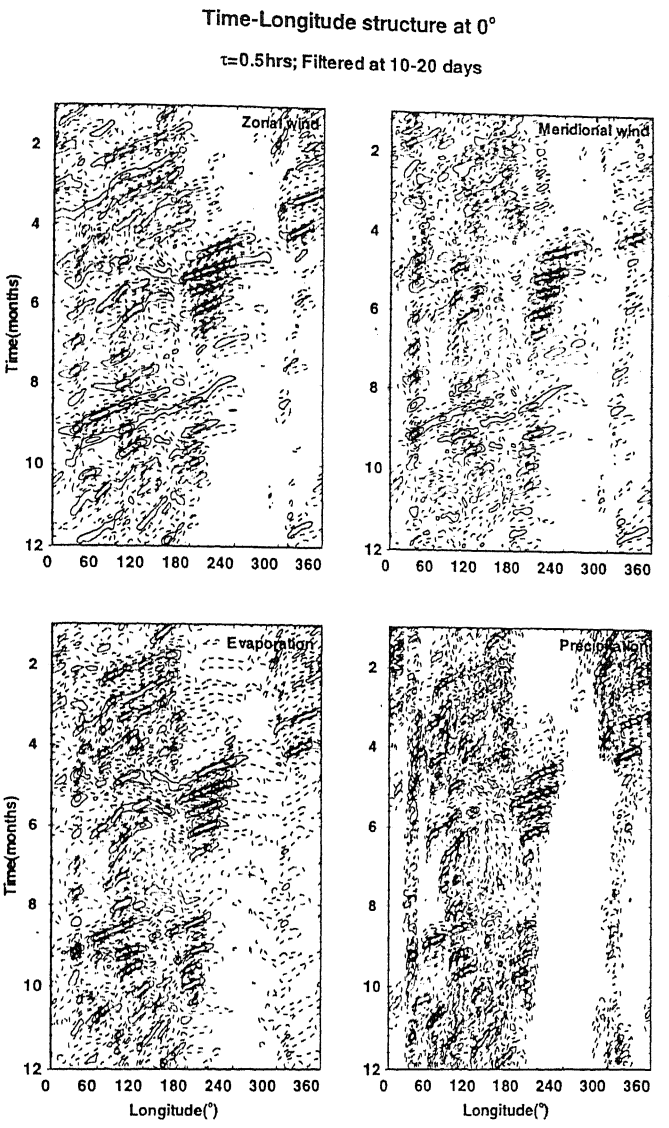

Figure 8.13: Same as the Fig 8.12, but over the equator

the Northern Hemispheric summer. As can be seen from 8.13, the model u at the equator exhibits strong zonal variation in its strength, while the corresponding meridional wind is more or less uniform in the zonal direction. The time-longitude structure of the evaporation field at the equator is very similar to that of the u, although it shows a more temporally uniform distribution than the zonal wind field. This implies that the evaporation field at the synoptic scale is largely determined dynamically. In contrast, the precipitation shows much higher degree of spatial and temporal uniformity in its distribution. A significant feature of the fields at the equator is their relatively weak strength, especially in the zonal wind

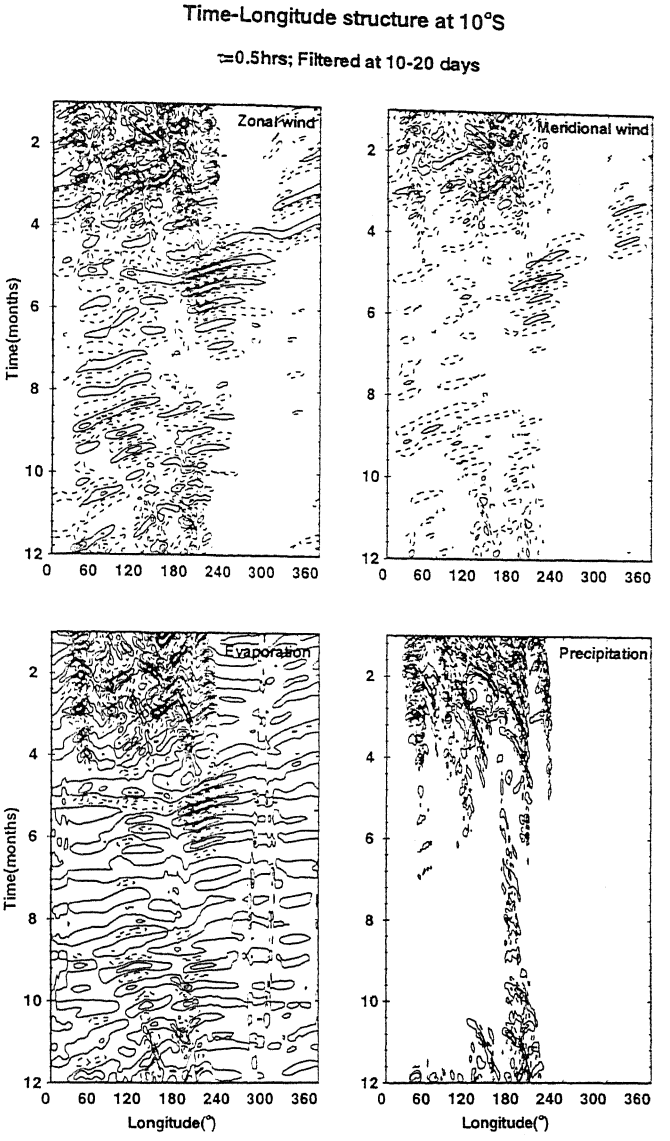

Figure 8.14: Same as the Fig 8.12, but over 10°S

component, during the summer months at most longitudes. The fields at 10°N, shown in figure 8.12, however, exhibit characteristics quite distinct from those at the equator. For one thing, the fields show a much stronger, and somewhat reversed, seasonality than those at the equator. While at the equator the u has stronger amplitudes during the winter months at most longitudes, at 10°N, both the zonal and the meridional winds are strongest during the summer months. This contrast is strongest in the distribution of the meridional wind, which shows a rather uniform distribution in time and zonal direction at the equator. Perhaps the strongest distinction between the fields at the equator and 10°N is in terms

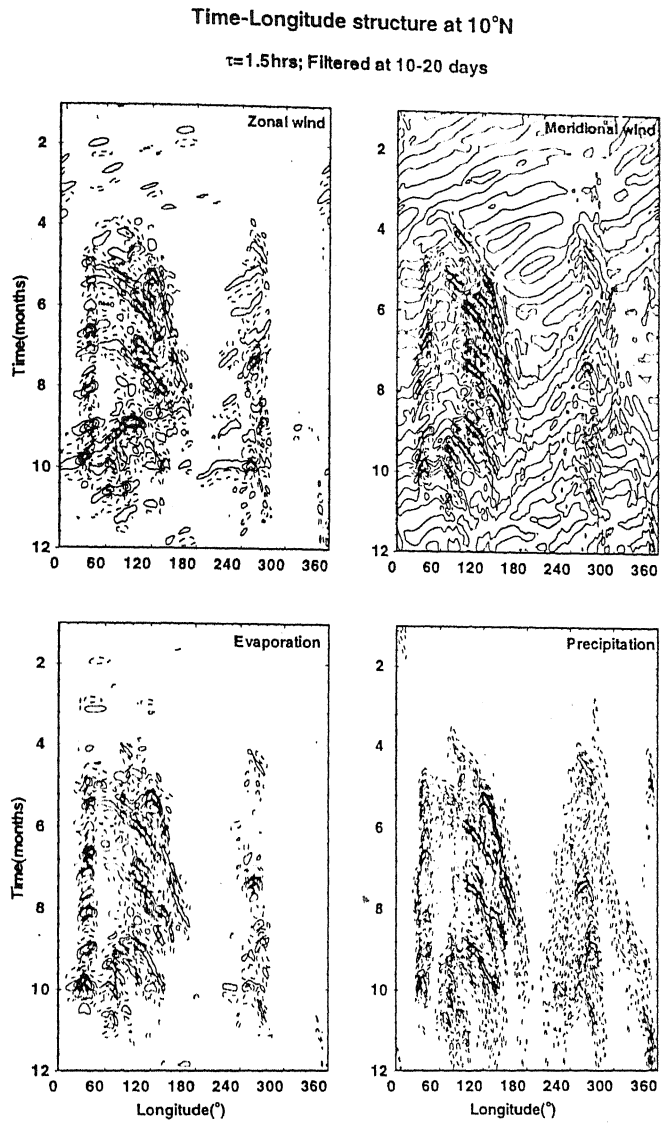

Figure 8.15: Same as the Fig 8.12, but for τ =1.5 hr.

of their phase propagation characteristics. While the fields at the equator quite generally exhibit a westward phase propagation, the fields at 10°N exhibit an eastward phase propagation in a characteristic manner. In particular, the fields tend to show an eastward propagation whenever amplitudes are large. Since this feature is present at several longitudes (and, in particular, in non-monsoon region where a seasonal reversal of the mean winds takes place), it is unlikely to be due to the mean winds. Thus, this feature is likely to be due to the dynamics of the system.

An interesting feature of the structure of the model fields is revealed by figures

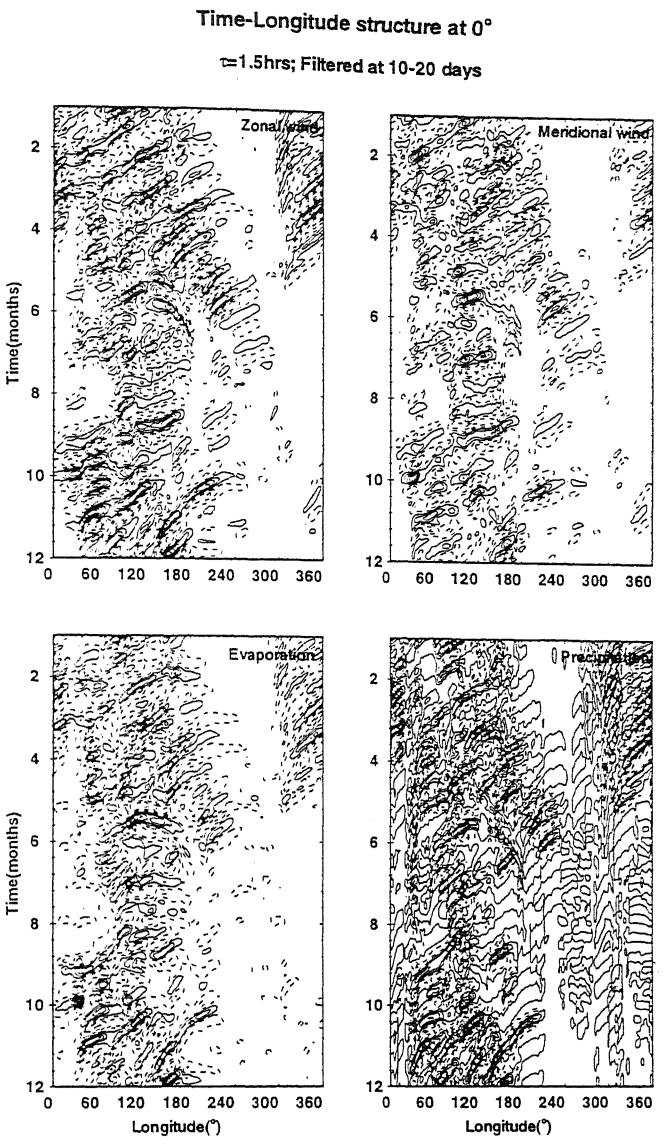

Figure 8.16: Same as the Fig 8.15, but over the equator

8.12 and 8.13. It can be seen that the u is weaker at the equator than at the Northern Hemisphere over the eastern pacific region, which would be consistent with a MRG wave structure for the u over this region. However, this feature is not present at other locations, especially over the monsoon region. The other feature is the presence of certain intense episodes, most prominent in the zonal wind and evaporation fields, both over the equator and the Northern Hemisphere.

The corresponding results for a value of τ=1.5 hr. are shown in figures 8.15 to 8.17. Comparison of the results for τ=0.5 hr. with the corresponding results for τ=1.5 hr. reveals no significant change in the phase propagation characteristics

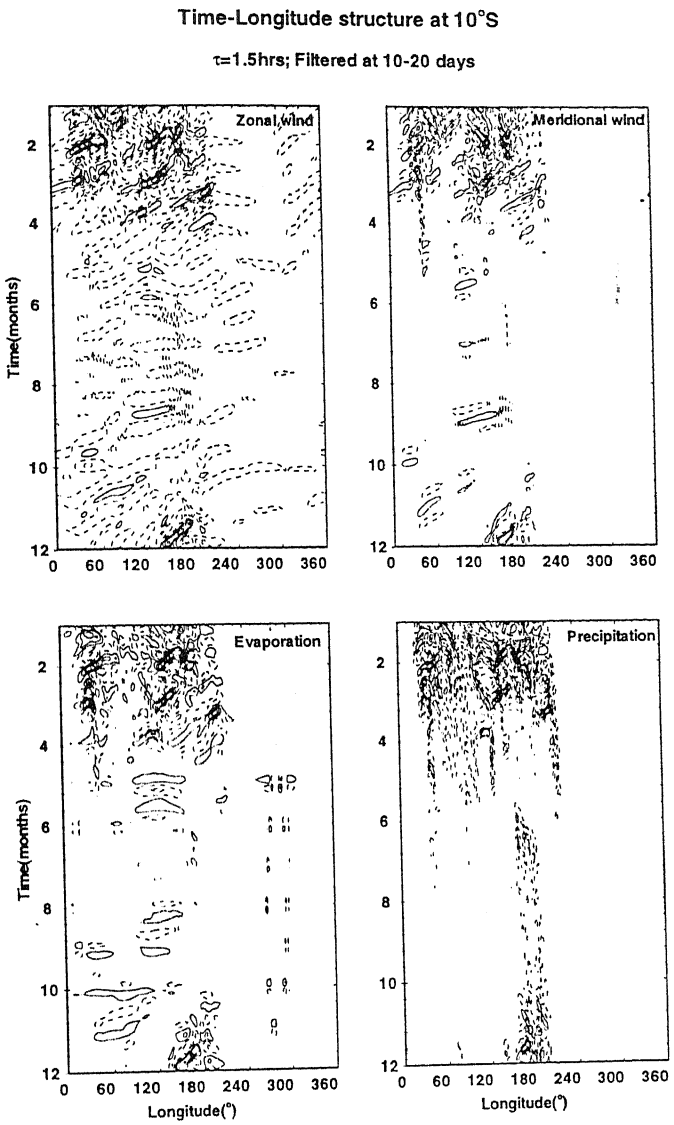

Figure 8.17: Same as the Fig 8.15, but over 10°S

for the two values of τ.

8.4 Time-Latitude Structure

We have seen that the model fields exhibit a pronounced annual cycle at certain longitudes, in agreement with observations. Here we examine the characteristics of the annual cycle specific to the 10-20 day wave. This will allow us to assess the contribution of the 10-20 day wave to the annual cycle of the anomaly circulation in the tropics. In addition, this will also provide us an insight into the detailed

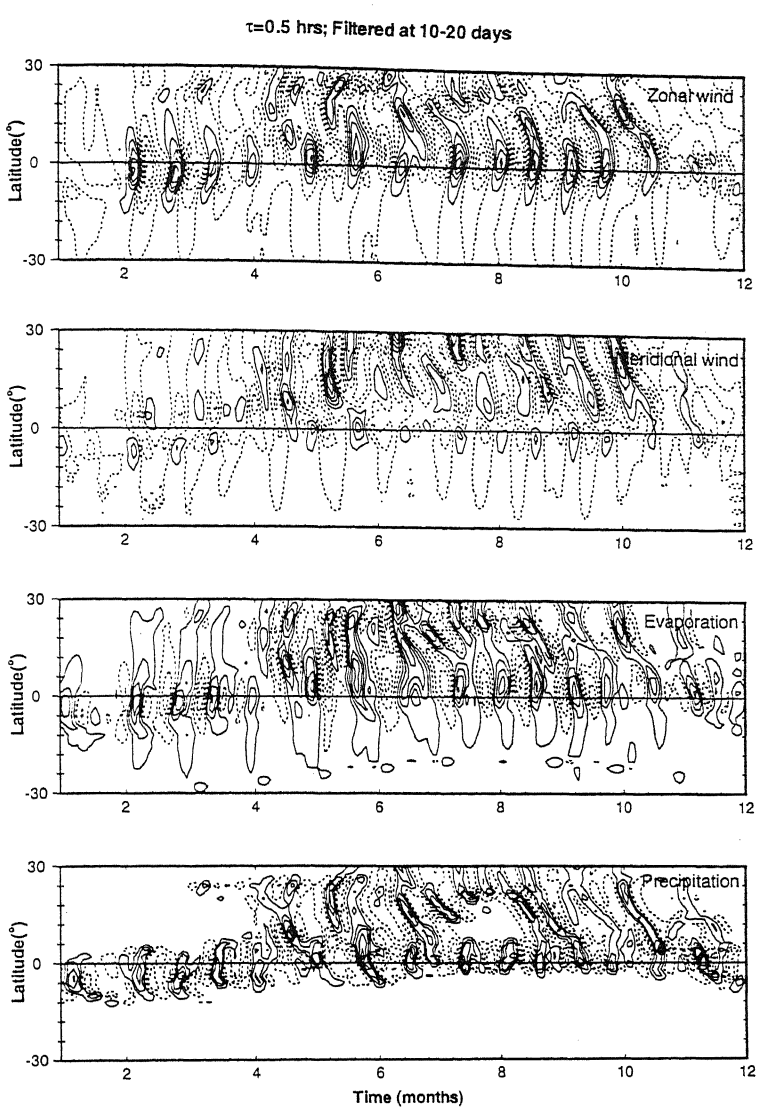

Figure 8.18: Time-latitude structure of the model fields from a composite one-year simulation at 90°E for τ =0.5 hr. Negative contours are dashed.

structure of the 10-20 day wave. The time-latitude plots of the model fields averaged around 90°E and filtered around 10-20 days are shown in figure 8.18. The corresponding results at 160°W and 80°W are shown in figure 8.19 and 8.20, respectively. A few striking zonal characteristics of the 10-20 day wave are discussed below. For example, at 90°E, the u is largely equator centered, although it also has prominent amplitudes in the Northern Hemisphere around 20°N, especially during the summer months. Thus this feature does not agree with the observed MRG wave structure of the 10-20 day wave, which should have u amplitude zero

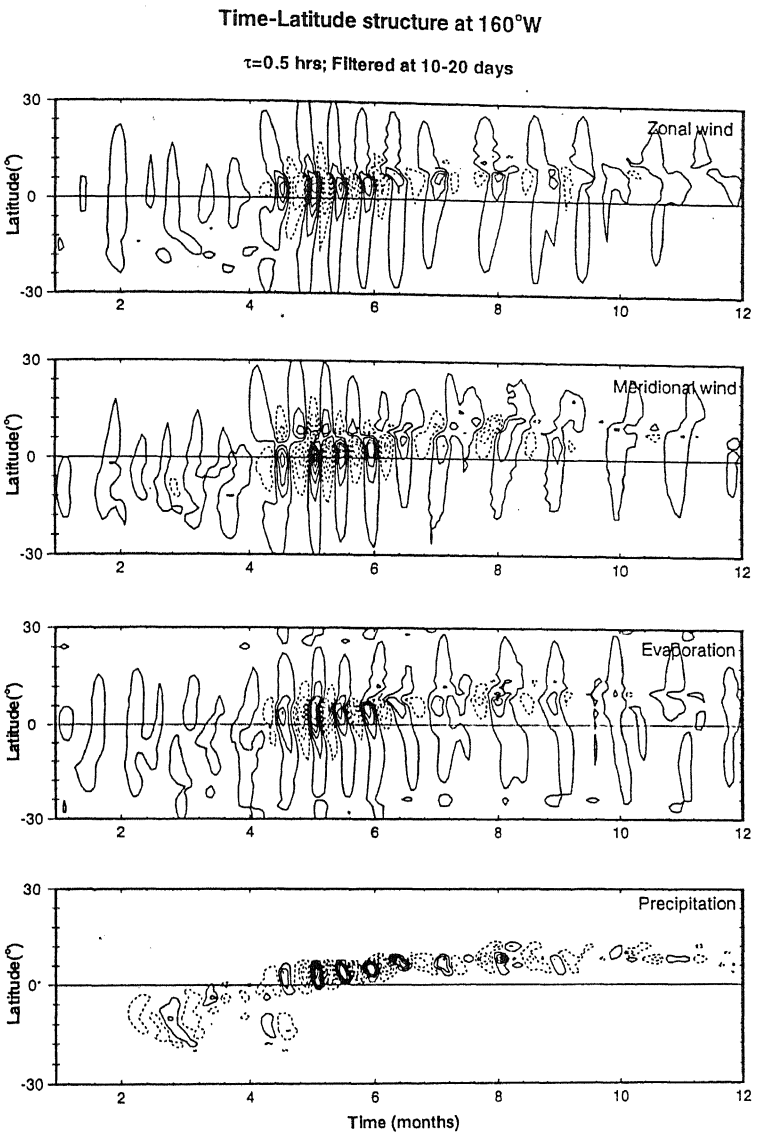

Figure 8.19: Same as the Fig 8.18, but over 160°W

over the equator. On the other hand, this structure agrees rather well with the *classical* easterly wave, which shows significant amplitude around 20°N. Further, the amplitudes at 20°N are strongest during the monsoon season. We have noted, in connection with our discussion with the time-longitude structures, that this is also the time and location when the 10-20 day wave exhibit a prominent eastward phase propagation. The picture emerges, therefore, is that our model simulation contains both *classical* easterly waves and the westward propagating 10-20 day wave. Over the Central and the Eastern Pacific, on the other hand, the model u is prominently off-equator, while the v is equator centered. Thus over this region,

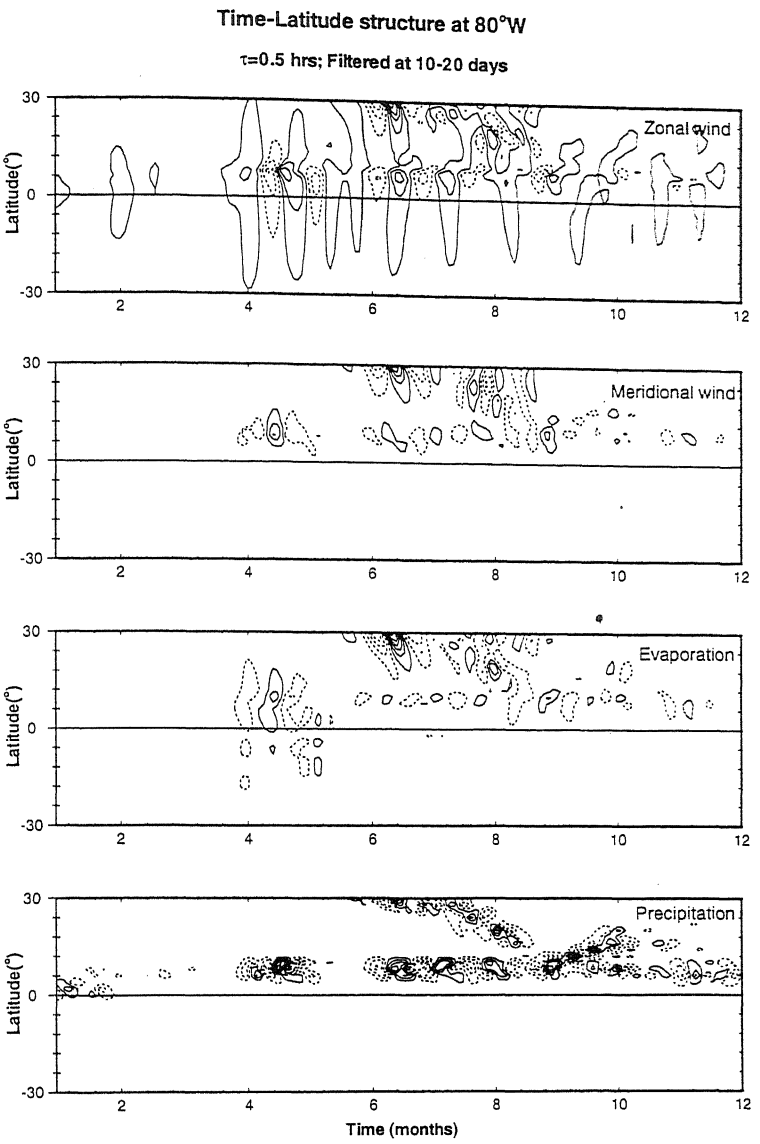

Figure 8.20: Same as the Fig 8.18, but over 80°W

the 10-20 day wave is essentially of MRG wave structure. Similar conclusions also hold for the Eastern Pacific sector, shown in figure 8.19.

The time-latitude diagrams show a prominent double-cell structure in all the model fields at 90°E (8.18 and 8.21). The two cells, one at the equator and the other at about 20°N, are related through an almost 90° phase difference in all the model variables. Such double-cell structure, however, is very weak or almost non-existent over the Pacific sectors. Over 80°W, this double-cell structure still exists to some extent, but the out-of-phase relation between the two cells prominent over 90°E has been now replaced by an in-phase relationship (8.20 and 8.23). Indeed,

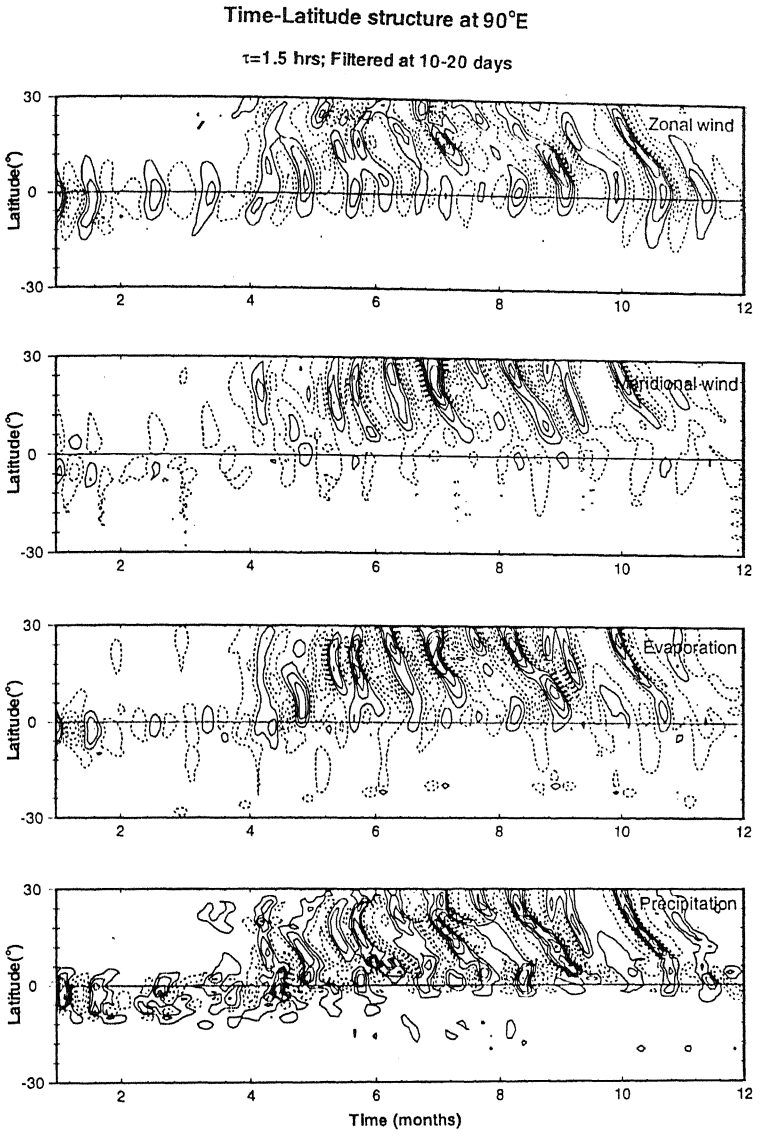

Figure 8.21: Same as the Fig 8.18, but for $\tau = 1.5$ hr.

over the 160°W, it is then, reasonable to conclude that the two cells merge at the mid-point of their separation to give rise to a single off-equatorial cell (8.19 and 8.22).

The time-latitude structures of the model fields also reveal that the annual cycle of the 10-20 day oscillations is quite different from the annual cycle of the unfiltered anomaly fields in general. In particular, over 90°E, we can discern two distinct components. One mode, with its u centered at the equator, shows very little or no change of its latitudinal distribution with the march of the season. The other, off-equatorial component, has a more distinct annual cycle. This (summer)

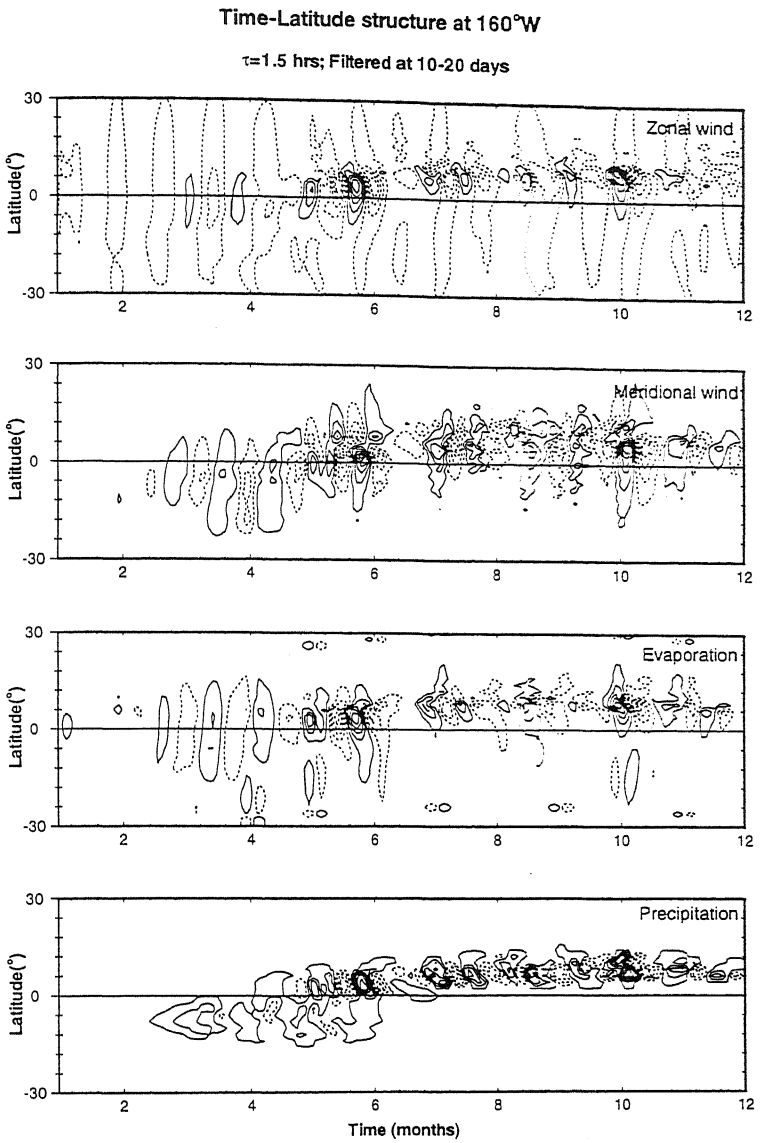

Figure 8.22: Same as the Fig 8.21, but over 160°W

component has significant activity at around 20°N, and has appreciable amplitude only during the summer months. Indeed, this Northern Hemisphere summer component of 10-20 day oscillation can be said to merge with the equatorial component with the march of the season as can be seen from figure 8.18. It is this second component of the 10-20 day oscillation that gives rise to the double-cell structure in the latitudinal direction. Such an equatorial expansion (or double-cell structure) in the meridional wind between 75-95°E was reported by Chen and Chen (1993) from an analysis of data generated by Global Data Assimilation System (GDAS) of the European Center for Medium-Range Weather Forecasts

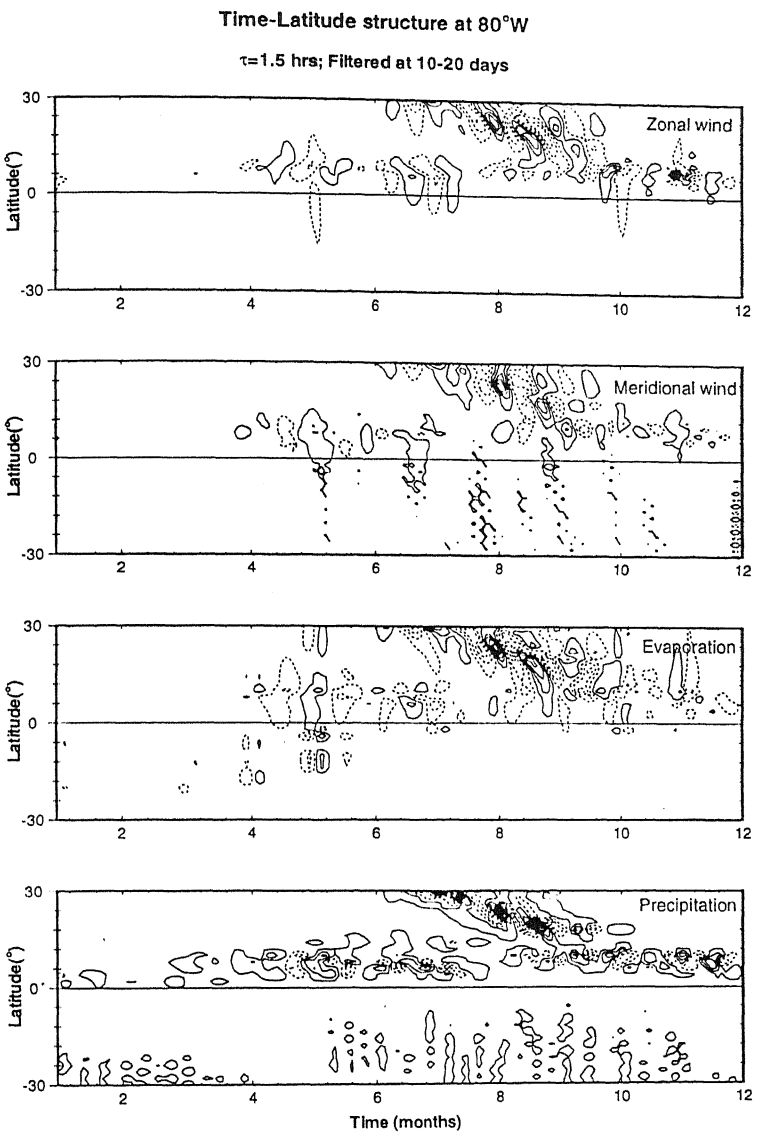

Figure 8.23: Same as the Fig 8.21, but over 80°W

(ECMWF). Although the analysis by Chen and Chen (1993) was carried out for only one year, and may not reveal the interannual variabilities of the characteristics of the 10-20 day mode, it is interesting that several of the observed features are also present in our composite model simulations. It can also be seen that the genesis of the two components with distinct zonal characteristics makes a significant contribution to the annual cycle of the total anomaly fields. In particular, the two components together determine the precipitation variabilities over the monsoon region at 10-20 day time scale.

8.5 Conclusions

A remarkable feature of the model simulation is its ability to simulate distinct features for the winter and the summer months, as well as for different zonal and meridional locations. In present model the distinctions between the summer and the winter as well as between different zonal and meridional locations come essentially through the mean fields. Hence, the results imply that detailed characteristics of the 10-20 day wave are to a large extent a response to the mean conditions. The mean conditions affect our model dynamics both dynamically and thermodynamically. Thus both the dynamical and the thermodynamical effects of the mean fields are essential for simulating the detailed structure of the intraseasonal variabilities.

To determine the role of the mean fields and the annual cycles of the mean wind and SST, the model simulations with only winter and only summer mean states are examined. In contrast to the 30-50 day oscillation which shows a prominent signal even in the absence of a mean annual cycle, the QBW disappears in the absence of a mean annual cycle. Thus not only the spatio-temporal structure but even the genesis of QBW is strongly linked to the mean annual cycle.

It appears that the contribution of QBO to the anomaly annual cycle is not negligible. Thus an inadequate simulation of QBW can adversely affect the simulation of the anomaly fields which, in turn, can change the characteristics of the total circulation in the tropics. The QBW, like the ISO1 is, therefore, likely to play a vital role in the tropical climate.

Chapter 9

The Spectrum of Oscillations: Interannual Variabilities

The most prominent oscillation of the tropical climate at longer than annual scale is the ENSO related variabilities. The atmospheric part of the ENSO scale variabilities, the Southern Oscillation (SO) arises from an interannual variations in the exchange of mass between the Indian and the Pacific Ocean and has been known to the meteorologists for a long time (Walker, 1932). The SO is known to have strong correlation with the oceanic variabilities known as the El Niño. Owing to its large climatic and associated socio-economic effects, the ENSO phenomena have received wide and sustained attention from both the communities of meteorologists and oceanographers. However, even from a purely dynamical point of view the ENSO phenomena, with its rich structure, play a crucial role in the tropical climate system. Although, following the conceptualization by Bjerkness (1969) and its subsequent development, ENSO is often regarded as an ocean-atmosphere coupled variability; it is possible that the *genesis* of the SO is a response of the tropical atmosphere to (SST-induced) convective forcing. Therefore, next the investigation is on the existence and structure of the interannual variability in our model simulation.

The SO variability is quasi-periodic, with a time scale between 3 and 7 years. It

is in this background of SO oscillations that the ENSO (warm and cold events) that brings about such drastic regional and global scale changes in the atmospheric and oceanic circulations is embedded (van Loon and Shea, 1985; Lau and Sheu, 1988). The SO signal is characteristic of the global tropics, although the oceanic counterparts of ENSO variabilities, El Niño and the La Niña that give rise to extreme warm and the cold events are more pronounced over the Pacific. However, contrary to earlier belief, ENSO phenomena are also more global in character. Thus warm events, in phase with ENSO events over the Pacific but with weaker amplitudes also appear over the Indian Ocean (Yasunari, 1987). We shall leave the question of the role of ocean-atmosphere coupling in the structure of ENSO variabilities to a later chapter.

While the mechanism and structure of ENSO related variabilities have received wide attention in recent years, the tropical atmosphere also supports other long-term variabilities. For example, the existence of a biennial variability in the atmosphere has been now known to the scientists for at least three decades. A summary of a number of earlier (prior to 1960) works on the existence of a biennial oscillation in the stratospheric and the tropospheric variables was prepared by Landsberg (1962). As it often happens in the atmospheric oscillations, the biennial variability was found to be quasi-periodic, with a time scale between 2 and 3 years. A more comprehensive analysis of the existence of a QBO in the tropospheric variables was provided by Landsberg *et al.* (1963) from an analysis of time series of surface temperature at a number of widely spaced locations over the globe. The subsequent years have seen a surge of research works emphasizing various characteristics of the QBO and its relation to various other oscillations.

A characteristic of the QBO is its rather global presence in a diverse set of variables. Thus QBO signal has been observed in East African rainfall (Rodhe and Virji, 1976) and United States surface temperature (Rasmusson *et al.* 1981). Biennial variability in the surface pressure has been documented by Trenberth in

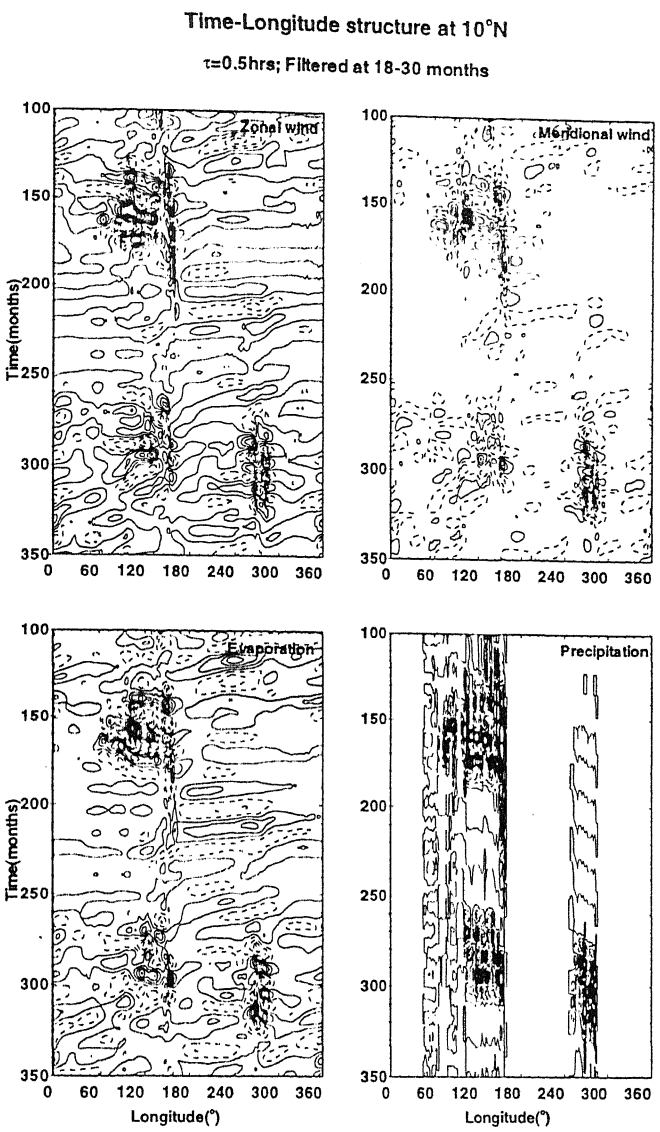

Figure 9.1: The time-longitude structure of model fields from a long term simulation at 10°N for τ =0.5 hrs.; filtered around 18-30 months. Negative contours are dashed

a series of studies (Trenberth 1975, 1976a, 1976b, 1980). Other studies (Trenberth and Paolino, 1981 and Trenberth and Shin, 1984) also provide ample evidence for the existence of a biennial signal in the tropospheric variables.

The QBO thus differs from many other tropical oscillations in that it is not necessarily confined to the tropics. Given this fact, it is not a priori obvious that our model, with essentially convective dynamics, is appropriate for investigating the genesis and structure of the QBO. Nor it is clear that a single mechanism generates the QBO the world over. We, therefore, wish to explore the possibility

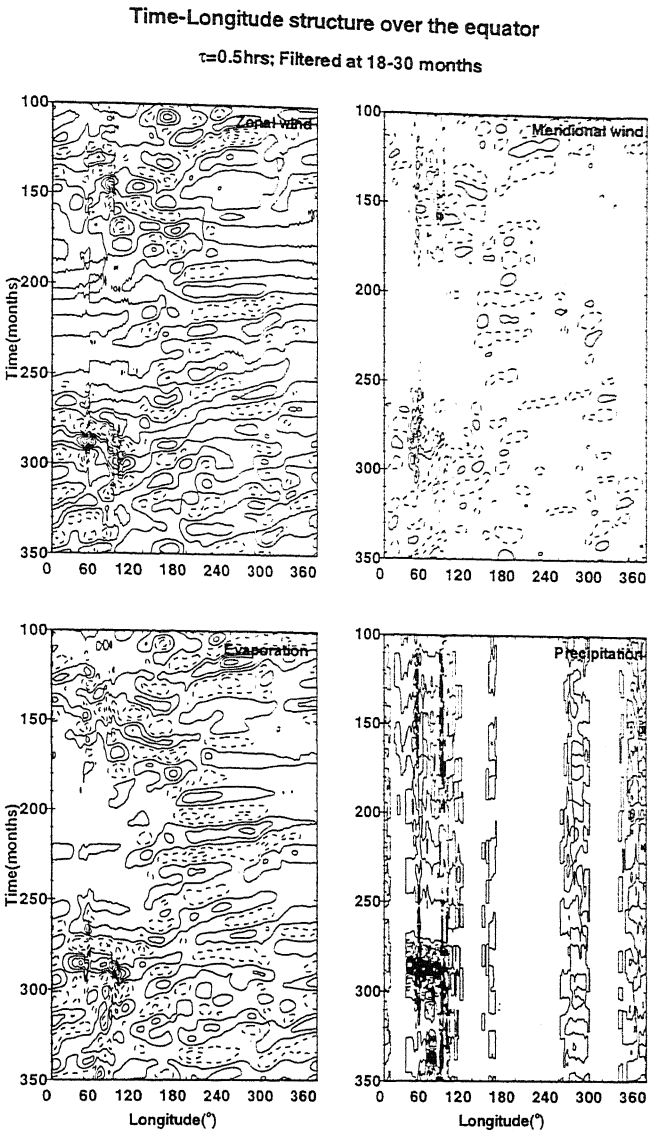

Figure 9.2: Same as figure 9.1, but over the equator

of a tropical QBO sustained by the convection induced dynamics in response to the mean fields.

The focus of the present chapter is on the structure of the interannual variability present in our model simulation and their comparison with observed structure. Also addressed is the question of essential mechanism necessary for the existence of interannual variability in our model simulation. To analyze the general properties of interannual variabilities in the simulation, the long-term simulations for different dynamical conditions are considered. To investigate the existence of any significant oscillation in the interannual scale, first the time series from the inter-

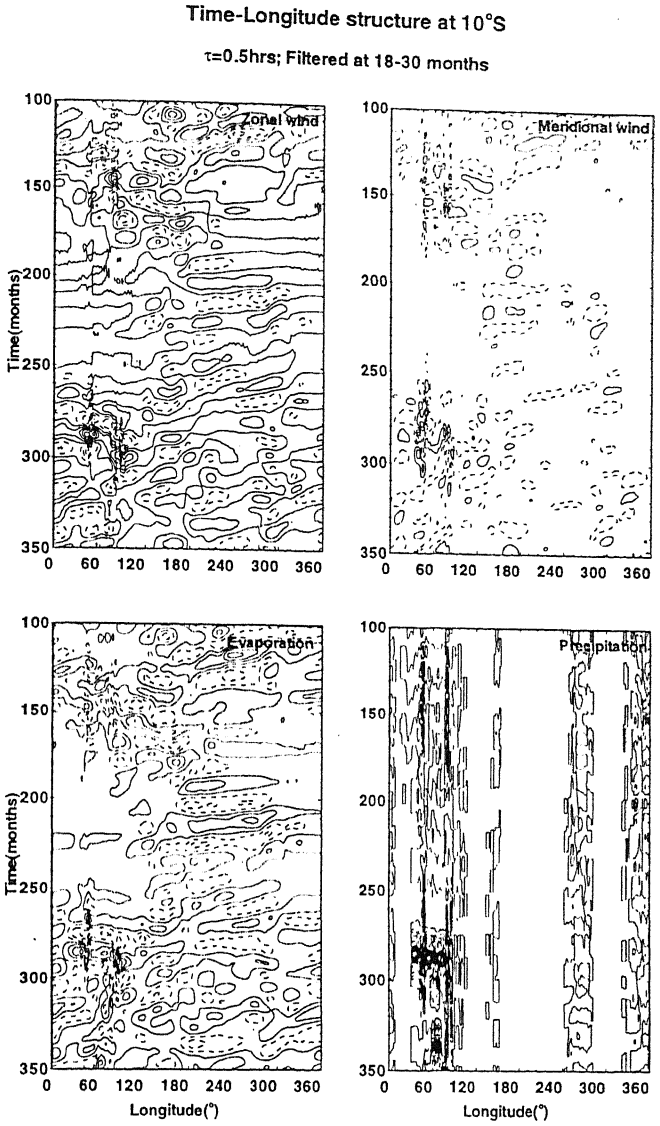

Figure 9.3: Same as figure 9.1, but over 10°S

annual model simulation is analyzed. It was shown that both for τ =0.5 hour and $\tau = 1.5$ hour there exist significant peaks in the 18-30 months and 3-7 years range above the corresponding red noise level. However, as we have seen in our earlier studies, the best simulations of the characteristics of the tropical variabilities at monthly and intraseasonal timescales are provided by a value of CTL=0.5 hour. We shall, therefore, investigate the characteristics of the interannual oscillations also for $\tau = 0.5$ hour.

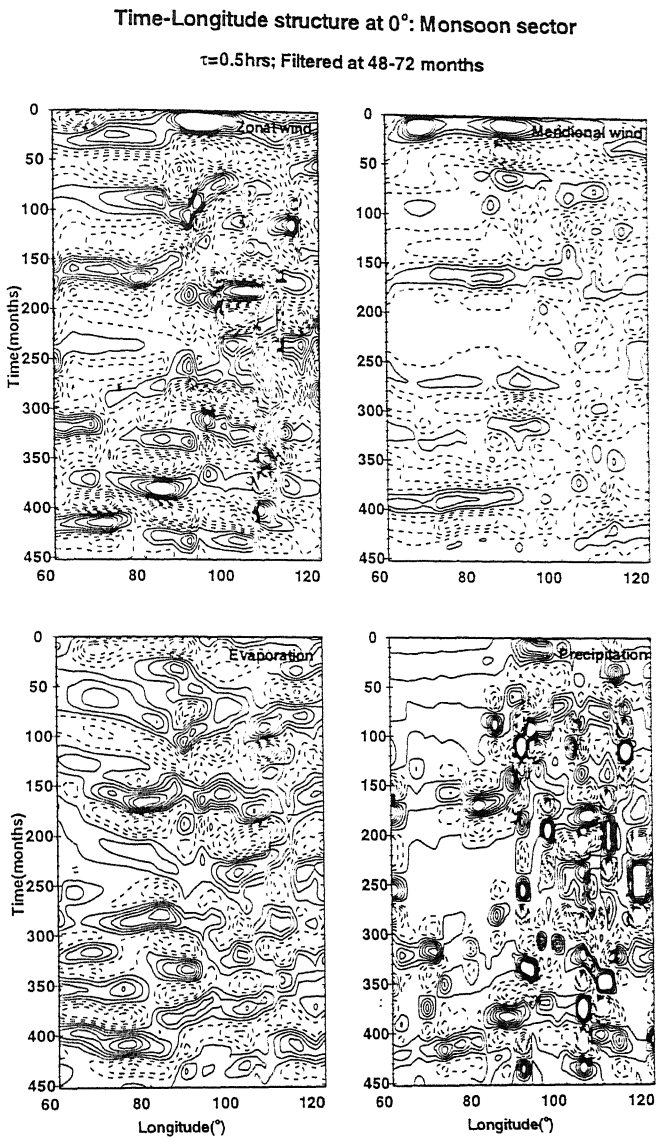

Figure 9.4: The time-longitude structure of model fields from a long term simulation at 10°N for τ =0.5 hrs.; filtered around 48-72 months. Negative contours are dashed

9.1 Longitude-Time Structure

Having seen the existence of significant signals at the two interannual periods in our model simulation, we have examined the phase propagation characteristics of these waves in detail to compare with observed structure. Hence, the time-longitude structures of the model fields filtered at the two interannual periods *viz.* 18-36 months and 3-7 years are examined. The data in these figures represent model simulations from the 38-year integration with an SST-dependent EWF. Once again, the results have been analyzed over three zonal regions, *viz.* the

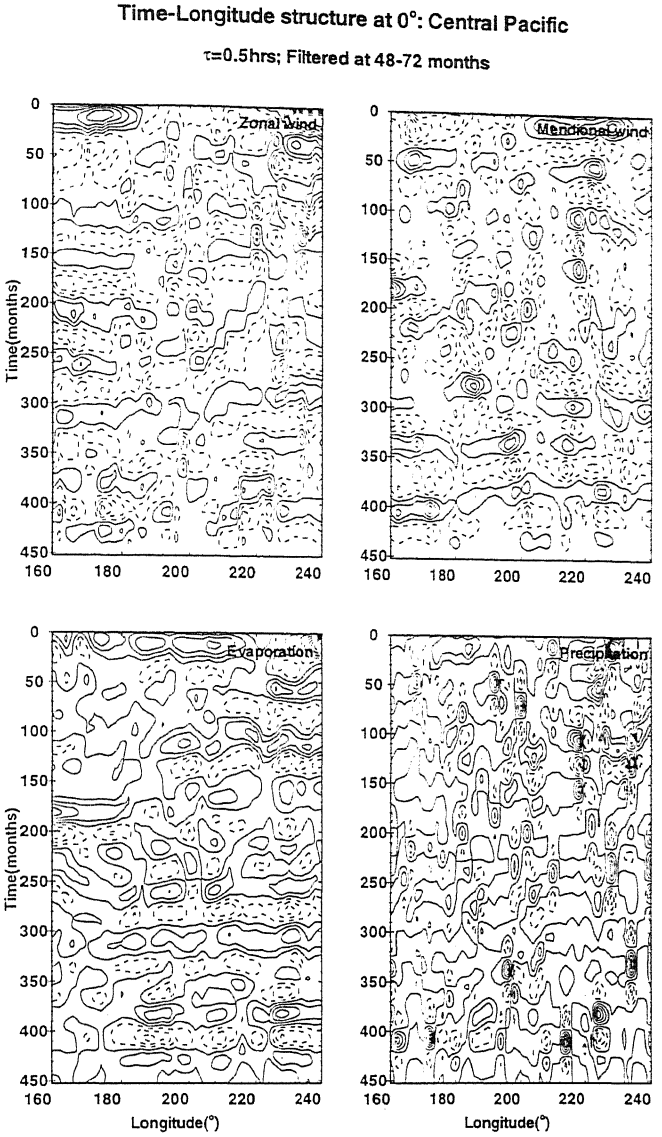

Figure 9.5: Same as figure 9.1, but over the equator

monsoon sector (60-120°E), the central Pacific (170°-130°W) and Eastern Pacific (110-50°W) and also over three latitudinal positions: equator, 10°N and 10°S. However, we shall present only the selected examples of simulations.

9.1.1 The Quasi-Biennial Oscillation

Figures 9.1 to 9.3 show the time-longitude structure of the model fields at 18-36 months. For clarity of presentation we plot only about twenty years (100-350 months) of total model simulation of 450 months. The most prominent feature in the time-longitude structures at the equator and the 10°N (figures 9.1 and 9.2

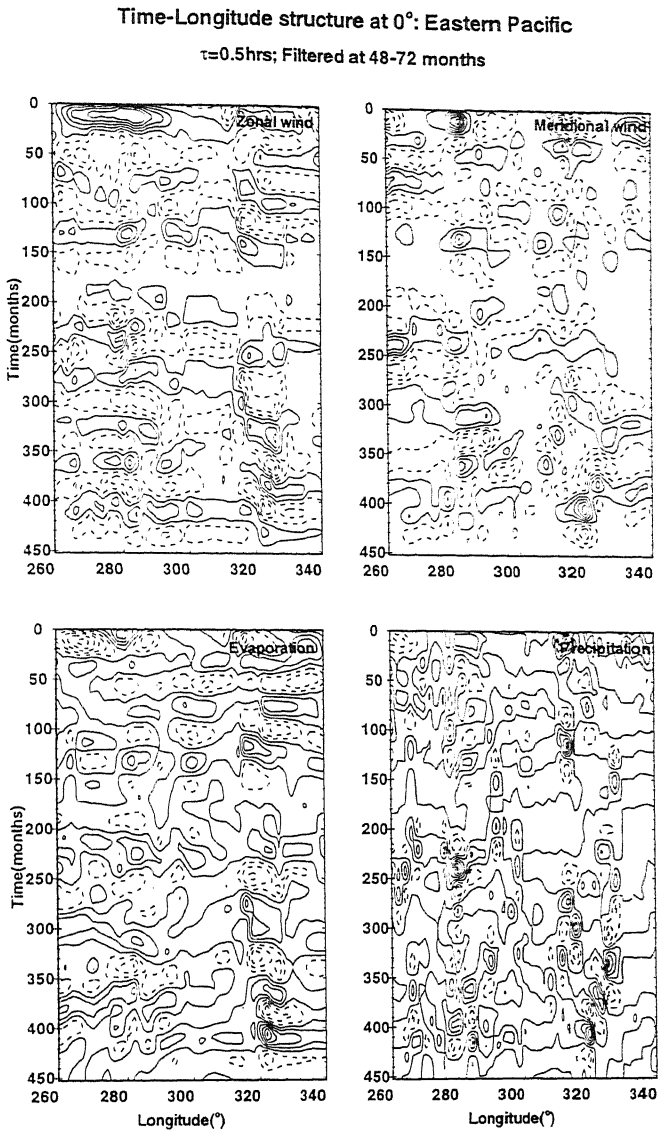

Figure 9.6: Same as figure 9.1, but over 10°S

respectively) is a clear eastward propagation, especially over the region 60°E and 160°W. In the southern hemisphere at 10°S (figure 9.3), the phase propagation is often westward. Besides, even over the equator and 10°N, the eastward phase propagation is not prominent over the zonal location beyond 160°W.

There are not many detailed analyses of the structure of QBO for comparison of our simulations. However, Ropelewski *et al.* (1992) analysed the time-longitude structure of QBO by filtering analysed COADS shipwinds at biennial frequency. The equatorial time-longitude structure of the biennially filtered data for the period 1956-1985 over the Indian and Pacific Oceans (40°E-80°W) clearly shows

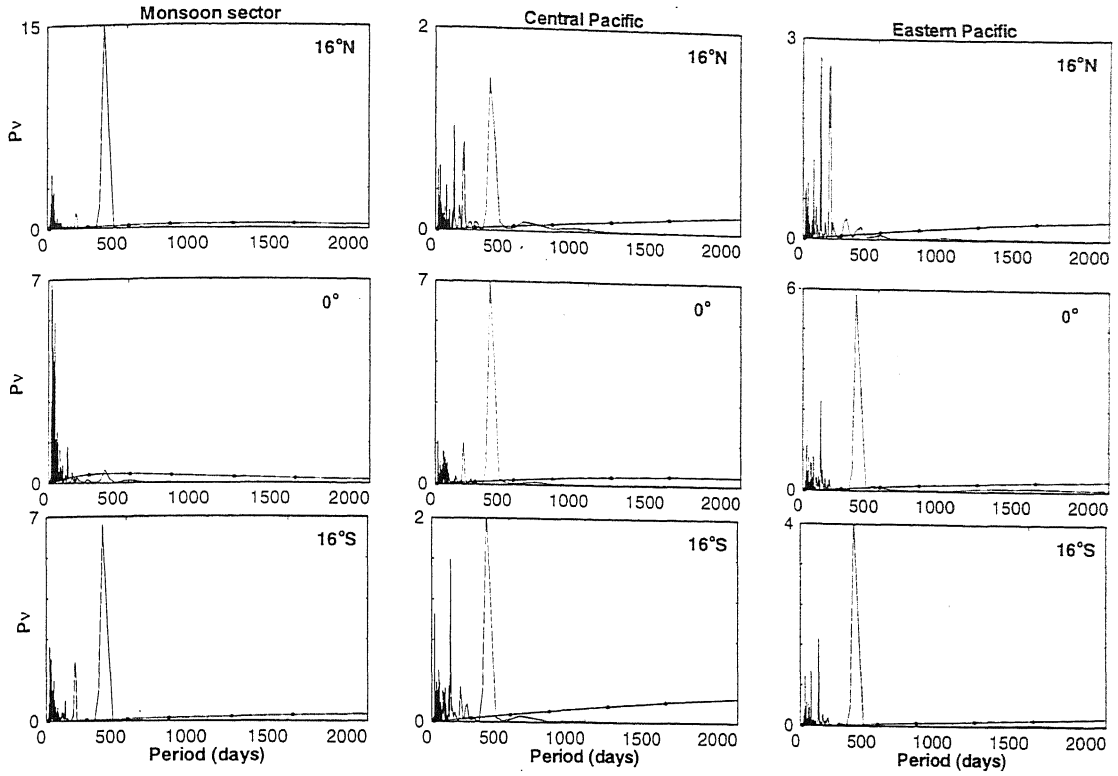

Figure 9.7: Power spectra of unfiltered time series of the model u field from long term simulation for climatological SST dependent EWF plotted with $\nu P(\nu)$ as the ordinate and period as abscissa.

an eastward phase propagation over this region. Our model simulations agree well with these observed structures. More detailed observational analyses are required for verifying the zonal and latitudinal distributions in the structure of QBO implied by our model simulations.

Another feature of the simulated time-longitude structure is the episodic nature of QBO activity with a time scale of about ten years. It has been recognized in recent years that there is considerable phase coherence among the annual cycle, the QBO and the low frequency variability of SO (Rasmusan, *et al.* 1996). The model simulations also support an oscillation with 8-10 years at several locations. The interrelationships among the annual cycle, QBO and ENSO are discussed later in this chapter.

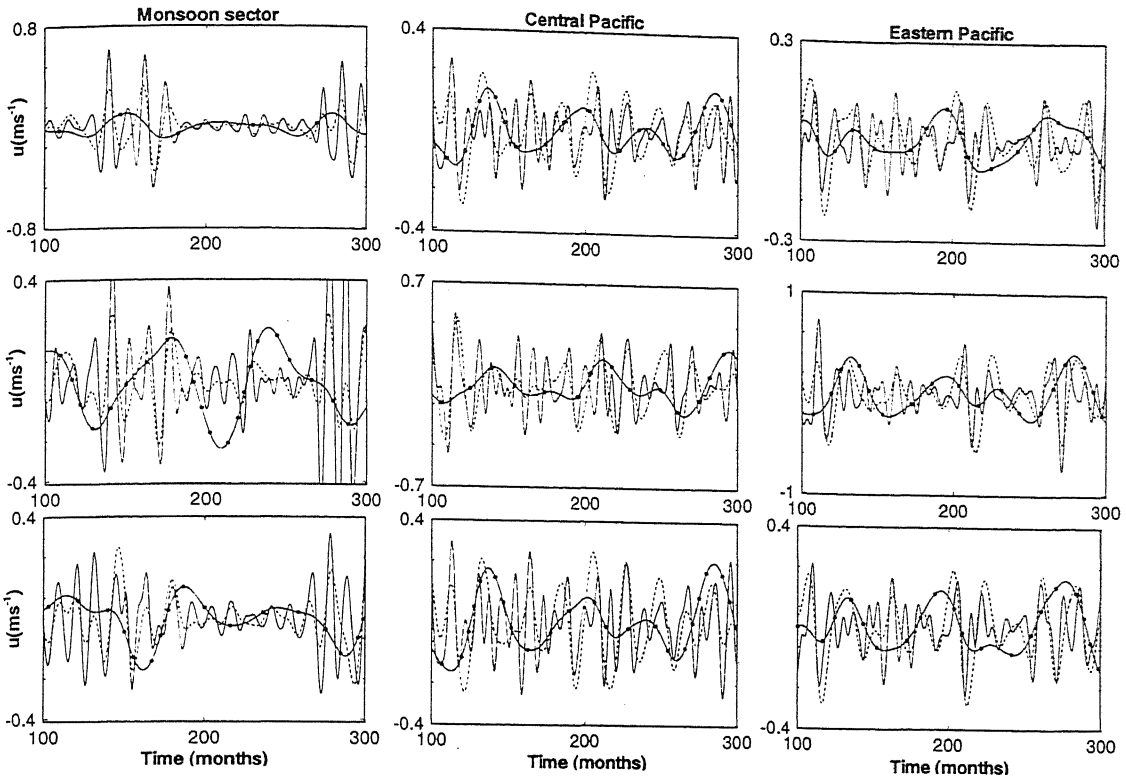

Figure 9.8: The time series of the u-field, filtered at annual (solid line), QBO (dashed line), and ENSO (solid with symbol) scales.

9.1.2 The ENSO Scale Oscillation

The time-longitude structure of the model fields for the entire 450 months of model simulation and over the equator are presented in figures 9.4 to 9.6 for three latitudinal positions. To describe regional structure of the 3-7 year variability in our mode simulations, we have presented the results for three zonal segments. A prominent feature of the simulated 3-7 year oscillation over the eastern Pacific is its strong eastward phase propagation (figure 9.6). This eastward propagation is also seen, but only weakly, over the other two zonal locations *viz* monsoonal region and Central Pacific (figures 9.4 and 9.5). There are, however, several other characteristics that distinguish the fields at three different zonal locations from one another. One such characteristic is the phase relationship between zonal wind and evaporation. While over the monsoon region, they are almost in phase and

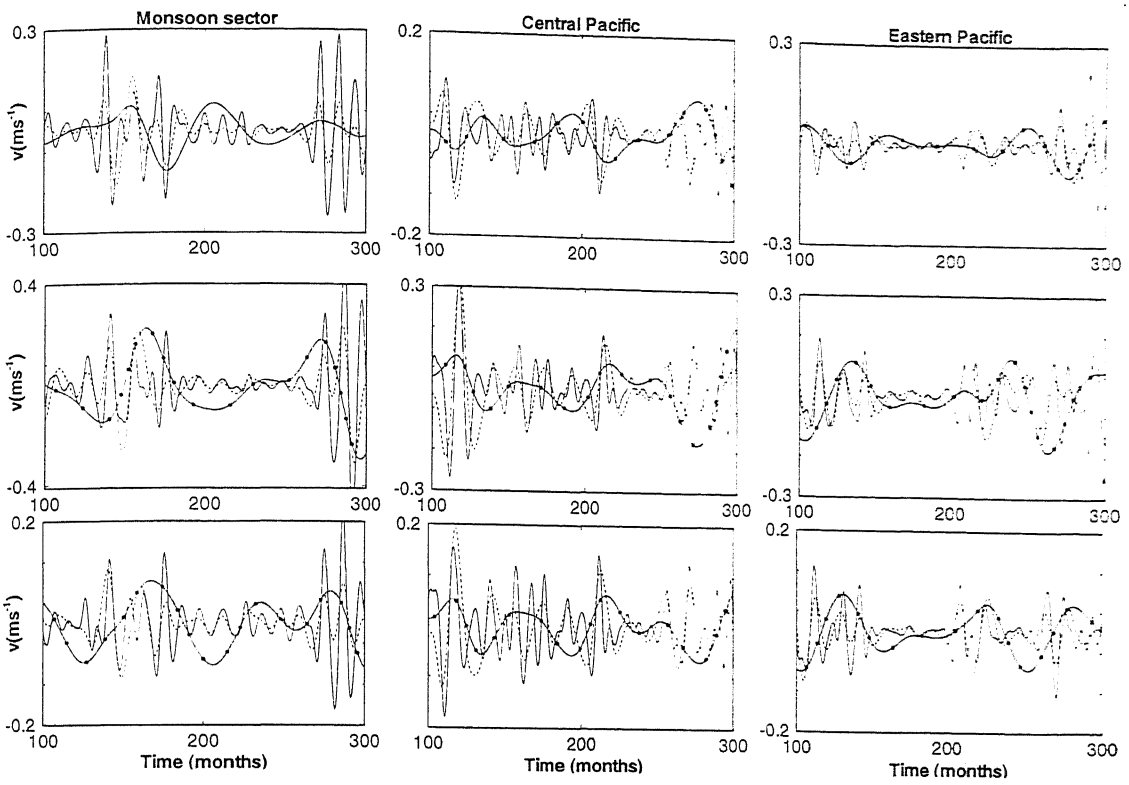

Figure 9.9: Same as figure 9.8, but for meridional wind

are nearly out-of-phase over the Pacific regions. In particular, over the Pacific regions strong evaporative forcing is associated with easterly wind anomalies. Figures show that the 3-7 year variability also exhibits episodic nature, more pronounced over the monsoon region with a low frequency variability.

9.2 Role of Interannual Variability of SST

Several studies suggest that the interannual oscillations are ocean-atmosphere coupled modes. Given the large time scale of these oscillations it is reasonable to expect that their evolution and structure is significantly affected by the ocean-atmosphere interaction. To determine the role of the interannual variability of SST on the genesis of QBO, we have integrated the model for 15 years with a climatological mean annual cycle of SST. The climatological mean annual cycle of

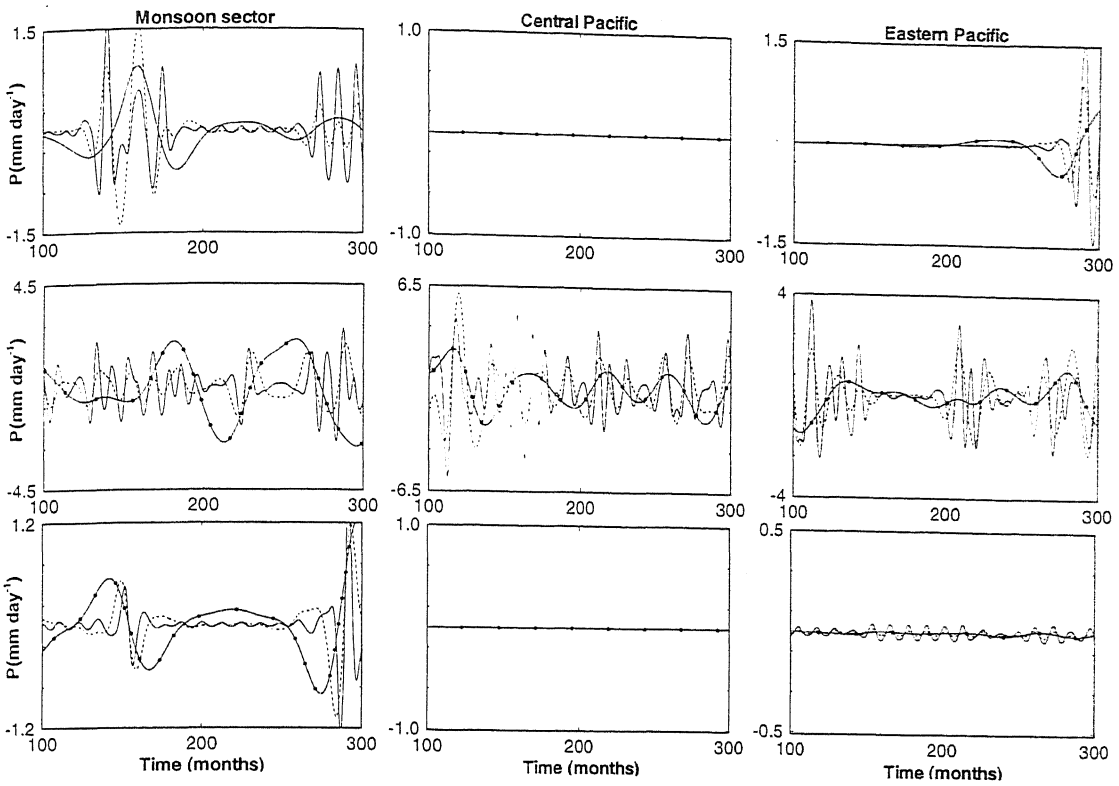

Figure 9.10: Same as figure 9.8, but for precipitation

SST was constructed by averaging the monthly mean SST fields for 38 years from COADS. We have examined the role of the absence of interannual variability of SST primarily in terms of power spectra of the model fields at different locations. Figure 9.7 represents the power spectra for the model u at three different zonal locations over the equator as indicated in the panels. The solid line and the solid line with symbol in figure 9.7 represent the power spectra for $\tau = 0.5$ hour and the corresponding red noise, respectively. As can be seen from this figure, there is no peak in the power spectra at the interannul periods above red noise level for any of the variables at any of the locations. The most prominent signal is centered around the annual time scale, followed by smaller but significant peaks at intraseasonal frequencies. Since the role of SST in our model is to modulate the strength of EWF, the above results imply that the interannual variation of convective forcing is necessary for the genesis of interannual oscillations. This in

turn emphasizes the importance of ocean-atmosphere interaction in interannual oscillations. Since the interannual variability in SST crucially dependents on the forcing by the surface winds.

9.3 The Interrelationships Among the Annual Cycle, QBO and ENSO

A question of great importance is the interrelationships among various oscillations with different time scales. This is related to the phase locking of various oscillations. There is a strong evidence of phase locking of the annual cycle with the ENSO cycle (Rasmusson and Wallace 1983). Similarly, there is evidence of phase locking between the QBO and ENSO (Lau and Sheu 1988). Brier (1978) and Nicholls (1978), on the other hand, suggested a mechanism of the tropospheric QBO involving a nonlinear interaction between the annual component of the surface wind, surface pressure and SST. Given the fact that our model supports strong signals at annual, QBO and ENSO scales, we have analyzed the phase locking among the three oscillations by considering time series for the model fields filtered at the three frequencies.

Figure 9.8 presents the time series of the model u field filtered at annual (solid line), QBO (dashed line) and ENSO (solid line with symbol) scales. The fields have been zonally averaged (before filtering) over three zonal locations as described before. Once again, we show the results for three latitudinal positions: 16°N (top panels), equator (middle panels) and 16°S (bottom panels). Figures 9.9 and 9.10 represent the corresponding results for the model v field and precipitation, respectively.

As can be seen from these figures, there exists a clear relationship between the QBO and the annual cycle. Not only are the two oscillations phase-locked, but their amplitudes vary proportionately in most of the time. In particular, they go through periods of intermittancy in phase. This is also largely true about the

ENSO signal (solid line with symbol), especially in the zonal wind (figure 9.8). A scrutiny, however, reveals a much richer structure in terms of zonal and meridional variations of the relationships among these oscillations, and highlights the need for more detailed analyses of observed data. For example, over the monsoon sector the ENSO is often of opposite phase with the QBO (and hence also with the annual cycle). The lack of phase locking decreases as we move to central Pacific where, over the equator, there exists a much greater phase coherence. However, the phase locking is generally weak over the off-equatorial regions. It should be noted that the zonal wind, especially over the Pacific sectors, exhibit strong equatorial trapping, while the signal in the meridional wind is small in general in all the three oscillations. While these relations between the three oscillations are indication of inter-period interactions, more elaborate analyses of observed as well as model simulations are required to build up a clear and consistent dynamical scenario.

9.4 Conclusions

The above results indicate that the convective tropical atmosphere, under the influence of SST, can support interannual variabilities with observed characteristics. Since we have used the observed SST, this variability is already present in the convective forcing in our model through its dependence on SST. What the above results show, therefore, is that our model with convective time lag can respond to this forcing and support the interannual oscillations with observed periodicities. The question, of course, arises as to how the interannual oscillation arises in the SST, and quite likely the genesis mechanism depends on ocean-atmosphere coupling. An important point, however, is that once the interannual oscillation is generated, its structure determined by the convective dynamics is quite similar to the observed one.

A number of studies have emphasised the interconnection between annual cy-

cle, biennial variability and the SO (Rasmussm *et al.* 1990). In particular, the biennial variability appears to be fundamental to SO itself (Ropelewski *et al.* 1992). A number of studies have emphasized the biennial component of the SO variability (Rasmussm *et al.* 1990; Barnett, 1991; Yasunari, 1987, 1989; Van Loo and Shea, 1985). On the other hand, there is also considerable evidence of a close relationship between the 30-50 day intraseasonal oscillation and SO both in terms of genesis and structure (Lau and Chau, 1986, 1988; Lau, 1985; Lau and Sheu, 1988). Our model with its ability to simulate this entire spectrum of SO is particularly suitable to investigate these aspects. Indeed, as we have seen, the model simulated annual cycle, QBO, and ENSO scale variabilities exhibits the observed phase coherence; the question of phase coherence between intraseasonal and interannual vraibilities needs to explained in future.

We have seen in the context of our discussion of the total spectra of simulated variabilities, there also exists a significant (above red noise) decadal scale oscillation in the model simulations at several locations. Although we have not explored this in the present discussion, the decadal variability is an important component of the tropical circulation. It is very encouraging that our model can capture this entire range of variabilities with a single basic mechanism. This paves the ground for a detailed investigation of each these oscillations under different dynamical and regional condtions.

Chapter 10

Convective Coupling and Tropical Variabilities

Recent analyses reveal that ocean-atmosphere coupling (OAC) plays a significant role in a wide spectrum of oceanic and atmospheric variabilities in the tropics. Following the conceptualization by Bjerknes (1969), it has long been held that the most prominent interannual oscillation (IAO), El Niño-Southern oscillation (ENSO), is an ocean-atmosphere coupled instability. Importance of OAC in the annual cycle has been shown for the eastern Pacific and the Atlantic Oceans by observational studies of Mitchell and Wallace (1992) and Wang (1994). Wang (1994) used monthly SST fields for the period 1950-1987 obtained from the Comprehensive Ocean Atmosphere Data Sets (COADS) to investigate the annual cycle in the tropical Pacific (between 30°S-30°N and 120°E-76°W). His analysis reveals two distinct components of variations in SST with respect to the equator. One antisymmetric, extratropical component that explains about 70% of the SST variance on the average and a symmetric equatorial annual cycle (SEAC). The SEAC is found to dominate the central-eastern equatorial Pacific, with amplitude decreasing with distance away from the equator. Wang (1994) concludes that while the antisymmetric component is essentially a delayed response to solar radiation with a maximum in the late summer (minimum in the late winter), the SEAC is

primarily governed by OAC, with maximum (minimum) in late fall (spring). In an earlier study Wang (1993) demonstrated the important role played by OAC in the annual development of the cold tongue in the eastern Pacific. In the intraseasonal scale the role of OAC has been less clear, although both the tropical atmosphere and ocean exhibit strong signals in the intraseasonal time scale (IST). The best known example of atmospheric intraseasonal oscillation (ISO) is the 40-60 day Madden and Julian oscillation (Madden and Julian, 1971; 1972). It is now known that a prominent intraseasonal signal is present also in the oceanic circulation. Analysis of time series data from surface moored buoys in the eastern equatorial Pacific (between 110 and 140^{0}W) for the period 1975-83 by McPhaden and Taft (1988 hereafter MT) revealed a very prominent ISO in zonal current, temperature and dynamic height. These signals were found to have characteristics of Kelvin waves, with eastward propagation, zero meridional velocity and with zonal velocity and temperature nearly in phase. Enfield (1987; E87) showed that the sea level fluctuations at IST during 1975-84 along the west coast of the Americas are remotely forced by atmospheric ISO in the western Pacific. These forced signals with Kelvin wave structure propagate eastward across the equator to reach the eastern boundary, where they propagate as coastal Kelvin waves. Although the analysis of MT revealed the period of the signals to be 60-90 days as against 40-60 days found by E87, it is likely that both the signals represent the same physical process (MT). A scenario that provides a qualitative understanding for such a situation is discussed later using the present model.

There have been several attempts to develop a dynamical mechanism to explain the coupled variabilities in the tropics, especially the ENSO. The basic premise of most of these studies is that while the linear atmosphere and the ocean may be by themselves stable, OAC can make the (coupled) system unstable. The OAC in these studies involves a mechanical coupling which determines a forcing of the oceanic current by the (lower) atmospheric wind stress and a thermal coupling

which determines the effect of SST on atmospheric heating. In most of the studies mentioned above, the latter is prescribed as a proportionality relation between SST anomaly and perturbation heating of the atmosphere. In such a formalism, SST acts like a direct heat source for the atmosphere, and the link between SST and atmospheric convection is an implicit one. Of course, the direct heat source provided by SST implicitely involves the convective processes, in the sense that the changed low-level circulation will result in modified intensity and distribution of convection. Although there have been a few attempts to incorporate the effects of convection directly into the formulation of OAC (Lau and Shen, 1988; Goswami and Selvarajan, 1991), these formulations can be termed as direct coupling where SST can heat the (lower) atmosphere, regardless of presence or absence of convection. The role of convection in these formulations is indirect or implicit. One reason for the indirect role of convection in these studies is that the moisture variable, and hence the precipitative heating, is determined by a balance equation. It should be noted that although Lau and Shen (1988 hereafter LS) begin with a dynamic moisture equation, their subsequent assumption of a convective regime effectively removes the time-dependence of the moisture variable. However, in a dynamical scenario the convective and non-convective regimes themselves evolve, one changing to the other depending on the local and time dependent forcing of the moisture variable. This is particularly true for a coupled environment, where SST plays a crucial role in the moisture variable. Indeed, recent analyses seem to indicate that the atmospheric convective activity is inseparably coupled to the oceanic processes. Several studies point to strong association between SST and the atmospheric convective activity at different time scales. In an analysis of data from International Satellite Cloud Climatology Project (ISCCP), Weare (1994) found significant correlation of SST with cloud variables both at IST and inter-annual time scales (IAT). The analysis of Weare (1994) further shows that not only SST but time rate of change of SST is also important for these processes.

From an analysis of intraseasonal variability of the tropical Pacific-Indian ocean and atmosphere using 7 year (1986-93) daily gridded data for variables like outgoing longwave radiation (OLR), surface stress and SST, Hendon and Glick (1995) report significant role of intraseasonal (30-50 day) cloud activity, and resultant short wave anomalies, on SST, especially over the Indian ocean eastward of about 165°E. The importance of the evaporative process in ENSO related variabilities has been emphasized by Myers *et al.* (1986).

The above analyses thus point to the possibility that the mechanism of OAC, in general, is different from the one usually assumed to explain ENSO. While a strong association between SST and (low-level) convection is quite expected, the observed association between SST and cloud activity, in particular, shows that the entire (lower) atmospheric column and the atmospheric convective activity are directly involved in OAC. It is possible that the primary mechanism of OAC is through the effect of SST on the atmospheric convection. This would imply that, unlike in the conventional formalism where the atmospheric heating is directly controlled by SST, the (OAC induced) atmospheric heating is possible only through deep heating by the column precipitation. In particular, in such a scenario, OAC behaves like a (second order) threshold process, somewhat akin to first order phase transition that results in precipitation. In the same way that precipitation cannot occur until the moisture content exceeds a critical value, the OAC induced atmospheric heating in our scenario is not effective until SST induced convection reaches a critical value. We shall call such a representation of OAC as convective coupling, to contrast it from the conventional (direct) coupling. Thus, if the basic mechanism of direct coupling can be summarized as the circular interaction between (low level) winds affecting the ocean which in turn affects the winds, then the basic mechanism of convective coupling can be represented as convective forcing affecting the winds which affect the ocean which in turn affects the winds and convective forcing.

The purpose of this study is to formulate such a convective coupling and to explore the dynamics of a convectively coupled system. A noteworthy feature of many of the observed variabilities in the tropics is their predominantly Kelvin wave character. The central role played by the Kelvin waves in ENSO has been emphasized and utilized in many studies (Hirst, 1988; Hirst and Lau, 1990; Philander, 1990). Similarly, the prominent atmospheric ISO with 40-60 day scale is also known to exhibit a prominent Kelvin wave character (Madden and Julian, 1971; Lau and Chan, 1985; Knutson and Weickman, 1987; Weickman *et al.* , 1985). Importance of the Kelvin waves in the dynamics of oceanic ISO has been also well recognized (MT; E87; Johnson and McPhaden, 1993; Hendon and Glick, 1995). These studies, along with the results quoted above indicate that Kelvin wave dynamics plays a central role in the tropical variabilities at IST, IAT as well as at intermediate time scales. We shall therefore consider convectively coupled Kelvin waves to explore a unified dynamical mechanism for origin of coupled oscillations at different time scales.

While we confine our dynamics to Kelvin waves, we address several questions pertaining to coupled variabilities in the tropics. In particular, we show that the convectively coupled system can support a wide spectrum of oscillations characterized by the selectively destabilized waves (the mode with the largest growth rate in the lower frequency regime; SDW) with different periods and wavelengths. Thus the two prominent oscillations, *viz.* ENSO and ISO, with two widely different times scales appear as manifestations of a single dynamical mechanism. However, such a unified dynamical framework for oscillations, with periods ranging from IST to IAT, must take into account the differences in the strengths and the relative roles of various processes at the widely separated time scales. Thus we consider two scenarios: one representative of IST and the other representative of IAT. These scenarios, as described below, are characterized by the strengths of certain physical processes appropriate for the respective time scale. In addition

we also consider scenarios which are region specific, such as the Indian ocean summer monsoon region. It will be seen that the same mechanism that gives rise to IAO generates ISO as one changes from the IAT to IST scenario. For intermediate scenarios the mechanism can generate oscillations of seasonal and annual time scales.

We also address the question of global nature of ENSO type of variability, as revealed by recent analysis (Yasunari, 1987; Nigam and Shen, 1993; Tourre and White, 1995). In particular, it is now recognized that ENSO type of variabilities, almost in phase with the Pacific events, also appear over the equatorial Indian ocean. It is possible that both regional mean conditions as well as basin-specific SST dynamics contribute to the genesis of IAO with relatively short zonal scale. We therefore consider two ocean models, characterized by different dynamics of SST. We then explore whether either of the SST models can support interannual variabilities with relatively shorter zonal scale.

In section 2 we describe the two components (atmospheric and the oceanic) of our basic model, the concept and formulation of the convective coupling and the two scenarios. Section 3 discusses the dispersion relation and the eigenfunctions for the two ocean models. In section 4 we discuss the mechanisms of ISO and IAO in the two ocean models and the relative roles of various processes. Section 5 presents our conclusions.

10.1 The basic model

10.1.1 The atmospheric component

Since in our scenario, the entire lower atmosphere is affected by OAC, we consider an atmospheric component of the coupled model which describes the dynamics of anomaly circulation of the lower troposphere. This component is represented by the shallow water equations describing the horizontal structure of the first

baroclinic mode on an equatorial β-plane. Thus the basic set of equations for our atmospheric model is constituted by equations from 3.31 to 3.36. However, for discussing the coupled dynamics in an analytical setting, these equations are linearized about the mean state of rest. Further, for reasons discussed above, only dynamics of the Kelvin wave in a coupled environment is investigated. For the Kelvin wave, the nondimensional forms of these equations are given by,

$$\frac{\partial u_a}{\partial t} - \frac{\partial \theta}{\partial x} + R u_a = 0 \tag{10.1}$$

$$\beta y u_a - \frac{\partial \theta}{\partial y} = 0 \tag{10.2}$$

$$\frac{\partial \theta}{\partial t} - \frac{\partial u_a}{\partial x} + R\theta = Q \tag{10.3}$$

$$\frac{\partial s}{\partial t} + \Gamma \frac{\partial u_a}{\partial x} = E - P \tag{10.4}$$

$$q = \overline{q}(1+s) \tag{10.5a}$$

The subscript 'a' denotes atmospheric variables. Here, R represents both Rayleigh damping and Newtonian cooling coefficients which we consider to be equal as their difference was not found to change the results qualitatively.

The length, time and temperature scales used for nondimensionalizing our equations are given by

$$T_0^2 = \frac{1}{2\beta_d c_a}\frac{\overline{\theta}}{\theta_0},\ L_0^2 = \frac{c_a}{2\beta_d}\frac{\overline{\theta}}{\theta_0},\ \theta_0 = H\frac{d\overline{\theta}}{dz} \text{ and } c_a^2 = \frac{gH\theta_0}{\overline{\theta}}.$$

The values of these quantities are given in Table 1A. The perturbation evaporation E is controlled by both atmospheric and oceanic processes. While a high SST (T) enhances potential evaporation, ventilation by the surface wind is necessary to make the evaporation process effective. The contribution from the atmospheric process to evaporation comes essentially from evaporation-wind feedback (EWF). If we assume these two processes to work in an additive manner (LS), then we can write,

$$E = \alpha T + \Lambda u_a \tag{10.5}$$

where the nondimensional forms for the evaporation-SST feedback parameter α and EWF parameter Λ are given in the following.

$$\alpha = \frac{\alpha_d \theta_0 T_0}{\overline{q}}, \text{ and } \Lambda = \frac{\rho_a C_D \Delta q L_0}{\overline{q}},$$

The various symbols with subscript 'd' used in this paper denote the corresponding dimensional value of the parameters which are represented by the symbols. The sign of Λ (as given in table 1) can be either positive or negative depending on whether the mean background winds are (implicitly) assumed to be westerlies or easterlies (Neelin *et al.* , 1987). Although the mean background winds in the tropics are easterlies in general, there are situations (*eg.* Indian ocean summer monsoon) when the mean winds are westerlies. Thus we shall consider either of the signs of Λ depending upon the situation. The values of Δq used are adopted from earlier studies (Weare *et al.* , 1981 and Zhang and McPhaden, 1995).

As in GR, the atmospheric heating is considered proportional to precipitation which in turn is proportional to s, as can be seen from eq.(10.6). Thus the nondimensional form of heating is given by

$$Q = \eta s; \tag{10.6}$$

where, $\eta = \dfrac{L_v B \overline{q}}{\theta_0 C_p H \rho_a}$.

The constants L_v, C_p, ρ_a and H are described in table 1. The nondimensional form of the other parameters in the model equations are $R = R_d T_0$, $B = T_0 \tau^{-1}$ and $\beta = \beta_d L_0 T_0$.

10.1.2 The oceanic component

The basic ocean model describes the dynamics of an oceanic mixed layer using reduced gravity equations for Kelvin waves. In addition we consider two equations which represent dynamics of SST in different ocean basins, or in different situations.

Ocean Model I

In the eastern Pacific, for example, there exists an observed positive correlation between the thermocline depth h and SST (Philande, 1990). Therefore, in our first SST model we take

$$T = \zeta h \tag{10.7}$$

where ζ is a constant of proportionality of the order of $10^{-2} Km^{-1}$. This is in accordance with the value of ζ used by Hirst (1986). Then the governing equations for model-I can written as

$$\frac{\partial u_o}{\partial t} + \epsilon \frac{\partial T}{\partial x} + a u_o = \tau_x \tag{10.8}$$

$$\beta y u_o + \epsilon \frac{\partial T}{\partial y} = 0 \tag{10.9}$$

$$\frac{\partial T'}{\partial t} + \zeta^* \frac{\partial u_o}{\partial x} + G u_o + b T' = 0 \tag{10.10}$$

where $\zeta^* = \dfrac{\zeta \overline{h}}{\theta_0}$, $\epsilon = \dfrac{\theta_0 g' T_0'^2}{\zeta L_0^2}$ and $G = \dfrac{\zeta L_0}{\theta_0} \dfrac{d\overline{h}}{dx}$

Ocean Model II

Unlike in the Pacific basin which has a shallow thermocline, the SST, in general, follows its own dynamics, although it is significantly affected by upwelling and downwelling. Thus in our second model SST is governed by an independent dynamical equation similar to one used in LS.

$$\frac{\partial u_o}{\partial t} + \epsilon\frac{\partial \phi}{\partial x} + au_o = \tau_x \quad (10.11)$$

$$\beta y u_o + \epsilon\frac{\partial \phi}{\partial y} = 0 \quad (10.12)$$

$$\frac{\partial T}{\partial t} + Gu_o + bT = \delta\frac{\partial \phi}{\partial l} \quad (10.13)$$

$$\frac{\partial \phi}{\partial t} + \frac{\partial u_o}{\partial x} + d\phi = 0 \quad (10.14)$$

where $\epsilon = \frac{\overline{\phi}T_0'^2}{L_0^2}$, $G = \frac{L_0}{\theta_0}\frac{d\overline{T}}{dx}$, $\delta = \frac{\overline{\phi}\delta_d}{\theta_0}$ and $\overline{\phi} = c_0^2$

In equations 10.10 to 10.16, a, b and d represent, respectively, damping coefficients for momentum, SST and the geopotential in nondimensional form (Table 1B). For convenience, we use same

Table 1B

Description of the coupling and scenario parameters

Parameter	Symbol	Nondimensional Value			
		Intraseasonal		Interannual	
		SST-M1	SST-M2	SST-M1	SST-M2
Evaporation-wind feedback	$\Lambda\,(10^{-1})$	5.0	-1.0	2.5	2.5
Convergence feedback	Γ	1.35	1.2	1.2	1.0
Zonal gradient of mean SST	$G\,(10^{-2})$	-10.5	12.5	-8.5	-7.5
Evaporation-SST feedback	α	4.6	4.6	4.6	4.6
Coefficient of mechanical coupling	$\gamma\,(10^{-3})$	9.5	9.5	9.5	9.5

SST-M1 stands for SST-model I and SST-M2 stands for SST-model II

symbols (ϵ and G) to represent the similar processes in two SST- models, though the values and forms of their nondimensional counterpart differ. The variables u_o and T are perturbations in zonal current and SST respectively. The thermocline height (in geopotential units) of the upper ocean is denoted by ϕ. The parameters appearing in equations 10.1 to 10.16 are described in tables 1A and 1B.

10.1.3 Ocean-Atmosphere Interaction (Convective Coupling):

The nature of the ocean-atmosphere coupling depends on the prescribed functional dependence of the wind stress τ and the atmospheric heating Q. For the mechanical coupling through the wind stress we have adopted the conventional parameterization, $\tau_x = \gamma_d u_a$ where γ_d represents the coefficient of mechanical coupling whose nondimensional form is given by $\gamma = \gamma_d T_o$.

In the convective coupling that we propose SST cannot heat the atmosphere directly; it influences the atmospheric heating by controlling the column moisture, and hence column precipitation. Further, the atmosphere is driven solely by precipitational heating. As such, the influence of the oceanic variables on the atmospheric flow would be absent in the absence of precipitative process. This process is included through equations 10.3, 10.4 and 10.7.

10.1.4 The Interannual and the Intraseasonal Scenarios:

One of the prime objectives of our study is to explore a common dynamical mechanism for the coupled variabilities in the tropics. However, while the basic dynamical mechanism may be the same, the oscillations with widely different timescales, like IAO and ISO, occur over different mean states. Although we have no explicit reference to a mean flow, we need to incorporate this difference in the mean conditions. One of the effects of the mean conditions is that the

Table 1A

Parameter	Dimensional symbol	value	Nondimensional symbol	Value
Time scale	T_o	$0.85\,days$	-	-
Length scale	L_o	$4400\,km$	-	-
Temperature scale	θ_o	$21\,K$	-	-
Moisture scale	q_o	$40\text{-}50\,kg\,m^{-2}$	-	-
Mean potential temperature	$\overline{\theta}$	$310\,K$	-	-
Mean thermoline depth	$\overline{h}$	$70\,m$	-	-
Oceanic gravity wave speed	c_o	$1\,m\,s^{-1}$	-	-
Tropopause Height	$H\pi$	$16\,km$	-	-
Atmospheric dry gravity wave speed	c_a	$200\,m\,s^{-1}$	-	-
Convective time lag	τ	$0.25\,days$	B	3.4
Upwelling coefficient	δ_d	$0.02^o K m^{-1}$	δ	9×10^{-4}
Oceanic Rayleigh friction coefficient	a_d	$80\,\text{days}^{-1}$	a	10^{-2}
Oceanic Newtonian cooling coefficient (for ϕ and T)	b_d	$200\,\text{days}^{-1}$	b	4.3×10^{-2}
Atmospheric Rayleigh friction coefficient	R_d	$1\text{-}5\,\text{day}^{-1}$	R	0.17-0.85
Atmospheric Newtonian cooling coefficent	R_d	$1\text{-}5\,\text{days}^{-1}$	R	0.17-0.85

strengths and the relative roles of various processes, especially those which depend on the mean conditions, are likely to be quite different for widely separated time scales. For example, selective destabilization of waves at ISO (IAO) scale cannot possibly be expected to occur for a parameter strengths which are representative of the IST (IAT). It is therefore important to take this aspect into account. In view of paucity of appropriate data, it is not easy to quantify these changes in the parameters as we change from one time scale to another. We shall, therefore, attempt to identify parameters that can provide a qualitative classification of scenarios with widely different time scales. In particular, we shall choose these parameters so as to be consistent in their characteristics with the respective time scale. Thus, for example, a value of Λ that is relevant for IST should only accompany a value of G relevant for the same time scale. Following this reasoning, we consider two scenarios *viz.* interannual and intraseasonal, for the same dynamical system described by the above equations. These two scenarios, for each ocean model, are characterized by parameters that reflect the mean conditions (and hence time scales). In general, quantities averaged over IAT are likely to be smaller than those averaged over IST. Therefore, we shall assume a value for a scenario parameter for IAT smaller than its corresponding value for IST. Specific reasons for this can vary from parameter to parameter and will be indicated below. Discussion on intermediate time scales can be accommodated by considering parameters of intermediate strengths. We choose the following scenario parameters:

Strength of EWF (Λ): This parameter is essentially determined by the time mean value of the air (anemometer level)-sea humidity difference. Following the reasoning outlined above, we assume that the interannual scale is characterized by a value of Λ smaller than that for the IST. This can happen, for example, because the air-sea humidity difference Δq in the IAT contains an average over summer as well as winter conditions, and hence would be smaller than the value

averaged over only summer conditions. In addition, for IST, as in the Indian Ocean summer monsoon region, the mean winds can be westerly. Thus for the ISO, both these cases are considered. For the values of mean wind assumed in our model ($5\,ms^{-1}$), the observed value of Δq is about 3 $gm\,kg^{-1}$ (Zhang and McPhaden, 1995) which corresponds to the value of Λ 0.5. We consider this value to characterize our intraseasonal scenario.

Zonal gradient of mean SST (G): It is well-known that zonal gradient of mean SST plays an important role in coupled dynamics (LS). However, the value of G is likely to be different for IAT and IST. In addition the value of G also varies from basin to basin. For example, the summer monsoon Indian Ocean is characterized by a positive east-west SST gradient, while, in the interannual scale, the Pacific is characterized by a negative east-west gradient of SST (Philander, 1990). We adopt a value of $\frac{d\overline{T}}{dx} = -5.0 \times 10^{-7}\,^{o}C\,m^{-1}$, similar to the one used in many earlier studies (Hirst, 1988; Lau and Shen, 1988), for the interannual time scale.

Strength of convergence feedback (Γ): The value of convergence feedback, whose nondimensional strength is measured by Γ, varies from IST and IAT. If we assume the IST to represent the summer situation, the value of Γ for the IAT will be less than that for the IST. For a variation of $q(z = 0)$ from 0.002 to $0.015\,gm\,kg^{-1}$ eq.(10.5.b) implies a range of $0.01<\Gamma<1.6$. Thus we adopt a value of Γ between 1 and 1.5 with the smaller limits to characterize IAT scenario.

It is possible to name other variables, like the mean thermocline depth ($\overline{h}$), strength of the mean wind and the mean lapse rate of the atmosphere, that are different for different time scales and for different regions. However, we shall confine ourselves mainly to these three parameters to characterize the scenarios; roles of certain other parameters are discussed in appropriate context. Certain important physical quantities as well as the parameters that do not change with time scale are described in table 1A while the standard values of the parameters

for the two scenarios are given in table 1B. The question of sensitivity of the results to these parameters will be taken up subsequently.

10.2 The dispersion relation and the eigenfunctions

For both the SST models, we seek separable solutions for the coupled systems in the form

$$\xi(x, y, t) = \xi(y)e^{i(kx-\omega t)} \tag{10.15}$$

Here ξ represents any of the variables $u_a, v_a, \theta, s, u_o, T$ and o. The conditions for obtaining nontrivial solutions then result in a dispersion relation for each ocean model.

(a) The dispersion relations Ocean model I:

$$i\alpha\gamma\eta kG^* - [\sigma_B(k^2 - \sigma_R^2) - i(\Gamma k - i\Lambda)\eta k][\sigma_a\sigma_b + k\epsilon G^*] = 0 \tag{10.16}$$

where $G^* = (iG - \zeta^* k)$.

Ocean model II:

$$\alpha\gamma\eta k(\delta\omega k - iG\sigma_d) - \sigma_b[i\sigma_B(k^2 - \sigma_R^2) + (\Gamma k - i\Lambda)\eta k][\sigma_a\sigma_d - k^2\epsilon] = 0 \tag{10.17}$$

where $\sigma_R = \omega + iR$, $\sigma_B = \omega + iB$, $\sigma_a = \omega + ia$, $\sigma_b = \omega + ib$ and $\sigma_d = \omega + id$.

Equations 10.18 and 10.19 can be expressed as polynomials in ω of degrees respectively 5 and 6. The expressions for these polynomials and the coefficients were arrived at using the MATLAB symbolic processor. The resultant polynomials are solved for various values of k (real). Hence, in general ω is a complex quantity. For further analysis of the dispersion relations we need to look at the structure of the eigenfunctions.

b. The eigenfunctions

Since the form of the equations governing the atmospheric part do not depend on the particular ocean model, the functional form of the atmospheric variables are also independent of the ocean model. So the eigenfunction of the zonal wind can be written as

$$u_a(x,y,t) = \exp(\mathrm{ikx} - i\omega t - \Delta y^2), \tag{10.18}$$

$$\text{where } \Delta = \frac{\beta k}{2\sigma_R}. \tag{21}$$

As stated earlier, ω is in general complex and hence the meridional structure of the waves are trapped only when $Re(\Delta) > 0$. The eigenfunctions for the other atmospheric variables are given below in terms of u_a.

$$\theta = -\frac{\sigma_R}{k} u_a \tag{10.22}$$

$$s = \frac{i(k^2 - \sigma_R^2)}{\eta k} u_a \tag{10.23}$$

The oceanic eigenfunctions: SST Model I

$$u_o = \frac{i\gamma\sigma_b}{\sigma_b\sigma_a + \epsilon k G^*} u_a \tag{10.24}$$

$$T = -\frac{i\gamma G^*}{\sigma_b\sigma_a + \epsilon k G^*} u_a \tag{10.25}$$

SST Model II:

$$u_o = \frac{i\gamma\sigma_d}{\sigma_d\sigma_a - k^2\epsilon} u_a \tag{10.26}$$

$$T = \frac{i\gamma(\delta\omega k - iG\sigma_d)}{\sigma_b(\sigma_d\sigma_a - k^2\epsilon)} u_a \tag{10.27}$$

$$\phi = \frac{i\gamma k}{\sigma_d \sigma_a - k^2 \epsilon} u_a \qquad (10.28)$$

The physical fields are the real parts of these complex functions.

(c) General Characteristics of the Dispersion Relation and the Eigenfunctions:

We have solved the dispersion relations (18) and (19) subject to the consistency condition: $Re(\Delta) > 0$. Before going into the detailed study of the full dispersion relations, it is instructive to analyze one of its limiting cases: $B = 0$. In our model the parameter B controls the atmospheric heating; thus, $B = 0$ corresponds to a case when precipitational heating is absent. As noted earlier there is no direct contribution of SST to atmospheric heating and SST controls the atmospheric heating only by controlling the moisture availability of the atmospheric column. Thus in absence of precipitational heating ($B = 0$), there is no contribution of the oceanic variables to the atmospheric heating. This is reflected in the dispersion relations by the fact that the terms involving $\alpha\gamma$ disappear for $B = 0$. The same argument also holds for EWF, which can affect the atmospheric heating only through affecting the atmospheric column moisture. Thus for $B = 0$, all the terms involving EWF parameter (Λ) dropout of the dispersion relations. In other words coupling cannot give rise to ocean-atmosphere instability in the absence of precipitational heating.

The other extreme case is represented by $\tau \longrightarrow 0$ which implies P $\longrightarrow \infty$. Although it is possible to analyse the case mathematically, it does not appear physically relevant. In the following we shall, therefore, explore the dispersion relations for the existence of selectively destabilized waves which can correspond to observed variabilities. Although we shall demonstrate that our framework can support a wide spectrum of coupled variabilities, our emphasis is on interannual and intraseasonal oscillations. In particular, we shall look for SDW with appropriate time period and zonal scale for values of the parameters that belong to

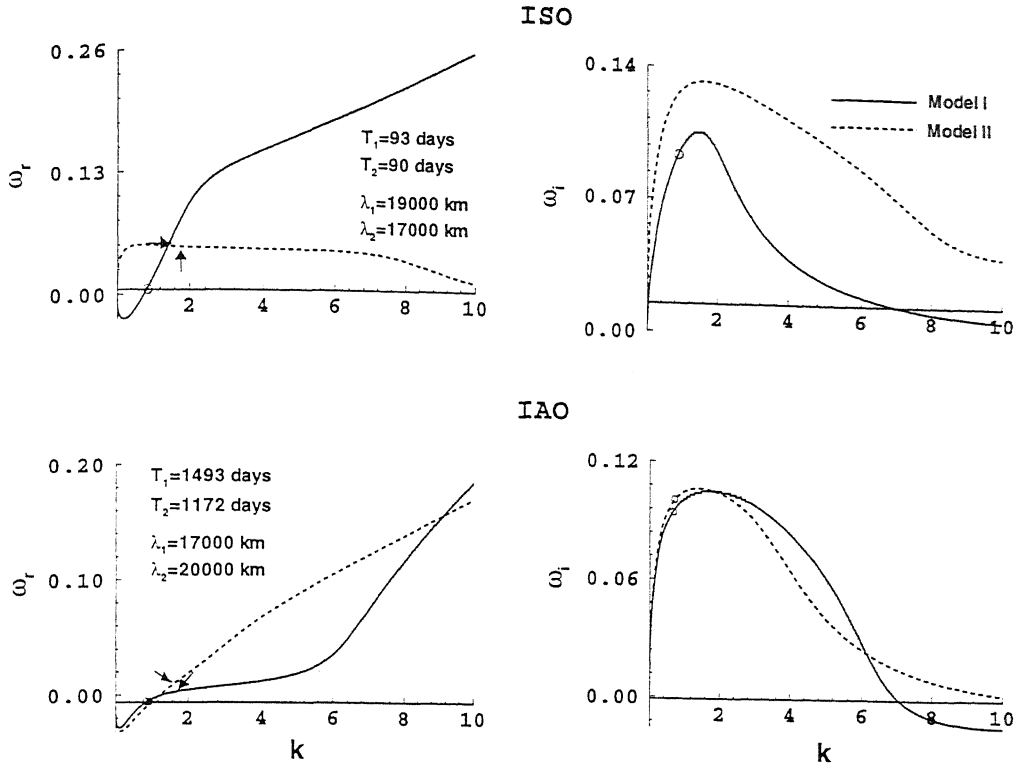

Figure 10.1: Dispersion curves for the standard case (refer table 1A and 1B). The left panels show the frequency (ω_r) as a function of wave number (k). The corresponding growthrates (ω_i) as a function of k are shown in the right panels. The top and the bottom panels represent the intraseasonal and the interannual scenarios, respectively. The solid and the dashed lines represent, respectively, the SST-model I and SST-model II. The allowed parts of the solutions are those starting from the circle marked at the smaller values of k. The arrow marks on the left panels indicate the wavenumbers corresponding to the SDW. The coordinates are in non-dimensional units.

either of the scenarios.

(d) Interannual and intraseasonal oscillations: The standard case

Out of the allowed solutions of the dispersion relation, only the ones that have positive growthrates are physically relevant. The growing solutions of the dispersion relation for the Ocean models I and II are accordingly presented in figure 10.1. The top panels represent the intraseasonal scenario while the bottom panels represent the interannual scenario. The left panels show the variation of the real part of ω (frequency) with wavenumber k in nondimensional units. The corresponding variations of the growthrate (imaginary part of ω) are shown in the

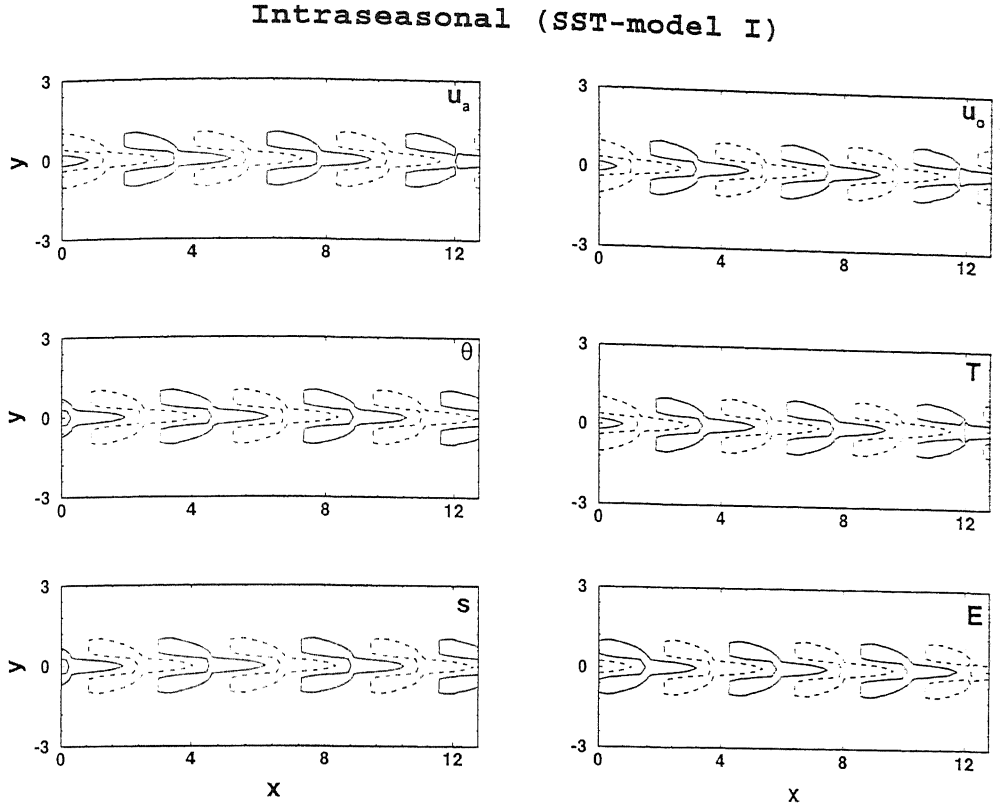

Figure 10.2: Longitude-latitude plots of the atmospheric and oceanic eigenfunctions and the evaporation field (E) for the maximally growing wave for intraseasonal scenario for the ocean model I. The negative contour are dashed. The coordinates are in non-dimensional units.

the IAT and IST. The significance of this fact can be appreciated from a scrutiny of the energetics of the perturbations.

The bottom right panel in each figure shows the structure of the corresponding evaporation field. Once again, the correlations of the evaporation field with SST, moisture anomaly and the zonal wind are different for different time scales and for the two SST models. The evaporation field is negatively correlated with SST and atmospheric temperature (T and θ respectively) for the intraseasonal case for SST Model I and interannaul case for SST Model II (figures 10.2 and 10.5 respectively). This feature is also present for SST-model I in the case of IST scenario (figure 10.2). Such a feature in the observed field was reported by Cornejo- Garrido and Stone (1977) who found negative correlation between SST and evaporation and atmospheric heating in the regions of the Walker circulation

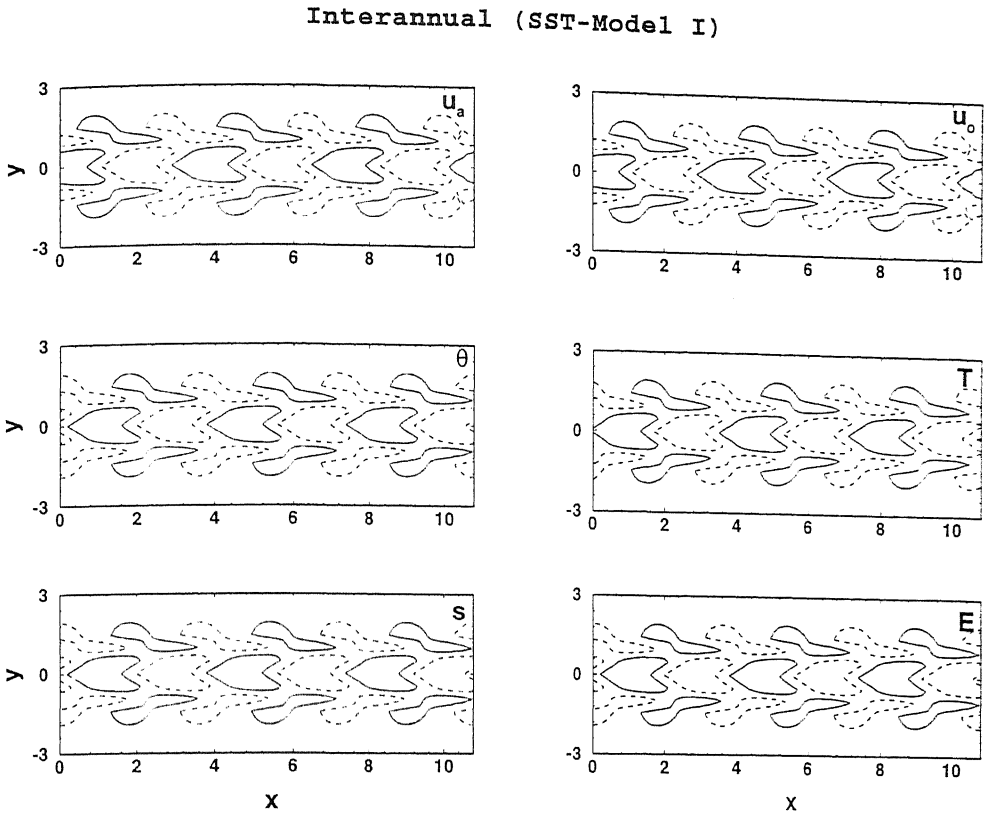

Figure 10.3: Longitude-latitude plots of the atmospheric and oceanic eigenfunctions and the evaporation field (E) for the maximally growing wave for interannual scenario for the ocean model I. The negative contour are dashed. The coordinates are in non-dimensional units.

near 10°S. Low correlation between SST and rainfall (s in our model) has been emphasized by also Ramage (1977). Murakami and Wang (1993) reported an out of phase relationship between OLR and SST from an investigation of annual cycle of the atmospheric circulation and SST over the equatorial Pacific and Indian ocean. Due to lack of extensive observational analysis, it is not easy to verify these relations. There are, however, some evidence of such differences in the SST-evaporation correlations for different scenarios (Liu, 1988).

(e) **Energetics:** To gain further insight into the model behavior and elucidate the role of various physical mechanisms, analysis of the perturbation energetics is carried out. The total energy of the atmospheric and oceanic part are given by

$$<E_a>_t = D_\theta^2 \frac{\eta_d \overline{q}}{\tau} <\theta s> + D_s^2 \alpha_d <sT> - \Lambda_d D_s^2 <s u_a> \qquad (10.29)$$

where $E_a = (u_a^2 + D_\theta^2 \theta^2 + D_s^2 s^2)/2$ and $\eta_d = \dfrac{L_v}{C_p H \rho_a}$.

SST- Model I :

$$<E_o>_t = \gamma_d <u_a u_o> - D_h^2 \frac{d\overline{T}}{dx} <T u_0>. \qquad \overline{T} = \zeta \overline{h} \qquad (10.30)$$

where $E_O = (u_O^2 + D_T^2 T^2)/2$

SST-model II:

$$<E_o>_t = \gamma_d <u_a u_o> - D_T^2 \frac{d\overline{T}}{dx} <T u_0> \qquad (10.31)$$

where $E_O = (u_O^2 + D_T^2 T^2 + \phi^2/g')/2$

where the angle bracket denotes average over a domain much larger than the disturbances. All 'D's appeared in above equations convert the dimension of corresponding term into dimension of energy. Exact forms of these conversion factors are not of much importance as we are interested in a qualitative study. The energy integrals of the oceanic equations show that, as found in earlier studies (Yamagata, 1985), one of the necessary conditions for the instability is the net positive correlation between atmospheric wind and oceanic current. It can be seen from the figures 10.2-10.5 that this condition is satisfied for both the models and scenarios. However, in the present case, this condition is neither necessary nor sufficient as evident from equations 10.30 to 10.32. The correlation represented by $< T u_o >$ in the case of IST scenario for model-II is negative which along with a positive SST-gradient gives a positive contribution to the growth rate. This correlation is positive for model-I for IST scenario which along with a $\frac{d\overline{T}}{dx} < 0$ gives a positive contribution. For the IAT, $\frac{d\overline{T}}{dx}$ for both the cases is negative, while corresponding $< T u_o >$ are generally positive, once again making the contribution

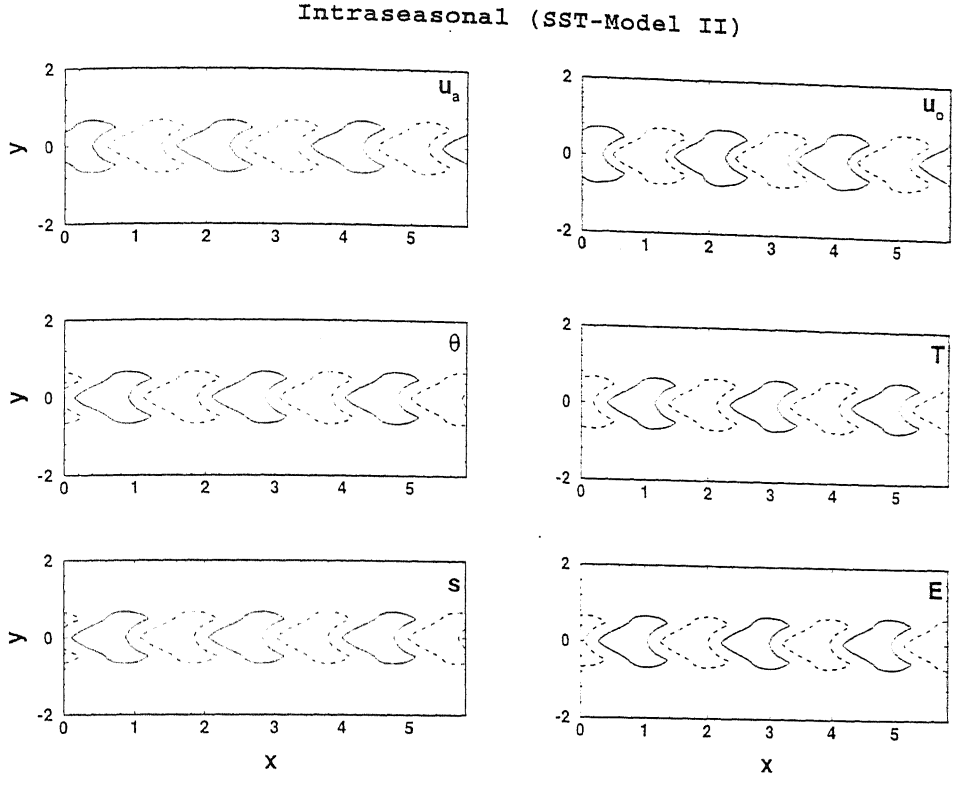

Figure 10.4: Longitude-latitude plots of the atmospheric and oceanic eigenfunctions and evaporation field (E) for the maximally growing wave for intraseasonal scenario for the ocean model II. The negative contours are dashed. The coordinates are in non- dimensional units.

positive. Another important source of energy, which is characteristic of convective coupling is $< su_a >$. which is different for different scenarios. It also depends on the SST modeling to some extent. In the IST scenario, for model-I, s and u_a are almost out of phase whereas for the model-II they are more in phase. For the model-II sign of Λ corresponding to IST scenario is negative. This implies a positive contribution to growthrate. This is also true for model-I as sign of Λ is positive. The term $< sT >$ which measures the contribution to the growth rate from SST-evaporation feedback is generally positive for both the scenarios and models.

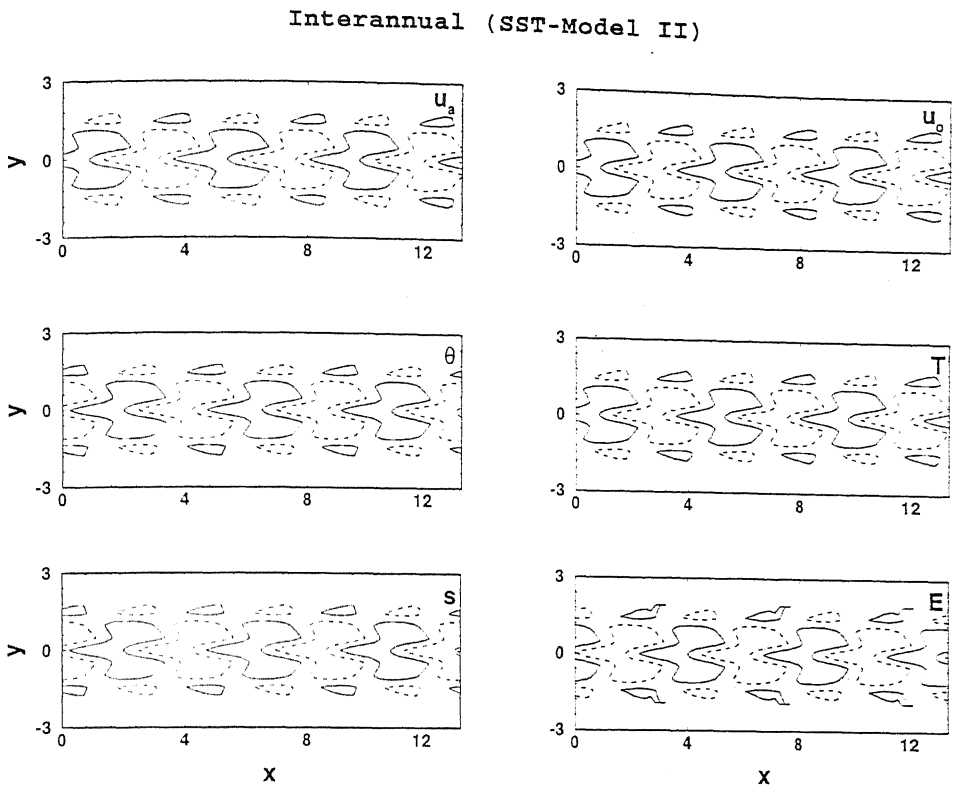

Figure 10.5: Longitude-latitude plots of the atmospheric and oceanic eigenfunctions and the evaporation field (E) for the maximally growing wave for interannual scenario for the ocean model II. The negative contours are dashed. The coordinates are in non- dimensional units.

10.3 Relative Roles of Various Processes

In view of the uncertainties involved in estimating many of the model parameters, it is important to address the question of sensitivity of our results to some of these parameters. As the number of parameters is rather large, we shall confine our study to those parameters which represent crucial physical processes in our model. It, however, may not be realistic to investigate the variation of certain parameters alone over wide ranges. Since these parameters also represent certain mean conditions their variations are likely to be accompanied by changes in certain other parameter. Hence, the characteristics of the SDW for different plausible combinations of these parameters are examined. Further, these sensitivity studies will be aimed at exploring certain specific issues of observed coupled

variabilities in the tropics.

(a) The spectrum of convectively coupled instabilities:

As mentioned above, a basic premise of this study is that it is essentially the same mechanism that accounts for many aspects of the OAC in the tropics. A large part of the variations in the characteristics of the oscillations at different time scales, we expect, is due to the variation in the strengths and the relative roles of various processes. Representative samples of the spectra of convectively coupled oscillations for the two ocean models are presented in table 2A and 2B, respectively for different

Table 2A

Spectrum of convectively coupled oscillations
(SST-model I)

Time Scales	Scenario Parameters			T	λ
	Λ (10^{-1})	G (10^{-2})	Γ	(Days)	$(10^3 km)$
Intraseasonal	5.5	-12.5	1.35	107	18
	5.0	-10.5	1.35	93	19
Seasonal	5.0	-8.5	1.35	175	38
	4.0	-10.5	1.35	150	34
Annual	2.5	-10.5	1.10	331	10
	2.0	-8.5	1.10	337	10
Interannual	2.5	-8.5	1.00	1493	17
	2.0	-6.5	1.00	1527	1.6

scenarios. It can be seen that for both the ocean models oscillations of appropriate period appear in a consistent manner as the scenario changes from one time scale

to another. Table 2 also shows that while the characteristics of the SDW depend on the scenario parameters, the existence of coupled oscillation for a particular time scale is not critically dependent on the choice of these parameters.

(b) Selectively destabilized oscillations:the governing processes:

Several processes are known to play significant role in the excitation and the characteristics of the SDW. Table 3 summarizes the relative roles of various key processes in the existence of

Table 2B

Spectrum of convectively coupled oscillations

(SST-model II)

Time Scales	Scenario Parameters			T	λ
	A (10^{-1})	G (10^{-2})	Γ	(Days)	$(10^3 km)$
Intraseasonal	5.0	6.5	1.4	89	26
	6.5	8.5	1.4	98	34
Seasonal	3.0	-21	1.5	206	33
	3.0	-12.5	1.3	202	15
Annual	3.0	-8.5	1.3	336	20
	2.5	-10.5	1.3	386	27
Interannual	2.5	-5.0	1.2	2310	23
	2.5	-7.5	1.2	1172	20

the SDW. It can be seen that there is no SDW in absence of OAC. The existence of an unstable mode (without scale selection) for $\alpha = 0$ is due to the fact that unlike in most linear analyses, the linear atmospheric component of our coupled model can by itself support unstable waves (GR). The important role played by east-west gradient of mean SST is also highlighted in this table.

(c) Effect of mean westerlies:

A well-known aspect of tropical circulation is the presence of strong surface westerlies over the monsoonal region due to the seasonal reversal of the winds. This reversal is also accompanied by a strong positive east-west gradient of SST over a large part

Table 3

Role of various processes in existence of selectively destabilized waves

(For respective standard set of values the other parameters)

Process	SST-Model I				SST-Model II			
	Scenerio				Scenerio			
	IST		IAT		IST		IAT	
	T Days	λ $10^3 km$	T Days	λ $10^3 km$	T Days	λ $10^3 km$	T Days	λ $10^3 km$
$\alpha = 0$	$\star$		$\star$		$\star\star$		$\star\star$	
$\Lambda = 0$	35	11	$\star\star$		$\star$		$\star\star$	
$\Gamma = 0$	$\star$		$\star$		182	41	$\star\star$	
$G = 0$	77	23	172	1.2	$\star\star$		224	2.8
$\delta = 0$	Not applicable				91	2.6	4064	2.3

$\star$ Selection at the smallest scale $\star\star$ No growing modes

of the Indian Ocean. Since the ISO signal is strongest over the Indian summer

monsoon region, it is important to investigate the effect of these changes in the mean conditions on the coupled oscillations at seasonal and intraseasonal time scales. Table 4 shows the characteristics of the SDW for the IST (and seasonal) scenario for mean westerlies ($\Lambda < 0$) and different strengths of the other scenario parameters G and Γ as well as for different strengths

Table 4

Effect of mean westerly on the selectively destabilized waves

Parameters				SST-model I		SST-model II	
α	Λ (10^{-2})	Γ	G (10^{-1})	T (days)	λ $(10^3\ km)$	T (Days)	λ $(10^3\ km)$
4.5	-11	1.1	1.25	212	15	94	24
4.5	-11	1.1	-1.25	**		**	
4.5	-11	1.1	12.5	47	22	39	19
4.5	-11	1.1	-12.5	*		**	
4.5	-11	1.2	1.25	356	10	90	17
4.5	-11	1.2	-1.25	**		**	
4.5	-11	1.2	12.5	48	16	38	15
4.5	-11	1.2	-12.5	*		**	
4.5	-22	1.2	1.25	*		111	18
4.5	-22	1.2	-1.25	**		**	
4.5	-22	1.2	12.5	57	16	43	15
4.5	-22	1.2	-12.5	*		**	
9.0	-11	1.2	1.25	226	8.0	68	16
9.0	-11	1.2	-1.25	**		**	
9.0	-11	1.2	12.5	35	15	30	15
9.0	-11	1.2	-12.5	*		**	

* Selection at smallest scale ; ** growing mode absent

of α, while the other parameters are kept at their standard values. It can be seen from this table that coupled ISO appears only when mean westerlies are accompanied by a positive east-west gradient of mean SST. This is consistent with the fact that the monsoonal Indian ocean is characterized by a positive gradient of mean SST. Another noteworthy feature is that SST- model I which is more appropriate for the eastern pacific region does not, in general, support modes of period less than seasonal time scale for mean westerlies, except for very high values of G. For SST model-II, on the other hand, the period of the SDW lies in the range of 30-110 days for a wide range of values of the scenario parameters. The corresponding wavelength also stays in the range of 15,000 to 24,000 km.

(d) Interannual oscillations with short zonal scales:

As mentioned above, recent analyses show interannual variability also over the equatorial Indian Ocean, almost in

Table 5

IAO with short zonal scale

(SST-Model II)

Parameters			T	λ
α	Λ (10^{-1})	G (10^{-2})	(Days)	$(10^3 km)$
9.5	-6.5	8.5	1201	8.7
4.5	-5.0	8.5	1336	9.1
12.5	-6.5	6.5	1827	8.7
4.5	3.5	5.0	1141	8.1
9	5	8.0	1985	7.1

phase with the El Niño over the Pacific, but with lower amplitudes. In addition, interannual signals are also observed over the Atlantic Ocean (Zebiak, 1987). In the conventional delayed oscillator mechanism, such variabilities need large

zonal extent (Hirst, 1988; Battisti and Hirst, 1989). Thus the delayed oscillator mechanism cannot provide a mechanism for the interannual oscillations in the global tropics. In order to explore whether a convectively coupled system can support interannual variabilities of different zonal scales, we have considered a number of scenarios for the interannual scale. The results are presented in table 5. It is interesting to note that while the SST model II can give rise to IAO with relatively short zonal scales for a number of scenarios, such a trend is not available for SST model I. As emphasized earlier, the SST model II, which does not assume a shallow thermocline as in SST model I is more appropriate for the Indian Ocean region. For SST-model II, interannual modes with period ranging from about three to five years appear for a very wide range of parameters. A comparison of table 2B and 5 reveals that EWF and zonal gradient of mean SST are two primary mechanisms that give rise to these IAO with short zonal scales.

(e) Role of convective time lag:

While the above investigations provide an extensive study of sensitivity of the results to the model parameters, we present below a summary of a conventional sensitivity study of the existence and the characteristics of the SDW with respect to model parameters. Of particular importance is the sensitivity of the results to the value of CTL. All of the above studies were done for a fixed value (0.25 day) of CTL. It is also one of the parameters that cannot be assigned a precise value since it embodies our hypothesis of CTL. As argued in GR, its value should be a few hours. It is, however, desirable that the existence and characteristics of the SDW for the two SST models and for different scenarios do not depend sensitively on the value of τ. The values of period and wavelength of the SDW for the two scenarios and for the two SST models are presented in table 6 for a range of CTL. We note that our results do not depend critically on the value of τ. Indeed, for a four fold change in the value of τ, from .1 to 0.4 day, the time periods for the SDW for the IST scenario remain within 115 and 66 days for

SST model I and between 95 and 83 days for SST model II. The corresponding wavelengths are between 15 and 28 thousand km. For the IAT scenario, the time periods of the SDW for the SST model II are between 1280 and 1144 days, with corresponding wavelengths between 15000 and 22000 km. For SST model I, however, the changes in the time period are much larger, from 663 days to 2308 days. Also, the trends of change in the time period as well as wavelength in the case of SST-model II for IAT scenario are

Table 6

Effect of convective time lag on characteristics of the maximally growing waves

Convective time lag		SST-Model I				SST-Model II			
		Scenario				Scenario			
		IST		IAT		IST		IAT	
τ	$B = \frac{T_0}{\tau}$	T	λ	T	λ	T	λ	T	λ
0.1	8.5	115	21	663	15	95	28	1280	22
0.2	4.2	101	20	1093	16	91	26	1253	21
0.3	2.8	85	18	2271	17	88	25	1158	18
0.4	2.0	66	15	2302	18	83	24	1144	15

opposite to those for other cases. Although the reasons for this are not clear, it was found that the solutions of the dispersion relations enter different regimes depending upon the relative strengths of the parameters.

(f) Effect of mechanical coupling and broad spectrum ISO:

Since the strength of the mechanical coupling (γ) is controlled by the strength of the mean wind, it is likely to have different strengths for different time scales or for different situations. The sensitivity of the coupled oscillations to the strength of the mechanical coupling (or, equivalently, the product $\alpha\gamma$, since α and γ always appear together in eqs. 18 and 19) is shown in table 7. The values of the mean winds corresponding to these values of γ are also given in the table. We assume that the strongest value of γ represents, qualitatively, the IST scenario, with strong mean wind. It can be seen that as the strength of the mean wind (coupling) is decreased from 10 m s $^{-1}$ (γ = 19) to 5 m s $^{-1}$ (γ = 9.6), the period of the coupled ISO increases, from 44 days to 87 days for SST model I, and from 69 days to 90 days for SST model II. The corresponding changes in the wavelengths are, however, marginal, especially for the SST model I. It is interesting to note that in an analysis of SST data for the period 1979-85, E87 had recorded eastward propagating oscillations with period 40-60 days, while MT, in their analysis for the period 1983-86 for the same region recorded Kelvin wave like disturbances of period 60-90

Table 7

Effect of mean wind strength and broad spectrum ISO

		SST-Model I*		SST-Model II**	
$\overline{u}$	γ	T	λ	T	λ
$m\,s^{-1}$	(10^{-3})	(Days)	$(10^3 km)$	(Days)	$(10^3 km)$
10	19.0	44	11	69	16
7	13.5	65	13	79	16
5	9.60	87	15	90	17

$\star$ Λ=0.65, Γ=1.3, G=-0.12, $\star\star$ Λ=-0.13, Γ=1.3, G=0.12

days. As observed by MT, this could be due to the changes in the variables due to

the El Niño of 1982-83. Indeed, the analysis of *E87* shows that subsequent to the El Niño the period increased to 70 days. MT concludes that the two oscillations

Table 8

Sensitivity of characteristics of SDW to scenario parameters (IST)

Parameter		SST-Model I		SST-Model II	
Symbol	Value	T (days)	λ (10^3 km)	T (Days)	λ (10^3 km)
$\Lambda(10^{-1})$	2.5	29	16	$\star$	$\star$
	3.5	53	16	$\star$	$\star$
	4.5	87	18	82	24
	5.5	104	19	101	29
	6.5	115	20	116	35
Γ	1.0	316	12	113	23
	1.1	106	6.7	103	22
	1.2	54	2.9	96	22
	1.3	71	15	93	24
	1.4	109	22	90	25
	1.5	125	27	87	27
$G(10^{-2})$	-2.0	82	22	165	30
	-4.0	87	21	114	27
	-6.0	92	20	90	26
	-8.5	93	19	73	24
	-10	93	18	62	22
	-12	94	18	52	20

$\star$ Selection at smallest scale

observed by *E87* and MT0 are essentially the same phenomenon. Table 7 provides

a qualitative support for such a broad spectrum ISO due to changes in the mean conditions, although, in practice, more than one mean process (such as zonal gradient of mean SST) is likely to be involved.

(g)Effect of EWF, mean SST gradient and Γ

As we have emphasized earlier, an arbitrary and independent variation of parameters like Λ and G is not justified as such a variation would imply a change in certain mean conditions and hence corresponding changes in the other scenario parameters. However, for the sake of completeness, we present in Table 8 and Table 9 variations in the characteristics of the SDW for both the ocean basins with respect to Λ, G and Γ, for the IST and IAT, respectively. In each of these cases only one parameter was varied when all other parameters were kept constant (at their standard values). As we have seen in table 3, the existence of SDW critically depends on the processes of evaporation- SST feedback (α) and EWF. There is no SDW for $\alpha = 0$, while there is SDW only at ISO for $\Lambda = 0$ (Table 3). Further, as discussed in the context of interannual and intraseasonal scenarios, Λ significantly affects the characteristics of the SDW. This trend is further reflected in Table 8 and Table 9. For both the scenarios, Λ has a profound effect on the existence and the nature of the SDW. The sensitivity of existence of SDW on Λ, however, is more sensitively dependent in the case IAT (Table 9), especially for SST- model II. The existence of IAO is also sensitive to Γ, as can be seen from Table 9. The characteristics of IAO are, relatively, less sensitive to variations in G. A scrutiny of tables 8 and 9 reveals that the existence of SDW with ISO characteristics is supported by a much wider range of scenario parameters in the intra-seasonal scale than in the interannual scenario. However, as we have mentioned earlier, conclusions from such independent variation of the scenario parameters may have only limited validity.

10.4 Conclusions

The central emphasis of the present work has been exploration of a unified dynamical framework for a wide class of tropical variabilities. In our scenario, there is a basic dynamical mechanism which, under the interplay of various processes

Table 9

Sensitivity of characteristics of SDW to scenario parameters (IAT)

Parameter		SST-Model I		SST-Model II	
Symbol	Value	T (days)	λ ($10^3\,km$)	T (Days)	λ ($10^3\,km$)
$\Lambda\,(10^{-1})$	1.5	**		320	16
	2.5	2221	17	3655	24
	3.5	366	14	*	
	4.5	223	12	*	
	5.5	170	11	*	
Γ	1.0	2986	18	*	
	1.1	192	8.0	*	
	1.2	*		1100	30
	1.3	*		893	40
	1.4	*		673	48
$G(10^{-2})$	-6.7	537	15	1394	20
	-7.1	634	15	1289	20
	-7.5	779	16	1132	19
	-7.9	1028	16	1009	18
	-8.3	1493	17	910	18

* Selection at smallest scale ; ** Growing mode absent

involved, gives rise to selective excitations at a number of observed spatial and temporal scales. The detailed structures of these observed oscillations, of course, will be enriched by various other processes, especially nonlinear processes, that operate beyond the genesis of the waves.

This dynamical framework for a class of tropical variabilities discussed here is dynamics of tropical Kelvin wave, and its selective excitation at various scales through internal forcing generated by OAC and moist processes. The motivation for exploring Kelvin waves has come from the predominantly Kelvin wave character of many observed tropical variabilities. The mechanism of selective excitation is through OAC and moist processes. The two distinguishing features of the present framework is an explicit dynamics of the moisture variable controlled by a convective time lag, and a convective OAC. The inclusion of an explicit moisture equation implies that we do not restrict our system to be necessarily in a 'convective regime' and assumed in many earlier studies (Goswami and Selvarajan, 1992; LS). The inclusion of CTL embodies the hypothesis that the selective destabilization (or high frequency cut-off) takes place through forcing by convection organized at certain time scales (characterized by CTL). The basic premise of convective coupling is that the atmosphere does not respond directly to SST heat source, but only through the deep column heating associated with precipitation. OAC controls this precipitational heating through the effect of SST on column moisture. However, as precipitation is a threshold process, convective coupling makes OAC also a (second-order) threshold process. Although more complex coupled dynamics have been considered with conventional direct coupling (Hirst, 1986; Hirst and Lau, 1990), the present study stands apart from these earlier studies for its emphasis on convective coupling which also incorporates the concept of convective time lag. Formulation of such an alternative OAC parameterization is motivated by the fact that the conventional formalism cannot account for many of the features of the observed variabilities as revealed by recent

involved, gives rise to selective excitations at a number of observed spatial and temporal scales. The detailed structures of these observed oscillations, of course, will be enriched by various other processes, especially nonlinear processes, that operate beyond the genesis of the waves.

This dynamical framework for a class of tropical variabilities discussed here is dynamics of tropical Kelvin wave, and its selective excitation at various scales through internal forcing generated by OAC and moist processes. The motivation for exploring Kelvin waves has come from the predominantly Kelvin wave character of many observed tropical variabilities. The mechanism of selective excitation is through OAC and moist processes. The two distinguishing features of the present framework is an explicit dynamics of the moisture variable controlled by a convective time lag, and a convective OAC. The inclusion of an explicit moisture equation implies that we do not restrict our system to be necessarily in a 'convective regime' and assumed in many earlier studies (Goswami and Selvarajan, 1992; LS). The inclusion of CTL embodies the hypothesis that the selective destabilization (or high frequency cut-off) takes place through forcing by convection organized at certain time scales (characterized by CTL). The basic premise of convective coupling is that the atmosphere does not respond directly to SST heat source, but only through the deep column heating associated with precipitation. OAC controls this precipitational heating through the effect of SST on column moisture. However, as precipitation is a threshold process, convective coupling makes OAC also a (second-order) threshold process. Although more complex coupled dynamics have been considered with conventional direct coupling (Hirst, 1986; Hirst and Lau, 1990), the present study stands apart from these earlier studies for its emphasis on convective coupling which also incorporates the concept of convective time lag. Formulation of such an alternative OAC parameterization is motivated by the fact that the conventional formalism cannot account for many of the features of the observed variabilities as revealed by recent

analyses. Chief among these are the global nature of the ENSO type variabilities and the rather broad spectrum nature of the coupled oscillations.

One of the chief merits of the convective coupling is that it naturally supports coupled modes at a number of time scales, which correspond to the spectrum of observed variabilities. The same mechanism that excites the intraseasonal mode for the IST scenario selectively excites the interannual mode when the scenario changes to IAT, as characterized by the relative strengths of the processes. This is in line with findings from several studies that there are marked similarities between ISO and IAO (Madden and Julian, 1971; Lau and Chan, 1985,1986; Lau and Lau, 1986; and Barnett, 1984). The close relationship between the ENSO and the annual and the seasonal cycles has also been emphasized. In our analysis, these different variabilities emerge as SDW of time and length scales governed by the mean conditions. Further, these variabilities can coexist with their respective characteristics as in nature, as they respond to different mean conditions. Indeed, for the IST scenario, only rarely an IAO signal is excited and vice-versa. Another interesting fact is that while the periods of SDW changes with scenario parameters, these changes are in bands, such as intraseasonal, seasonal and interannual, as we change the parameter regimes.

The present formalism also supports interannual oscillation with relatively small zonal scale when the SST dynamics corresponds to a situation with a deep thermocline. Such a framework may have relevance in the genesis of interannual oscillations over the Indian Ocean almost in phase with ENSO, as shown by recent observational analysis. Since the IAO with shorter zonal scales can coexist with interannual oscillations of comparable periods but larger zonal scales in an ocean basin with different SST dynamics, like the ENSO with larger zonal scale over the Pacific, the present formalism offers a unified dynamical framework for genesis of coupled IAO in the global tropics.

It is needless to emphasize that the simple mechanism of genesis of coupled oscillations proposed in this study cannot account for the entire structure of the observed spectrum. It is perhaps equally needless to emphasize the many limitations that a simple model like ours suffers from. One of the major limitations of the present study is that it exclusively discusses the dynamics of the coupled Kelvin waves. Such an approach, however, may not always work as in a real situation other modes may be excited which may significantly affect the dynamics. Such studies, with conventional formulation of OAC have been already carried out by several authors. However, as emphasized earlier, the focus of our study is the proposed parameterization of OAC, for which an investigation with the simplest but a physically relevant dynamical system appeared a logical first choice. The results, we feel, provide valuable insight into the relevance and effect of convective coupling in the dynamics of coupled oscillations in the tropics. This, we hope, will pave the way to investigate convective coupling in a realistic modeling exercise.

Chapter 11

Concluding Remarks

We would now like to synthesize our results from the previous chapters to arrive at the main conclusions regarding the role of convective forcing and convective time lag in the dynamics and simulation of tropical variabilities. We would also like to identify the major successes and failures, and the need and the scope for future improvements.

The first and the main conclusion that emerges is that a significant part of the tropical variabilities can be understood as forced by convection induced dynamics. We have examined this aspect from a number of angles, such as comparison of average structure of observed and simulated anomaly fields, the anomaly annual cycle and the existence and structure of various observed oscillations. These multi-pronged analyses have helped us to arrive at a robust and consistent dynamical picture of the genesis and structure of the tropical variabilities. In particular, the same dynamical condition as well as parameter range provide the best and the consistent simulations of various aspects of tropical variabilities like the structure of the monthly anomaly fields, genesis and structure of ISO and the structure of the annual cycle.

An important parameter in our formalism is convective time lag, which represents a time scale for interaction between *organized* convection and large-scale

dynamics. It was shown in earlier studies in analytical setting that the inclusion of convective time lag provides a high-frequency cutoff to the tropical eigen modes destabilized by the moist feedbacks (Goswami and Rao, 1993, Goswami and Mathew, 1994). Such a scenario holds also in the present case, although, the relevant value for the CTL in the detail and the non-linear case is about an hour as against a few hours implied by the analytical studies. This, we argue, is because the detailed structure of the variabilities requires contributions from a hierarchy of convective organizations, the smallest of which is characterized by a time scale of about 0.5 hour. As we have seen in the context of coupled dynamics with convective time lag, the relevant value of CTL is once again a few hours in an analytical (linear) setting.

A question that naturally arises at this point is a dynamical description of the effect of CTL: mechanism through which it effects a high frequency cutoff. There is perhaps more than one way of looking at this aspect. One possible explanation is in terms of what the convective time lag basically implies: an adjustment time scale over which precipitation, and hence convective heating, takes place. Thus oscillations with periods much shorter than this convective adjustment time scale would not have time to be forced by the convective heating. Thus a high frequency cut-off naturally results.

A significant finding from the present work has been that SST can significantly affect the tropical variabilities even at monthly and other intraseasonal scales. This has been seen in the contexts of structure of the monthly anomaly fields as well as the genesis and the structure of the intraseasonal oscillations. While SST plays a central role in most dynamical scenarios of interannual oscillations, the significant role of SST in the dynamics of monthly anomaly fields and intraseasonal oscillations in our formulation may appear surprising. The primary dynamical reason for this, we believe, is that in the present model the effect of SST is essentially through its modulation of the moist feedback, and not as a di-

rect heat source. Thus SST directly controls the convective process which is the one of the main driving mechanisms. We have seen that this concept of direct association between SST and convection formulated and applied more explicitly in convective coupling excites the entire spectrum of oscillations under appropriate mean conditions.

There are several directions in which the present model needs to be and can be improved. These improvements can be in terms of both dynamics and physics. Improvements in terms of dynamics would primarily involve a model with vertical structure and global (meridional) domain with more advective nonlinearity. More important, we feel, would be the improvements in the physics. Thus a phased programme for further development of our model of anomaly circulation in the tropics would involve improving certain physics in the present first-baroclinic model itself. There are several such factors whose relative importance in the simulation of the anomaly fields needs to be investigated.

Since in our scenario the large part of the tropical variabilities is due to the response of the convection driven dynamics to the prevailing mean conditions, a major area of improvement would be to involve the mean conditions as comprehensively as possible. For example, the present simulations were generated for a spatially and temporally uniform value of the mean value of the column integrated moisture, $\overline{q}$. Since $\overline{q}$ in our model determines the distribution and intensity of precipitation, and hence convective forcing, inclusion of spatial and temporal (seasonal or monthly) variations of $\overline{q}$ is likely to have significant effect on the model simulations. Another possibility is to use not only the mean dynamical fields but also the mean precipitation field in the dynamics of anomalies through an appropriate parameterization. In another approach adopted by Saji and Goswami (1996) a considerable degree of success in simulating the anomaly climate in the tropis was achieved by directly relating precipitation to SST.

Another area where our model needs improvement was evident from the simu-

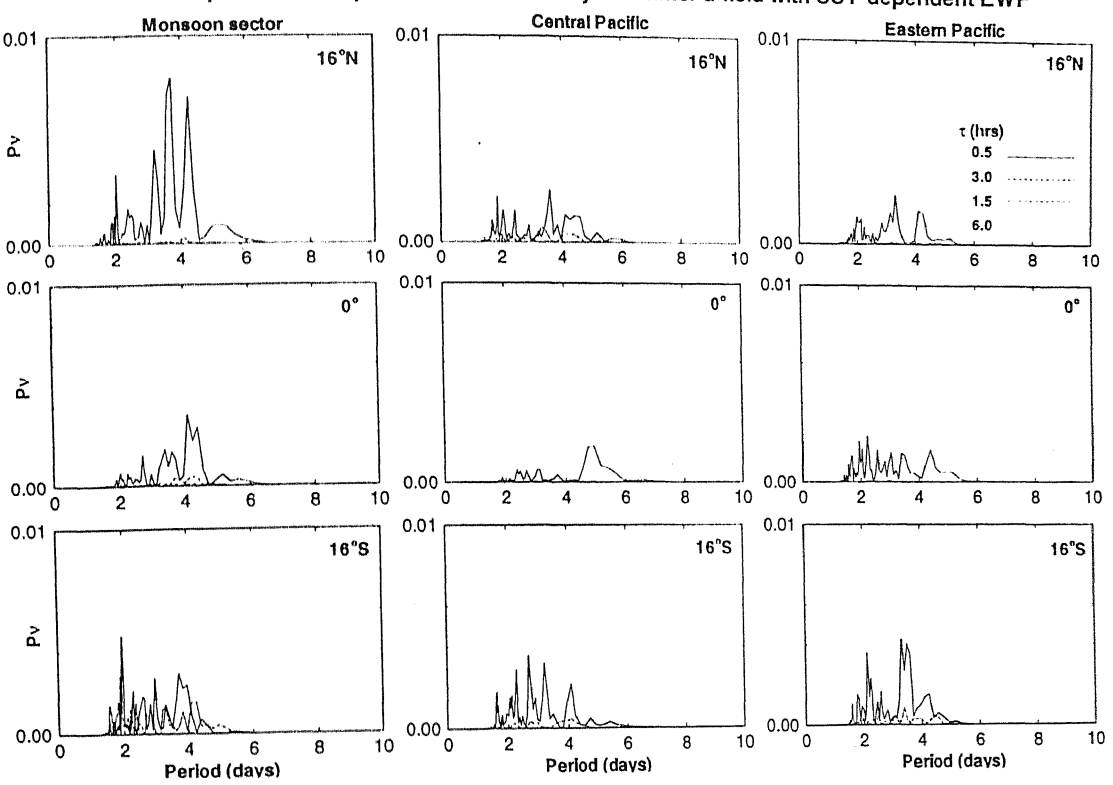

Figure 11.1: Power spectra of zonal wind filtered at 3-7 days plotted for four values of CTL with $\nu P(\nu)$ as the ordinate and period as abscissa, where P is the power and ν is the frequency. For each value of CTL the fields have been normalized to their respective maximum.

lation of the structure of the monthly anomaly fields. It was found, in particular, that the simulations showed consistently high errors over the land regions. This is understandable, since our model has no land physics. The importance of the land surface processes in the dynamics of tropical circulation has been emphasized in many works. While our simulations clearly bring out the deficiencies brought about by the absence of the land surface processes, it needs to be examined how and whether inclusion of a (parameterized) land surface process in our model would shift the model simulations closer to the observed structure. An important first step, of course, is to consider a realistic land-ocean distribution, as close as possible to the observed distribution. This would automatically imply certain change in the structure of the lower boundary forcing and, in particular, moist

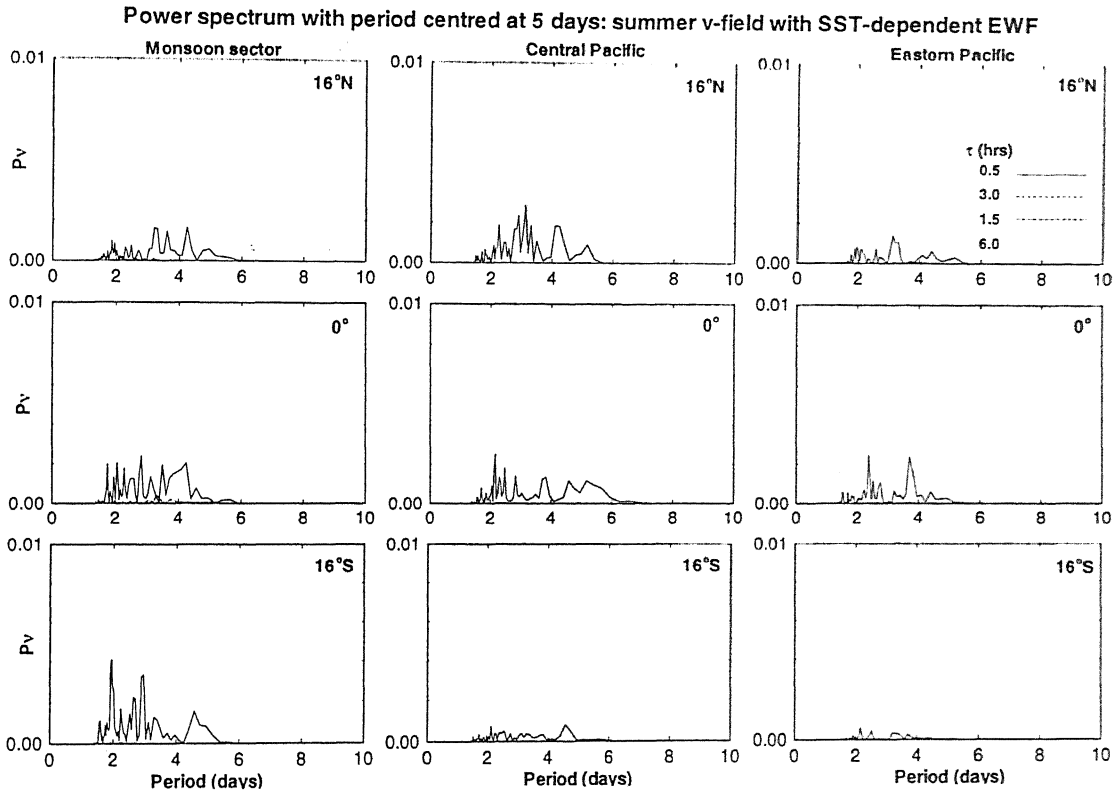

Figure 11.2: Same as figure 11.1, but for meridional wind

feedback. In the second phase, an appropriate formulation of the moist feedback over the land region has to be incorporated.

It is worth noting that the first-baroclinic mode model developed by us can support a rich spectrum of physics. Indeed, the power spectrum shows, although not at all locations with equal strength, peaks almost at all the observed periodicities relevant for the model simulations. In observation also various oscillations are not seen at all locations and at all seasons with equal strength. The scenario that emerges, therefore, is one in which a very broad spectrum of the observed tropical oscillations is excited by the convection induced internal dynamics in the tropics. These oscillations then respond to the seasonally and spatially varying mean conditions and also to ocean-atmosphere coupling with varying strengths and characteristics. This variation of response of the oscillations of different periodicities to these factors then result in the observed structure of the tropical

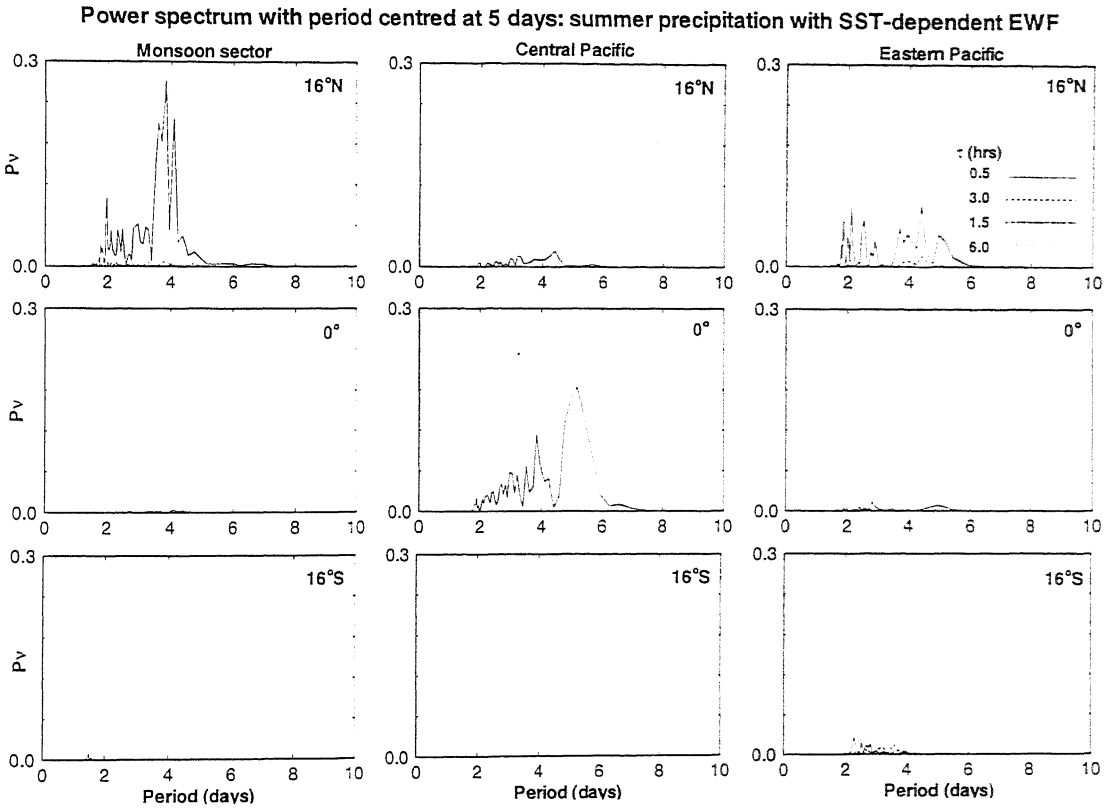

Figure 11.3: Same as figure 11.1, but for precipitation

oscillations. We have seen that such a scenario is also borne out by our investigation of the convectively coupled tropical dynamics.

Although our model can simulate a very wide spectrum of tropical oscillations it is still not complete. There are well-known tropical oscillations both at the high frequency end as well as with longer periods than what we have covered here. At the higher frequency end of the intraseasonal oscillations lies the 'synoptic frequency' easterly waves. There are, however, two distinct classes of easterly waves. One class is characterized by an off-equatorial (20°N) maximum in the amplitude with a zonal wavelength of about 2000 km. The other class is characterized by a westward phase propagating (relative to the basic current), longer wavelengths than the first type, equatorially trapped structure. Most of our knowledge about the 3-7 day westward propagating wave with a zonal scale of about 6000 km. comes from recent analyses of analyzed global data sets (Liebmann and Hendon,

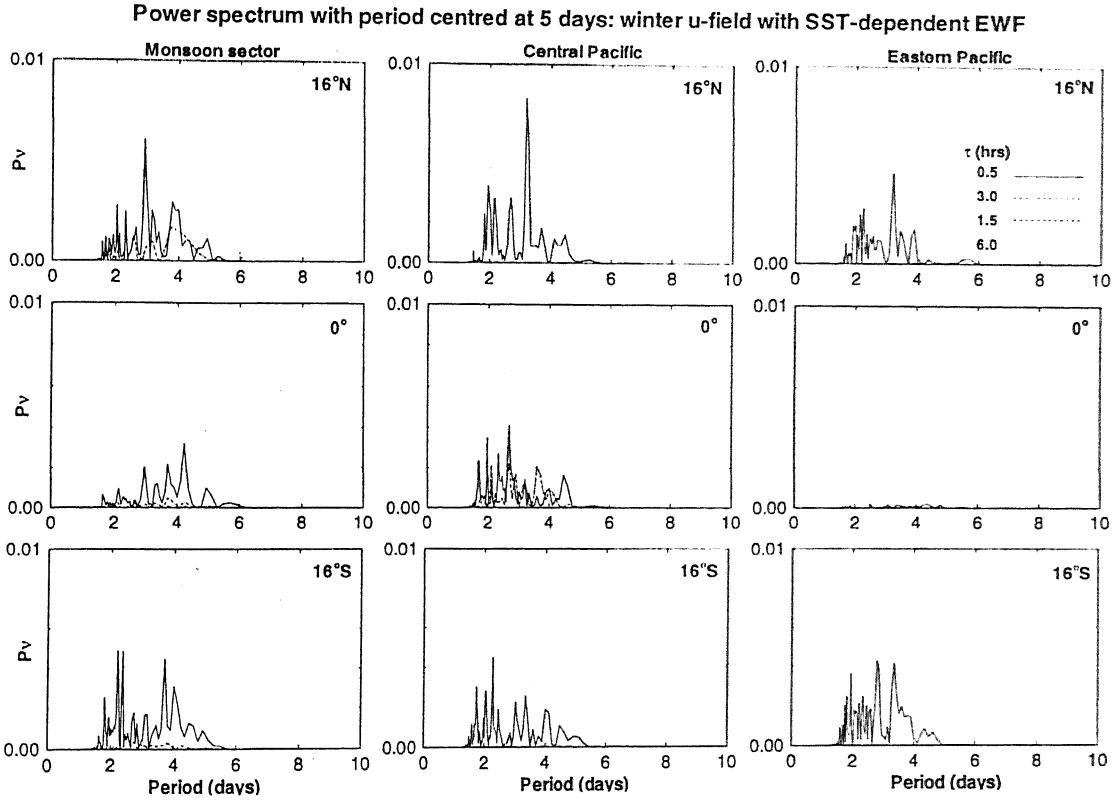

Figure 11.4: Same as figure 11.1, but for winter months

1990, hereafter LH90).

The discovery of these synoptic frequency waves with relatively large zonal scales raises several interesting theoretical problems. These questions range from one of genesis of these waves, related to the general driving mechanism, to the variation of the characteristics of these waves in space and time. While there have been a large number of theoretical investigations of the 30-50 day eastward propagating wave, a very few studies have addressed the question of dynamical mechanism of 3-7 day wave. A successful dynamical scenario for the genesis of 3-7 day wave was advanced by Goswami and Goswami (1991), who showed that inclusion of combined effect of EWF and convergence feedback and dissipation selectively destabilizes the mixed Rossby gravity (MRG) wave at 3-7 day time scale. Since the observed spectral characteristics of the 3-7 day wave were by then available from the analysis of LH90, it was possible to verify the predictions

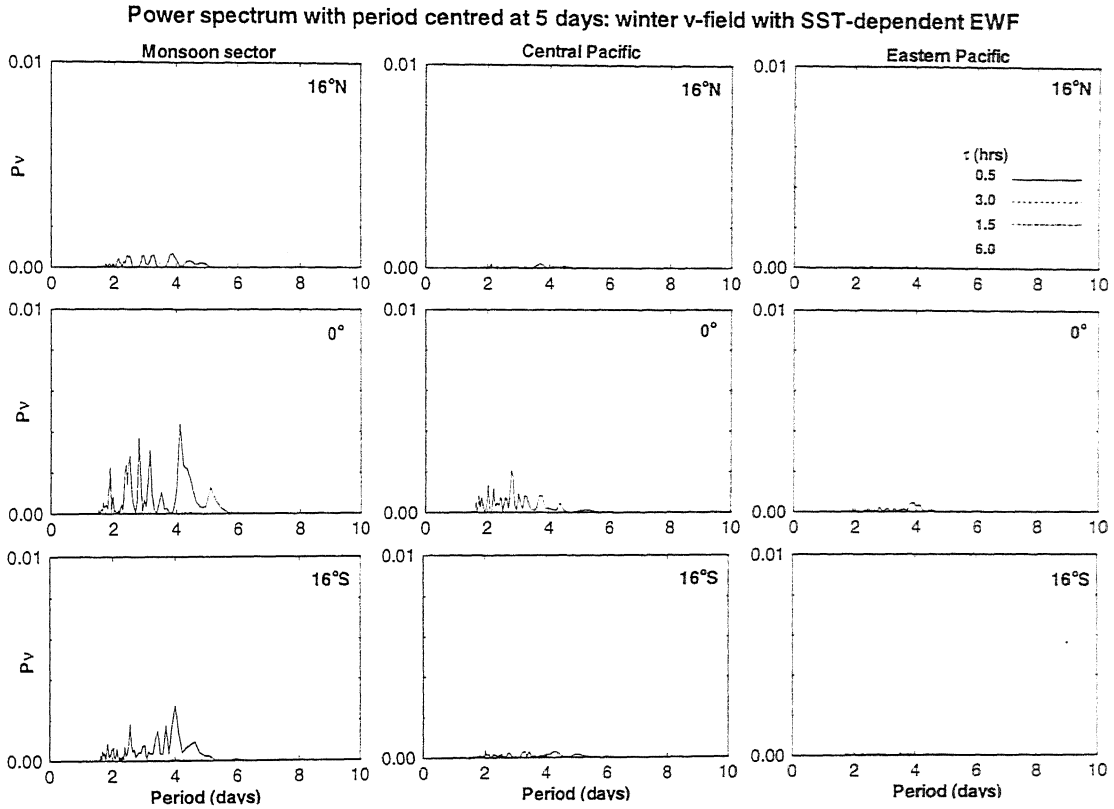

Figure 11.5: Same as figure 11.4, but for meridional wind

from the theory with observations. Thus it was shown that not only the period but also the zonal wavelength and the e-folding length (characteristic equatorial trapping length) were also in close agreement with observations. The investigation of genesis and structure of 3-7 day wave in presence of a CTL was carried out in Goswami and Mathew (1994). In particular, it was shown in Goswami and Mathew that the same mechanism that selectively destabilizes the MRG wave at 3-7 day time scale in presence of mean easterlies excites the 10-20 day wave in presence of mean westerlies. These analytical results thus provide an excellent motivation for examining the existence and the characteristics of the 3-7 day wave presence of CTL and non-linear heating. Indeed there are peaks at 3-7 day range in our composite one-year simulation. However, as the associated power is rather weak, we have not carried out a detailed analysis of this oscillation in our present study. It is, nonetheless, interesting to note that the power spectra of

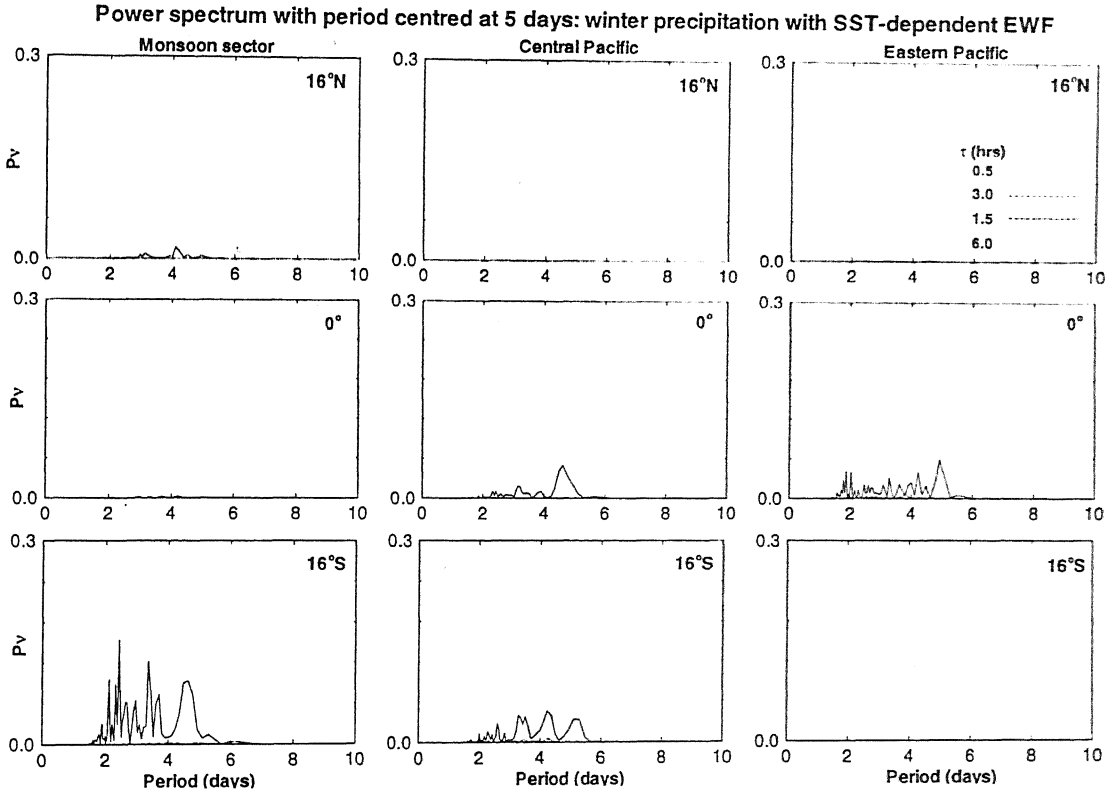

Figure 11.6: Same as figure 11.4, but for precipitation

the model fields filtered at 3-7 day window exhibit many characteristics similar to the observed.

Figures 11.1-11.3 show the power spectra of the model u, v and the precipitation fields from the composite one-year simulation, with an SST-dependent EWF, filtered at 3-7 days. As before, the unfiltred time series have been generated by averaging the fields over a zonal extent of 60° centered at 90°E (monsoon sector), 80°W (Central Pacific) and 160°W (Eastern Pacific). We shall consider three latitudinal positions, *viz.* equator, 16°N (NH) and 16°S (SH). The results are shown from analysis of the fields for the summer months (June-October) at different locations as indicated in the panels. The four curves in each panel represent the power spectra for four different values of CTL. The corresponding power spectra for the winter months (January-May) are shown in figures 11.4-11.6 As can be seen from these figures, the model in general supports ISO with 3-7

day time scale, although the power is relatively weaker than that for the 30-50 day and the 10-20 day waves in the model simulation. Since our model fields are normalized to its maximum value for ease of comparing results for different values of CTL, the smallness of power is not necessarily an indicator of weakness of the spectrum in the absolute sense. Figures 11.1-11.6 show that $\tau = 0.5hr$ gives rise to the strongest signal at 3-7 days.

The first striking feature of the power spectra of the winter fields is their distinctly different characteristics from the corresponding summer fields. Thus, in contrast to the summer u, the winter u shows much weaker power over the equator than over the off-equatorial positions. This is especially true over the eastern Pacific region, where the the equatorial u has very little power. This characteristic is in consistent with an MRG wave structure of the 3-7 day wave as found by Liebmann and Hendon (1990). The MRG wave character of the winter fields is further borne out by the power spectra of the winter v (figure 11.5), which shows the highest amplitude over the equator. The precipitation, however, shows rather distinct zonal and latitudinal characteristics from the dynamical fields (figure 11.6). It was found that many other characteristics of the 3-7 day wave, like its westward propagation, are also consistently reproduced by the model simulation. But a more detailed analysis of the structure of the high-frequency part of our model simulation is necessary.

At the low frequency (but less than centennial scale) end of the tropical oscillation are the decadal and inter-decadal (about 25 years) oscillations. Very little is known about the structure and dynamics of these variabilities. Although our long-period simulation is upto 38 years and hence can not be used to investigate interdecadal oscillations, it is interesting to note that there exists a significant peak above the red noise level in the 8-10 year range at several locations. Once again, this aspect needs to be investigated through elaborate analyses of simulations for much longer period.

Another aspect of the tropical oscillations that is discussed here is the question of their phase speeds. Although it is possible to compute a measure of the wavelength associated with each periodicity, and hence an associated phase speed, this discussion has been left out in the the present work. This and other spectral as well as dynamical characteristics of the simulated fields must be carried out in a detailed and objective manner for further evaluation of the model simulations.

Considering the model's present level of success and its understandable and conceptually consistent failures, it is a potential candidate for a tropical atmospheric model with more detailed structure like vertical variations. This would allow not only a discussion of the three dimensional structure of the (simulated) anomaly fields, but inclusion of a more detailed structure of the mean fields. The latter is quite important in view of the significant role of the mean circulation in the dynamics of the variabilities. The success of the present formulation in the context of tropical variabilities indicates that the concept of a convective time lag may be useful in parameterizing convective forcing in more complex GCMs.

References

Anderson, D. T. L., 1976: The low-level jet as a western boundary current. *Mon. Wea. Rev.* 104, 907-921.

Bannon, P., 1979: On the dynamics of the East African Jet. II. Jet transients. *J. Atmos. Sci.*, 36, 2139-2168.

Barnett, T. P., 1984: Interaction of monsoon and pacific trade wind system at interannual time scales. Part III a partial anomaly of southern oscillation. *Mon. Wea. Rev.*, 112, 2380-2387.

Barnett, T. P., 1991: The interaction of multiple time scales in the tropical climate system, *J. Climate*, 4. 269-285.

Battisti, D. S., and A. C. Hirst. 1989: Interannual variability in a tropical atmosphere-ocean model: Influences of basic state, ocean geometry and non-linearity. *J. Atmos. Sci.*, 46. 1687-1712.

Bergman, J. W. and M. L. Salby, 1994: Equatorial wave activity derived from fluctuations in observed convection. *J. Atmos. Sci.*, 51, 3791-3806.

Betts, A. K, 1986: A new convective adjustment scheme. Part- I: Observational and theoretical basis, *Quart. J. Roy. Meteorol. Soc.*, 112, 677-691.

Betts, A. K. and M. J. Miller. 1986: A new convective adjustment scheme. Part-II: Single column tests using GATE wave, BOMEX, ATEXand Artic air-mass data sets. *Quart. J. Roy. Meteorol. Soc.* 112. 693-709.

Bjerknes, J 1969: Atmospheric teleconnections from the equatorial Pacific, *Mon. Wea. Rev.*, 97, 163-172.

Blade, L and D. L. Hartmann, 1993: Tropical intraseasonal oscillations in a simple nonlinear model. *J. Atmos. Sci.*, 50, 2922-2939.

Brier, G. W, 1978: The Quasi-Biennial oscillation and feedback processes in the atmosphere-ocean-earth system, *Mon. Weath. Rev.*, 106, 938-946.

Cane, M. A. and Zebaik, S. E., 1985: A theory for El Niñ and Southern Oscillation. *Science*, 228, 1085-1087.

Chang, C. P. and H. Lim 1988: Kelvin wave-CISK: a possible mechanism for the 30-50 day oscillation. *J. Atmos. Sci.*, 45, 1709-1720.

Chang, C. P., 1976: Vertical structure of tropical waves maintained by internally-induced cumulus heating, *J. Atmos. Sci.*, 33, 729-739.

Chang, C. P., 1977: Viscous internal-gravity wave and low- frequency oscillations in the tropics. *J. Atmos. Sci.*, 29, 90-110.

Chao, W. C, 1995: A critique of wave-CISK as an explanation for the 40-50 day tropical intraseasonal oscillation. *J. Meteorol. Soc. Japan*, 73, 677-684.

Chao, W. C. and S.-J. Lin, 1994: Tropical intraseasonal oscillation, super cloud clusters, and cumulus convection schemes. *J. Atmos. Sci.*, 51, 1282-1297.

Chen T, and Chen J-M., 1993: The 10-20 Day mode of the 1979 Indian Monsoon: Its relation with the time variation of monsoon rainfall. *Mon. Wea. Rev.* 121, 2465-2482.

Cho, H.-R., K. Fraedrich and J. T. Wang, 1994: Cloud clusters, Kelvin waves-CISK, and the Madden-Julian oscillations in the equatorial troposhere. *J. Atmos. Sci.*, 51, 68-76.

Cornejo-Garrido, A. G., and P. H. Stone, 1977: On the heat balanceof the Walker circulation. *J. Atmos. Sci.*, 34, 1155- 1162.

Davey, M. K., 1985: Result from the moist equatorial atmosphere model. Coupled Ocean-Atmosphere models, *J. C. J Nihoul, Ed., Elsevier*, 41-49.

Davey, M. K., A. E. Gill, 1987: Experiment on tropical circulation with a simple moist model. Quart. *J. Roy. Meteorol. Soc.*, 113, 1237-1269.

Dunkerton, T. J., and M. P Baldwin, 1995: Observation of 3-6 Day Meridional wind oscillations over the tropical Pacific, 1973-1992: Horizontal structure and propagation. *J. Atmos. Sci.*, 52, 1585-1601.

Emanuel, K. A., 1987: An air-sea interaction model of intraseasonal oscillations in the tropics. *J. Atmos. Sci.*, 44, 2324-2340.

Emanuel. K. A., 1993: The effect of convective response time on WISHE modes. *J. Atmos. Sci.*, 50, 1763-1775.

Enfield. D. B., 1987: The intraseasonal oscillation in eastern Pacific sea levels: How is it forced? *J. Phys. Oceanogr.*, 17, 1860-1876.

Gill, A. E., 1980: A simple solution for heat-induced tropical circulation. *Quart. J. R. Met. Soc.*, 106, 447-462.

Gill, A. E., and Philips, P. J., 1986: Nonlinear effect on the heat-induced circulation of the tropical atmosphere. *Q. J. R. Meteorol. Soc.*, 112, 69-91.

Goswami B. N. and J. Shukla, 1984: Quasi-periodic oscillation in a symmetric general circulation model. *J. Atmos. Sci.*, 41, 20-37.

Goswami B. N. and Sudha Selvarajan 1991: Convergence feedback and unstable low frequency oscillation in a simple coupled ocean-atmospheric model. *J. Geophys. Res.* 18, 991- 994.

Goswami P. and B. N. Goswami 1991; Modification of n=0 equatorial waves due to interaction between convection and dynamics, *J. Atmos. Sci.* 48, 2231-2244.

Goswami P. and R. Koteswar Rao 1994; A dynamical mechanism for selective excitation of the Kelvin mode at timescale of 30-50 days. *J. Atmos. Sci.* 51, 2769-2779.

Goswami P. and V. Mathew 1994; A mechanism for scale selection in Tropical circulation at observed intraseasonal frequencies, *J. Atmos. Sci.*, 51, 3155-3166

Gruber, A., 1974: Wavenumber-frequency spectra of sat-measured brightness in

Davey, M. K., A. E. Gill, 1987: Experiment on tropical circulation with a simple moist model. Quart. *J. Roy. Meteorol. Soc.*, 113, 1237-1269.

Dunkerton, T. J., and M. P Baldwin, 1995: Observation of 3-6 Day Meridional wind oscillations over the tropical Pacific, 1973-1992: Horizontal structure and propagation. *J. Atmos. Sci.*, 52, 1585-1601.

Emanuel, K. A., 1987: An air-sea interaction model of intraseasonal oscillations in the tropics. *J. Atmos. Sci.*, 44, 2324-2340.

Emanuel. K. A., 1993: The effect of convective response time on WISHE modes. *J. Atmos. Sci.*, 50, 1763-1775.

Enfield. D. B., 1987: The intraseasonal oscillation in eastern Pacific sea levels: How is it forced? *J. Phys. Oceanogr.*, 17, 1860-1876.

Gill, A. E., 1980: A simple solution for heat-induced tropical circulation. *Quart. J. R. Met. Soc.*, 106, 447-462.

Gill, A. E., and Philips, P. J., 1986: Nonlinear effect on the heat-induced circulation of the tropical atmosphere. *Q. J. R. Meteorol. Soc.*, 112, 69-91.

Goswami B. N. and J. Shukla, 1984: Quasi-periodic oscillation in a symmetric general circulation model. *J. Atmos. Sci.*, 41, 20-37.

Goswami B. N. and Sudha Selvarajan 1991: Convergence feedback and unstable low frequency oscillation in a simple coupled ocean-atmospheric model. *J. Geophys. Res.* 18, 991- 994.

Goswami P. and B. N. Goswami 1991; Modification of n=0 equatorial waves due to interaction between convection and dynamics, *J. Atmos. Sci.* 48, 2231-2244.

Goswami P. and R. Koteswar Rao 1994; A dynamical mechanism for selective excitation of the Kelvin mode at timescale of 30-50 days. *J. Atmos. Sci.* 51, 2769-2779.

Goswami P. and V. Mathew 1994; A mechanism for scale selection in Tropical circulation at observed intraseasonal frequencies, *J. Atmos. Sci.*, 51, 3155-3166

Gruber, A., 1974: Wavenumber-frequency spectra of sat-measured brightness in

the tropics, *J. Atmos. Sci.,* 31, 1680.

Hayashi, Y. and D. G. Golder, 1980: The seasonal variation of tropical transient planetary waves appearing in a GFDL general circulation model, *J. Atmos. Sci.*, 37, 705-716.

Hayashi, Y-Y. and A. Sumi, 1986: The 30-40 day oscillation simulated in a "aqua-planet" model, *J. Meteorol. Soc. Japan*, 64, 451-466.

Hayashi, Y-Y., and T. Nakazawa, 1989: Evidence of the existence and eastward motion of superclusters at the equator, *Mon. Wea. Rev.*, 117, 236-243.

Hendon H., and John Glick, 1995: Observed intraseasonal atmosphere-ocean variability in the tropical pacific and Indian oceans, Paper H004, Abstract International TOGA conference 1995.

Hendon, H. H., and M. L. Salby, 1996: Planetary-scale circulations forced by intraseasonal variations of observed convection, *J. Atmos. Sci.*, 53, 1751-1758.

Hendon, H. H., and M. L. Salby, 1994: The life cycle of the Madden-Julian oscillation, *J. Atmos. Sci.*, 51, 2225-2237.

Hendon, H. H., 1988: A simple model of the 40-50 day oscillation, *J. Atmos. Sci.*, 45, 569-584.

Hentel, M. and Baader, H. 1978: Diabatic heating climatology of the tropical circulation, *J. Atmos. Sci.,* 35, 1180-1189.

Hirst A. C., and K. M. Lau 1990: Intraseasonal and interannual Oscillations in Coupled Ocean-Atmosphere Models, *J. Climate*, 3, 713-725.

Hirst, A. C., 1986; Unstable and damped equatorial modes in simple coupled ocean-atmospheric models, *J. Atmos. Sci.* 43, 606-630.

Hirst, A. C., 1988; Slow instabilities in tropical ocean basin-global atmosphere models, *J. Atmos. Sci.* 45, 830-852.

Hirst, A., and K. M, Lau, 1990: Intraseasonal and interannual oscillations in couple ocean-atmosphere model. *J. Clim.*, 3, 713-725.

Horel, J. D, 1982: On the annual cycle of the tropical Pacific atmosphere and

ocean. *Mon. Wea. Rev.*, 110, 1863-1878.

Hsu, H.-H, B. J. Hoskins, and F.-F. Jin, 1990: The 1985/86 intraseasonal oscillation and the role of the extratropics. *J. Atmos. Sci.*, 47, 832-839.

Itoh, H., 1989: The mechanism for the scale selection of tropical intraseasonal oscillation, *J. Atmos. Sci.*, 46, 1779-1798.

Johnson, E. S. and M. J. Mcphaden, 1993: Structure of intraseasonal Kelvin waves in the equatorial Pacific Ocean. *J. Phys. Oceanogr.*, 23, 608-625.

Julian, P. R. and Chervin, R. M., 1978: A study of the Southern Oscillation and Walker circulation phenomenon. *Mon. Wea. Rev.*, 106, 1433-1451.

Kirtman, B. P. and A. D. Vernekar 1992: a note on CISK and the E-W feedback mechanism for the Madden-Julian oscillation, *J. Atmos. Sci.* 25, 143-169

Knutson, T., and K. M. Weickmann, 1987: The 30-60 day atmospheric Oscillations: Composite life cycles of convection and circulation anomalies. *Mon. Wea. Rev.*, 115, 1407-1436.

Knutson, T. R., and K. M. Weickmann, 1987: 30-60 day atmospheric oscillation: composite life cycles of convection and circulation anomalies. *Mon. Wea. Rev.*, 115, 1407-1436.

Krishnamurti, T. N., Molinari, J. and pan. H. L., 1976: Numerical simulation of the Somali jet. *J. Atmos. Sci.*, 33, 2350-2362.

Krishnamurti, T. N., and P. Ardanuy, 1980: The 10-20 day westward propagating mode and breaks in the monsoon. *Tellus*. 32,15-26.

Krishnamurti, T. N., P. K. Jayakumar, J. Sheng, N. Surgi and A. Kumar, 1985: Divergent circulations on the 30-50 day time scale. *J. Atmos. Sci.*, 42, 364-375.

Krishnamurti, T. N., and S. Gadgil, 1985: On the structure of the 30 to 50 day mode over the globe during FGGE. *Tellus*, 37A, 336-360.

Krishnamurti, T. N., D. K. Oosterhof and A. V. Mehta, 1988: Air-sea interaction on the time scale of 30 to 50 days. *J. Atmos. Sci.*, 45, 1304-1322.

Landsberg, H. E, 1962: Biennial pulses in the atmosphere *Beitr. Phycs. Atmos.*,

35, 184-194.

Landsberg, H. E, J. M Mitchell, H. L Jr. Crutcher and F. T Quinlan, 1963: Surface signs of the biennial atmospheric pulse, *Mon. Weather Rev.*, 101, 549-556.

Lau, K.-M 1985: Elements of a stochastic-dynamical theory of the long-term variability of the El Nino/Southern Oscillation, *J. Atmos. Sci.*, 42, 1552-1558.

Lau K.-M and P. H. Chan, 1985a: Aspect of 40-50 day oscillation during northern winter as inferred from outgoing long wave radiation *Mon. Wea. Rev.*, 113, 1889-1901.

Lau K.-M and P. H. Chan, 1985b: Aspect of 40-50 day oscillation during northern summer as inferred from outgoing long wave radiation *Mon. Wea. Rev.*, 114, 1354-1367.

Lau K.-M. and L. Peng, 1987: Origin of low-frequency oscillation in the tropical atmosphere. Part I: basic theory. *J. Atmos. Sci.*, 44, 950-972.

Lau K.-M and P. H. Chan, 1988: Intraseasonal and Interannual variations of the tropical convection: A Possible link between the 40-50 day oscillations and ENSO? *J. Atmos. Sci.,* 45, 506-521.

Lau K.-M. and S. Shen 1988; On the dynamics of the intraseasonal oscillation and ENSO. *J. Atmos. Sci.*, 45, 1781- 1797.

Lau, K.-M. and L. Peng, 1990: Origin of low-frequency (intraseasonal) oscillations in the tropcial atmosphere. Part III: monsoon dynamics. *J. Atmos. Sci.*, 47, 1443-1462.

Lau, K.-M. and P. H., Chan, 1986: Aspects of the 40-50 day oscillation during Northern Winter as inferred from outgoing longwave radiation. *J. Atmos. Sci.*, 43, 1889-1909.

Lau, K.-M., and P. H., Chan, 1988: Intraseasonal and interannual variations of tropical convection: A possible link between the 40-50 day oscillation and ENSO ? *J. Atmos. Sci.*, 45, 506-521.

Lau, K.-M, and P. J. Sheu, 1988: Annual cycle, Quasi-Biennial Oscillation, and Southern Oscillation in global precipitation. *J. Geophys. Res.*, 93, 10975-10988.

Lau, K.-M., T. Nakazawa and C. H. Sui. 1991: Observations of cloud cluster hierarchies over the tropical western Pacific. *J. Geophys. Res.*, 96, 3197-3208.

Lau, N.-C, and Lau, K.-M, 1986: The structure and propagation of intraseasonal oscillations appearing in a GFDL general circulation model. *J. Atmos. Sci.*, 43. 2023- 2047.

Lau N.-C. and K.-M. Lau 1986: Structure and propagation of intraseasonal oscillations appearing in a GFDL GCM. *J. Atmos. Sci.* 43, 2023-2047.

Lau, N.-C., I. M. Held and J. D. Neelin, 1988: The Madden- Jullian oscillation in an idealized general circulation model. *J. Atmos. Sci.*, 45, 3810-3832.

Levey, K. M. and M. R. Jury, 1996: Composite intraseasonal oscillations of convection over southern Africa.*J. Climate*, 9, 1910-1920.

Li, T and B. Wang, 1994: A thermodynamic equilibrium climate model for monthly mean surface winds and precipitation over the tropical Pacific. *J. Atmos. Sci.*, 51, 1372-1385.

Liebmann, B, and H. H. Handon, 1990: Synoptic scale disturbances near the equator. *J. Atmos. Sci.*, 43, 3138-3158.

Lim, H., T.-K. Lim and C. P Chan, 1990: Re-examination of wave-CISK theory: existence and properties of non-linear wave-CISK modes. J. Atmos. Sci., 47, 3078-3091.

Lin Xin and Johnson, R. H, 1996: Kinematic and thermodynamic characteristics of the flow over the western Pacific Warm pool during TOGA COARE. *J. Atmos. Sci.*, 53, 695-758.

Lindzen, R. S., 1974: Wave-CISK in the tropics. *J. Atmos. Sci.*, 28, 156-179.

Liu W. T., 1988: Moisture and latent heat flux variabilities in the Tropical Pacific derived from satellite data, *J. Geophys. Res.*, 93, 6749-6760.

Lukas, R., P. J. Webster, M. Ji, and A. Leetmaa. 1995: The large-scale context

Lau, K.-M, and P. J. Sheu, 1988: Annual cycle, Quasi-Biennial Oscillation, and Southern Oscillation in global precipitation. *J. Geophys. Res.*, 93, 10975-10988.

Lau, K.-M., T. Nakazawa and C. H. Sui, 1991: Observations of cloud cluster hierarchies over the tropical western Pacific. *J. Geophys. Res.*, 96, 3197-3208.

Lau, N.-C, and Lau, K.-M, 1986: The structure and propagation of intraseasonal oscillations appearing in a GFDL general circulation model. *J. Atmos. Sci.*, 43. 2023- 2047.

Lau N.-C. and K.-M. Lau 1986: Structure and propagation of intraseasonal oscillations appearing in a GFDL GCM. *J. Atmos. Sci.* 43, 2023-2047.

Lau, N.-C., I. M. Held and J. D. Neelin, 1988: The Madden- Jullian oscillation in an idealized general circulation model. *J. Atmos. Sci.*, 45, 3810-3832.

Levey, K. M. and M. R. Jury, 1996: Composite intraseasonal oscillations of convection over southern Africa.*J. Climate*, 9, 1910-1920.

Li, T and B. Wang, 1994: A thermodynamic equilibrium climate model for monthly mean surface winds and precipitation over the tropical Pacific. *J. Atmos. Sci.*, 51, 1372-1385.

Liebmann, B, and H. H. Handon, 1990: Synoptic scale disturbances near the equator. *J. Atmos. Sci.*, 43, 3138-3158.

Lim, H., T.-K. Lim and C. P Chan, 1990: Re-examination of wave-CISK theory: existence and properties of non-linear wave-CISK modes. J. Atmos. Sci., 47, 3078-3091.

Lin Xin and Johnson, R. H, 1996: Kinematic and thermodynamic characteristics of the flow over the western Pacific Warm pool during TOGA COARE. *J. Atmos. Sci.*, 53, 695-758.

Lindzen, R. S., 1974: Wave-CISK in the tropics. *J. Atmos. Sci.*, 28, 156-179.

Liu W. T., 1988: Moisture and latent heat flux variabilities in the Tropical Pacific derived from satellite data, *J. Geophys. Res.*, 93, 6749-6760.

Lukas, R., P. J. Webster, M. Ji, and A. Leetmaa. 1995: The large-scale context

for the TOGA coupled ocean-atmosphere response experiment. *Meterol. Atmos. Phys.*, 56, 3-16.

Madden, R. A., 1986: Seasonal variations of the 40-50 day oscillation. *J. Atmos. Sci.*, 43, 3138-3158.

Madden, R. A. and P. R. Julian 1971: Detection of a 40-50 day oscillation in the zonal wind in the tropical pacific *J. Atmos. Sci.*, 28, 702-708.

Madden, R. A., and P. R. Julian, 1972: Description of global scale circulation cells in the tropics with 40-50 day period. *J. Atmos. Sci.*, 29, 1109-1123.

Madden, A. R. and P. R. Julian, 1994: Observation of the 40- 50 day tropical oscillation - A review. *Mon. Wea. Rev.*, 122, 814-837.

Matsuno, T. 1966: Quasi-geostrophic motions in the equatorial area. *J. Met. Soc. Japan.*, 44, 25-43.

Mayers, G., J. R. Donguy, and R.K. Reed, 1986: Evaporative cooling of western equatorial Pacific Ocean by anomalous winds, *Nature*, 323, 523-526.

McPhaden, M. J., 1982: Variability in the cetral equatorial Inadian Ocean, I Ocean dynamics. *J. Mar. res.*, 40, 157-176.

McPhaden, M. J., and B. A. Taft, 1988: Dynamics of seasonal and intraseasonal variability in the eastern Pacific. *J. Phys. Oceanogr.* 18, 1713-1732.

Meehl, G., 1993: A coupled air-sea biennial mechanism in the tropical Indian and Pacific regions: Role of the ocean, *J. of Climate*, 6, 31-41.

Meehl, G., 1987: The annual cycle and interannual variability in the tropical Pacific and Indian Ocean regions, *Mon. Wea. Rev.*, 115, 27-49.

Mertz, G. J., and Mysak., 1984: Evidence for a 40-60 day oscillation over the western Indian ocean during 1976 and 1979. *Mon. Wea. Rev.*, 112, 383-386.

Milliff, R. F. and R. A. Madden, 1996: The existence and vertical structure of fast, eastward moving disturbances in the equatorial troposphere. *J. Atmos. Sci.*, 53, 586-597.

Mitchell, T. P., and J. M. Wallace, 1992: The annual cycle in equatorial convec-

tion and sea surface temperature. *J. Climate*. 5, 1140-1156.

Miyahara, S., 1987: A simple model of the tropical intraseasonal oscillation. *J. Meteorol. Soc. Japan*. 65.341-351.

Murakami, T., 1976: An analysis of summer monsoon fluctuations over India. *J. Meteorol. Soc. Japan*, 54. 15-32.

Murakami, T., and Frydrych, 1974: On the preferred period of upper wind flutuations during the monsoon. *J. Atmos. Sci.*, 31. 1549-1555.

Murakami, T., L.-X Chen. and A. Xie. 1986: Relationship among seasonal cycles. low-frequency oscillations. and transient disturbances as revealed from outgoing longwave radiation data. *Mon. Wea. Rev.*, 114. 1456-1465.

Murakami, T. and Wang. B, 1993: Annual cycle of equatorial east-west circulation over the Indian and Pacific oceans. *J. Climate*. 6, 932-952.

Nakazawa, T, 1986: Intraseasonal Variation in OLR in the tropics during the FGGE year. *J. Meteorol. Soc. Japan*., 64. 17-34.

Nakazawa, T, 1995: Intraseasonal oscillations during the TOGA-COARE IOP. *J. Meteorol. Soc. Japan*, 73, 305-319.

Neelin, J. D. and Jia-yuh Yu 1994: Modes Tropical variability under convective adjustment and Madden-Julian oscillation Part I: Analytical Theory *J. Atmos. Sci.* 51, 1876-1914.

Neelin, J. D., I. M. Held and K. H. Cook, 1987: Evaporation- wind feedback and low-frequency variability in the tropical atmosphere. *J. Atmos. Sci.*, 44. 2241-2248.

Neelin, J. D., I. M. Held. and K. H. Cook. 1987: Evaporation- wind feedback and low frequency variability in tropical atmosphere. *J. Atmos. Sci.*, 43, 2341-2348.

Nicholls, N. 1978: Air-Sea interaction and the Quasi-Biennial oscillation, *Mon. Wea. Rev.*, 106, 1505-1508.

Nigam Sumant and H. S. Shen 1993: Structure of oceanic and atmospheric low frequency variabilities over the tropical Pacific and Indian oceans Part 1: COADS

observation, *J. Climate*, 6, 657-677.

Nishi, N., 1989: Observational study on the 30 60 day variation in the geopotential and temperature fields in the equatorial region. *J. Meteorol. Soc. Japan.*, 67,187-203.

Numaguti, A., 1993: Dynamics and energy balance of the Hadley circulation and the tropical precipitation zones: significance of the dstribution of evaporation. *J. Atmos. Sci.* 50, 1874-1887.

Numaguti, A., and Y. Y. Hayashi, 1991a: Behavior of cumulus activity and structure of circulations in an "aqua-planet" model Part I: the structure of the super clusters. *J. Meteorol. Soc. Jap.*, 69, 541-561.

Numaguti, A., and Y. Y. Hayashi, 1991a: Behavior of cumulus activity and structure of circulations in an "aqua-planet" model Part II: eastward-moving planetary scale structures and the intertropical convergence zone. *J. Meteorol. Soc. Jap.*, 69, 563-579.

Parker. D. E., 1973: Equatorial Kelvin waves at 100mb. *Quart. J. Roy. Meteorol. Soc.,* 99, 116-129.

Philander, S. G. F, T. Yamagata, and R.C. Picanowski, 1984: Unstable Air-Sea interaction in the tropics. *J. Atmos. Sci.*, 41, 604-613

Philander, S. G. F. 1990: El Niño, La Niña, and southern oscillation., *Academic press. Inc.*

Philander, S. G. F. 1992: Ocean-atmosphere interactions in the tropics: A review of recent theories and models. *J. Appl. Metoer.* 8, 939-945.

Philips, P. J., Gill, A. E., 1987: An analytical model of the heat-induced tropical circulation in the presence of a mean wind. *Q. J. R. Meteorol. Soc.*, 113, 213-236.

Rasmusson, E. M., X. Wang and C. F. Ropelewski, 1990: The biennial component of ENSO variability, *J. of Marine Systems*, 1, 71-96.

Rasmusson, E. M, P. A. Arkin, W. Y Chen, and J. B Jalickee, 1981: Biennial variations in surface temperature over the United States as revealed by singular

decomposition, *Mon. Weather Rev.*, 109. 181-192.

Rasmusson. E. M, and J. M Wallace, 1983: Meteorological aspects of the El Niño/Southern Oscillation, *Science*, 222. 1195-1202.

Ramage. C. S., 1977: Sea surface temperature and local weather. *Mon. Wea. Rev.*, 105.540-544.

Rodhe, H. and H. Virji. 1976: Trends and periodicities in east African rainfall. *Mon. Weather Rev.*, 104. 307-315.

Ropelewski. C. F., Halpert. M. S and X. Wang, 1992: Observed tropospheric biennial variability and its relationship to the southern oscillation, *J. Climate*, 5. 594-614.

Rui, H., and B. Wang 1990: Development characteristics and dynamical structure of tropical intraseasonal convection anomalies. *J. Atmos. Sci.*, 47, 357-379.

Salby, M. L. and H. H. Hendon, 1994: Intraseasonal behavior of clouds, temperature, and motion in the tropics. *J. Atmos. Sci.*, 51. 2207-2224.

Salby, M. L., R. R. Garcia and H. H. Hendon, 1994: Planetary- scale circulations in the presence of climatological and wave-induced heating. *J. Atmos. Sci.*, 51, 2344-2367.

Saji N. H. and B. N. Goswami. 1996: An improved linear model of the tropical surface wind variability. *Q. J. R. Meteorol. Soc.*, 122 23-53

Seager, R and S. E. Zebiak. 1994: Convective interaction with dynamics in a linear primitive equation model. *J. Atmos. Sci.*, 51, 1307-1331.

Seager, R., Zebiak, S. E. 1995: Simulation of tropical climate with a linear primitive equation model *J. Climate*, 8, 2497-2520

Schopf, P. S., and Suarez. 1988: Vacillations in a coupled ocean-atmosphere. *J. Climate,*

Sui, C. H., and K. M. Lau, 1989: Origin of low-frequency (intraseasonal) oscillations in the tropical atmosphere. Part II: Modification of mobile wave-CISK modes by boundary forcings. *J. Atmos. Sci.*, 46, 37-56.

Swinbank, R., T. N. Palmer and M. K. Davey, 1988: Numerical simulations of the Madden-Jullian oscillation. *J. Atmos. Sci.*, 45, 774-788.

Takayabu, Y. N., K..-M. Lau and C.-H. Sui, 1996: Observation of a Quasi-2-day wave during TOGA COARE. *Mon. Wea. Rev.*, 124, 1892-1913.

Toure and white 1995: abstract, TOGA International conference.

Trenberth, K. E., 1975: A Quasi-Biennial standing wave in the Southern Hemisphere and interactions with sea surface temperature, *Q. J. R. Meteorol. Soc.*, 101, 55-74.

Trenberth, K. E., 1976a: Fluctuations and trends in indices of the Southern Hemisphere circulation. *Q. J. R. Meteorol. Soc.*, 102, 65-75.

Trenberth, K. E., 1976b: Spatial and temporal variations in the Southern Oscillation, *Q. J. R. Meteorol. Soc.*, 102, 639-653.

Trenberth, K. E., 1980: Atmospheric Quasi-Biennial oscillations, *Mon. Weather Rev.*, 108, 1370-1377.

Trenberth, K. E. and W. K Shin, 1984: Quasi-biennial fluctuations in sea level pressures over the Northern Hemisphere, *Mon. Weather Rev.*, 112, 761-777.

Trenberth, K. E. and D. A. Paolino, 1981: Characteristic patterns of variability of sea level pressure in the Northern Hemisphere, *Mon. Weather Rev.*, 109, 1169-1189.

Van Loon, H. and Shea, D. J. 1985: The Southern Oscillation. Part IV The precursors south of 15°S to the extremes of the oscillation, *Mon. Weather Rev.*, 113, 2063-2074.

Walker., G. T and E. W. Bliss, 1932: World weather V. Mem., *R. Meteorol. Soc.*, 4, 53-84.

Wang, B and Y. Xue, 1992: Behavior of a moist Kelvin wave packet with nonlinear heating. *J. Atmos. Sci.*, 49, 549-559.

Wang, B. and H. Rui, 1990: Dynamics of the coupled moist- Kelvin-Rossby wave on the equatorial β-plane. *J. Atmos. Sci.*, 47, 397-413.

Wang, B. and Tianming Li, 1993: A simple tropical atmosphere model of relevance to short-term climate variations. *J. Atmos. Sci.*, 50, 260-284.

Wang, B. and X. Xie, 1997: A model for the boreal summer intraseasonal oscillation. *J. Atmos. Sci.*, 54, 72-86.

Wang, X-L and T. Murakami, 1988: Intraseasonal disturbance activity before, during and after the 1982-83 ENSO. *J. Atmos. Sci.*, 45, 3754-3770.

Wang, X. L. 1994: The coupling of annual cycle and ENSO over the tropical Pacific *J. Atmos. Sci.*, 51, 1115-1138.

Weare, B. C., 1994: Interrelationships between cloud properties and sea surface temperature on seasonal and interannual time scales *J. Climate*, 7, 248-260

Weare, B. C., P. T. strub and M.D. Samuel, Marine climate atlas of tropical Pacific Ocean, Contrib to atmos. Sci. 20, 147pp., Univ. of Calif., Davis, 1980.

Weare, B. C., Strub, P. T and Michel D, 1981: Annual mean surface heat fluxes in the tropical Pacific Ocean, *J. Phys. Oceanogr.* 705-717.

Weickman, K. M., G. R. Lussky, and J. E. Kutzbach, 1985: Intraseasonal (30-50 day) fluctuations in outgoing long wave radiation and 250 mb streamfunction during northern winter. *Mon. Wea. Rev.*, 113, 941-961.

Weickmann, K. M., 1983: Intraseasonal circulation and outgoing longwave radiation modes during Northern Hemisphere winter. *Mon. Wea. Rev.*, 111, 1838-1858.

Weickmann, K. M., and Khalsa, 1990: The shift of convection from the Indian Ocean to the Western Pacific ocean during a 30-60 day oscillation *Mon. Wea. Rev.*, 118, 964-978.

Xie, S.-P., A. Kubokawa and K. Hanawa, 1993: Evaporation- wind feedback and the organizing of tropical convection on the planetary scale. Part I: Quasi-linear instability. *J. Atmos. Sci.*, 50, 3873-3893.

Xu, K.-M. and Emanuel, K. A. 1989: Is the tropical atmosphere conditionally unstable? *Mon. Wea. Rev.*, 117,1471-1479.

Yamagata T., 1985: Stability of simple air-sea coupled model in the tropics.Coupled ocean-Atmosphere Models, J. C. J. Nihoul, Ed., Elsevier, 637-657

Yamagata, T., and Y. Hayashi, 1984: A simple model for the 30-50 day oscillation in the tropics. *J. Meteorol. Soc. Japan,* 62, 709-717.

Yasunari T. 1987: Global structure of El Niño Southern oscillation Part 1: El niño composites, *J. Meteorol. Soc. Japan*, 65, 65-8.

Yasunari T. 1989: A possible link of the QBO's between the stratosphere, troposphere and the surface temperature in the tropics, *J. Meteorol. Soc. Jap.*, 67, 483-493.

Zangvil, A., 1975: Temporal and spatial behavior of large-scale disturbances in tropical cloudiness deduced from satellite brightness data. *Mon. Wea. rev.,* 103, 904-920.

Zebiak, S. E., 1990: Diagnostic studies of Pacific surface winds *J. Climate.* 3, 1016-1031.

Zhang, C., 1996: Atmospheric intraseasonal variability at the surface in the tropical western Pacific Ocean. *J. Atmos. Sci.*, 53, 739-757.

Zhang, G. J., MacPhaden, M. J., 1995: The relationship between sea surface temperature and latent heat flux in the equatorial Pacific, *J. Climate*, 8, 589-605.

Zheng, Q., X.-H. Yan, W. Timothy Liu, W. Tang and D. Kurz, 1997: Seasonal and interannual variability of atmospheric convergence zones in the tropical Pacific observed with ERS-1 scatterometer, *Geophys. Res. Lct.*, 24, 261-263.

Appendix

Description of the model parameters

Parameter	symbol	value
Mean potential temperature	$\overline{\theta}$	$310\,K$
Tropopause Height	$H\pi$	$15\,km$
Atmospheric dry gravity wave speed	c_a	$200\,m\,s^{-1}$
Atmospheric Rayleigh friction coefficient	R_d	1-5 days^{-1}
Atmospheric Newtonian cooling coefficent	R_d	1-5 days^{-1}
Density of air	$\overline{\rho}$	$1.225\ kg\,m^{-3}$